Scientific Session Abstracts

SS1. Cardiopulmonary Imaging . . . . . pages 55-58

SS2. Efficacy, Education, Administration and PACS . . . . . pages 59-62

SS3. Neuroradiology/Head and Neck . . . . . pages 63-66

SS4. Vascular and Interventional Radiology . . . . . pages 67-69

SS5. Efficacy, Education, Administration and PACS . . . . . pages 70-72

SS6. Genitourinary/OB/GYN (Kidney/Calculi) Imaging . . . . . pages 73-76

SS7. Cardiopulmonary Imaging . . . . . pages 77-79

SS8. Genitourinary/OB/GYN (Prostate/Adrenal) Imaging . . . . . pages 80-82

SS9. Neuroradiology/Head and Neck . . . . . pages 83-86

SS10. Pediatric Imaging . . . . . pages 87-90

SS11. Vascular and Interventional Radiology . . . . . pages 91-93

SS12. Cardiopulmonary Imaging . . . . . pages 94-96

SS13. Genitourinary/OB/GYN (Pelvis) . . . . . pages 97-99

SS14. Cardiopulmonary Imaging . . . . . pages 100-103

SS15. Gastrointestinal (Colon) Imaging . . . . . pages 104-107

SS16. Breast Imaging . . . . . pages 108-111

SS17. Breast Imaging . . . . . pages 112-115

SS18. Musculoskeletal (Pelvis/Lower Extremity) . . . . . pages 116-120

SS19. Genitourinary/OB/GYN (Female Genitourinary) . . . . . pages 121-124

SS20. Breast Imaging . . . . . pages 125-128

SS21. Gastrointestinal (Pancreas/Biliary) Imaging . . . . . pages 129-133

SS22. Musculoskeletal (Upper Extremity) Imaging . . . . . pages 134-138

SS23. Gastrointestinal (Diffusion/Perfusion) Imaging . . . . . pages 139-143

SS24. Musculoskeletal Imaging (and Treatment Innovations) . . . pages 144-148

SS25. Vascular and Interventional Radiology . . . . . pages 149-152

SS26. Gastrointestinal (Bowel/Peritoneum) Imaging . . . . . pages 153-157

SS27. Nuclear Medicine . . . . . pages 158-160

SS28. Gastrointestinal (Liver) Imaging . . . . . pages 161-165

SS29. General and Emergency Radiology . . . . . pages 166-168

SS30. Musculoskeletal (Systemic Disease/Spine) Imaging . . . . . pages 169-173

AMERICAN ROENTGEN RAY SOCIETY

RESIDENTS IN RADIOLOGY AWARDS

Award-winning papers will be presented at the

2010 ARRS Annual Meeting

May 2-7, 2010, San Diego, CA

President's Award ($2,000)
Executive Council Awards ($1,000 each)

General Information

Papers must be submitted on the clinical application of the discipline of radiology and radiological science.

The awards are available to residents and fellows in radiology and radiological sciences. One of the three awards may be given to a fellow.

If the resident or fellow is not the sole author, it is expected that he or she has performed the majority of the work and is the first author.

The paper should not have previously been presented, published or submitted for presentation or publication while it is being considered for an award.

Each candidate may submit only one application.

Submission Procedure

Each applicant must submit the following materials:

- A manuscript and any applicable illustrations,
- A curriculum vitae,
- A letter from the program director attesting that the author is a radiology resident or fellow, that the work is primarily the effort of the resident or fellow, that each coauthor has contributed to the work, and that the manuscript has not previously been presented or submitted for presentation or publication while it is being considered for an award.

The manuscript format should follow the instructions to authors, which can be viewed on www.ajronline.org.

Award-winning papers will be submitted to the *AJR* by the Research Committee for possible publication.

Log on to www.arrs.org for more information.

Deadline for submission: February 15, 2010
Winners will be announced by March 15, 2010

American Roentgen Ray Society
ARRS

www.arrs.org

PB00

Scientific Session 1

Cardiopulmonary Imaging Papers

Room: 208, Level 2

Monday, April 27, 2009, 10:00 am–11:30 am

Abstracts 001-008

Moderators: *U.J. Schoepf, B. Sundaram*
Keynote: CT of the Heart at the Crossroads—*U.J. Schoepf*

10:10 am

001. Low-Risk Chest Pain Patients in the Emergency Department: Negative 64-Channel Cardiac CT Angiography May Reduce Length of Stay and Hospital Charges

May, J.; Shuman, W.; Strote, J.; Branch, K.; Mitsumori, L.; Lockhart, D.; Caldwell, J. University of Washington, Seattle, WA*
Address correspondence to J. May (jbonny@u.washington.edu)

Objective: The current standard of care (SOC) workup of chest pain patients in an emergency department (ED) takes 12-36 hours and is expensive. The majority of low risk chest pain patients in this setting do not have coronary artery disease. Cardiac CT angiography (CCTA) is known to have a very high negative predictive value for significant coronary artery disease in low risk chest pain patients. A negative (CCTA) early in the workup of such patients may enable shortening of the length of stay (LOS) and reduction of charges in the ED.

Materials and Methods: We obtained informed consent to add a cardiac CT to the SOC workup of low-risk ED chest pain patients (TIMI-risk 0-2). Of the first 53 consecutive patients, 50 had a negative 64 channel CCTA and were included in this series; three had a positive CCTA with significant coronary artery disease and were excluded. The SOC workup consisted of serial cardiac enzymes, serial ECGs, and either stress Tc99m SPECT sestamibi (n=47) or stress echocardiography (n=3). LOS and hospital charges were analyzed for all patients in this SOC workup and also in two CCTA based earlier discharge scenarios using actual patient data: 1. CCTA plus serial enzymes and serial ECGs followed by discharge if all were negative (CCTA1); and 2. CCTA plus one set of enzymes and one ECG followed by discharge if all were negative (CCTA2). LOS time points were extracted from the patient medical record and charges were extracted from the institutional billing databases. Comparisons were made by paired t-tests.

Results: For the SOC workup, mean LOS was 25.4 hours. Mean LOS for CCTA1 (end point one hour after last enzyme results were available) was 14.3 hours (11.1 hours less than SOC, $p<0.001$), and for CCTA2 (end point one hour after CT results were available) was 5.0 hours (20.4 hours less than SOC, $p<0.001$). For SOC workup, mean charges were $7,597. CCTA1 mean charges were $6,153 (19% less than SOC, $p<0.001$), and CCTA2 mean charges were $4,251 (44% less than SOC, $p<0.001$).

Conclusion: In this population of low-risk ED chest pain patients, discharge based on negative CCTA, negative cardiac enzymes, and negative ECG may significantly decrease both LOS and hospital charges compared to SOC. With the current focus on ED cost containment and congestion, cardiac CT may have a role in the evaluation of low risk chest pain patients.

10:20 am

002. Prevalence of Extracoronary Ancillary Findings in Coronary CT Angiography

Sullivan, J.; Francois, C.; Ozel, B.; Yu, Z.; Keevil, J.; Reeder, S. University of Wisconsin School of Medicine and Public Health, Madison, WI*
Address correspondence to J. Sullivan (jrsullivan@wisc.edu)

Objective: The objective was to quantify and categorize the prevalence of ancillary findings identified on coronary CT angiography (CCTA).

Materials and Methods: This retrospective study compared two patient populations; group one consisting of 49 patients (mean age 61.6 years; 31 males, 18 females) scanned for a CCTA vs. angiography comparison trial and group two consisting of 246 consecutive patients (mean age 54.6; 126 males, 120 females) undergoing clinically indicated CCTA. All patients were scanned on a 64-slice MDCT (GE Healthcare, Waukesha, WI). For group one, images were reviewed by consensus of two board certified radiologists. For group two, the clinical report was reviewed for ancillary findings. For both groups, "major" findings included those requiring intervention or follow-up, or those that provided an alternative diagnosis to explain symptoms. Examples of major findings include: myocardial thinning, septal defects, pericardial masses, pulmonary emboli, noncalcified pulmonary nodules >4 mm, lymphadenopathy >/=1cm, hiatal hernias, compression fractures, hepatoma, aortic aneurysms, soft tissue masses, etc. "Minor" findings were those considered benign, which would not affect clinical management or require follow-up. Rates of ancillary findings between the two groups were compared using Fisher's exact test.

Results: For both groups combined, a total of 383 major findings were found in 195 (66%) patients and 541 minor findings were noted among 241 (82%) patients. More than half of the patients had at least one finding in both the major and minor categories (161/295, 55%). Only 19 patients out of 295 (6.4%) had no ancillary findings. There were no statistically significant differences in group demographics, except patient age ($p<0.01$) and hypertension ($p=0.02$), both of which were greater in group one. Rates of major findings and minor findings were 71% and 59% for group one and 65% and 86% for group two. There were no significant differences in overall rates of major findings between groups ($p=0.42$), although the number of minor findings was greater in group two ($p<0.001$).

Conclusion: CCTA has an expanding role in managing patients with chest pain and risk factors for CAD. A large proportion of patients undergoing CCTA have important ancillary findings, which may impact clinical management, indicating the importance of having a qualified physician involved in the interpretation of extracoronary structures.

CME credit forms and course evaluations are available online at https://www.directsurv.net/arrs/. Your user name is arrs then your badge number (for example, arrs123456) The password is arrs2009. (Please note that your badge number is also your ARRS ID number.) Please visit this site to claim your CME credit. The site opens on April 26 and will be open through May 16. In an effort to be green, ARRS is not including CME credit forms in your registration packet.

10:30 am

003. Contrast Injection Strategies for Short Scan Coronary CT

Numburi, U.[1,2]; Halliburton, S.[1,2] 1. Cleveland Clinic, Cleveland, OH; 2. Cleveland State University, Cleveland, OH*
Address correspondence to U. Numburi (numburu@ccf.org)

Objective: New MDCT systems with an increased number of detector rows enable extremely short scan times for coronary imaging (less than five seconds). Existing contrast injection protocols (average of 100 ml of 350-400 mgI/ml at 3-5 ml/second) must be modified to insure optimal contrast-enhancement during data acquisition. The objective of this study was to use data from 64-slice level scanners to develop injection protocols for short duration cardiac imaging on faster systems.

Materials and Methods: A total of 25 cardiovascular patients were imaged on a 64-slice scanner with approximately 20 cm of z-axis coverage per rotation (Siemens Medical Solutions, Forchheim, Germany). Each patient received a test injection of 20 ml of contrast (Iopromide 370 mgI/ml, Berlex, Montville, NJ) at 4.5 ml/second followed by 60 ml (<90 kg) or 80 ml (>=90 kg) of saline at the same flow rate. The time to peak maximum enhancement of the test injection was measured in the ascending aorta and used to time the 63–130 mL diagnostic injection relative to data acquisition. Using methods described in previous work, the patient was considered to be a linear, time-invariant system where attenuation (output) can be obtained by convolving the patient transfer function (patient response to a Dirac impulse input) with the contrast injection profile (input) [Fleischmann, JCAT, 1999]. The transfer function for each patient was computed from the test bolus data in the discrete domain. The patient specific transfer function was then used to approximate the injection profile necessary to achieve cardiac enhancement of 300 HU for scan duration of four seconds.

Results: Individual transfer functions were obtained in all patients [16 male, 9 female patients; mean age 59 years (30-71 years); mean weight 96 kg (59-135 kg)]. The contrast injection profile required to achieve optimal enhancement during a four second scan was predicted for all patients. On average, contrast profiles could be described as biphasic injections with an initial flow rate of 4 ml/second for eight seconds, followed by 3 ml/second for eight seconds and requiring a total average volume of 56 ml.

Conclusion: Biphasic contrast injection protocols requiring on average less than 60 ml of contrast may be appropriate for short scan duration cardiac imaging enabling a reduction in contrast volume compared to current practice.

10:40 am

004. Normal Myocardial Enhancement on 64-Slice CT

Stanton, C.[1]; Jain, V.[1]; Travin, M.[1]; Levsky, J.[1]; Burton, W.[2]; Jacobi, A.[1]; Haramati, L.[1] 1. Albert Einstein College of Medicine, Montefiore Medical Center, Bronx, NY; 2. Albert Einstein College of Medicine, Bronx, NY*
Address correspondence to L. Haramati (lharamati@aecom.yu.edu)

Objective: There is no standard method for characterizing myocardial enhancement on cardiac CT and few analyses have been described. We hypothesized that intrinsic differences in enhancement exist between myocardial segments and between patient populations. The purpose of this study was to describe myocardial enhancement on CT in patients with normal hearts.

Materials and Methods: The study population comprised 33 sequential patients (13 men, 20 women, mean age 52 years) who were prospectively recruited to undergo cardiac CT and SPECT and whose CT coronary angiograms and myocardial perfusion on SPECT were normal. Myocardial enhancement on CT was measured for each patient in HU using a region of interest in diastole (n=33) and in systole (n=29) for each of the 17 segments in the American Heart Association model. To potentially correct for variability in enhancement, aortic HU was measured and incorporated into an aorta:myocardial ratio for each segment. These ratios were compared to raw myocardial HU. We analyzed the myocardium according to the three vascular territories: left anterior descending coronary artery, left circumflex coronary artery, and right coronary artery; according to basal, mid and apical segments; and into septal or nonseptal walls. Population differences including sex, age (above, below mean) and body surface area (BSA) and left ventricle (LV) mass were evaluated for their effect on myocardial HU.

Results: The mean myocardial HU for the population was 98 (standard deviation [SD]=4.55) in systole, and 94 (SD=.12) in diastole (p=no significant difference). The mean aortic HU was 356 (SD=82.24). The raw myocardial HUs showed a narrower coefficient of variation (.15) than the ratio values (.25). Hence, raw myocardial HU were used in subsequent analysis. There was no significant difference in HU between the basal, mid and apical segments or between the three vascular territories. The septal segments showed greater mean HU vs. all other segments in both systole (112 vs. 93, $p<0.0001$) and diastole (111 vs. 87, $p<0.0001$). Women had higher mean myocardial enhancement than men in both systole (101 vs. 93, p=0.0002) and diastole (98 vs. 88, $p<0.0001$). There was no relationship between myocardial HU age, BSA or LV mass.

Conclusion: The normal myocardium has characteristic anatomic and gender differences. Women's myocardium enhances more than men's and the septum enhances more than the other walls of the heart.

10:50 am

005. Automated Diagnosis of Stenosis on Coronary CT Angiography

Zhang, S.; Levin, D.; Halpern, E. Thomas Jefferson University, Philadelphia, PA*
Address correspondence to S. Zhang (shaoxiong.zhang@jefferson.edu)

Objective: The objective was to evaluate the diagnostic accuracy of a new automated system designed for preliminary rapid interpretation of coronary CT angiography (CCTA).

Materials and Methods: Interpretation of CCTA studies with software (Rcadia Medical Imaging, Haifa, Israel) was compared with a consensus interpretation of two experienced cardiac imagers. One-hundred CCTA examinations were selected from a series of more than 1,000 cases performed on a 64-slice scanner (Philips Healthcare, Bothell, WA) during 2006-2007. Only those studies judged to have excellent image quality for evaluation of the coronary arteries during a single phase of the cardiac cycle were included. Comparison of the interpretations of the software and the experienced cardiac imagers was based upon detection of stenosis with =50% vessel diameter reduction in ten coronary segments, including the left main, left anterior descending artery (LAD), left circumflex artery (LCX) and right coronary artery (RCA). Evaluation of the LAD, LCX and RCA was divided into proximal, mid and distal segments. Diagonal and obtuse marginal arteries were not evaluated.

Results: Among the 100 cases submitted for evaluation, the software failed to process seven cases, leaving 930 segments in 930 patients for the current analysis. The software detected 10/13 patients with = 50% stenosis (sensitivity=77%) and correctly identified 59/80 patients with < 50% stenosis (specificity=74%), yielding a negative predictive value of 95% in our study population. The software correctly identified stenosis in 8/22 coronary segments (sensitivity=36%) and correctly identified < 50% stenosis in 869/908 segments (specificity=96%). Segments in which a stenosis was missed included the left main coronary artery (n=1), the LAD (n=8), the LCX (n=3) and the RCA (n=2).

Conclusion: New technology for automated interpretation of CCTA examinations demonstrates promising results for the diagnosis of stenosis in the major coronary arteries, with moderate sensitivity and specificity. However, even with excellent quality studies, further improvements in this technology are needed to improve sensitivity for the detection of stenosis. Rapid, automated interpretation of CCTA studies can provide a preliminary study interpretation, allowing better prioritization of cases for evaluation by the expert reader.

11:00 am

006. Effect of Heart Rate and Reconstruction Interval on Image Quality Using Dual-Source CT Coronary Angiography: A Per-Segment Analysis

Malik, S.[1,2]; Sassani, A.[1]; Marfori, W.[1]; Arellano, C.[1]; Sayre, J.[1]; Ruehm, S.[1] 1. University of California, Los Angeles, Los Angeles, CA; 2. Case Western Reserve University, Cleveland, OH*
Address correspondence to S. Malik (sbm11@case.edu)

Objective: The purpose of this study was to evaluate the influence of heart rate and image reconstruction interval on the image quality of individual coronary artery segments using dual-source CT (DSCT) coronary angiography in a clinical patient population with a wide variety of heart rates during data acquisition.

Materials and Methods: Coronary DSCT angiographic data sets of 61 consecutive patients collected without administration of beta blockers were analyzed. For each patient fifteen data sets were reconstructed with reconstruction intervals ranging from 20-90% of the R-R interval at 5% increments. Image quality was graded by two blinded readers through consensus reading using scores ranging from one (clear delineation of segment) to four (vessel structures not differentiable). Fifteen coronary artery segments per patient were classified according to the guidelines of the American Heart Association.

Results: The mean heart rate during coronary CT angiography was 72.8 ± 16.5 (range: 40-109). Diagnostic image quality (Score 1-2) was found in 90.22% of all segments (720 of 798). In patients with a heart rate <75 bpm the optimal reconstruction interval was at 70%. This was significantly better than the best systolic phase of 30% ($p<0.01$). In patients with a heart rate >75 bpm the optimal reconstruction interval was 35%. This was significantly better than the best diastolic phase of 70% ($p<0.01$). In 12 of 15 segments (excluding the posterior descending artery, middle left anterior descending artery, and left main artery, optimal image quality was obtained at heart rates <60 bpm. At heart rates <60 bpm and 60-75 bpm optimal image quality at diastole was obtained for all segments at 60-75% and 65-80% respectively, and at systole at 25-50% and 20-35%, respectively. At these heart rates diastolic images were significantly better ($p<0.05$) than systolic images. At heart rates > 75 bpm optimal image quality was obtained for all segments during diastole from 65-90% of the R-R interval and during systole from 30-40% of the R-R interval. Systolic images were significantly better ($p<0.05$) than diastolic images.

Conclusion: DSCT allows for diagnostic imaging of coronary arteries without beta blocker administration in patients with a wide variety of heart rates. In patients with heart rates <75 bpm, diastolic reconstruction intervals generate optimal image quality in 12 of 15 segments. In patients with heart rates >75 bpm, a reconstruction interval at 30-40% of the systolic phase yields optimal image quality in 12 of 15 segments. The remaining three segments (first diagonal artery, proximal right coronary artery and distal left anterior descending artery) show no significant difference in image quality at systolic or diastolic reconstructions. Therefore, diagnostic DSCT imaging appears feasible for heart rates <60 bpm and 60-75 bpm, with a narrow pulsing window from 60-75%, 65-80% and 30-40% of the R-R interval, respectively. The selection of a single reconstruction interval appears sufficient for the diagnostic display of all segments of the coronary tree enabling a substantial reduction in radiation exposure during routine coronary artery imaging.

11:10 am

007. Effectiveness of Best R-R Reconstruction Interval Detection Software for the Evaluation of Dual-Source Coronary CT Angiography Examinations

Erol, B.; Karcaaltincaba, M.; Hazirolan, T.; Akata, D. Hacettepe University School of Medicine, Ankara, Turkey*
Address correspondence to M. Karcaaltincaba (musturayk@yahoo.com)

Objective: We aimed to investigate effectiveness of best R-R interval detection software for evaluation of coronary CT angiography examinations.

Materials and Methods: We enrolled 109 consecutive patients who underwent dual-source coronary CT angiography. Indications were chest pain in low-intermediate risk group patients and/or nonspecific ECG changes (n=91), poststent evaluation (n=10), bypass graft evaluation (n=8). All examinations were performed by dual-source CT with temporal resolution of 83 milliseconds using slice thickness of 0.6 mm. None of the patients received beta blockers. The software calculated best R-R reconstruction interval for both diastole and systole. The visibility of coronary artery segments were evaluated using 15 segment (total of 1,635 segments) American Heart Association classification by two radiologists in consensus.

Results: Mean patient age was 55 years. Mean heart rate was 73 bpm (range 47-110). Mean best diastole and systole R-R reconstruction interval determined by the software was 73 (95 CI:63-83) and 38 (95% CI:85-5), respectively. When only best diastole, only best systole and both best systole and diastole reconstructions were evaluated, all coronary artery segments were visualized in 65 (60%), 61 (56%) ve 93 (85%) patients, respectively. In 12 patients evaluation of additional one (n=11) or two (n=1) R-R reconstruction intervals allowed visualization of all coronary artery segments. In four patients with arrhythmia all segments cannot be visualized, but after ECG editing all segments were visible in three of four patients.

Conclusion: Automatic determination of best R-R reconstruction interval allows evaluation of all coronary artery segments in most patients (85%) without additional reconstructions. Coronary artery CT angiography examinations can be evaluated faster and easily by using this tool. A major limitation is patients with arrhythmia.

11:20 am

008. Optimal Phase Reconstruction of Coronary Artery Segments: The CORE 64 Experience

Paul, N.[1]; Arbab-Zadeh, A.[2]; Vavere, A.[2]; Gottlieb, I.[2]; Hoe, J.[3]; Brinker, J.[2]; Dewey, M.[4]; Yoshioka, K.[5]; Clouse, M.[6]; Lima, J.[2]; Lardo, A.[2]; Miller, J.[2] 1. University of Toronto, Toronto, Canada; 2. Johns Hopkins University Hospital, Baltimore, MD; 3. Mount Elisabeth Medical Center, Singapore, Singapore; 4. Charite University, Berlin, Germany; 5. Iwate University Hospital, Moriyoka, Japan; 6. Beth Israel Deaconess, Boston, MA*
Address correspondence to N. Paul (narinder.paul@uhn.on.ca)

Objective: The objective was to assess the feasibility of using prospective EKG gating with 64-row MDCT in CT coronary angiography (CTCA), by analyzing the optimal phase reconstructions used in retrospectively gated acquisitions during the CORE 64 trial.

Materials and Methods: Nine cardiac centers recruited 405 patients to have CTCA and coronary angiography from October, 2005-January, 2007 (CORE 64 Trial). CTCA was performed on 64-row MDCT (Toshiba Medical Systems, Tochigi-ken, Japan), targeting a heart rate = 65 bpm. Raw data were analyzed by a central core lab to determine the optimal phase of reconstruction for motionless coronary artery segments (CAS) using a 19 segment model. Image analysis was performed by two blinded, independent readers. Readers could use volume rendered images, curved multiplanar reformats (MPR's), maximum intensity projection (MIPs), and cross-sectional images. A single phase of reconstruction (SPR) was recorded when both readers agreed that a single acquisition window was optimal for all CAS. In all other scenarios, more than one phase was recorded.

Results: To date, 291 patient datasets have been analyzed; 214 men (73%), mean age 59 years (40-89) totaling 559 segments. On a per patient basis, overall 70% of patients required a single phase for optimal CTCA reconstruction, on a per segment basis, 5,064 segments (91.6%) were optimally reconstructed using a single phase (SPR) for the entire exam. SPR as follows: HR (number of patients, % SPR) per patient analysis; <55 (94; 84%), 55-59 (74; 68%), 60-64 (53; 66%), 65-69 (36; 58%), =70 (18; 53%). Per segment analysis: HR (number of segments, %SPR); <55 (1,786; 97%), 55-59 (1,406; 88%), 60-64 (1,007; 90%), 65-69 (36, 58%), =70 (646, 88%). HR determined the optimal phase for SPR as follows: HR (mean phase in milliseconds, two standard deviation, minimum, maximum); <55 (911.5; 105.5; 360; 1,260), 55-59 (780.8; 87.0; 280; 1,140), 60-64 (718.0; 98.0; 280; 860), 65-69 (622.0; 131.0; 320; 760), =70 (574.6; 159.4; 140; 940).

Conclusion: At lower heart rates, there is increased likelihood of using a single phase for optimal reconstruction (SPR) of coronary artery segments using conventional 64-row MDCT. At heart rates below 55 bpm, a SPR is used in 84% of patients. With increasing heart rate, the optimal phase of reconstruction shifts from the diastolic toward the systolic phase of the cardiac cycle. Prospective EKG gated cardiac CT is a feasible proposition. To optimize radiation dose reduction, the heart rate should be controlled, ideally to 55 bpm or less.

Scientific Session 2

Efficacy, Education, Administration and PACS Papers

Room: 309, Level 3
Monday, April 27, 2009, 10:00 am–11:30 am
Abstracts 009-016

Moderators: *D. Heitkamp, R. Gunderman*
Keynote: What Counts in Education—*R. Gunderman*

10:10 am

009. Interpretive Services in Radiology: An Analysis of Trends, Growth and Cost
Sarwar, S.; Khosa, F.; Gomez, S.; Romney, B.; Khan, A.; Raptopoulos , V.; Clouse, M. Beth Israel Deaconess Medical Center, Brookline, MA*
Address correspondence to F. Khosa (fkhosa@hotmail.com)

Objective: This retrospective study was done to assess the impact of interpreter services (IS) in Radiology at a large metropolitan academic institution to determine if there were deficiencies, and need to improve service and delivery of care. We also analyzed the trends, growth and cost associated with increasing demands on IS.

Materials and Methods: We analyzed current needs and trends in utilization of IS services in radiology with attention to number of languages, total cost, wait times for interpreter service in radiology and ethnic mix between 2003 and 2007. In addition, a detailed survey of 50 radiology personnel was done at random and included (21 in CT, 13 in MRI, nine in ultrasound, seven in radiography) to identify possible barriers and obstacles faced in encounters with members of the IS and our non-English speaking patients.

Results: At our institution, IS caters to almost all languages, the four most common being Russian, Spanish, Chinese and Cape Verdean/Portuguese. There is increasing growth and language requirements in IS. In fiscal year 2003, there were 41,882 IS encounters in comparison to 68,344 for 2007 and 70,127 projected for 2008. The most rapid increase in need for language requirement has been for Spanish, followed by Chinese, Russian and Cape Verdean. These increases in encounters resulted in the cost of $1,403,536 for 2003 compared to $2,665,882 for 2007. The results of a survey of 78% of radiology personnel given at random estimated that IS staff was present 66% of the time during the encounter and radiology staff waited for discourse between patient and interpreter 58% of the time. Almost all (94%) believed the IS decreased procedure time when present, although 88% indicated that time was wasted in the waiting for IS personnel.

Conclusion: With an increase in the immigrant population, language barriers can be major obstacles in delivery of service and can have medico-legal implications. Having an efficient and effective IS helps physicians and health care providers. In a global village, the ever increasing demands on IS in health care calls for continual evaluation and remodeling. Through our study, we hope to improve and encourage further development of a simple and important service and diminish prospective barriers encountered in IS and its use in radiology.

10:20 am

010. Industry Analysis: Implications for Radiology
Friese, J.; Schmitz, J. Mayo Clinic, Rochester, MN*
Address correspondence to J. Friese (friese.jeremy@mayo.edu)

Objective: The objective was to evaluate the competitive landscape for the field of diagnostic and interventional radiology.

Materials and Methods: Professor Michael Porter of Harvard Business School pioneered the field of strategic analysis in the business community. These frameworks, including five forces industry analysis, competitive strategy, and value chain analysis, were used to understand the current business landscape in which radiologists operate. Based on these analyses, general recommendations are offered which can be implemented by radiology leaders and groups.

Results: Three of the five forces affecting the imaging industry remain positive. Few substitutes exist currently. Despite the promise of genetic and molecular diagnosis, clinical applications remain limited. Capital barriers to entry for new entrants are relatively high. Accreditation requirements will also limit nonradiologist participation. Supplier power is generally favorable for radiologists. While an oligopoly of suppliers exists, adequate competition remains to ensure competitive pricing and technology advancement. Two forces, customer power and competitive rivalry, have positive and negative attributes. Patients are slowly demanding and obtaining information on practice quality and alternatives. Referring physicians remain skeptical of the value radiologists provide. Consequently, these physicians are increasingly moving up market in imaging services. For-profit imaging corporations, national and international, are eager to grow and possess the infrastructure to further commoditize the industry. Value chain analysis shows limited internal and external strategic consistency of primary and secondary activities of radiology groups. For example, it highlights the inconsistency of generalist training of radiologists despite increasing specialization among referring physicians, increasing radiologist isolation secondary to increasing IT capabilities, focus on imaging quality over customer service, and dependence on others for patient procurement.

Conclusion: Strategic analysis is an important exercise for radiology leaders and individual practices. Five forces and value chain analyses highlight opportunities and challenges in the imaging industry. Radiologists should make an effort to further specialize, focus on customer service, proactively participate in accreditation, and consider consolidation into larger organizations.

CME credit forms and course evaluations are available online at https://www.directsurv.net/arrs/. Your user name is arrs then your badge number (for example, arrs123456) The password is arrs2009. (Please note that your badge number is also your ARRS ID number.) Please visit this site to claim your CME credit. The site opens on April 26 and will be open through May 16. In an effort to be green, ARRS is not including CME credit forms in your registration packet.

10:30 am

011. To Err is Human: How to Avoid Errors of Laterality in Radiology Reports

Jagtiani Sangwaiya, M.; Saini, S.; Blake, M.; Dreyer, K.; Kalra, M.*
Massachusetts General Hospital, Boston, MA
Address correspondence to M. Jagtiani Sangwaiya (mjagtiani@partners.org)

Objective: The objective was to determine the frequency of side discrepancies in the body and impression sections of radiology reports. In addition, we determined the frequency of corrected side discrepancies between radiology reports and images in a larger database of radiology reports.

Materials and Methods: In this cross-sectional study, all radiology reports (n=1,065,322) with an addendum were assessed with a radiology reports search engine, using search words "left" and "right" and "addendum" from January 1, 2007 through December 31, 2007 for discrepancy between the body and impression sections. For reports with discrepancies, we recorded the patient's gender, true side of the lesion and the imaging modality. All unaddended reports (n=13,281) in January 2007, containing the words "left and right" were evaluated using the same search engine for similar discrepancies. Follow up of reports for addenda was performed for an average of nine months. Imaging studies of reports with errors were reviewed to determine the correct side of the lesion.

Results: Of the 1,065,322 reports, 88 addended side discrepancies were reported. The errors in mislabeling the side of lesion were more common in female (n=58) than in male (n=30) patients. Of the 88 addended errors, 27 were labeled incorrectly in the body, 29 in the impression section, and 32 were mislabeled in both body and impression sections. Amongst the addended reports with side errors, mammography (25%, 22/88) and plain radiography (18%, 16/88), followed by MRI (16%, 14/88) and ultrasound (16%, 14/88), were the most commonly reported modalities with mislabeling of the side of lesion. In January 2007, there were 43/13,821 (0.31%) reports with side discrepancy of which seven had addenda and 36 had no correction for side mislabeling. In the 43 reports with uncorrected errors in laterality, most findings with side errors were observed in lungs (34.8%, 15/43), brain (16.3%, 7/43) and blood vessels (11.6%, 5/43).

Conclusion: In conclusion, laterality errors of findings are uncommon (0.008% in our institution) but do occur in radiology reports. The radiology departments and oversight safety committees should create a monitoring process to identify, track and rectify the wrong side errors in radiology reports. Radiologists should countercheck their reports before signing off their reports.

10:40 am

012. The ACR Appropriateness Criteria: An Effective Tool to Teach Evidence-Based Imaging in the Radiology Core Clerkship

Dillon, J.[1]; Slanetz, P.[2] 1. Boston Medical Center, Boston, MA; 2. Beth Israel Deaconess Medical Center, Boston, MA*
Address correspondence to P. Slanetz (slanetzp@verizon.net)

Objective: With escalating healthcare costs and limited resources, effective utilization of imaging is essential to permit optimal patient care. Students have limited exposure to evidence-based medicine in medical school, and even less exposure to the science behind utilizing specific imaging modalities for patient care. With less than 20% of medical schools requiring a rotation in radiology, most students do not understand the indications for and clinical effectiveness of many imaging tests. Therefore, we introduced two focused sessions on evidence-based imaging during the required radiology core clerkship at our institution to meet these needs.

Materials and Methods: From June, 2008 to present, 31students in the radiology core clerkship underwent a didactic session on principles of evidence-based imaging and then participated in a small group case-based session and self-directed learning exercise using the ACR Appropriateness Criteria website as the primary resource. Twenty-five topics were covered ranging from shortness of breath, acute abdominal pain, and thoracic and abdominal trauma to headache, head trauma, stroke and postmenopausal bleeding. At the end of the clinical rotation, students evaluated the exercise on a five-point scale for its effectiveness in teaching imaging strategies and its impact on their future career.

Results: Of 31 students (17 third years, 14 fourth years), none were aware of the ACR website as a resource prior to this exercise; however, 29 (94%) found the ACR Appropriateness criteria a useful resource and 28 (90%) stated that they would likely use this resource in other clinical rotations and future practice. Twenty-five (81%) felt challenged to think differently about radiology as a result of these sessions and 23 (75%) felt they had a solid understanding of the indications for certain imaging tests following the sessions. Only five (16%) would have preferred a didactic session rather than the interactive small group and self directed sessions. Students praised the ACR website for its comprehensive coverage of the different modalities and their relative radiation risks but noted the absence of relative cost information. Nearly half of the students would have preferred covering all of the topics during dedicated sessions rather than as a self-directed exercise.

Conclusion: The ACR Appropriateness Criteria is a valuable resource to teach evidence-based imaging to medical students. A majority of students indicated that they will continue to use this resource in future practice.

10:50 am

013. Accuracy of On-Call Resident's Interpretation of Total Spine MRI Performed for Evaluation of Cord Compression

Booya, F.; Bhadilia, R.; Rojas, R.; Hackney, D.; Hochberg, A. Beth Israel Deaconess Medical Center, Jamaica Plain, MA*
Address correspondence to F. Booya (fargolbooya@yahoo.com)

Objective: The objective was to evaluate the accuracy of on-call resident's interpretation of total spine MRI performed for evaluation of cord compression.

Materials and Methods: We reviewed total spine MRI cases performed from January, 2008 to September, 2008 in our emergency department requested for the evaluation of cord compression. We compared the preliminary reading provided by the on-call resident during off hours with the final reading by an attending physician. We recorded the accuracy of resident reading for evaluation of cord compression and other significant findings.

Results: There were 36 cases that had preliminary reading provided by an on-call resident. Twenty-two cases were performed for new onset neurological symptoms, 11 for excruciating back pain, two for high risk spinal fractures and one case was performed for sudden loss of distal pulses. Resident readings were concordant with the final readings in 36/36 cases for cord compression evaluation. In five patients, significant findings were not called in the preliminary reading that affected subsequent clinical management. These were sacral fracture, cord contusion and multiple ligamentous injuries, paraspinal mass and aortic thrombus.

Conclusion: There is high degree of concordance between resident preliminary reading and final attending reading for evaluation of cord compression. However, in about 13% of cases resident readings did not include important spinal and extraspinal findings that affected subsequent clinical management. Elucidation of the patterns may prevent future occurrences.

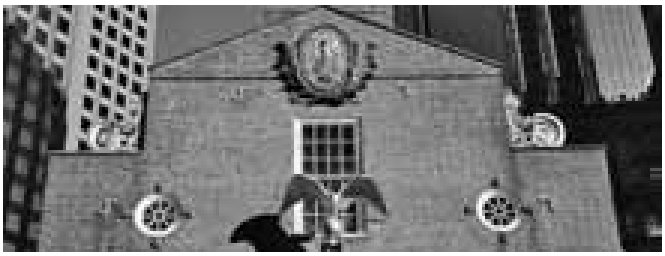

11:00 am

014. Archiving of Thin Slice CT Images in Follow-Up of Lung Nodules Not of Additional Benefit

Chan, M.; Hong, T.; Kohno, Y.; Salahudeen, S.; Soboleski, D. Queen's University, Victoria, Canada*
Address correspondence to T. Hong (3tsch@queensu.ca)

Objective: The objective of this study was to determine whether archiving of reconstructed 7 mm thick axial CT slices are sufficient in the follow-up of nonspecific pulmonary nodules on CT scans of the thorax.

Many studies have attempted to address the increasing need for condensed storage to accommodate the ever-expanding accumulation of imaging data. Proposed solutions have suggested multiple methods of lossy file compression [5, 6, 7] and conversion to alternate formats [8]. Meanwhile, the continual advancement in imaging and medicine is resulting in an exponential increase of acquired data. As a result, it is an ongoing project to search for more effective alternatives to store the mass amounts of imaging data [9]. A reduction in the number of archived images can be a more practical and simplified approach. Current storage of an average CT chest study with 200 3 mm slice thick images occupies approximately 52 megabytes of space.

Materials and Methods: This was a quantitative and qualitative comparison of 153 noncalcified lung nodules in 58 patients monitored by routine follow-up CT over at least a two year time frame. The nodules identified on the 3 mm thick CT slices stored as digital data were compared with reconstructed 7 mm thick slices archived on film.

Results: Of the total 153 nonspecific pulmonary nodules visualized on 3 mm axial CT slices, only two nodules were not identified on the reconstructed 7 mm thick slices on film. These two unobserved nodules were 2.3 mm and 2.5 mm in diameter.

Conclusion: Digital storage of chest CT images in reconstructed 7 mm thick slices, in comparison with 3 mm thick slices, will not result in significant reduced visual sensitivity nor deduct from future patient management in follow-up of nonspecific lung nodules. This potentially could result in an ~ 60% decrease in storage computer space.

11:10 am

015. Acute Appendicitis: Performance of Readers With Various Levels of Experience Using Independent Coronal MPR vs. Independent Transverse Images

Sebastian, S.; Khan, M.; Sabourin, S.; Hartman, M.; Ibraheem, O.; Small, W. Emory University School of Medicine, Decatur, GA*
Address correspondence to S. Sebastian (ssebast@emory.edu)

Objective: The objective was to assess the performance of readers with varied levels of experience and training using independent coronal multiplanar reformats (MPR) vs. transverse images for diagnosis of acute appendicitis.

Materials and Methods: This was an IRB approved study; 60 patients referred for MDCT with suspicion of acute appendicitis were included. Presence of abnormal appendix on surgery and pathology reports was the reference standard for acute appendicitis (n=45), while the remaining patients (n=15) did not have acute appendicitis, since they did not undergo surgery and had an unremarkable clinical follow up report. Transverse images were reconstructed at 5 mm thick sections and .625 mm thick sections. The .625 mm sections were subsequently reformatted to obtain 3 mm thick coronal MPR images. In a retrospective image review, only the coronal MPR images were independently reviewed for diagnosis, confidence scores and image quality by four readers (Rs): first year resident with one abdominal CT rotation (R1), third year radiology resident (R3), abdominal imaging fellow (R3), and a staff radiologist with five years of experience in abdominal imaging (R4). After an interval of at least two weeks, only the independent transverse images were reviewed. Image quality was subjectively assessed on a five-point scale (1=very poor; 5=excellent). A diameter of 8 mm was used as the cutoff on CT for acute appendicitis in both planes. Confidence scores pertaining to final diagnosis were assessed with a three-point scale (1=poor; 3=excellent).

Results: Sensitivities and specificities for detection of acute appendicitis for four readers for independent coronal MPR images were (R1; 88, 90), (R2; 94, 92), (R3; 94, 94) (R4; 96, 95) respectively and for independent axial scans were (R1; 92, 92), (R2; 94, 94), (R3; 92, 94) (R4; 96, 96) respectively. Differences were not statistically significant ($p>0.05$). There was good reader agreements (range, 0.80 to 0.88) among readers for coronal scans alone and for axial scans alone (range, 0.82 to 0.9). Mean image quality was 4.51 for coronal images and 4.62 for axial images. There was no statistically significant difference in the confidence scores of all readers in both planes ($p>0.05$).

Conclusion: Independent coronal MPR images may be used regardless of reader experience and training for the detection of acute appendicitis. Training of first year radiology residents could benefit with routine use of coronal MPR images for the detection of acute appendicitis.

11:20 am

016. The Impact of Introducing Cine Clips in Routine Ultrasound Protocols

Bragg, A.; Angtuaco, T. University of Arkansas for Medical Sciences, Little Rock, AR*
Address correspondence to T. Angtuaco (angtuacoteresital@uams.edu)

Objective: The objective was to determine the changes brought about by the introduction of cine clips in routine ultrasound protocols relative to efficiency of daily work load and assess the effect of these changes in sonographer and sonologist behavior.

Materials and Methods: A review of examinations of the neonatal head, complete abdominal ultrasound and complete pelvic ultrasound was performed before and after the introduction of cine clips into routine protocols. Cases performed for one month were used to measure the average scan time in each category. Using the old protocol the following number of studies were reviewed: 36 neonatal heads, 60 complete abdomen and 52 complete pelvic exams. With the new cine protocol the following studies were reviewed: 97 neonatal heads, 56 complete abdomen and 68 complete pelvic exams. The results were compared to determine time savings and impact on efficiency. Subjective survey of responses to the protocol change among sonographers and sonologists were recorded.

Results: Average scan times using the old protocol were as follows: 6.5 minutes for neonatal heads, 16.3 minutes for complete abdomen and 24.06 minutes for complete pelvic studies. For the new protocol the average scan times were as follows: 3.4 minutes for neonatal heads, 13.07 minutes for complete abdomen and 11.8 minutes for complete pelvic exams. Survey responses from sonographers included the following: decrease in repetitive stress disorders, less resistance to portable examinations and less repeat studies. Among sonologists, the following changes were recorded: easier distinction between artifact and true findings; less rescan time to confirm sonographer findings, easier communication with clinicians, and more confidence in diagnosis.

Conclusion: Introduction of cine clips to the routine scanning protocols results in significant time savings, more confidence in diagnosis, less rescan times, less repetitive stress disorders among sonographers, and better communication between sonologists and clinicians.

Scientific Session 3

Neuroradiology/Head and Neck Papers

Room: 210, Level 2
Monday, April 27, 2009, 10:00 am–11:30 am
Abstracts 017-024

Moderators: D. Nguyen, K. Saltzman
Keynote: Neuroradiology Education Update 2009—M. Mullins

10:10 am

017. Follow-Up of Initial Nondiagnostic Fine-Needle Aspiration Biopsy: Is Rebiopsy Necessary? Experience in a Cohort of 2,348 Patients

Baier, N.; Hahn, P.; Gervais, D.; Mueller, P.; Samir, A.; Harisinghani, M. Massachusetts General Hospital, Boston, MA Address correspondence to N. Baier (baier.nina@mgh.harvard.edu)*

Objective: Fine-needle aspiration biopsy (FNAB) as a main diagnostic test to distinguish benign from malignant thyroid nodules may be nondiagnostic in up to 20% of the patients. The purpose of this study was to evaluate patients with nondiagnostic thyroid FNAB assessing subsequent outcome including surgery, repeated biopsy and imaging and to calculate the accuracy of repeated FNAB.

Materials and Methods: Between January, 2002 and November, 2007, of 2,348 radiologist-performed ultrasound-guided thyroid FNABs 408 (17%) were nondiagnostic; 192 of these (79.7% female, 20.3% male, average age: 57.43 years) were included in this study. Inclusion criteria were: nondiagnostic first FNAB and follow-up records available for retrospective review, classified as follows: 1) surgery within less than three months, 2) repeated FNAB within less than three months, 3) diagnostic ultrasound follow-up for at least 12 months.

Results: Malignancy was identified in 34 (17.7%) of all nodules (n=5 papillary thyroid carcinoma, n=21 microfollicular adenoma, n=1 follicular thyroid carcinoma, n=5 other malignancies). Group 1: 21 nodules (10.9%) underwent total thyroidectomy (mean follow-up time 2.04 months) of which 52% were malignant. Group 2: 113 (58.9%) and 11 (5.7%) nodules had a first and second follow-up FNAB (mean follow-up time 1.34 months), respectively. The first rebiopsy was again nondiagnostic in 35.4% (40/113) and the second in 27.7% (3/11). 20.4% of first (23/113) and none of second repeated biopsies were malignant. Of these malignant nodules 56.5% were true positive and 13% false positive by surgery. Group 3: Follow-up imaging by thyroid ultrasonography was performed in 58 (30.2%) nodules (mean follow-up time 31.6 months) of which 96.6% were stable in size, 3.4% showed interval growth.

Conclusion: The high overall prevalence of thyroid cancer (17.7%) in patients with thyroid nodules diagnosed on initial FNAB as nondiagnostic necessitates the recommendation for follow-up.

10:20 am

018. Reasons for a Nondiagnostic Fine-Needle Aspiration Biopsy in Thyroid Nodules Based on Individual or Combined Ultrasonographic Features

Baier, N.; Hahn, P.; Gervais, D.; Mueller, P.; Samir, A.; Harisinghani, M. Massachusetts General Hospital, Boston, MA Address correspondence to N. Baier (baier.nina@mgh.harvard.edu)*

Objective: This study was performed to determine the likelihood for a nondiagnostic fine-needle aspiration biopsy (FNAB) in thyroid nodules based on demographic and ultrasonographic assessment.

Materials and Methods: Between 2002 and 2007, 946 thyroid nodules (198 male; 748 female) were identified retrospectively which had undergone an ultrasound (US) followed by a FNAB. Four sonographic features were recorded from previous reports: longest dimension (<10 mm, =10 mm), morphology (solid, cystic, mixed), presence of microcalcifications, and presence of lymphadenopathy. Final FNAB outcome of each nodule was classified as diagnostic or nondiagnostic.

Results: The overall prevalence of a nondiagnostic FNAB was 17.4% (165 of 946 nodules). Older age was significantly associated with a nondiagnostic FNAB (mean age 55.3 years for diagnostic vs. 58.2 years for nondiagnostic FNAB; p=0.001), whereas gender had no influence. Intragroup comparison of US features among nodules with diagnostic and nondiagnostic FNAB could not identify a statistically significant difference between both groups for one of the individual US features or a combination of two to four of them, even not for size (longest dimension 11.8 mm for nodules with diagnostic vs. 11.3 mm for nodules with nondiagnostic FNAB; p=0.714). Solid nodules =10 mm containing microcalcifications and concomitant presence of lymphadenopathy showed the highest risk for a FNAB to be nondiagnostic (odds ratio 1.44), but this result was not significant (p=0.443).

Conclusion: US features cannot predict the risk of nondiagnostic FNAB in thyroid nodules, even not the previously suspected features size and morphology. Only older age significantly increases the risk for a FNAB to be nondiagnostic.

CME credit forms and course evaluations are available online at https://www.directsurv.net/arrs/. Your user name is arrs then your badge number (for example, arrs123456) The password is arrs2009. (Please note that your badge number is also your ARRS ID number.) Please visit this site to claim your CME credit. The site opens on April 26 and will be open through May 16. In an effort to be green, ARRS is not including CME credit forms in your registration packet.

10:30 am

019. Arterial Spin Labeling MR Perfusion is Equally Accurate to (18)FDG-PET in Distinguishing Recurrent Tumor from Radiation Necrosis

Booya, F.; Hackney, D.; Alsop, D. Beth Israel Deaconess Medical Center, Jamaica Plain, MA*
Address correspondence to F. Booya (fargolbooya@yahoo.com)

Objective: The objective was to compare arterial spin labeling (ASL) technique with (18)FDG-PET imaging for differentiation of tumor necrosis from recurrence in patients with brain tumors.

Materials and Methods: Seventeen patients with 24 histologically proven brain tumors (six cases of glioblastoma multiforme and 11 cases of metastases) who were treated with radiation or chemoradiation and had enhancing lesions at the site of primary tumor treatment in the follow up imaging were included. ASL and PET were done within an average 16 days of each other (range 0-50). In each patient, the gadolinium enhanced MRI and PET and ASL study were independently interpreted as tumor or not. Using an enhanced MRI study as a road map, the uptake/perfusion of the lesion and the normal white matter were measured in FDG-PET and ASL studies. The ratios of FDG uptake of the lesions to normal white matter in PET and ratio of cerebral blood perfusion of the lesion to normal white matter were compared. The results were compared with the gold standard (pathology and/or long term clinical follow up).

Results: In tumor recurrence, FDG uptake ratio was 2.9 + 0.8 and ASL perfusion ratio was 5.9 + 2.1. All recurrences had standard uptake value (SUV) greater than 5.7 and perfusion greater than 50 cc/minute/gram. In radiation necrosis the uptake or perfusion were equal to or less than normal white matter and reliable region of interest could not be placed. No radiation necrosis had uptake greater than 4.9 SUV or perfusion greater than 29 cc/minute/gram. There was a close correlation between FDG-PET findings and arterial spin labeling in the tumor region of interest ($p<.05$). The PET was concordant with gold standard in 19/24 lesions and ASL was concordant with the gold standard in 23/24 lesions.

Conclusion: Both methods are highly concordant with one another and with the gold standard. The slight superiority of ASL was not statistically significant. However, since ASL is a five minute acquisition at the time of MR imaging, collecting perfusion data with ASL is a more efficient approach to answering a diagnostic question.

10:40 am

020. Finding Ectopic Parathyroid Adenomas Missed by Ultrasound, Nuclear Scintigraphy or Surgery: Preliminary Results of 4-Phase MDCT in 18 Patients

Beland, M.[1,2]; Grand, D.[1,2]; Dupuy, D.[1,2]; Yoo, D.[1,2]; Monchik, J.[1,2]; Mayo-Smith, W.[1,2] 1. Brown University, Providence, RI; 2. Rhode Island Hospital, Providence, RI*
Address correspondence to M. Beland (mbeland@lifespan.org)

Objective: We review our experience performing a multiphase (4D) MDCT to localize ectopic parathyroid adenomas not seen on ultrasound or nuclear medicine exams or failed prior surgery.

Materials and Methods: This retrospective review received IRB approval and is HIPAA compliant. Eighteen patients with primary hyperparathyroidism underwent a multiphase (4D) CT scan of the neck and chest including noncontrast and multiphase postcontrast imaging. All had nonlocalizing ultrasound and nuclear medicine imaging or failed prior surgery. The medical records and imaging studies of these patients were reviewed with particular attention to operative and pathology reports and postoperative therapeutic response. Correlation of imaging studies with operative results and pathology, when available, was performed to determine accuracy of CT findings. Region of interest measurements were performed of pathologically proven lesions and cervical lymph nodes to determine what phase of contrast yielded maximum lesion conspicuity.

Results: Single or multiple enlarged parathyroid glands were identified on 4D MDCT in 15 of 18 patients. Average maximum diameter was 1.1 cm. Seven of the 15 patients have undergone surgical excision at the time of the study. Nine parathyroid adenomas were identified on CT in these seven patients, all of which were confirmed on pathology (specificity 100%). All patients demonstrated a biochemical treatment response with mean pretreatment parathyroid hormone assay 141.7 pg/mL and posttreatment hormone assay 19.1 pg/mL. Mean HU densities for the confirmed adenomas were 46, 129, 136 and 113 at 0, 30, 60 and 90 seconds after intravenous contrast administration, respectively. Mean HU densities for the largest identifiable cervical lymph node were 39, 58, 92 and 100 at 0, 30, 60 and 90 seconds after intravenous contrast administration, respectively. Adenoma enhancement was statistically significantly higher than nodes at 30 ($p=0.0001$) and 60 ($p=0.0061$) seconds.

Conclusion: Multiphase MDCT is an extremely useful exam to localize ectopic parathyroid glands. Parathyroid adenomas have a characteristic appearance and enhance avidly on early phase imaging which can be useful in distinguishing these lesions from lymph nodes.

10:50 am

021. Residual Pituitary Adenomas after Surgical Treatment: Improved Depiction with Gadobenate Dimeglumine Compared to Gadopentetate Dimeglumine

Anzalone, N.; Vezzulli, P.; Scola, E.; Picozzi, P.; Iadanza, A. Scientifc Institut San Raffaele Hospital, Milan, Italy

Objective: The objective was to intraindividually compare 0.1 mmol/kg doses of gadobenate dimeglumine and gadopentetate dimeglumine for MR imaging of residual pituitary adenoma postsurgery.

Materials and Methods: Fifteen patients (six males, nine females) with residual pituitary adenoma amenable to gamma knife surgery were enrolled. Patients underwent two MR examinations at 1.5T separated by 48 hours. The imaging parameters were identical for the two studies. Ten patients received gadobenate dimeglumine for the first examination and gadopentetate dimeglumine for the second while the remaining five patients received the two agents in the reverse order. The first of the two examinations was performed after positioning the stereotaxic helmet. The volume and injection rate were identical for the two examinations. Images were evaluated in terms of lesion morphology, dimension and border delineation, degree and pattern of lesion enhancement, and definition of the involvement of nearby structures (e.g. cavernous sinuses). Overall preference for one examination over the other was assigned in blinded fashion in terms of lesion detectability and diagnostic confidence.

Results: Preference for gadobenate dimeglumine was expressed for 11/15 patients while preference for gadopentetate dimeglumine was expressed for 3/15 patients. For the remaining patient the two agents were considered equivalent. Where a preference for gadobenate dimeglumine was expressed, the choice was primarily due to greater contrast enhancement and better lesion border definition both of which led to improved depiction of the residual pituitary adenoma

Conclusion: Improved depiction of residual pituitary adenoma on follow-up MR imaging after surgical treatment is achievable with gadobenate dimeglumine compared to gadopentetate dimeglumine.

11:00 am

022. Subcentimeter Thyroid Nodules: Utility of Sonographic Characterization and Ultrasound-Guided Needle Biopsy

Sharma, A.[1,2]; Gabriel, H.[1,2]; Nikolaidis, P.[1,2]; Nemcek, A.[1,2]; Nayar, R. [1,2] 1. Northwestern University Feinberg School of Medicine, Chicago, IL; 2. Northwestern Memorial Hospital, Chicago, IL*
Address correspondence to A. Sharma (a-sharma3@northwestern.edu)

Objective: Although current practice guidelines exist for biopsy of nodules >1 cm, no specific paradigm has been established for the management of subcentimeter nodules. In addition, the incidence of nodal metastasis from a thyroid cancer is not necessarily nodule size-dependent. The purpose of this study is to determine the significance of these thyroid nodules by evaluating the utility of sonographic characterization and subsequent ultrasound (US)-guided biopsy of thyroid nodules less than 1 cm.

Materials and Methods: We performed a retrospective review of more than 2,000 thyroid biopsies between March, 2006 and August, 2008 and identified a subset of patients who underwent needle biopsy of thyroid nodules 9 mm or smaller. The patients ranged in age from 24 to 87 with a mean of 53 years. Two fellowship-trained ultrasound attendings reviewed images on a PACS workstation and noted specific sonographic features including internal echogenicity, margins, height/width ratio, presence of microcalcifications, posterior acoustic features, solid/cystic ratio, presence of a halo, and color Doppler characteristics. Subjective assessment scores for level of suspicion were also noted for each lesion. All ultrasound-guided biopsy procedure notes and histopathologic reports were reviewed and correlated with the ultrasound assessments.

Results: A total of 108 subcentimeter thyroid nodules underwent ultrasound-guided biopsy; 11/108 (10%) of the nodules had a nondiagnostic biopsy and were excluded from further analysis; 14/97 (14%) nodules were malignant at cytology. For another 15 (15%) neoplasm could not be excluded and repeat US fine needle aspiration (FNA) was suggested. Overall, 16 (17%) were malignant at final surgical pathology. Malignant nodules had a size range of 3-9 mm and mean of 7.7 mm. All 16 (100%) malignant nodules were solid, 15/16 (94%) were hypoechoic, 11/16 (69%) had at least partially ill-defined margins, 9/16 (56%) were taller than wide or spherical, 13/16 (81%) had calcifications, and 15/16 (94%) had a very high level of suspicion for malignancy.

Conclusion: By not biopsying certain subcentimeter nodules, a significant number of small, neoplastic nodules will be missed. In addition, US-guided FNA of these subcentimeter lesions can be successfully performed with a low nondiagnostic rate. Certain sonographic features correlate highly with the presence of malignancy, most notably solid, hypoechoic nodules with microcalcifications, and an equal or greater height/width ratio. Thus, subcentimeter nodules with suspicious characteristics may be malignant and may be successfully diagnosed with ultrasound-guided biopsy.

11:10 am

023. A Controlled Vocabulary to Represent Sonographic Features of the Thyroid and its Application in a Bayesian Network to Predict Thyroid Nodule Malignancy

Liu, Y.; Kamaya, A.; Desser, T.; Rubin, D. Stanford University, Stanford, CA*
Address correspondence to Y. Liu (yliu@stanford.edu)

Objective: It is challenging to distinguish benign from malignant thyroid nodules on high resolution ultrasound. Many ultrasound features have been studied individually as predictors for thyroid malignancy, none with a high degree of accuracy, and there is no consistent vocabulary used to describe the features. This study aims to create a controlled vocabulary for sonographic features of the thyroid with the goal of providing a means of creating standard descriptions of the images. We hypothesize that such a controlled vocabulary can be used to drive decision support applications such as a Bayesian network for thyroid nodule classification.

Materials and Methods: We performed a systemic review and identified 16 articles that discussed either one or a number of sonographic features associated with either benign or malignant thyroid nodules. We then built a Bayesian classifier to predict thyroid nodule malignancy using both imaging and demographic factors. To evaluate our classifier, we randomly selected 21 benign thyroid nodules and 20 malignant nodules from 37 patients who had pathologically-established diagnosis from ultrasound-guided biopsies. We compared the performance of our classifier to that of two radiologists specializing in thyroid imaging.

Results: We identified eight sonographic features that are well known to be associated with either benign or malignant thyroid nodules. An aggregate sensitivity and specificity of each feature was calculated as the weighted average of these parameters from all the articles. The weight used was the number of thyroid nodules studied in each article, so that the aggregate values were biased toward large studies. The Bayesian classifier built from this controlled vocabulary had comparable or even slightly better performance to that of the two expert radiologists: area under the ROC curve (Az) for the Bayesian classifier was 0.85. The Az for the two radiologists was 0.85 and 0.72, respectively.

Conclusion: Controlled vocabularies have been advocated to standardize radiology reporting and to facilitate communication, data retrieval, and data analysis. Our results demonstrate the benefit of controlled terminology for creating a decision support application—in our case, a Bayesian network to help diagnose malignant thyroid nodules. The malignant potential of thyroid nodules can be quantitatively assessed in such a model to provide decision support to practitioners deciding whether to biopsy suspicious lesions.

11:20 am

024. Risk of Cancer Associated With Ultrasound Findings: Results from a Population-Based Cohort Study

Sellami, D.; Chu, P.; Feldstein, V.; Goldstein, R.; Smith-Bindman, R. University of California San Francisco Medical Center, San Francisco, CA*
Address correspondence to D. Sellami (dorra.sellami@radiology.ucsf.edu)

Objective: The objective was to determine the prevalence of thyroid nodules on ultrasound (US) and features predictive of cancer. The goal is to identify nodules with low risk of cancer so that fine needle aspiration (FNA) can be deferred in patients at lowest risk.

Materials and Methods: This was a retrospective cohort study of patients who had a thyroid US at a single academic institution between January, 2000 and March, 2005 (4,370 patients and 6,684 exams). Patient data were linked with the Northern California SEER cancer registry. Patients in whom cancer was diagnosed within two years of US were considered cases and patients in whom cancer was not diagnosed within two years were considered controls. US images of all cases (n=105), and random sample of controls (n=378) were prospectively reviewed by two radiologists blinded to cancer status.

Results: The preliminary analysis of 83 patients (16 cancers, 66 controls) demonstrates good to outstanding agreement between observers in US interpretation (kappa 0.73-1.0). Overall, 121 nodules were identified among 57 patients. Among the controls, 53% (35/66) had at least one nodule >10 mm. Several nodule features were significantly associated with the risk of cancer, including microcalcifications (15.4% of cancers, 1.2 % of controls, likelihood ratio [LR] 12.83); a cyst with a mural nodule (10.3% of cancers, 2.5% of controls, LR 4.12); and hypoechoic echo-texture (17.9% of cancers, 7.4% of controls, LR 2.42). US features significantly associated with benign outcome include hyperechoic echo-texture (0% of cancers, 8.6% of controls, LR 0.06) and the presence of a halo (23.1% of cancer, 37% of controls, LR 0.62). Some features previously reported as predictive of cancer, such as shape, or predictive of benignity, such as ring down artifact, did not discriminate between cancers and controls. A multivariate analysis will be used to develop a scheme for combining nodule features for interpreting thyroid US, resulting in US assessment that parallels the BIRADS system for breast imaging.

Conclusion: The prevalence of benign thyroid nodules is high. Clinical guidelines that recommend FNA of all lesions >10 mm would result in large numbers of benign thyroid biopsies. Several US features are significantly associated with the risk of cancer and should prove useful for development of an evidence-based management algorithm for thyroid US.

SCIENTIFIC SESSION 4

VASCULAR AND INTERVENTIONAL RADIOLOGY PAPERS

Room: 310, Level 3

Monday, April 27, 2009, 10:00 am–11:30 am

Abstracts 026-031

Moderators: *C. Ray, D. Madoff*
Keynote: Paradigm Shifts in Hepatic Arterial Tumor Embolotherapy—*C. Ray*

10:30 am

026. Angiographic Cone Beam C-Arm Volume CT With a Flat Panel Detector Prior to Transcatheter Arterial Chemoembolization: Does it Add Useful Information on the Arterial Tumor Supply and Portal Veins?

Meyer, B.[1]; Witschel, M.[1]; Frericks, B.[1]; Wolf, K.[1]; Wacker, F.[1,2]*
1. Charité - University Medicine, Campus Benjamin Franklin, Berlin, Germany; 2. Johns Hopkins Medical School, Baltimore, MD
Address correspondence to B. Meyer (b.meyer@marleben.de)

Objective: The study was done to assess arterial tumor supply and portal vein with C-Arm CT (CACT) in comparison to digital subtraction angiography (DSA) in patients undergoing transcatheter arterial chemoembolization (TACE) of the liver.

Materials and Methods: Thirty patients (hepatocellular carcinoma, n=10, malignant ocular melanoma, n=12, hypervascular liver metastases, n=8) underwent arterial and portal-venous CACT (breath-hold technique, resolution 0.4 mm^3) of the liver using intra-arterial contrast media administration as well as DSA immediately prior to TACE. After assessing the DSA images, CACT images were reviewed on a 3D workstation. Number and origin of the tumor feeding arteries, ideal position of the catheter for TACE, presence of segmental portal vein thrombosis and of breathing artifacts in both, DSA or on CACT, were assessed and correlated.

Results: The number of vessels identified as tumor feeders was significantly higher in C-Arm CT than in DSA (CACT: 1.4 ± 0.6 and DSA: 1.0 ± 0.3, p=0.003, t-test). After consideration of the CACT images, the position of the catheter for TACE was changed in 15 cases to a less selective position (n=9) or to a more selective position to preserve healthy liver tissue (n=3) or the gall bladder (n=3). Breathing artifacts were observed in both, CACT (n=3) and DSA (n=2), but did not interfere with image interpretation. A segmental portal vein thrombosis was seen in three patients in CACT, but only in one in DSA.

Conclusion: As CACT depicts both, soft tissue as well as small vessels in high spatial resolution, tumor-vessel-allocation is facilitated and the ideal catheter position for TACE can be chosen more precisely. Due to the higher contrast resolution of CACT in comparison to DSA, portal vein pathologies are better visualized.

10:40 am

027. Chemoembolization Combined with Radiofrequency Ablation for Hepatocellular Carcinoma; Survival Benefits and Tumor Treatment Response

Dhanasekaran, R.[1]; Khanna, V.[1]; Kooby, D.[1]; Delman, K.[1]; Staley, C.[1]; Kauh, J.[1]; Carew, J.[2]; Kim, H.[1] 1. Emory University School of Medicine, Atlanta, GA; 2. Emory University, Atlanta, GA*
Address correspondence to R. Dhanasekaran (renumathyd@gmail.com)

Objective: The objective was to investigate survival benefits and tumor treatment response among patients who received treatment with transcatheter therapy (TACE) combined with radiofrequency ablation (RFA) and TACE alone.

Materials and Methods: The study included 108 hepatocellular carcinoma (HCC) patients who were treated with TACE between the period of 1998 and 2008; 51 (47.2%) received TACE followed by planned RFA and 57 (52.8%) received TACE alone; 57 patients received Precision TACE with Doxorubicin drug eluting beads and 51 received conventional TACE. The primary endpoint of the study was survival from TACE and the secondary was tumor treatment response. Survival analysis was performed using Kaplan Meier Estimator with a log rank test, Fischer exact test was performed for categorical variables and the t test for continuous variables.

Results: Patient demographics (age, sex and race) were comparable between the two groups. The average MELD score among the TACE-RFA group and TACE-only group were 12.87 and 12.33 respectively (p=0.64). The number of patients in Child's class A, B, C in the two groups were 28/15/8 and 23/23/11 (p=0.30). The number of patients in Okuda class I, II and III in the two groups were 22/23/6 and 14/30/9 (p=0.2). The median survival among patients who received TACE + RFA and TACE alone were 566 days and 209 days (p=0.01). One year, two year and three year survival rates among patients who received TACE + RFA and TACE alone were 53%, 44%, 30% and 35%, 15%, 7%. Median survival of patients treated with Precision TACE + RFA was 566 days and that of patients treated with conventional TACE + RFA was 336 days (p=0.510). Mean progression-free duration by RECIST criteria among the TACE + RFA group was 210 days vs. TACE only group 97 days (p=0.04).

Conclusion: Combination therapies of TACE and RFA were associated with improved survival compared to TACE alone. No significant survival difference was associated with Precision TACE + RFA vs. conventional TACE + RFA. TACE + RFA was associated with improved imaging response and progression-free duration compared to TACE alone.

CME credit forms and course evaluations are available online at https://www.directsurv.net/arrs/. Your user name is arrs then your badge number (for example, arrs123456) The password is arrs2009. (Please note that your badge number is also your ARRS ID number.) Please visit this site to claim your CME credit. The site opens on April 26 and will be open through May 16. In an effort to be green, ARRS is not including CME credit forms in your registration packet.

10:50 am

028. Volumetric Quantification of Necrosis in MDCT of Tumor Phantoms and Colon Cancer Hepatic Metastasis Treated with Y-90 Radioembolization: Initial Results

Tochetto, S.[1]; Rezai, P.[1]; Soud, H.[2]; Yaghmai, V.[1] 1. Northwestern University, Chicago, IL; 2. Siemens Medical Solutions, Malvern, PA*
Address correspondence to V. Yaghmai (v-yaghmai@northwestern.edu)

Objective: The objective was to evaluate the feasibility of volumetric quantification of the necrotic component of colon cancer hepatic metastasis after treatment with Yttrium-90 radioembolization using prototype software.

Materials and Methods: Initially three phantoms with different shapes and volumes simulating hepatic tumors with central necrosis were constructed, imaged by MDCT and segmented by a prototype software to validate volumetric measurement of necrosis. The phantoms were constructed using an agarose gel, suspended in diluted contrast solution (180 HU) and scanned by 64-MDCT. The outer layer of each phantom and its internal core were constructed with different densities, mimicking the higher density of viable tumor (40-45 HU) and necrotic center (18-20 HU). Different densities were achieved by adding different concentrations of iodinated contrast material to the gel. The volume of phantoms and their "necrotic" core were then quantified using the prototype semiautomated segmentation software designed specifically for this purpose. Fourteen colon cancer hepatic metastases in patients treated with Yttrium-90 radioembolization and imaged by contrast-enhanced MDCT were also segmented and evaluated. The mean density of each metastasis, its entire volume, as well as the volume of its necrotic component, were obtained.

Results: The volume of the phantom and its "necrotic" component calculated by the prototype software had strong correlation with the actual phantom volume (r=0.89 for both necrotic and viable components). The volumes calculated for the whole/"necrotic" component of the three phantoms were: 53.0/7.3 mL (the actual volume 58.0/8.0 mL); 55.0/17.5 mL (60.0/16.0 mL) and 76.0/29.4 mL (75.0/30 mL). For all hepatic metastases (14/14;100%), the necrotic portion was segmented and its volume was automatically calculated by the prototype software. Segmentation of necrosis and its volumetry was achieved in less than 60 seconds for all cases.

Conclusion: Volumetric quantification of the necrotic component of treated colon cancer hepatic metastasis is feasible. Its role in assessment of treatment response is currently being evaluated.

11:00 am

029. Analysis of Complications of Percutaneous Nephrostomies Stratified by Imaging Guidance Technique, Fluoroscopy, CT, Ultrasound, and Experience of Operator

Lang, E.[1]; Hanano, A.[1]; Rudman, E.[1]; Jaworsky, J.[1]; Thomas, R.[2]; Myers, L.[2]; Derbes, A.[1] 1. SUNY Downstate Medical Center, Brooklyn, NY; 2. Tulane University Medical Center, New Orleans, LA*
Address correspondence to E. Lang (erich.lang@downstate.edu)

Objective: The objective is to analyze the impact of guidance methods such as fluoroscopy, CT, ultrasound (US), and the experience of the operator on occurrence and type of complications seen with percutaneous nephrostomy.

Materials and Methods: A total of 1,763 percutaneous nephrostomies (PCN) (nonaccess tract procedures) were performed in 1,022 male, 614 female, 22 children, two months-87 years age, from LSU Medical Center, New Orleans Veterans Administration Hospital, Tulane Health Science Center, SUNY Downstate Medical School, and Johns Hopkins Bayview Center. Standard trocar or needle-guide-wire exchange access was used. Underlying pathology necessitating PCN were obstruction by stones 426, by neoplasms 297, strictures 36, upper urinary tract infection-sepsis 343, stones and UTI 634, diagnostic 27.

Results: When using fluoroscopic guidance, experienced operators (+20 procedures, mean 178) had 11 complications (nine bleeding, two leakage) in 862 patients of which one mandated intervention. Conversely, inexperienced operators (less then 20, mean 5.6 procedures) incurred 37 complications in 218 patients (31 bleeding, 11 leakage, three major), ten requiring embolization or surgery. When using CT or ultrasound guidance, experienced operators had 14 complications (two of which were major) in 229 patients (ten bleeding, four leakage) with four requiring intervention; inexperienced operators had 88 complications (14 of which major with two fatalities) in 454 patients (64 bleeding, and/or 34 leakage) 31 requiring intervention. Of 22 major complications 13 occurred when using CT or ultrasound guidance by inexperienced operators; as did both observed fatalities.

Conclusion: Fluoroscopic-guided PCN appears to have fewer complications than CT or ultrasound- guided PCN. As might be expected, experience of the operator is the major factor impacting on complications, emphasizing the need for close supervision of trainees.

11:10 am

030. Focal Hyperperfusion in the Tumor Liver After Thermal Ablation and Peri-Interventional Bleeding Risk

Rosenberg, C.; Abe, N.; Hosten, N. University of Greifswald, Greifswald, Germany*
Address correspondence to C. Rosenberg (christian.rosenberg@uni-greifswald.de)

Objective: When performing percutaneous thermal ablation in the liver focal hyperperfusion, that is not due to residual or recurrent tumor, has been a frequent finding in peri-interventional imaging. The aim of the study was characterization of these hyperperfusional phenomena and evaluation of their influence on bleeding risk in reablation.

Materials and Methods: Between 2001 and 2007, 82 patients underwent laser-induced thermal ablation of primary and secondary liver malignancies. Pre- and postablational dynamic contrast imaging using 1.5T MR and 8-slice CT (Siemens Medical Solutions, Forchheim, Germany) was retrospectively evaluated. Hyperperfusions were subgrouped as lobar, segmental, wedge-shaped, intramural, peritumoral or subcapsular. Occurrence of nonmalignant hyperperfusion was correlated with incidence of bleeding events according to medical records and imaging.

Results: Incidence of intratumoral focal hyperperfusion ranged from 4-6% over a one-year period, pertumoral hyperperfusion from 11-40%, segmental hyperperfusion was seen in up to 40% of the cases. Peri-interventional bleeding occurred in 17 cases, 12 were minor parenchymal bleedings, four were subcapsular and one was a major parenchymal bleeding. In 4/17 patients with bleeding complication focal hyperperfusion was evident before ablation. There was no significant difference in bleeding incidence between the groups with focal hyperperfusion and the group without.

Conclusion: There is a diverse pattern of nonmalignant hyperperfusion in the tumor liver after multimodal local treatment, which has to be taken into account dealing with liver imaging and intervention. In the group evaluated, data shows no influence on bleeding risk in reablation.

11:20 am

031. Laser Ablation of Lung Metastases: Differences in Survival According to Tumor Entity

Rosenberg, C.; Bock, K.; Hosten, N. University of Greifswald, Greifswald, Germany*
Address correspondence to C. Rosenberg (christian.rosenberg@uni-greifswald.de)

Objective: The aim of the study was the measuring of survival after laser ablation of lung metastases from different primary entities. Results were supposed to provide a patient- and disease-specific outcome evaluation for laser-induced thermal ablation as a complimentary modality in multimodality cancer therapy.

Materials and Methods: Sixty-four patients underwent CT-guided laser ablative therapy of pulmonary metastases using a miniaturized internally cooled applicator system (Trumpf Medizinsysteme, Umkirch, Germany). Twenty patients suffered from colorectal carcinoma, ten from renal cell carcinoma, six from melanoma and four from breast carcinoma metastasis. Diverse entities accounted for metastatic disease in 24 other cases. Kaplan-Meier analysis was performed.

Results: Median time to death was 12.2 months in all 64 cases, 24.3 months in the group of patients suffering from renal cell carcinoma and 33.6 months for colorectal carcinoma metastasis. No therapy-related deaths occurred in 129 procedures. Pneumothorax drainage was needed in 5% (7/129) of the cases. Parenchymal bleeding (13%, 17/129) always was self-limited. A median recurrence-free interval of 10.9 months could be achieved for patients with colorectal metastasis.

Conclusion: The primary tumor causing pulmonary metastasis influences prognosis and outcome after image-guided laser ablative therapy. Analogous to the surgical experience performing local resection of secondary lung malignancies, best results could be achieved for colorectal metastasis. Long-term outcome and postinterventional survival do not necessarily correlate with the disease-specific primary effectiveness rate.

EFFICACY, EDUCATION, ADMINISTRATION AND PACS PAPERS

Room: 310, Level 3
Monday, April 27, 2009, 3:30 pm–5:00 pm
Abstracts 032-038

Moderators: *B. Richmond, D. Piraino*
Keynote Address: Imaging Work Places: Little Things Make a Big Difference—*D. Piraino*

3:50 pm

032. Factors Affecting Report Turnaround Time Reduction after Implementation of a Voice Recognition System
Krishnaraj, A.; Lee, J.; Laws, S. University of North Carolina Hospitals, Chapel Hill, NC*
Address correspondence to A. Krishnaraj (akrishna@unch.unc.edu)

Objective: Computerized voice recognition (VR) has existed for more than 30 years but has only recently been implemented in large scale in the field of radiology. Prior studies have documented reductions in report turnaround time (RTT) after implementation of VR. Our preliminary observation suggests that improvement in RTT is not uniform across the department. The purpose of this study is to analyze the causes for such variations.

Materials and Methods: Data from our 700-bed academic hospital radiology department was collected nine months prior to and nine months after the implementation of a VR system after a six month "wash-in" period. Faculty members were ranked according to their average RTT (defined as the interval between the time when a study is available for interpretation, usually on PACS, and the time when a study has been verified by an attending physician) before and after implementation of VR. The percentage of reduction in RTT after implementation of VR was calculated for each faculty member. Causes for variations in percent of RTT reduction were determined by observation of faculty work habits.

Results: The average RTT for 30 faculty members ranged from 4.6 hours to 65.9 hours before VR and from 1.2 hours to 47.3 hours after VR. The percent of reduction in RTT ranged from (-) 33% to (+) 93%. Seven faculty members had greater than 75% reduction in their RTT; ten faculty members had 51-75% reduction in their RTT; nine faculty members had 26-50% reduction in their RTT and four faculty members had less than 25% reduction (including two faculty members whose RTT increased after VR). Of the 13 faculty members who had less than 50% improvement in their RTT, two distinct subgroups were identified: five faculty members were in the top RTT group both before (average 6.8 hours, range 4.6-8.5) and after VR (average 4.3 hours, range 2.6-5.7) whereas the remaining eight faculty members were more heterogeneous and had various reasons for the modest improvement. The reasons include inconsistent use of VR, waiting for prior studies for comparison, lagging technology (e.g., PACS in mammography) and work habits.

Conclusion: Improvement in RTT as a result of VR varies significantly among faculty members in an academic department. Multiple reasons, including pre-VR RTT and work habits, may account for such variations. Recognition of various factors contributing to improvement in RTT with VR may allow more customized intervention to achieve even better results in the future.

4:00 pm

033. Repetitive Stress Symptoms Among Radiology Technologists Working in a PACS Environment: Prevalence and Response to Ergonomic Interventions
Boiselle, P.; Levine, D.; Horwich, P.; Barbaras, L.; Siegal, D.; Shillue, K.; Affeln, D. Beth Israel Deaconess Medical Center, Boston, MA*
Address correspondence to P. Boiselle (pboisell@bidmc.harvard.edu)

Objective: The objective was to determine the prevalence of repetitive stress symptoms among technologists working in a PACS-based environment and to assess their response to ergonomic interventions.

Materials and Methods: A survey instrument was designed by occupational health specialists and administered to 209 technologists working in a PACS-based radiology department. Data gathered included: presence of repetitive stress symptoms, prior diagnosis of repetitive stress syndrome, and number of hours per day working at a personal computer or PACS monitor. Respondents were also asked whether they spent > 2 hours per day in an awkward posture (a screening question to identify those at risk for repetitive stress symptoms and injuries). Additionally, respondents who had received ergonomic chairs, ergonomic workstations or ergonomic training were asked to rank the impact of these interventions upon the severity of repetitive stress symptoms using a seven-point Likert scale (-3 markedly worse to +3 markedly better). A space for narrative comments was also provided.

Results: A total of 128 responses were received (61% response rate). Repetitive stress symptoms were reported by 74% of respondents, and a prior diagnosis of repetitive stress syndrome was reported by 41%. A slight majority of respondents (59%) reported working at a computer or PACS station more than four hours per day, and 70% reported spending >2 hours per day in an awkward position. Improvement in repetitive stress symptoms (Likert scale +1 to +3) was reported by 55% of respondents who received ergonomic chairs (n=58), 42% who received ergonomic workstations (n=33), and 35% who underwent ergonomic training (n=17). The most common narrative responses related to the need for additional ergonomic chairs and workstations (n=10).

Conclusion: Practical ergonomic initiatives are modestly successful at reducing repetitive stress symptoms among radiology technologists and should be implemented to help reduce the risk of injuries.

4:10 pm

034. Wireless Device Enhances Resident Case Conferences

Amans, M.; Yeh, C.; Brown, M.; Zheng, L.; Shih, G. 1. Weill Cornell College of Medicine, New York, NY*
Address correspondence to M. Amans (drmatty01@yahoo.com)

Objective: Radiology resident teaching conferences typically consist of viewing significant images of different cases. While acceptable for plain film radiography, the viewing of significant images restricts the interaction of the resident with the cases of cross-sectional modalities such as CT or MR. In order to reproduce a more realistic case environment, we have developed a novel technique to allow residents to scroll through an entire imaging examination utilizing a portable wireless hand held device.

Materials and Methods: We present a novel method to navigate through cross-sectional studies using a Nintendo Wii remote (wiimote). The wiimote is a lightweight wireless Bluetooth device with three orthogonal accelerometers, infrared camera, and 12 buttons. Programming interfaces with computers allow users to control a set of images wirelessly with a range of 30 feet (enough for a medium sized lecture room). The lightweight hand held wireless device can also easily be handed from resident to resident. Using the gyroscopic and/or infrared interface, the resident can navigate the case simply by tilting the wiimote in different directions.

Results: In multiple case conferences this term, we have implemented our device and received very positive feedback from the residents. Viewing of only key images prepares a resident for generating differential diagnoses, but does not optimally allow a resident to identify the key findings within a stack of CT or MR images. Training residents to review entire exams during teaching conferences enhances the educational experience as it better simulates the reality of working and also the radiology oral boards environment. While we recognize the limitations of utilizing a proprietary hand held device, this highly programmable input device is inexpensive for the level of technology.

Conclusion: Using a wireless device reprogrammed and repurposed for education, we have developed an interface to allow residents to review stacks of cross-sectional images, thus improving resident case conferences.

4:20 pm

035. Nintendo Wii Remote (Wiimote) as Alternative Input Device for Reviewing Radiology Exams

Yeh, C.[1]; Amans, M.[1]; Shih, G.[1]; Kutch, III, F.[2]; Brown, M.[3]; Zheng, L.[3] 1. New York Hospital-Presbyterian: Cornell Campus, New York, NY; 2. University of Florida - Gainesville, Gainsville, FL; 3. National University of Singapore, Singapore, Singapore*
Address correspondence to C. Yeh (cliff.yeh@gmail.com)

Objective: With the ever-increasing workload for the radiologist tied almost exclusively to the traditional keyboard-mouse user interface, repetitive motion injury has become a growing concern. In addition, there are inherent limitations of a keyboard-mouse user interface that constrain the way the radiologist can interact with radiology studies. Using an inexpensive wireless device from the Nintendo Wii gaming system, we offer an innovative way of using hand movement for the radiologist to manipulate a given set of images.

Materials and Methods: To explore an alternative user interface with radiology data, a novel technique using infrared technology (either via a hand held device or special light reflectors) was developed to navigate cross-sectional imaging studies, such as CT and MRI. Instead of employing basic keyboard and mouse clicks, we created an infrared handheld device with motion sensing capability that allows the user to scroll/pan/window/zoom through a set of images via hand movement and pointing. Alternatively, with the use of special light reflectors that can be attached to the hand or even onto an article of clothing, a certain set of programmed movements is tracked by an infrared camera to control basic image manipulation.

Results: Preliminary trials demonstrate radiologists are able to effectively use our input devices to review radiology images. The essential features that a radiologist routinely requires can be performed using either our infrared hand held device or special light reflectors. With increasingly larger number of studies and larger datasets per study, our alternative user interface offers the potential to interact with image studies more intuitively and more ergonomically. This technology may also alleviate the health concerns associated with the traditional keyboard-mouse user interface. And with the growing use of complex 3D image data sets, this infrared technology can allow the user to more seamlessly interact with these images than would normally be available through the traditional keyboard-mouse interface.

Conclusion: The traditional keyboard mouse user interface limits the way the radiologist can interpret images and manage an ever-increasing workload, while at the same time contribute to injuries due to repetitive motion. We offer an inexpensive alternative input device utilizing infrared technology that may improve the radiologist workflow and alleviate repetitive motion injuries.

4:30 pm

036. Effect of Caseload on Radiology Report Turnaround Time

Krishnaraj, A.; Lee, J.; Laws, S. University of North Carolina Hospitals, Chapel Hill, NC*
Address correspondence to A. Krishnaraj (akrishna@unch.unc.edu)

Objective: Computerized voice recognition (VR) has been gradually implemented in the field of radiology in the last two decades. Numerous articles have documented reduction in report turnaround time (RTT) after the implementation of a VR system. Our own observation suggests that the improvement in RTT secondary to VR varies significantly among different academic subspecialties and among faculty within the same subspecialty section. The purpose of this study is to assess the relationship between caseload and RTT before and after implementation of VR.

Materials and Methods: Data from our 700 bed academic hospital radiology department was collected nine months prior to and nine months after the implementation of VR system after a six month "wash-in" period. Faculty members were ranked according to the average RTT before and after implementation of

VR as well as percentage of reduction in RTT. The RTT were then compared to the total number of verified reports for the same two study periods for each individual faculty member and subspecialty section.

Results: During the study periods, RTT for the faculty members with the highest number of verified reports per month (1,812 before VR and 2,100 after VR) were 18.1 hours and 1.2 hours respectively; the RTT for the faculty members with the lowest number of verified reports (53 before VR and 33 after VR) were 30.9 hours and 22.5 hours respectively. Before VR, each faculty member in the section with the shortest RTT (13.3 hours) verified 575 reports and the section with the longest RTT (50 hours) verified 526 reports per month. After VR, each faculty member in the section with the shortest RTT (1.8 hours) verified 1,864 reports and the section with the longest RTT (23.2 hours) verified 144 reports per month. In three of eight sections, members within the same section had a three-fold difference in average RTT before or after VR.

Conclusion: Caseload does not seem to have an adverse effect on RTT either before or after implementation of VR. Recognizing that factors other than caseload may be more important in determining RTT in an academic institution may allow us to explore more targeted solutions.

4:40 pm

037. An Open Source Application that Can Display the History of Opened Studies on the GE PACS Workstation

Laks, M.; Latson, L. Montefiore Medical Center, Flushing, NY*
Address correspondence to M. Laks (mlaks2000@yahoo.com)

Objective: The GE PACS system does not display the history of recently viewed studies on the workstation. This was problematical for us because we sometimes would like to return to a study that we had closed or a resident working with us had closed thinking that we were done with it. The study also could have been closed because it exceeded the number of studies (30) that can be opened at one time, the workstation crashed, or for other reasons. It was difficult to return to the study if we had no idea of the name or medical record numbers of the patients that we were looking at. This was a major problem on a daily basis.

Materials and Methods: We utilized freely available software tools to write a program to display the recent studies opened on the GE workstation. We make this software freely available to other radiologists who may need it.

Results: We have been able to solve the problem of display of recently opened studies on our workstation by using freely available tools. We make this available to other radiologists who need it for their daily work.

Conclusion: Radiologists are a small segment of the software utilizing community, and our needs are great for our daily work. In the wider world of computer users, solutions for frequently encountered problems are met and widely distributed via web sites designed for these purposes. We see this particular software tool as a paradigm for the sort of tool that needs to be developed and distributed by radiologists to each other, to make our work lives better.

4:50 pm

038. Effect of Baroque Classical Music on Mood, Concentration, Perceived Diagnostic Accuracy, Productivity, and Work Satisfaction of Diagnostic Radiologists.

Mohiuddin, S.[1,2]; Lakhani, P.[1,3]; Chen, J.[1,3]; Siegel, E.[1]; Mohiuddin, A[4].; Safdar, N.[1] 1. University of Maryland, Baltimore, MD; 2. Harbor Hospital, Baltimore, MD; 3. University of Pennsylvania Health System, Philadelphia, PA; 4. University of North Carolina*
Address correspondence to S. Mohiuddin (mohiuddin.sohaib@gmail.com)

Objective: The purpose of this study is to assess the impact of classical chamber music from the Baroque period on mood, concentration, perceived diagnostic accuracy, productivity and work satisfaction among radiologists.

Materials and Methods: In this cross sectional survey, radiologists were recruited to listen to one hour of classical chamber music from the baroque period while interpreting radiological studies during a typical workday. Participants rated mood, concentration, perceived diagnostic accuracy, productivity, and work satisfaction on a seven-point Likert scale. Subgroup analyses were performed. Unpaired nonparametric Mann-Whitey tests resulting in p values less than 0.5 was considered statistically significant.

Results: Eight radiologists participated in the study (age 27-62 years; four male, four female; five trainees, three attendings). All participants noted a neutral or positive effect on mood, productivity, perceived diagnostic accuracy, and work satisfaction. The greatest positive effects were noted with regard to mood and work satisfaction, with 63% and 50% of respondents reporting a positive impact respectively. No participants indicated a negative effect on mood, perceived diagnostic accuracy, productivity, or work satisfaction. Only one (12.5%) participant indicated a negative effect of music on concentration. Females reported a greater effect on mood than males, with mean scores of 6.0 ± 0.8 and 4.3 ± 0.6 respectively ($p<0.03$). There was a greater effect on mood for those with experience playing instruments than those without, with mean scores of 6.3 ± 0.6 and 4.4 ± 0.5 respectively ($p<0.03$). Participants who listened to music more than 5 hours per week had greater scores for mood (5.0 ± 0.8) than those that did not (3.8 ± 0.5) $p<0.06$.

Conclusion: Classical music was associated with an increased mood and work satisfaction. Overall, these results indicate there may be a role for ambient music in radiology working environments. Further investigations may further illuminate the potential role of music improving efficiency and accuracy in reading environments.

SCIENTIFIC SESSION 6

GENITOURINARY/OB/GYN (KIDNEY/CALCULI) IMAGING PAPERS

Room: 309, Level 3
Monday, April 27, 2009, 3:30 pm–5:30 pm
Abstracts 039-047

Moderators: *E. Remer, D. Grand*
Keynote Address: Diagnosing Urinary Calculi: What Can We Do Better?—*E. Remer*

4:00 pm

039. Urolithiasis (Urinary Stone Disease) in Asymptomatic Adults Identified with Low Dose Noncontrast CT
Lawrence, E.[1,2]; Boyce, C.[1]; Kim, D.[1]; Taylor, A.[1]; Winter, T.[1]; Bruce, R.[1]; Hinshaw, J.[1]; Pickhardt, P.[1] 1. University of Wisconsin, Madison, WI; 2. Albert Einstein College of Medicine, Bronx, NY*
Address correspondence to P. Pickhardt (pj.pickhardt@hosp.wisc.edu)

Objective: The prevalence of urolithiasis in asymptomatic adults has not been established by objective means. Unenhanced CT represents the gold standard for in vivo detection of urolithiasis. We evaluated the prevalence of urolithiasis in a large cohort of asymptomatic adults, as well as the incidence of symptoms over a ten-year interval.

Materials and Methods: Low dose noncontrast CT was performed in 5,056 consecutive asymptomatic adults (mean age, 56.9 years; 2,752 women, 2,304 men) undergoing routine colorectal cancer screening (CT colonography). The presence, size, and location of urinary calculi were recorded. Prevalence was assessed according to gender, age, obesity, and diabetes. Electronic medical record review was used to assess the incidence of asymptomatic stone disease over a ten-year interval.

Results: The prevalence of urolithiasis was 7.8% (395/5,056 adults), with an average of 2.1 stones per case (range, 1-29). In addition to nephrolithiasis in 391 individuals, ureteral and bladder calculi in six and two cases respectively. Four of the cases of unsuspected ureteral calculi showed obstructive hydronephrosis. Mean stone size was 3 mm (range, 1-20 mm). Over a ten-year period, 20.5% (81 of 395) with stones (1.6% of the entire cohort) had at least one symptomatic episode. Males were more likely to have urolithiasis than females (9.7% vs. 6.3%; $p<0.001$). Diabetes (9% vs. 7.7%; p=0.45), obesity (7.9% vs. 7.7%; p=0.78) and age greater than or equal to 60 (8% vs. 7.7%; p=0.73) did not affect prevalence, but diabetes and obesity did correlate with symptom development ($p<0.001$ and $p<0.05$, respectively).

Conclusion: This is the first objective population-based objective assessment of the prevalence of urolithiasis in an asymptomatic cohort. Of the 8% of asymptomatic adults with urolithiasis, most cases were unsuspected and remained asymptomatic. Although there was no correlation between asymptomatic urolithiasis and diabetes, obesity, or older age, both diabetes and obesity were associated with symptomatic stone disease.

4:10 pm

040. Application of Noise Projection Software and 2D Nonlinear Adaptive Filters for Radiation Dose Reduction With a Renal Calculus CT Protocol
Singh, S.[1]; Kalra, M.[1]; Forsberg, A.[2]; Toth, T.[3]; Blake, M.[1] 1. Massachusetts General Hospital, Boston, MA; 2. Sharpview AB, Linkoping, Sweden; 3. General Electric Company, Waukesha, WI*
Address correspondence to S. Singh (ssingh6@partners.org)

Objective: Noise projection software has been validated for obtaining simulated low dose images. The purpose of our study was to assess if 2D adaptive filters can help decrease radiation dose by improving image quality and lesion conspicuity on the simulated low radiation dose CT images for kidney stone assessment.

Materials and Methods: We processed MDCT image data of 44 subjects (age range=21.2-80.2, mean age=51.9, M:F 21:23) who underwent a kidney stone protocol with noise projection software to obtain simulated low radiation dose images at 25%, 50%, and 75% dose reduction. The original CT images, which were the standard of reference for the number of stones, were acquired at 120 kVp, 75-380 mA and 15-noise index. All three simulated low dose CT image series were processed with a 2D filter (SharpView AB, Linkoping, Sweden) to improve image quality. The original CT (n=1), simulated low dose (n=3), and 2D filtered (n=3) image series were anonymized and randomized for blinded and independent review by two radiologists (n=total number of series=44 x 7= 308). Each radiologist compared image series for noise, number of urinary calculi, conspicuity and diagnostic acceptability on a five-point scale (1=unacceptable; 5=excellent). Circular regions of interest were drawn in the posterior spinal muscle to measure the CT numbers and objective noise. Statistical analysis was performed with Student t test.

Results: Both radiologists detected all 206 kidney stones with all 2D filtered images, including three kidney stones (1-3 mm) that were not visualized on unfiltered images with 75% dose reduction. There was no significant difference between 25% and 50% images with and without 2D filters for diagnostic acceptability and conspicuity (p=.5). At 75% dose reduction, the 2D filters resulted in significant improvement in these parameters over corresponding nonfiltered low dose images ($p<0.0001$). The mean objective noise decreased by 20.1 to 33.5% compared to the low dose CT images ($p<0.0001$).

Conclusion: The 2D filters can help visualize tiny renal calculi not visualized on ultra low dose CT images with 75% dose reduction, while improving the image noise and diagnostic acceptability of low dose images.

4:20 pm

041. Measurement of Stone Size on CT: Effect of Window Settings and Magnification in an In-Vitro Study
Kambadakone Ramesh, A.; Eisner, B.; Dretler, D.; Sahani, D.*
Massachusetts General Hospital, Boston, MA
Address correspondence to A. Kambadakone Ramesh (akambadakone@partners.org)

Objective: In patients with urinary calculi, crucial management decisions are based on the stone size measurements obtained

on CT and patients with calculi equal to 5mm are usually treated conservatively. The purpose of this study was to assess the most accurate method of measuring calculi on CT and determine the effect of window settings, image magnification and stone composition on stone dimensions obtained on CT in an ex-vivo study.

Materials and Methods: In this ex-vivo experiment, 24 urinary calculi (12 oxalate, 5-17.5 mm and 12 uric acid, 3.5-17 mm) were embedded into human kidney sized potatoes and scanned using 64 MDCT with a section thickness 0.625 mm and standard technique (120 kVp and 200mAs). Transverse and longitudinal dimensions of the calculi were recorded on a PACS workstation using electronic calipers at soft tissue (WW-320 and WL-50) and bone window (WW-1120 and WL-300) settings and repeated with 5x magnification. The measurements obtained with micro calipers acted as the gold standard. Comparison between the CT measurements and the gold standard measurements were done using paired T-test.

Results: Excellent correlation with the true measurements was observed for CT measurements obtained in bone window with 5x magnification (mean difference 0.13 mm, p=0.6). Stone composition also affected the measurement as the error in values was greater for oxalate stones compared to uric acid stones ($p<0.001$). Poor correlation was seen for measurements obtained in soft tissue window with or without magnification (mean difference 1.2-1.9 mm, $p<0.03$) and in bone window without magnification (mean difference 1.4 mm, p=0.0002).

Conclusion: In this ex-vivo study, stone measurement performed with bone window and 5x magnifications provided the most accurate measurement of the renal calculi. The measurement error for calcium oxalate stones was greater than that of uric acid stones suggesting that stone composition may be responsible for measurement inaccuracies.

4:30 pm

042. Determining Renal Stone Volume Following Surgical Intervention—A Pilot Study Using Calcium Scoring Software to Assess Therapeutic Efficacy

Shah, S.; Allen, B.; Chokshi, P.; Berger, A.; Desai, M. Cleveland Clinic, Broadview Heights, OH*
Address correspondence to S. Shah (shahs2@ccf.org)

Objective: Nephrolithiasis is a common disorder with increasing prevalence in the United States. To our knowledge, no standardized method exists to determine renal stone burden prior to and following lithotripsy for kidney stone disease. The purpose of this study is to describe a novel method to assess renal stone volume in hopes of using it to guide management and predict clinical outcomes.

Materials and Methods: An IRB approved HIPPA retrospective review of the urology database from 2003 through 2006 yielded 160 patients who had unenhanced CT of the urinary tract before and after lithotripsy, with two years follow-up. Patients with indwelling stents or percutaneous drainage catheters were excluded. A workstation with calcium scoring software (Siemens Medical Solutions, Forchheim, Germany) was used to determine renal stone volume (RSV), stone size, density, and location. Symptoms and recurrent episodes were studied.

Results: Twenty-six patients (mean age: 50 years; M:F 1.4:1) are studied to date. Following lithotripsy there was mean 82% decrease in RSV (1,021 mm^3 pretherapy to 185 mm^3 post-therapy). With at least a 50% reduction in residual stone volume, 0% of which resided in the upper pole), only 15% of patients required a repeat surgical procedure. The lowest clinical success rate for surgical intervention was with posterior, interpolar stones (50% success rate). Hydronephrosis improved in 69% of patients within a week. Overall, 25% of patients returned with symptoms within two years following surgery.

Conclusion: Calcium scoring software is a feasible postprocessing method to rapidly determine renal stone volume and may help determine treatment efficacy and predict long term clinical outcome.

4:40 pm

043. Added Criteria of Phase Enhancement and Morphology of Calcifications Improve Accuracy and Positive Predictive Value of Diagnosis of Renal Cell Cancer vs. Complex Multiseptated Cyst

Lang, E.[1]; Rudman, E.[1]; Zinn, H.[1]; Thomas, R.[2]; Myers, L.[2]; Hanano, A.[1]; Brodsky, J.[1]; Macchia, R.[1] 1. SUNY Downstate Medical Center, Brooklyn, NY; 2. Tulane University Medical Center, New Orleans, LA*
Address correspondence to E. Lang (erich.lang@downstate.edu)

Objective: The objective was to establish the impact of added criteria of enhancement and de-enhancement phase and morphology of calcifications on the accuracy and hence positive predictive value of diagnosis of renal cell carcinoma (RCC) vs. complex multiseptated cyst.

Materials and Methods: In a retrospective study 112 patients with a diagnosis of 2F or 3A renal cystic mass lesions were identified from files from LSU Medical Center, Tulane Health Science Center, New Orleans Veterans Administration Hospital, SUNY Downstate Medical School and Johns Hopkins Bayview Center, from 1998 to 2007. Reinterpretation by two blinded uroradiologists concurred with the diagnosis in 69 patients.(46 2F and 23 3A lesions, 38 male, 31 female, age 27–77; mean 49). The lesions were then reclassified adding criteria of early phase enhancement with later parenchymal phase de-enhancement and thick granular calcifications in the wall of cysts and/or soft tissue elements (1-2 mm thick) extending outside the calcific shell, indicating a RCC.

Results: Based on these added criteria 19 of the 26 RCC were properly classified. Criteria based on morphology of calcifications and tissue elements outside of shell-calcifications established another four correct RCC diagnoses. Thus with added criteria 23 of 26 RCC were properly diagnosed as were 32 of 39 complex multiseptated cysts. Diagnosis based on Bosniak criteria established a correct diagnosis in 15 of 26 RCC, and 33 of 39 complex multiseptated cysts, with an overall diagnostic accuracy of 69%. With added criteria 23 of 26 RCC and 32 of 39 complex multicystic lesions were correctly diagnosed, thus establishing a diagnostic accuracy of 79%. Both techniques failed to diagnose four benign solid mass lesions.

Conclusion: The diagnostic accuracy and positive predictive value for the important group of RCCs has increased to 88% when applying expanded criteria of enhancement and morphology of calcifications from 57% achievable when using Bosniak criteria. However, solid mass lesions remain a problem and the categorization of benign cysts relies on Bosniak criteria.

4:50 pm

044. Subtraction CT: Is There a Role in the Characterization of Renal Lesions?

Kambadakone, A.; Samir, A.; Eisner, B.; Saini, S.; Sahani, D. Massachusetts General Hospital, Boston, MA*
Address correspondence to A. Kambadakone Ramesh (akambadakone@partners.org)

Objective: The objectives were to evaluate the utility of subtraction CT in the improved characterization of renal masses and its effect on reader confidence in detecting enhancement in renal lesions and evaluate the feasibility of performing image subtraction and its impact on routine workflow.

Materials and Methods: In this ongoing IRB approved study, 150 patients (M:F-69:81, age 22-88) who underwent unenhanced and contrast-enhanced MDCT examination for characterization of the renal mass were included. Image subtraction was performed between the unenhanced and the enhanced images using software on the scanner console. Two experienced radiologists independently reviewed the images and recorded their level of confidence for detecting presence or absence of enhancement on a six-point scale (1-definitely absent and 6-definitely present). The lesions were further evaluated for their size, attenuation characteristics (HU values) and the final diagnosis was established in all enhancing lesions either by histopathology or followup imaging with clinical data. The impact of generating and interpreting subtraction images on the workflow was evaluated.

Results: Out of the 240 lesions (0.6-11.2 cm, mean-2.9 cm) analyzed 184 lesions (mean size-2.8 cm) showed no enhancement and 56 lesions (mean size-3.2 cm) showed enhancement. Combined evaluation of the routine images with the subtraction images provided the highest sensitivity (100%) and specificity (99%) in determining enhancement for both the readers (kappa >0.8) and improved reader confidence compared to evaluation of routine images and subtraction images alone ($p<0.05$). The positive predictive value for determination of enhancement was modest with evaluation of subtraction images alone (71-74%) however improved when they were interpreted in conjunction with the unenhanced and enhanced images (95-97%). Subtraction images improved reader confidence in 62-71% of lesions for the determination of enhancement particularly in hyperdense cysts and in small lesions (<2 cm). The average time spent in generating the subtraction images was three minutes (2-8 minutes).

Conclusion: Inclusion of subtraction imaging is feasible with CT examinations for renal masses and does not impede the routine workflow. Subtraction CT considerably improves the diagnostic confidence in identifying the presence or absence of enhancement in the renal mass thereby enabling better characterization.

5:00 pm

045. Treated Metastatic Renal Cell Carcinoma: Assessing Therapeutic Success of Biologic Therapy Using a Novel Response CT Criteria Based on Lesion Size, Attenuation and Morphology

Shah, S.; Smith, A.; Remer, E. Cleveland Clinic, Broadview Heights, OH*
Address correspondence to S. Shah (shahs2@ccf.org)

Objective: As in the case of gastrointestinal stromal tumors (GIST), morphologic and attenuation changes have been observed in metastatic renal cell carcinoma (mRCC) following tyrosine kinase inhibitor (TKI) therapy. We examine the effectiveness of a novel response criteria based on lesion size, attenuation, and morphology on contrast-enhanced CT (CECT) in predicting clinical outcome, with respect to RECIST and Choi criteria.

Materials and Methods: An IRB approved HIPAA compliant retrospective review of charts and CECT of 53 patients with mRCC (mean age 60; 3:1 male:female, 219 lesions) was performed. Tumor size and mean volumetric lesion attenuation (Siemens Medical Solutions, Forchheim, Germany) prior to and after initiating TKI therapy (mean: 57d) were correlated with time of disease progression (Fisher's Exact test). Sensitivity and specificity of our novel response criteria, RECIST criteria, and Choi criteria were compared (McNemar test).

Results: Post-therapeutic decreased mean attenuation of >40 HU was seen in one or more lesions in 51% of patients with progression free survival (PFS) at greater than nine months vs. 0% of patients whose disease progressed within nine months ($p<0.001$). For the PFS group, the sensitivity and specificity of our response criteria was 84% and 90%, compared with 91% and 40% using the Choi criteria, and 14% and 90% using the RECIST partial response criteria.

Conclusion: Assessing therapeutic effectiveness of biologic therapy for mRCC based on size alone (RECIST criteria) is felt to underscore tumor morphologic changes. Our response criteria based on tumor size, attenuation, and enhancement morphology, when applied to the initial post-therapy CT scan, predicted a favorable clinical outcome with relatively high sensitivity and specificity.

5:10 pm

046. Incidence of Contrast-Induced Nephropathy Following Intravenous Injection in a Large Population of Patients with Chronic Kidney Disease Undergoing CT Imaging

Sahani, D.[1]; Chen, K.[2]; Kuhn, M.[3]; Chen, N.[4]; Heiken, J.[5]; Soulez, G.[6]; Reimer, D.[7] 1. Massachusetts General Hospital, Boston, MA; 2. Rui Jin Hospital, Shanghai, China; 3. Southern Illinois University School of Medicine, Springfield, IL; 4. Shanghai Jiaotong University, Shanghai, China; 5. Washington University, St. Louis, MO; 6. University of Montreal, Montreal, Canada; 7. Radiologists PC, Mobile, AL*
Address correspondence to D. Sahani (dsahani@partners.org)

Objective: The objective was to evaluate the rate of contrast-induced nephropathy (CIN) in patients with chronic kidney disease

(CKD) undergoing MDCT and to evaluate risk factors for the development of CIN, including choice of contrast medium (CM).

Materials and Methods: A total of 401 patients with CKD (serum creatinine [SCr] =1.5 mg/dL and/or creatinine clearance [CrCl] =60 mL/minute) were enrolled. All patients were randomly assigned to receive either a low-osmolar contrast agent (iopamidol; n=202) or an iso-osmolar contrast agent (iodixanol; n=199) for their CT procedure. All CM were injected IV at 4 mL/second followed by a 20 mL saline flush; 153 patients received 40 g iodine (gI); the remaining patients received at least 65 mL of CM. SCr was measured at screening, baseline and 48-72 hours postcontrast. CIN was defined as a postcontrast increase in SCr ≥25% from baseline. The incidence of CIN in various groups was compared using Fisher's exact test. Multivariate logistic regression analysis was performed using >25% increase in SCr as a dependent variable and treatment group, baseline SCr, age, gender, iodine dose (gI/kg), hydration, diabetes, and exposure to nephrotoxic medications as covariates.

Results: Total gI was higher in patients receiving iopamidol; no other significant differences were seen in demographics or risk factors. Baseline SCr levels were similar (iopamidol 1.52 ± 0.36 mg/dL vs. iodixanol 1.49 ±0 .38 mg/dL; p=0.48). The rate of CIN was low (19/401 [4.7%]) and similar between the two CM groups (iopamidol = ten patients; iodixanol = nine patients; p=1.0). No case of acute renal failure was observed. Mean postdose SCr changes were comparable (iopamidol 0.03 ± 0.22 mg/dL vs. iodixanol 0.04 ± 0.25 mg/dL, p=0.619). Similar findings were seen in the 284 patients (iopamidol =140, iodixanol =144) with both CKD and diabetes: CIN in 14/284 (4.9%) patients, seven patients in each CM group, p=1.0. Ninety-three patients had a baseline SCr =2.0 mg/dL and/or baseline CrCl =40 mL/minute (iopamidol =53, iodixanol =40). CIN was seen in four patients (4.3%) in this high-risk group, including two patients in each CM group (p=1.0). In a multivariate logistic regression analysis no risk factor predicted CIN, however hydration proved marginally beneficial (p=0.042).

Conclusion: The rate of CIN in a large group of patients with CKD and other risk factors undergoing MDCT was less than 5%. Both iopamidol and iodixanol may be used safely in patients with CKD undergoing CT.

5:20 pm

047. Potential Laparoscopic Kidney Donors: Comparison Between MDCT Measurement of Renal Volume and 99m Tc-DTPA Split Function

Malek, S.; Ersoy, H.; Mitsouras, D.; Whitmore, A.; Tullius, S.; Rybicki, F. Brigham and Women's Hospital, Boston, MA*
Address correspondence to F. Rybicki (frybicki@partners.org)

Objective: Preoperative MDCT evaluation of potential laparoscopic kidney donors focuses on the number and location of renal arteries and veins; craniocaudal size discrepancies are evaluated with 99m Tc-DTPA split function renography. The purpose of this study is to test the hypothesis that CT kidney volume measurements are comparable to split function renogram findings.

Materials and Methods: For 21 potential laparoscopic donors (13 females, mean age=45 years, range=27-71 years,) who underwent both MDCT and renography between August, 2005-October, 2007, retrospective CT renal volumes were compared to the reported split function results. 99m Tc-DTPA (15 mCi) split function used a dual energy window acquisition (140 +/- 28 keV). CT protocol: 64-slice three-phase (bolus tracking, 100 seconds, six minutes),100 mL iopromide 370 mg I/ml at 5 mL/second, no saline, 120kV, 200 mA, 0.6 x 0.4 mm axial slices analyzed by region of interest evaluation of renal volume using bolus tracking (arterial phase) images using a dedicated postprocessing workstation.

Results: The mean difference between the left kidney CT derived percent volume (CTPV) and the renogram derived percent function (RPF) was -1.7% (95% CI: -3% to -0.43%). The mean of the difference (CTVP-RPF) was significantly different from 0 (p=0.01, Wilcoxon sign rank). The CTVP was moderately correlated to RPF (r^2=0.7624, p<0.001). The fitted linear model was CTVP=0.85 x RPF + 6.4%.

Conclusion: Although the mean percentage difference between scintigraphy function and CTA volume findings are not equivalent, using 95% confidence intervals the difference between the renogram and CT volume findings in potential renal donors is within 3%. MDCT kidney volume measurements demonstrate promise as a single comprehensive examination for potential laparoscopic renal donors.

Scientific Session 7

Cardiopulmonary Imaging Papers

Room 208, Level 2
Tuesday, April 28, 2009, 9:30 am–11:00 am
Abstracts 048-055

Moderators: *P. Woodard, S. Patel*
Keynote Address: Cardiac Imaging: 2009 Update—*P. Woodward*

9:40 am

048. Coronary Calcium Scoring: Do Workstations of Different Vendors Generate Comparable Results?
Weininger, M.; Ritz, K.; Ritter, C.; Hahn, D.; Beissert, M. University Hospital of Wuerzburg, Wuerzburg, Germany*
Address correspondence to M. Weininger (weininger@roentgen.uni-wuerzburg.de)

Objective: The objective was to investigate if the specific coronary calcium scoring software of three different workstations does generate comparable and vendor-independent results.

Materials and Methods: Coronary calcium scoring using a 64-slice CT scanner (Siemens Medical Solutions, Forchheim, Germany) was performed on 30 patients (18 males, 12 females; 58 ± 11 years). Images were reconstructed in 10%-increments from 40%-80% of the RR-interval. Two experienced observers in consensus calculated Agatston (AS) and volume scores (VS) for every image series using the specific calcium scoring software of three workstations (*WS 1*: Leonardo, Siemens; *WS 2:* Aquarius, TeraRecon; *WS 3*: Vitrea, Vital Images).

Results: Mean values of coronary calcium scores for all reconstruction intervals were as follows: *WS 1*: AS, 344 ± 12; VS, 305 ± 13; *WS 2*: AS, 333 ± 6; VS, 297 ± 13; *WS 3:* AS, 340 ± 9; VS 319 ± 13. Mean values of calcium scores for all patients were as follows: *WS 1*: AS, 342 ± 615; VS, 305 ± 529; *WS 2*: AS, 333 ± 595; VS, 297 ± 523; *WS 3:* AS 338 ± 614; VS 317 ± 560. No significant differences between the obtained calcium scores could be found. Concerning the cardiac risk stratification at different reconstruction intervals the same 4/30 patients could be assigned to two different risk groups by each workstation ($p<0.05$). No specific reconstruction interval was identified that displayed a significant less variability for each score.

Conclusion: Workstations of different vendors seem to produce comparable coronary calcium scoring results, suggesting a vendor independence of the method. Furthermore, the variability of coronary calcium scoring depending on the reconstruction interval was reproduced by each workstation, suggesting that none of the workstations contributes to an increase in accuracy regarding the risk stratification.

9:50 am

049. Bismuth Breast Shielding and its Effect on Calcium Score and Dose
Ciancibello, L.; Gilkeson, R.; Fei, B. University Hospitals Case Medical Center, Cleveland, OH*
Address correspondence to L. Ciancibello (leslie.ciancibello@uhhospitals.org)

Objective: The increased public sensitivity of under-diagnosed heart disease in women has resulted in an increased use of coronary artery calcium scoring in the female population. While early recognition of heart disease is valuable, the effect of CT dose has been of increasing concern. The purpose of our study was to determine the effect of bismuth breast shielding on patient dose as well as calcium score results.

Materials and Methods: The effects of bismuth breast shielding were studied on an anthropomorphic phantom using a 64-MDCT scanner. Ten dose measurements were obtained using an ion chamber positioned on top of the anthropomorphic phantom with zero, one, two, three and four layers of bismuth shielding using the standard CT calcium score protocol. Ten datasets were obtained of the anthropomorphic phantom with zero, one, two three and four layers of bismuth shielding using the routine calcium score protocol. The image data sets were then individually analyzed using market available coronary artery calcium score software.

Results: The average radiation dose of prospective ECG gated calcium scoring without shielding is 2.48 rads. While there appeared to be a reduction in dose with one breast shield layer, the reduction was not statistically significant (2.06 rads, $p=0.181$.). There was significant dose reduction with two layers (1.51 rads, $p<0.03$), with three layers (1.62 rads, $p<0.02$) and four layers (1.29 rads, $p<0.000$) of breast shielding. Because of the concern for the increase in image noise, coronary calcium score was measured at all levels of breast shielding. The total calcium score of the unshielded anthropomorphic phantom was 647.34 +/- 10.6. The reduction in calcium score with one breast shield was not significant (638.33 +/- 21.2 $p<.3418$). There was a small but significant decrease with two layers of bismuth shield (598.3 +/- 9.8 $p<0.002$), with three layers (606.29 +/- 18 $p<.0002$), and four layers (618.23 +/- 14.8, $p<0.005$).

Conclusion: The use of multiple layers of bismuth breast shielding significantly reduces radiation dose in a cardiac phantom. While the use of multiple layers of bismuth shields will have a real effect on the total calcium score determination, this small decrease in total calcium score should not significantly change medical management. Therefore, we propose increased levels of bismuth breast shielding should be used in women undergoing MDCT calcium scoring exams.

10:00 am

050. Breathing Artifacts in CT Coronary Angiography Performed With 64-Row MDCT: Incidence and Effect on Vessel Evaluability
Torres, F.; Ayyappan, A.; Abadi, S.; Nguyen, E.; Doyle, D.; Crean, A.; Menezes, R.; Paul, N. Toronto General Hospital, University of Toronto, Toronto, Canada*
Address correspondence to F. Torres (felipe.torres@uhn.on.ca)

Objective: The purpose of this study is to evaluate the incidence of breathing artifacts (BA) in CT coronary angiography (CTCA) performed with 64-row MDCT and the effect of these artifacts on vessel evaluability.

Materials and Methods: A retrospective review of 115 consecutive CTCA studies performed on a 64-row MDCT (Toshiba Medical Systems, Tochigi-ken, Japan) for exclusion of native coro-

nary artery disease during March and April, 2007 involving 63 males (54.8%) and 52 females (45.2%), with a mean age of 59.6 years (range 24 to 84). Breathing artifact was defined as the occurrence of motion artifact in axial images and the presence of stair step artifact in the thoracic wall on sagittal reformatted images. The presence of BA was graded on a three-point scale by two cardiac radiologists as follows; 1=absent, 2=mild BA (mild RA, blurring of vessels and bronchial walls on axial images, but stair step artifact in the chest wall on sagittal reformations); 3=severe BA (stair step artifact clearly visible on the chest wall on sagittal reformations). The effect of BA on evaluation of the coronary arteries was graded as evaluable or unevaluable. The association between BA incidence ad patient biometrics, medication and scan parameters was examined.

Results: Breathing artifacts were detected in 13 patients (11.3%). In 7 (6.1%) of these patients, respiratory motion caused at least one unevaluable coronary artery segment. For the studies affected by breathing artifacts, the mean number of coronary segments affected was 2.7 (0-14), and the mean number of nonevaluable segments was 2.2 (0-14). There was no association between the occurrence of BA and age, sex, body mass index, history of asthma or chronic obstructive pulmonary disease, use of beta-blocker and scan duration. Patients experiencing breathing artifacts had a higher median heart rate (84.8 bpm, 51.5-80.8) than those who did not (58.1 bpm, 44.6-92.7; p=0.02).

Conclusion: Breathing artifacts are common in CT coronary angiography with 64-row MDCT and adversely affect the diagnostic value of the examination in 6.1% of patients.

10:10 am

051. Prevalence of Myocardial Bridging in Taiwan
Chen, Y.; Sheu, M.; Wu, M.; Chang, C. Taipei Veterans General Hospital, Taipei, Taiwan*
Address correspondence to Y. Chen (ydchen@vghtpe.gov.tw)

Objective: The objective was to retrospectively assess the prevalence of myocardial bridging (MB) in Taiwan with MDCT coronary angiography.

Materials and Methods: Between September, 2006 and May, 2007, 440 men and 220 women underwent electrocardiogram–gated 64-slice MDCT coronary angiography in our institution and were enrolled in the study. Written informed consent was obtained from all subjects included in the study. Mean age of patients in the study group was 58.8 years old ± 15.2. MDCT data were analyzed by three dedicated cardiovascular radiologists.

Results: Prevalence of MB was 18.5% (122/660). The prevalence of MB in men and women was (21.1%, 93/440) and (13.2%, 29/220) respectively, without statistical difference ($p>0.05$). Mean age of patients with MB was 57.4 years old ± 16.1. A total 168 coronary segments with MB were depicted. Fifty bridging segments (29.8%) were located at the distal segment of the left anterior descending artery (LAD) branch, 32 bridging segments (19%) at the middle segment of the LAD branch, 25 bridging segments (15.9%) at the first diagonal branch; 26 bridging segments (15.5%) at the first obtuse marginal branch of the left circumflex artery; only four bridging segments (2.4%) were at the right coronary artery; 17 bridging segments (8.3%) were at the ramus intermedius branch.

Conclusion: Electrocardiogram–gated MDCT is an effective noninvasive tool for evaluating MB in a clinical setting. The most common location of MB is LAD. The prevalence of MB in Taiwan is higher than that reported in the conventional coronary angiography studies in the literature.

10:20 am

052. Variability of Myocardial Blood Flow During the Cardiac Cycle is Reflected in Coronary CT Angiography Series
Knollmann, F. University of Pittsburgh, Pittsburgh, PA*
Address correspondence to F. Knollmann (knollmanfd@upmc.edu)

Objective: MDCT has evolved into a powerful diagnostic tool for the assessment of coronary artery disease. Myocardial contrast enhancement does reflect myocardial blood flow, but is seldom used for diagnostic purposes. The aim of this investigation was to determine if physiologic changes in myocardial blood flow during the cardiac cycle are reflected in myocardial contrast enhancement of EKG-gated, helical coronary CT angiography (CTA) examinations.

Materials and Methods: Patients in whom coronary MDCT angiography ruled out any high grade stenosis were included in the retrospective analysis. All 21 patients were examined using a 64-row MDCT unit with retrospective EKG-gating and retrospective image reconstruction covering the entire cardiac cycle, in steps of 10% of the R-R interval. Myocardial contrast enhancement was measured in a full thickness region of interest within the free left ventricular wall for each phase, and the difference between maximum and minimum enhancement calculated.

Results: There was marked variability of myocardial contrast enhancement during the cardiac cycle (analysis of variance for repeated measurements, $p<0.0001$). The mean variability of myocardial contrast enhancement during the cardiac cycle was 58 HUs (standard deviation: 26 HUs). Typically, the highest attenuation was observed during late diastole, and the least attenuation during end systole.

Conclusion: Helical coronary CTA reflects physiological variability of myocardial blood flow during the cardiac cycle in patients without high grade coronary artery stenosis, with decreased blood flow at end systole. This finding indicates that myocardial attenuation of an EKG-gated CTA series can be used to assess myocardial blood flow and may help to diagnose myocardial ischemia using standard helical coronary CTA exam data.

10:30 am

053. MDCT Coronary Angiography: Influence of Heart Rate on Coronary Enhancement
Chen, Y.; Chiu, C.; Sheu, M.; Wu, M.; Chang, C. Taipei Veterans General Hospital, Taipei, Taiwan*
Address correspondence to Y. Chen (ydchen@vghtpe.gov.tw)

Objective: The objective was to prospectively evaluate the influence of heart rate on coronary enhancement during 64-slice MDCT coronary angiography.

Materials and Methods: From January, 2007 to January, 2008, 218 subjects who received 64-slice MDCT coronary angiography were enrolled. Patients were divided into five groups according to their heart rates: less than 45/minute (Group A); 46-50/minute (Group B); 51-55/minute (Group C); 56-60/minute (Group D); more than 61/minute (Group E). MDCT coronary angiography was performed using retrospective ECG-gating and automated bolus triggering with biphasic injection of iodinated contrast agent at a fixed rate of 5 mL/second followed by a saline chaser. Attenuation measurements of coronary segments were performed by region of interest measurements along the z-axis. Age, body weight, coronary calcium score, and heart rate in each case were recorded.

Results: Analysis of variance revealed age, body weight, and coronary calcium score in these five groups had no statistical difference ($p>0.05$). Different heart rate groups had significant influence on the arterial attenuation in each coronary segment ($p<0.05$). In each coronary segment, Group C had the highest vessel attenuation ($p<0.05$); Group A or Group E had the lowest vessel attenuation ($p<0.05$). Vessel attenuation of each coronary segment was higher in Group B than in Group A ($p<0.05$), and higher in Group D than in Group E ($p<0.05$).

Conclusion: Heart rate has significant influence on coronary enhancement during MDCT coronary angiography. Optimal coronary enhancement can be achieved with heart rate between 51-55/minute.

10:40 am

054. Fully Automated 3D-Coronary Endothelial Shear Stress Based on 320-Detector Row CT Angiography

Rybicki, F.; Mitsouras, D.; Nallamshetty, L.; Coskun, A.; Feldman, C.; Stone, P.; Steigner, M.; Chatzizisis, Y. Brigham and Women's Hospital, Boston, MA*
Address correspondence to F. Rybicki (frybicki@partners.org)

Objective: Coronary segments with reduced endothelial shear stress (ESS) are more likely to have rapid progression of atherosclerosis than those with more stable ESS patterns. Coronary ESS is typically obtained from the lumen geometry derived from intravascular ultrasound (IVUS), with increasing interest in noninvasive approaches. The purpose of this study is to demonstrate fully automated 3D coronary lumen geometry extraction based on 320-detector row coronary CT angiography images.

Materials and Methods: The contrast-enhanced coronary lumen from axial 320 x 0.5 mm detector row CT (Toshiba Medical Systems, Tochigi-ken, Japan) images was automatically segmented (Vital Images, Minnetonka, MN). The geometric mesh of the segmented lumen surface was over-determined for computational fluid dynamic (CFD) simulation requirements along the circumference. Decimation along the circumference was performed with low-pass spatial filtering. This had the additional advantage of reducing small irregularities in the detected endoluminal surface. Blood velocities through the left main and left anterior descending artery (LAD) were obtained using commercial CFD software (CHAM, Wimbledon, UK). Standard assumptions were used: blood a Newtonian fluid; viscosity estimated from hematocrit; zero tangential gradient of velocity at outlet; flow discharging to zero gauge pressure; uniform velocity profile at the inlet section. ESS was calculated as the spatial gradient of the simulated blood velocity field at the inner boundary of the lumen times the viscosity of blood.

Results: Manual correction of the lumen segmentation was not required. Axial velocity profiles and ESS maps are obtained from the fully automated 3D coronary lumen geometry extraction. ESS maps demonstrate axisymmetric patterns with circumferential uniformity.

Conclusion: Coronary images obtained from 320 x 0.5 mm detector row CT enable a fully automated algorithm to extract the 3D coronary lumen geometry for ESS computations. A significant challenge to CT coronary ESS modeling is the ease at which the lumen geometry can be obtained. 320-detector row CT images enable an algorithm to obtain this geometry without user input.

10:50 am

055. CT Visualization of Coronary Artery Vasa Vasorum

Knollmann, F.; Raval, J.; Usas, A.; Nichols, L. University of Pittsburgh, Pittsburgh, PA*
Address correspondence to F. Knollmann (knollmanfd@upmc.edu)

Objective: Coronary vasa vasorum have been implicated as a key factor in the pathogenesis of acute coronary syndromes. While these vessels are much smaller than the resolution of any clinically established imaging technique, secondary effects of their presence may still be detectable. In a post mortem investigation, the presence of coronary vasa vasorum should be investigated using a micro CT method.

Materials and Methods: At autopsy, the coronary arteries of seven hearts were cannulated and filled with either a barium sulfate based contrast agent, or Microfil, and then depicted on a clinical multidetector row unit (GE Healthcare, Waukesha, WI), and a micro CT unit (SCANCO Medical AG, Brüttisellen, Switzerland). Micro-CT scans were obtained at 10 micrometer isotropic resolution. Images were reformatted and coronary vasa vasorum depicted by maximum intensity projection.

Results: Coronary vasa vasorum were detected in the tunica adventitia of the left anterior descending coronary artery, and could be followed from their ostium onwards. They would typically traverse the coronary artery wall without giving off any branches into the neither tunica intima nor media. They then form an adventitial network and evolve into venous vasa vasorum.

Conclusion: Micro CT analyses of human coronary arteries confirm the presence of coronary vasa vasorum, and are well suited to investigate the proliferation, size and distribution of such vessels. It has been hypothesized that the proliferation of vasa vasorum into atherosclerotic plaques and subsequent intra plaque hemorrhage are the ultimate cause of plaque rupture and coronary thrombosis, and the availability of a true 3D, nondestructive imaging technique opens new research pathways. Further investigations will address how far the presence of coronary vasa vasorum can be inferred in lower resolution imaging studies from periarterial contrast enhancement, as has been suggested for intra-arterial ultrasound.

SCIENTIFIC SESSION 8

GENITOURINARY/OB/GYN (PROSTATE/ADRENAL) IMAGING PAPERS

Room: 210, Level 2
Tuesday, April 28, 2009, 9:30 am–11:00 am
Abstracts 056-062

Moderators: *R. Abbott, N. Rofsky*
Keynote Address: Prostate MR: New Opportunities and Insights—*N. Rofsky*

9:50 am

056. 320-Detector Row CT Renal Perfusion for Potential Laparoscopic Renal Donors - Initial Experience
Steigner, M.; Jerosch-Herold, M.; Nallamshetty, L.; Mitsouras, D.; Whitmore, A.; Rybicki, F. Brigham and Women's Hospital, Boston, MA*
Address correspondence to F. Rybicki (frybicki@partners.org)

Objective: The objective was to investigate 320-detector row CT renal perfusion as a supplement to renal CT angiography.

Materials and Methods: For two potential laparoscopic renal donors, axial 320 x 0.5 mm detector row CT (Toshiba Medical Systems, Tochigi-ken, Japan) perfusion was performed with a protocol using aortic bolus tracking at the renal artery ostia, followed by four more phases with 2.5 second temporal resolution, 100 kV, 400 mA, 120 mL iopromide 370 mg I/mL at 5 mL/second, no saline. 0.5 mm axial reconstructed images underwent region of interest Hounsfield Unit (HU) analysis in the juxtarenal aorta plus the cortex and medulla of both kidneys. The data (HU vs. time curves) were fit with JSIM, a Java-based SIMulation environment (URL: http://www.physiome.org), using a spatially distributed model with plasma and interstitial spaces. The plasma space fraction was assumed = 0.2. Flow was optimized by least squares minimization. Peak enhancement contrast to noise (CNR) was calculated as peak cortical HU/standard deviation in fat.

Results: The renal cortical flow estimates of 4.5 ml/g/minute were not significantly different between left and right kidney and are consistent with previously reported estimates from MR perfusion, albeit at the high end of the normal range. Flow estimates for the medulla were not significantly different from zero, due to the relatively short acquisition window. The peak cortical CNR=38:1.

Conclusion: 320 x 0.5 mm CT (16 cm craniocaudal coverage) enables whole-kidney CT acquisition and modeling for potential laparoscopic renal donors. This is one of the first estimates of CT renal perfusion with direct detection of iodine as the tracer, as opposed to MRI estimates that rely on indirect detection of gadolinium as the tracer through the water signal. This initial protocol will incorporate glomerular filtration rate by extending the current acquisition window and the model-based analysis. Because of the high peak CNR, protocol optimization will minimize iodine load and radiation while expanding temporal coverage. 320-slice CT renal perfusion estimates show promise as a single study of morphologic and functional data in general, with improved preoperative assessment for potential laparoscopic renal donors.

10:00 am

057. Incidental Findings of Abnormal Prostate T2-Weighted Signal in Pelvic MRI Examinations
Oliveira, G.[1]; Haker, S.[2]; Tempany, C.[2]; Mulkern, R.[2] 1. University of Washington, Seattle, WA; 2. Brigham and Women's Hospital, Boston, MA*
Address correspondence to G. Oliveira (grachid@u.washington.edu)

Objective: The objective was to determine the incidence of abnormal T2-weighted (T2W) signal in the peripheral zone (PZ) of the prostate in men undergoing pelvic MRI with no history of prostate cancer (PC).

Materials and Methods: Pelvic MRI exams of more than 1,500 male patients scanned between 2005 and 2008 were considered. Patients with a history of known PC were excluded and inclusion required availability of prostate specific antigen (PSA) and digital rectal exam (DRE) results. A total of 43 men with diagnostic quality T2- and T1-weighted images of the prostate were enrolled. The ages ranged from 36 to 79 years and the clinical indications for the exams were non-PC genitourinary and gastrointestinal cancers. Imaging was performed at 1.5T with either phased array coils only (n=35), an endorectal coil/phase array combination (n=2) or endorectal coil only (n=6) using T2-weighted FSE sequences with TR values ranging from 4-6 s, effective TE values from 96 to 105 milliseconds (ms), slice thicknesses from 3-5 mm, and in-plane spatial resolutions of ~ 1 x 1 mm^2. Images were reviewed by two radiologists for the presence of areas of abnormal T2 signal within the PZ. These were defined as focal, linear or diffuse. T1-weighted images were evaluated for the presence of hemorrhage.

Results: Of the 43 subjects, 30 (70%) had abnormal hypointensities in the PZ. No T1 abnormalities consistent with hemorrhage were found. Of these 30 subjects, five (17%) were classified as focal or suspicious for PC while 13 (43 %) and 12 (40%) were classified as diffuse and linear, respectively, and interpreted as likely benign such as chronic prostatitis. Of the 30 patients with abnormal signal, five (16%) had abnormal PSA and/or DRE while of the 13 patients with normal PZ signal, two (15%) had abnormal PSA and/or DRE.

Conclusion: T2-weighted imaging of the prostate has a relatively high rate of detection of abnormal hypointensities within the PZ. As an incidental finding, the value of abnormal signal in PZ is questionable as it is often not associated with suspicious PSA or DRE. This finding suggests that T2W images alone are not useful for cancer detection and other techniques such as spectroscopy, diffusion imaging and/or dynamic contrast enhancement are required.

10:10 am

058. MR Spectroscopic Imaging of Benign Prostatic Tissue: Findings at 3T Compared to 1.5T-Initial Experience
Chitkara, M.; Westphalen, A.; Kurhanewicz, J.; Qayyum, A.; Poder, L.; Reed, G.; Coakley, F. University of California, San Francisco, San Francisco, CA*
Address correspondence to F. Coakley (fergus.coakley@radiology.ucsf.edu)

Objective: The objective was to compare the metabolic findings at MR spectroscopic imaging of benign prostatic tissue performed at 3T vs. 1.5T.

Materials and Methods: This study was approved by our institutional Committee on Human Research with waiver of the requirement for written consent and was HIPAA compliant. We retrospectively identified 71 voxels of benign peripheral zone tissue from three men who underwent endorectal MR spectroscopic imaging of the prostate at 1.5T and 3T. Two readers independently scored the matched spectra from these voxels on a scale from one (likely benign) to five (likely malignant). In voxels rated as more malignant at 3T by either reader, the integral peaks of choline, polyamine, and creatine normalized to the citrate peak were compared at 3T vs. 1.5T, using a Wilcoxon ranked-sum test.

Results: Twenty-one voxels were considered to have more malignant spectra at 3T and only three voxels were considered more benign ($p<0.001$). The mean choline to citrate integral peak ratio in the 21 more malignant-appearing voxels was significantly higher at 3T compared to 1.5T (0.39 vs. 0.11; $p<0.001$), as was the mean polyamine to citrate integral peak ratio (0.25 vs. 0.07; $p<0.001$). Creatine to citrate peak integral values were unusable due to noise.

Conclusion: At endorectal MR spectroscopic imaging of benign peripheral zone prostatic tissue, choline and polyamine peaks are more prominent at 3T compared to 1.5T, resulting in significantly higher choline and polyamine to citrate ratios; awareness of this selective amplification may help avoid over-diagnosis of prostate cancer.

10:20 am

059. MRI and Pathologic Stage of Prostate Cancer

McClure, T.; Gomez, A.; Gulati, M.; Nagarajan, R.; Margolis, D.; Thomas, A.; Reiter, R.; Raman, S. University of California, Los Angeles, Los Angeles, CA*
Address correspondence to T. McClure (tmcclure@mednet.ucla.edu)

Objective: Clinicians are increasingly using MRI as an imaging modality in the diagnosis of prostate cancer. We assessed prostate MRI's ability to accurately predict pathologic stage and capsular involvement of the prostate.

Materials and Methods: We retrospectively reviewed MRI reports and pathology reports of 119 patients who were referred for prostate MRI prior to radical prostatectomy. The MRI reports were scored for staging and micro- and/or macroscopic extracapsular extension (ECE). Differentiation between T2 and T3 disease on MR was based on gross ECE or seminal vesicle invasion (SVI). Evaluation for capsular involvement included those cases suggestive of microscopic invasion. Final pathology reports were then reviewed and compared to MR findings.

Results: MRI's ability to differentiate between T2 and T3 disease was: sensitivity=75%, specificity=95%, positive predictive value=55%, and negative predictive=98% (p=0.001). MRI's ability to determine capsular involvement was: sensitivity=71%, specificity=74%, positive predictive value=86%, and negative predictive value=54% (p=0.001).

Conclusion: An important component in the management of prostate cancer is the differentiation of T2 and T3 disease. This study demonstrates that MR is accurate in the staging of prostate cancer and suggests that MR may be a useful aid in assessing capsular involvement.

10:30 am

060. Impact of MRI on Preoperative Surgical Planning for Robotic Assisted Laparascopic Prostatectomy

McClure, T.; Raman, S.; Margolis, D.; Gomez, A.; Nagarajan, R.; Thomas, A.; Reiter, R. University of California, Los Angeles, Los Angeles, CA*
Address correspondence to T. McClure (tmcclure@mednet.ucla.edu)

Objective: In robotic-assisted laparascopic prostatectomy (RALP), which is increasingly used in the surgical management of prostate cancer, the surgical decision making regarding the extent of dissection is tempered by loss of tactile feedback. Because preoperative MR is accurate for detection of extracapsular extension, we evaluate the utility of endorectal MR guiding surgical decision making during RALP.

Materials and Methods: After IRB approval, the preoperative endorectal coil prostate MR in 19 men who subsequently underwent RALP were reviewed. The surgical plan with regards to neurovascular bundle (NVB) resection preoperative plan was assigned prior to and after MR review. The actual surgical technique was then recorded. A total of 38 NVB were evaluated. The use of MR in changing surgical plan was compared.

Results: Of 38 NVB, preoperative MR imaging changed the plan in 53% of patients. Of patients for whom the plan was changed, 60% underwent more aggressive NVB sparing surgical technique and 40% had more conservative NVB surgical technique. The rate of positive margins was 2.5%

Conclusion: The benefits of RALP are limited by loss of tactile feedback during surgery. This limits the decision making process of the surgeon in how aggressive he/she can be with regards to nerve-sparing techniques. Preoperative endocoil prostate MR helps the urologic surgeon compensate for the lack of tactile feedback to optimize the nerve sparing technique without compromising oncological outcome.

10:40 am

061. Improved Evaluation of the Adrenal Gland at MDCT Using Thin-Client PACS

Jagtiani, M.[1]; Kalra, M.[1]; Sahani, D.[1]; Cushing, M.[1]; Schirmacher, H.[2]; Saini, S.[1] 1. Massachusetts General Hospital, Boston, MA; 2. No Institutional Affiliation*
Address correspondence to M. Jagtiani Sangwaiya (mjagtiani@partners.org)

Objective: A thin-client PACS platform stores the thinnest MDCT images and lets the radiologist manipulate the viewing slice thickness at the time of image interpretation. We investigated the utility of a thin-client PACS for evaluating the adrenal gland at 16-detector row MDCT.

Materials and Methods: In this IRB approved and consent waived retrospective study, 51 (M:F 25:26, age range 26-95) randomly selected abdominal CT scans from March, 2008 were evaluated. Images were obtained at a detector collimation of 1.25 mm on a 16-detector row MDCT scanner (GE Healthcare, Waukesha, WI). Two experienced radiologists (R1 and R2) independently evaluated the adrenals randomly either on 5 mm contiguous images or on 1.2 mm contiguous images, separated by a week, on a thin-client server based system (Visage Imaging, Carlsbad, CA). Reader's (R1 and R2) confidence in the detection and characterization of adrenal lesions on thick and thin slices were determined on a five-point scale (1=definite lesion, 5=no definite lesion). A third independent reader, who had access to all image datasets and prior CT scans and clinical information, served as reference standard. The additional lesions detected on thin slices, change in confidence from thick to thin slices and improvement of definition in lesions was determined.

Results: Improved confidence was found in 10% (10/100) for R1 and 17% (17/100) of adrenals for R2 with thin slices. By the McNemar's (two sided) test, the first reader's confidence did not change significantly (p=0.61) while R2 did become significantly (p=0.0025) more confident. Improved definition and conspicuity was seen in three and ten lesions by R1 and R2 respectively. On thin slice data, R1 detected 14 additional lesions (11 true positives), and R2 detected 16 new lesions (15 true positives). The third reader detected 37 lesions in total. Overall, substantial inter-observer correlation (r^2= 0.7) was observed on thin slices.

Conclusion: Thin-client PACS allow maximum exploitation of MDCT technology by permitting the radiologist to select slice thickness at the time of image interpretation. In our experience, the use of thin slice data enabled improved definition of adrenal gland with enhanced detection of subtle abnormalities. Interpretation of routine abdominal CT with thick (5 mm) images can miss a substantial number of adrenal lesions. A thin client system can help view thinner and thick images without burdening PACS.

10:50 am

062. Characterization of Adrenal Masses: Can Dual Energy CT Improve Differentiation Between Adenomas and Metastases?

Gupta, R.; Ho, L.; Marin, D.; Boll, D.; Nelson, R. Duke University Medical Center, Durham, NC*
Address correspondence to L. Ho (ho000004@mc.duke.edu)

Objective: Based on prior studies which showed that the attenuation (HU) of lipid decreases with decreasing peak kilovoltage (kVp), we hypothesize that adrenal adenomas will decrease in HU at low kVp owing to the presence of intracellular lipid. The purpose of this study is to determine if adenomas can be distinguished from metastases by demonstrating HU decrease at 80 kVp compared with 140 kVp.

Materials and Methods: Thirty-one adrenal nodules were prospectively identified in 17 patients who underwent standard CT of the chest for a variety of indications. These patients then underwent dual energy CT of the adrenals using a 64-MDCT scanner equipped with a dual energy software package (GE Healthcare, Waukesha, WI) which enables a conventional single source MDCT scanner to produce 140 and 80 kVp nearly simultaneously during a single imaging acquisition. Adrenal nodules were classified as follows: lipid rich adenoma if the attenuation value was less than 10 HU at 140 kVp (n=20); lipid poor adenoma if the attenuation value was greater than 10 HU at 140 kVp and stable for greater than one year (n=6); adrenal metastasis if rapid increase in size over one year and history of primary lung malignancy (n=5). Sensitivity, specificity, negative predictive value (NPV) and positive predictive value (PPV) were also calculated for diagnosis of an adenoma using dual energy CT (DECT).

Results: Mean HU ± SD at 140 and 80 kVp was 2.1 ± 9.9 and 2.6 ± 13.3 for adenomas; 28.5 ± 2.9 and 37 ± 6.0 for metastases, respectively (p<0.01). Half (13/26) of adenomas demonstrate mean decrease of 5.5 ± 2.9 HU at 80 kVp. The other 50% of adenomas demonstrated a mean increase, 6.3 ± 4.5 HU at 80 kVp. At 80 kVp, all adenomas demonstrate a mean increase of 0.4 ± 7.1 HU and all metastases demonstrated a mean increase of 9.2 ± 4.3 HU, p=0.012) Using a decrease in attenuation at 80 kVp as an indicator of intracellular lipid within an adenoma, DECT has 50% sensitivity, 100% specificity, 100% PPV and 28% NPV for diagnosis of adenoma.

Conclusion: A decrease in attenuation in an adrenal lesion between 140 kVp and 80 kVP is a highly specific sign for an adrenal adenoma. However, because an increase in attenuation at 80 kVp is seen with metastases and some adenomas, the sensitivity of this test is low. Based on this data, it appears that DECT can be used to help differentiate some adrenal adenomas from metastases.

Scientific Session 9

Neuroradiology/Head and Neck Papers

Room: 207, Level 2
Tuesday, April 28, 2009, 9:30 am–11:00 am
Abstracts 063-070

Moderators: *M. Johnson, C. Lascola*
Keynote Address: MR Imaging Characterization of Cervical Spinal Cord Injury—*M. Omojola*

9:40 am

063. Single-Tensor vs. Multitensor Tractography to Visualize the Corticospinal Tract for Neurosurgical Planning
Radmanesh, A.; Whalen, S.; Jolesz, F.; Golby, A. Brigham and Women's Hospital/ Harvard Medical School, Boston, MA*
Address correspondence to A. Radmanesh (aradmanesh@partners.org)

Objective: Depiction of hand and face motor fibers using diffusion tensor imaging (DTI) is a well known challenge in neurosurgical planning. Single-tensor tractography methods cannot successfully demonstrate the hand and face components of the corticospinal tract (CST) due to the presence of crossing fibers. The extended streamline two-tensor tractography method (XST) was recently introduced to address the issue of crossing fibers. To evaluate its clinical usefulness, we compared XST to the commonly used single-tensor method (ST).

Materials and Methods: XST was evaluated on simulated data. Tractography was performed in eight brain tumor patients (eight diseased hemispheres) and five volunteer subjects (ten healthy hemispheres) using 3D-slicer (www.slicer.org). Functional MRI was obtained during hand clenching (all cases) and lip pursing (four patients and three controls). Tractography was performed in the posterior limb of the internal capsule (PLIC) using a 1 mm seed-point grid. A method-blind neuroradiologist scored the generated tracts on a scale of zero to three ("0" no tracts, "1" marginal tracts, "2" a few (<7) correct tracts, "3" many (seven or more) correct tracts). A correct tract is defined as a tract that reaches the functional MRI activation after being seeded from PLIC. We tabulated and compared the scores.

Results: XST showed the correct trajectory around the simulated crossing point. Hand: mean (and standard deviation) of scores for patients: 2 (1.1) vs. 2.9 (0.3) using ST vs. XST, respectively. For controls: 0.9 (1.2) vs. 2.7 (0.5). In four diseased and two healthy hemispheres, the scores were similar using either method. In 12 hemispheres XST showed higher scores. Face: mean (and SD) of scores for patients: 0 vs. 2 (1.4) using ST and XST, respectively. For controls: 0.2 (0.4) vs. 1(0.6).

Conclusion: By allowing tracking through regions of crossing fibers, extended two-tensor tractography can delineate the putative hand and face fibers better than ST in both patients and healthy subjects. This is often important for operative planning for lesions in and adjacent to the motor cortex. This method is also potentially useful for other areas with crossing fibers, such as the brain stem.

9:50 am

064. High-Resolution Diffusion-Weighted Imaging of the Orbit Compared to Whole-Brain Diffusion-Weighted Imaging: A Comparative Analysis
Sepahdari, A.; Rohany, M.; Abramson, S.; Goldin, D.; Michals, E. University of Illinois Medical Center at Chicago, Chicago, IL*
Address correspondence to A. Sepahdari (alisepahdari@gmail.com)

Objective: Diffusion-weighted imaging (DWI) is an increasingly utilized technique and an area of active research. Although DWI has long been used to detect acute cerebral infarct, it is increasingly used to evaluate neoplasms and mimicking lesions. Recent studies have focused on quantitative apparent diffusion coefficient (ADC) as a means for differentiating lesions, including lesions of the orbit. As DWI evolves from a means of detection to one of characterization, it is important to explore new methods and techniques. Our purposes were to test whether a high-resolution (HR) DWI sequence targeted to the orbit could better characterize a small anatomic structure (the lacrimal gland) than a whole-brain DWI sequence, and whether similar ADC values were obtained for lacrimal gland and pons using both techniques.

Materials and Methods: Orbit MRIs of 17 consecutive adult patients were reviewed. Imaging was performed on a 1.5T magnet (GE Healthcare, Waukesha, WI) using single-shot spin-echo echoplanar DWI with parallel imaging. Whole brain DWI was performed at 5 mm slice thickness with 0 mm interslice gap. HR orbit DWI was performed at 2 mm slice thickness with 0 mm interslice gap. Three small (~5 mm^2) regions of interest (ROIs) were obtained in the lacrimal gland and three larger (~15 mm^2) ROIs were obtained in the pons in each patient on ADC maps of both sequences. ADCs for each structure were compared between techniques, and ADC ratios between lacrimal gland and pons were compared using a Student's *t* test.

Results: The lacrimal gland was visible in 76% of cases using HR technique, and in 100% of cases using whole brain technique. ADC values for lacrimal gland and pons were significantly different between techniques ($p<0.0001$). Lacrimal gland ADC was 0.99 +/- 0.20 using HR technique, compared to 1.33 +/- 0.14 using whole brain technique. Pons ADC was 0.52 +/- 0.09 using HR technique, compared to 0.69 +/- 0.07 using whole brain technique (all values in units of 10^{-3} mm^2/second). Lacrimal gland/pons ADC ratio was not different between techniques (1.95 vs. 1.96).

Conclusion: Decreasing slice thickness without altering other parameters does not result in improved visualization of small structures with DWI, as reduced partial volume averaging is more than offset by worse signal to noise ratio. Choice of slice thickness can also heavily influence the ADC of a given structure. ADC ratio may be a more externally valid tool than quantitative ADC for lesion characterization.

10:00 am

065. Subtle Pathology Detection with Multidetector Row Coronal CT Reformations in Acute Head Trauma

Zacharia, T.; Nguyen, D. Penn State Hershey Medical Center, Hershey, PA*
Address correspondence to T. Zacharia (ttz100@yahoo.com)

Objective: We sought to analyze retrospectively the added value of coronal reformations obtained with MDCT in patients with acute head trauma.

Materials and Methods: Multidetector 16-section CT was performed in 200 adult patients (110 men and 90 women; age range, 21-87 years; mean age, 51 years) with acute head trauma. Scans were performed sequentially and axial 5 mm thick slices were obtained from base of skull to vertex. The source data set was reformatted coronally, with 2-mm-thick sections at 2-mm intervals. The study was approved by the Institutional Review Board (IRB). Images were analyzed retrospectively by two independent, blinded readers with the same level of training, who interpreted first the axial scans alone followed immediately by the coronal scans. Confidence in the visualization of neuroanatomy and pathology was scored on a five-point scale. The final diagnosis was determined by clinical follow-up.

Results: In 145 patients with acute head trauma, no CT abnormalities were detected. Remaining patients (n=55) had imaging abnormalities that warranted admission and clinical follow up and in some instances surgery (n=8). Acute traumatic intracranial abnormality was detected on axial scans in 46 patients. Additional findings were elicited on coronal CT reformations in nine cases and these were missed initially on axial CT. Coronal reformations detected additional findings in 16.3% (9/55) of the cases. These additional findings included subarachnoid hemorrhage (n=1), tentorial subdural hemorrhage (n=2), interhemispheric subdural hemorrhage (n=2), posterior fossa subdural hemorrhage (n=1), inferior frontal lobe contusions (n=2) and temporal lobe contusions (n=1). Overall, coronal reformations improved diagnostic confidence and interobserver agreement over axial images alone for visualization of normal structures and in the diagnosis of acute abnormality.

Conclusion: Subtle neuroimaging findings detected by coronal CT head reformations include tentorial and interhemispheric fissure subdural hemorrhage, subarchnoid hemorrhage and inferior frontal and temporal lobe contusions. Coronal reformations detected additional findings in 16.3% of the cases. Coronal CT head reformations improve the sensitivity and diagnostic confidence in the clinical setting of acute trauma. Therefore, radiology departments should consider routinely generating coronal reconstructions in such patients.

10:10 am

066. Imaging of the Brain on Coronal Whole-Body Short-Tau Inversion Recovery: Comparison with Dedicated Brain MR Imaging for the Evaluation of Abusive Head Trauma

Tung, G.; Mehan, W.; Jenny, C.; Evangelista, P. The Warren Alpert Medical School of Brown University/Rhode Island Hospital, Providence, RI*
Address correspondence to W. Mehan (wmehan01@hotmail.com)

Objective: Coronal, whole-body, short-tau inversion recovery (WB-STIR) has been used to investigate soft tissue and skeletal injuries in cases of suspected physical abuse. The purpose of this study is to compare MR images of the brain from WB-STIR with dedicated brain MR imaging for the detection of traumatic head injuries.

Materials and Methods: From November 2004 to 2007, contemporaneous coronal WB-STIR and dedicated brain MR imaging (DBM) was performed under conscious sedation on children referred by the Child Protection Program. An average of 34 coronal images (range, 25-44) of the brain were obtained as part of the coronal WB-
STIR examination (repetition time [TR]/echo time [TE]/inversion time [TI], 4,000-7,000/50-60/150-160; matrix, 320 x 147; FOV, 32-48 cm; average, 1; slice thickness, 4 mm; acquisition time, 21 minutes). Dedicated brain MR imaging (DBM) consisted of six series (sagittal conventional spin echo [CSE] T1- and transaxial turbo spin echo [TSE] T2-, T2*-, magnetization prepared rapid gradient echo [MPR] T1-, fluid attenuated inversion recover [FLAIR], and diffusion-weighted imaging [DWI]) with an average acquisition time of 28 minutes.

Results: MR imaging was performed on 20 boys and 11 girls (mean age, 5.4 months; range, 0.3-20.2). Twenty (65%) children had sustained accidental head trauma and 11 (35%) had suffered abusive head trauma. Coronal WB-STIR and DBM were concordant in all seven normal cases and in 31 (84%) diagnoses of traumatic brain injury, including all cases of cortical edema from contusion or hypoxic-ischemic injury (n=7), skull fracture (n=6), scalp contusion (n=3), and axonal injury (n=2). They were also in agreement for presence and size of 13 (87%) cases of subdural hemorrhage (SDH). In five (83%) cases, benign enlargement of the subarachnoid space was distinguished from SDH by absence of the cortical vein sign. Coronal WB-STIR and dedicated brain MR imaging were discordant for six (16%) diagnoses of traumatic brain injury, including two (13%) cases of SDH. Small intraventricular hemorrhages (n=3) and superficial siderosis (n=1) were not identified on WB-STIR.

Conclusion: Compared to dedicated MR imaging of the brain, imaging of the brain from the WB-STIR examination identifies all negative cases of brain injury and the majority of traumatic brain injuries.

10:20 am

067. Lumbar Vertebral Endplate Changes on CT: Correlation with MR Imaging

Stollman, N.; Kazmi, K. Hahnemann University Hospital, Drexel College of Medicine, Philadelphia, PA*
Address correspondence to K. Kazmi (kkazmi@msn.com)

Objective: Endplate signal (Modic) changes within the lumbar vertebral bodies have been well characterized on MR imaging and have been divided into three subtypes. The purpose of this study is to describe these endplate changes on CT and to correlate with concurrent MRI with a specific focus on characterizing the CT findings in each subtype.

Materials and Methods: Twenty-nine patients who had evidence of vertebral endplate changes on lumbar MRI and had concurrent CT examinations were retrospectively reviewed at our

institution. Endplate signal changes were detected at 37 levels. Two radiologists reviewed the MRI examinations and the changes were categorized by subtype: Type 1 edema, Type 2 fatty or Type 3 sclerosis. Concurrent lumbar CT examinations were then reviewed for the presence of endplate changes. Endplate changes were divided into the following categories: no sclerosis (normal density), mildly sclerotic (increased density, but with visible trabeculae), moderately sclerotic (obscured trabeculae), densely sclerotic (density similar to cortical bone) or lytic (decreased density).

Results: Of the 37 levels at which endplate changes were detected on MRI, nine (24.3%) were type 1 changes. There were 22 (59.4%) levels that had type 2 changes and there were six (16.2%) levels with type 3 changes. Among the nine levels with type 1 changes on MRI, three (33.3%) had no sclerosis on CT and six (66.6%) were mildly sclerotic. For the type 2 changes, one (4.5%) had no sclerosis, nine (40.9%) were mildly sclerotic and 12 (54.5%) were moderately sclerotic. The type 3 changes demonstrated moderate sclerosis in two cases (33.3%) and dense sclerosis in four cases (66.6%). There were no lytic changes seen on CT. The overall prevalence of sclerosis in endplate changes of all types was 89.2% (33 out of 37).

Conclusion: Preliminary data indicates that the degree of sclerosis on CT increases as one progresses from type 1 to type 2 and type 3 endplate changes with the most dense sclerosis seen in type 3. One possible explanation is that the more chronic changes have more time to develop sclerosis, even though one might expect a decrease in density with type 2 changes due to fat deposition. There is also an overall high rate of sclerosis of any severity (89.2%). This holds true even among those with type 1 and type 2 changes, both of which may be expected to decrease density on CT. Further study with pathologic correlation is required to better understand the significance of the lumbar endplate changes seen on CT and MRI.

10:30 am

068. 3D Fast FLAIR MR Imaging of the Inner Ear: Normative Data and Application in Patients with Sensorineural Hearing Loss

Moon, J.[1]; Kim, H.[2]; Choi, J.[1]; Lim, Y.[2]; Lee, I.[1]; Kim, S.[1]; Jung, W.[1]*
1. Samsung Medical Center, Seoul , South Korea; 2. Seoul National University Hospital, Seoul, South Korea
Address correspondence to C. Jin Wook (jwchoi95@hanmail.net)

Objective: 3D fast fluid attenuated inversion recovery (FLAIR) MR imaging is reported to be useful for the evaluation of patients with sensorineural hearing loss (SNHL) by providing thin slices with high signal to noise ratio (SNR) with attenuation of fluid signal. The purposes of this study are to establish the normative data of the inner ear seen on 3D (FLAIR) and also to identify the inner ear abnormalities in patients with SNHL.

Materials and Methods: Precontrast axial 3D FLAIR was obtained in 53 audiometrically normal subjects and 30 patients with SNHL on a 3T unit. Postcontrast images were also obtained in 29 subjects with normal hearing and all 30 patients with SNHL. In 30 patients with SNHL, abnormal audiometry was found in 40 ears. Fifty 0.8 mm thick slices with voxel size of 0.8 x 0.8 x 0.8 mm were obtained with an acquisition time of five minutes 20 seconds. Signal intensity (SI) of inner ear was graded 0-3 with zero as no or poor visualization and 1, 2, and 3 as visualization with SI less than, same as, and greater than cerebellar cortex, respectively. The degree of enhancement was also graded 0-3 with zero as no enhancement (NE), one as mild enhancement (Mi), two as moderate enhancement (Mo), and three as marked enhancement (Ma). All Image interpretation was done by two neuroradiologists in conference.

Results: Of 91 ears with normal audiometry, the SI of the cochlea was graded zero in 18 (20%) and one in 73 (80%), and that of the vestibule was graded zero in 87 (96%) and one in four (4%). No case showed grade 2 or 3. Of 47 ears with contrast enhancement, NE of the cochlea was seen in 23 (49%), Mi in 20 (43%) and Mo in 4(8%). In the vestibule, NE was noted in 41 (87%) and Mi in six (13%). Of audiometrically abnormal 40 ears in 30 patients with SNHL, the SI of the cochlea was graded zero in five (12.5%), one in 27 (67.5%), and two in eight (20%), and that of the vestibule was graded zero in 33 (82.5%), one in five (12.5%) and two in two (5%). After enhancement, NE of the cochlea was seen in 18 (45%), Mi in 15 (37.5%), Mo in six (15%) and Ma in one (2.5%). In the vestibule, NE was noted in 33 (82.5%), Mi in four (10%), and Mo in three (7.5%).

Conclusion: The SI of the inner ear equal to or greater than that of the cerebellar cortex on 3D FLAIR seems to be abnormal. However, visualization of some SI, usually hypointense to cerebellar cortex, within the inner ear is a frequent finding on 3D FLAIR, and should not be interpreted as pathology.

10:40 am

069. Normal Values for the Atlantala-Axial Relationships on MDCT

Bertozzi, J.; Rojas, C.; Hayes, A.; Guidi, C.; Martinez, C.; Marulanda, G. University of South Florida College of Medicine, Tampa, FL*
Address correspondence to J. Bertozzi (christopher_bertozzi@verizon.net)

Objective: We aim to establish normal values on MDCT images for the atlantal-axial relationships including the atlanto-axial interval (AAI), atlanto-dental interval (ADI), and lateral atlanto-dental interval (LADI) as methods to detect craniocervical junction injuries in adults and children.

Materials and Methods: Two-hundred normal adult patients between 20 and 40 years of age and 133 pediatric patients between two months and ten years of age underwent cervical spine MDCT with multiplanar reconstructions. The width of the joint space between the lateral mass of C1 and the lateral mass of C2 was measured at three equidistant points on both the left and right side on coronal reformatted images to determine the AAI. The distance between the anterior surface of the dens and the posterior surface of the anterior arch of C1 was measured on the sagittal reformatted images to determine the ADI. The distance between the lateral surface of the dens and the medial surface of the lateral mass of C1 was measured in the coronal plane to determine the LADI bilaterally. Two examiners evaluated the patient populations to establish interexaminer variability.

Results: Greater than 95% of the adult population was found to have an AAI less than 3.4 mm, an ADI less than 2 mm right LADI of 4.8 mm and left LADI of 7 mm. Greater than 95% of the pedi-

atric population was found to have an AAI less than 3.9 mm, an ADI less than 2.5 mm, a right LADI less than 7.4 mm, and a left LADI less than 7.6 mm. No significant interexaminer variability was found when performing these measurements in adults or in the pediatric population.

Conclusion: The establishment of normal values for the atlantal-axial relationships in the adult and pediatric population is important in the detection of craniocervical junction injuries. We suggest that these values should be considered as the normal ranges in the adult and pediatric population on MDCT images.

10:50 am

070. Nephrogenic Systemic Fibrosis: A Prospective Methodology for Follow-Up of Patients with Chronic Kidney Disease Undergoing MRI with Gadolinium Contrast Agent

Mamillapalli, N.; Minn, M.; Vallurupalli, K.; Kuhn, M. Southern Illinois University School of Medicine, Springfield, IL*
Address correspondence to M. Kuhn (mkuhn@st-johns.com)

Objective: The objective was to evaluate the incidence of nephrogenic systemic fibrosis (NSF) in patients with stages 3 to 5 chronic kidney disease (CKD) undergoing MRI with gadobenate dimeglumine.

Materials and Methods: As part of a prospective multi-center study, patients referred for MR neuroimaging with contrast were screened with a calculated estimated glomerular filtration rate (eGFR), modification of diet in real disease (MDRD) method from a serum creatinine value obtained within 24 hours prior to MRI. Patients were stratified by entry eGFR 30-59 mL/minute/1.73 meter squared (Cohort 1) or eGFR< 30 mL/minute/1.73 meter squared (Cohort 2). Patients with a history of gadolinium exposure within the previous year were excluded. After signing their informed consent, eligible patients received 0.1 mmol/kg gadobenate dimeglumine (Bracco Diagnostics, Princeton, NJ) intravenously. Patients are followed up to two years with scheduled telephone calls and office visits to evaluate for any signs of nephrogenic systemic fibrosis. A skin biopsy by a dermatologist is part of the protocol for any suspected NSF cases. To date we have enrolled 17 patients over six months at our site and enrollment is ongoing at our center and other sites participating in this multicenter study

Results: No confirmed cases of NSF have been seen so far in the group of 17 patients enrolled at our site. One patient was lost to follow-up and another patient died of unrelated causes.

Conclusion: A prospective study to evaluate the incidence of NSF in patients undergoing gadolinium enhanced MRI has not been previously accomplished. The methodology of our study may serve as a model for other institutions.

SCIENTIFIC SESSION 10

PEDIATRIC IMAGING PAPERS

Room: 310, Level 3

Tuesday, April 28, 2009, 9:30 am–11:00 am

Abstracts 071-079

Moderators: *S. Puig, I. Kim*

9:30 am

071. Effect of kVp Adjustment on Noise Level in Astute Low Dose CT Scanning

Gamberoni, J.; Davros, W.; Reid, J. Cleveland Clinic Children's Hospital, Cleveland, OH*
Address correspondence to J. Reid (reidj@ccf.org)

Objective: There is a concerted movement to decrease radiation dose in pediatric CT in order to reduce the long term risk of radiation-induced cancers. Currently this is done through decreasing mAs by age or weight without regard to size. Our hypothesis is that kVp can be an effective parameter to lower dose in pediatric CT while maintaining an acceptable noise level. We propose a protocol that more accurately guides dose reduction through manipulation of kVp and mAs according to patient size.

Materials and Methods: All measurements were taken using a 16-slice CT scanner (Siemens Medical Solutions, Forchheim, Germany). Center line dose was measured using a 100 mm pencil probe ion chamber with an electrometer (Victoreen Instruments, Moedling, Austria) and standard CT dose index phantoms with diameters of 10, 16, and 32 cm. Noise was measured by recording the standard deviation from a region of interest (ROI) near the center of selected images while kVp, mAs and phantom diameter were varied in turn. One hundred and twenty dose measurements were made at 80, 100, 120, and 140 kVp. At each kVp measurements were taken at 50, 100, 200, 300 and 400 mAs. For each combination of kVp and mAs, dose measurements were taken at the center line of the 10, 16 and 32 cm diameter phantoms. Trend lines for paired parameters were created in Microsoft Excel.

Results: Dose increases in a linear fashion with mAs according to (16 cm phantom): dose at 80 kV=0.019 (mAs) - 0.087; dose at 100kVp=0.044 (mAs) - 0.36; dose at 120 kVp=.063 (mAs) - 0.52; dose at 140 kVp=0.079 (mAs) + 0.70 with goodness of fit greater than 0.98. This is true for each phantom diameter and each kVp tested. For a fixed mAs, dose increases with kVp in a linear fashion according to dose (at 400 mAs) =0.41 (kVp) - 24.3. There are absolute size limitations to dose reduction with kVp for an acceptable noise value such that increases in mAs at low kVp in larger patients would lead to unacceptably large dose levels without achieving an acceptable noise level.

Conclusion: Although dose reduction is easily achieved through manipulation of mAs, it may be preferable to accomplish this by adjustments in kVp especially in the setting of iodinated contrast-enhanced scans which takes advantage of the higher k-edge absorption at lower kVp. This can be achieved while maintaining an acceptable noise level at lower dose and varying patient sizes however thresh-hold limitations do exist related to patient size.

9:40 am

072. Pediatric Fluoroscopy - Reducing Patient Effective Dose

Moffatt, H.[1]; Reed, M.[1]; Ingleby, H.[2]; Zaporozan, G.[2]; Fife, I.[2] 1. Health Science Centre, Winnipeg, Canada; 2. CancerCare Manitoba, Winnipeg, Canada*
Address correspondence to H. Moffatt (hayleymoffatt@yahoo.ca)

Objective: Knowledge about radiation dose from diagnostic imaging is of great importance, especially given its stochastic effects. This is of particular concern in the more radiosensitive pediatric population. The goal of this study is to determine, quantitatively, the effect of altering easily manipulated settings on a fluoroscopic machine on effective dose.

Materials and Methods: Four different trials were performed for this study. An initial baseline trial was obtained for each in which no magnification or collimation was used, the image intensifier height was at a minimum, and the pulse rate was at a maximum. Subsequent trials were performed in which the magnification (three different settings), collimation (three different settings), image intensifier height (five different settings), or pulse rate (three different settings) was altered. An ionization chamber embedded in plexiglass on top of the fluoroscopy table was used to measure the exposure rate of the primary beam for each trial. The amount of scatter radiation was also measured with a second ionization chamber. Exposure rates were then converted to effective doses using a Monte Carlo computer simulation

Results: A significant reduction ($p<0.01$) in effective dose and scattered radiation was observed with decreasing magnification, decreasing the height of the image intensifier, decreasing the pulse rate, and increasing collimation. Up to a 57% and 62% decrease in effective dose was observed with collimation and pulsed fluoroscopy, respectively. Similarly, increasing magnification and increasing the image intensifier height increased effective dose significantly, up to 165% and 142%, respectively. Similar results were obtained for scattered radiation.

Conclusion: Easily manipulated settings on fluoroscopy machines can be used to significantly reduce patient effective dose and should be used during all fluoroscopy procedures, particularly for pediatric patients. Including these dose reduction methods contributes to overall optimization in diagnostic radiology procedures.

9:50 am

073. Role of MDCT in the Diagnosis of Mechanical Intestinal Obstruction in Children

Saxena, A.[1]; Chatterjee, S.[2]; Suri, S.[3]; Rao, K.[1] 1. Post Graduate Institute of Medical Education and Research, Chandigarh, India; 2. Sree Chitra Tirunal Institute of Medical Science and Technology, Trivandrum, India; 3. No Institutional Affiliation*
Address correspondence to A. Saxena (fatakshay@yahoo.com)

Objective: CT is an established modality for evaluation of intestinal obstruction in adults. However, there is lack of data on the role of the CT scan in evaluation of pediatric intestinal obstruction. The purpose of this study was to evaluate the role of MDCT in the diagnosis of mechanical intestinal obstruction in children.

Materials and Methods: This was a prospective study which was approved by our institute ethics board. Thirty-two children underwent MDCT scans for clinically suspected mechanical intestinal obstruction. Twenty-two of these patients were subsequently operated on and were included in the study. Of the 22 children included, there were 16 males and six females. Median age was 3.5 years (range four months to 12 years). Fourteen MDCT scans were performed on a 16 detector scanner while eight MDCT scans were done on a four detector scanner. The scans were evaluated for presence and level of intestinal obstruction, any possible cause and viability of bowel.

Results: There were 19 true positive, two false negative, one true negative and no false positive cases of mechanical intestinal obstruction on the MDCT scans. Thus, MDCT had 90.48% sensitivity, 100% specificity, 100% positive predictive value and 33.33% negative predictive value in diagnosing mechanical intestinal obstruction. MDCT scan could correctly predict the level of obstruction in all (19 out of 19) true positive cases. MDCT scan could predict the cause of intestinal obstruction completely in 11/21(52.38%) patients and partially in five out of 21 (23.81%) patients. MDCT could detect bowel wall ischemia in patients with mechanical intestinal obstruction with a sensitivity of 75%, specificity of 88.24%, positive predictive value of 60%, negative predictive value of 93.75% and overall accuracy of 85.71%.

Conclusion: The MDCT scan is useful in management of pediatric patients with intestinal obstruction.

10:00 am

074. Coronary CT Angiography in the Detection of Congenital Malignant Coronary Arteries

Sultani, T.[1]; Richardson, R. [3]; Musil, I.[2, 3]; Nigro, J. [3]; Diab, K. [3]; Pophal, S. [3]; 1. St. Joseph Hospital and Medical Center, Phoenix, AZ; 2. University of Arizona College of Medicine, Phoenix, AZ; 3. Catholic Healthcare West, Phoenix, AZ*
Address correspondence to T. Sultani (TimSultani@hotmail.com)

Objective: Cardiac CT angiography (CCTA) is an established modality for the detection of coronary artery disease in adults. However, in pediatric populations, given fast heart rates, smaller body size, and the concern for radiation exposure, little has been said about its use for detection of coronary artery anomalies. Congenital coronary artery anomalies, although rare, are important because they can often present with sudden death or myocardial infarction as the first clinical manifestation making early diagnosis paramount. Modern advances in CT have made this modality superior to others as it can quickly and clearly identify the coronary anatomy in 3D representations. We present a set of pediatric cases in which EKG gated CCTA was used to detect "malignant" type coronary artery anomalies.

Materials and Methods: A retrospective study was performed searching our institution's database of 150 children with complex congenital heart disease for patients with malignant coronary arteries. CCTA was performed with a 64-slice MDCT, with EKG gating, followed by 3D reformations.

Results: A total of 20 patients were found to have an anomalous malignant coronary artery. In six patients, there was a right coronary artery (RCA) origin from the left aortic sinus of Valsalva (LSV) with an interarterial course between the pulmonary outflow tract and aorta. Seven patients were found to have anomalous left coronary artery (LCA) origination from pulmonary artery (ALCAPA). One patient had an anomalous RCA originating from pulmonary artery (ARCAPA). The remaining six patients all had different malignant anomalies (with an interarterial course) which included RCA origin from LCA, LCA from RCA, RCA originating from left anterior descending (LAD) artery, RCA from right sinus of Valsalva (RSV), RCA from left ascending aorta, and finally LCA originating from right aortic sinus of Valsava.

Conclusion: Congenital anomalous coronary arteries are a major cause of sudden death in adolescents making early detection vital. MDCT has proven to be a superior modality in providing an unambiguous diagnosis of congenital anomalous coronary arteries in the pediatric population.

10:10 am

075. Coronal Whole-Body Short Tau Inversion Recovery MR Imaging in the Investigation of Nonaccidental Traumatic Injury in Children

Evangelista, P.; McCarten, K.; Jenny, C.; Barron, C.; Goldberg, A.; Tung, G. Rhode Island Hospital/Warren Alpert Medical School of Brown University, Providence, RI*
Address correspondence to P. Evangelista (pevangelista@lifespan.org)

Objective: The objective was to investigate coronal, whole-body, short tau inversion recovery (WB-STIR) MR imaging in the evaluation of nonaccidental trauma (NAT).

Materials and Methods: After referral by the Child Protection Program (CPP) for suspected NAT, 51 children (mean age, 6.3 months; range, one week-37 months) underwent WB-STIR between February, 2003 and November, 2007. All bone and soft tissue injuries identified by WB-STIR and radiographic bone survey (RBS) were tabulated for each child.

Results: The cause of injury was NAT in 40 (78%) children and accidental trauma in 11 (22%) children. Of 200 fractures, 160 (80%) were detected by WB-STIR. WB-STIR did not change the clinical decision regarding the cause of trauma in any case but did strengthen the case for NAT by revealing four bone contusions and 14 additional fractures [13 (93%) confirmed on follow-up RBS and one on post mortem radiography], of which five (36%) were not identified on initial RBS. WB-STIR identified 37 soft tissue lesions: 28 (76%) were associated with fractures, four (11%) were primary injuries, and five (13%) were iatrogenic. Five fractures were identified on both initial RBS and WB-STIR in 11 children with accidental injury. There were also six soft tissue lesions detected, five (83%) associated with fracture and one (17%) was iatrogenic

Conclusion: WB-STIR did not change the clinical assessment of the cause of traumatic injury in children presenting with suspected NAT. However, WB-STIR did add value by demonstrating both bone contusions and fractures not identified on initial RBS as well as traumatic soft tissue injuries.

10:20 am

076. Feasibility of Real Time Diagnostic Imaging Central Review in Multicenter Cancer Trials

McCarten, K.[1,2]; Rosen, N.[2]; Friedman, D.[3]; Schwartz, C.[1]; Voss, S.[4]; Bishop-Jodoin, M.[2]; Kessel, S.[2]; Johnson, C.[2]; Laurie, F.[2]; FitzGerald, T.[2] 1. Rhode Island Hospital, Providence, RI; 2. University of Massachusetts Medical School Quality Assurance Review Center, Providence, RI; 3. Vanderbilt Children's Hospital, Nashville, TN; 4. Dana-Farber Cancer Institute and Children's Hospital, Boston, MA*
Address correspondence to M. Bishop-Jodoin (MJodoin@QARC.org)

Objective: The objective was to demonstrate that real time diagnostic imaging centralized review performed by a selected group of imagers in a multicenter Childrens Oncology Group (COG) trial, using protocol specified response definitions, is feasible.

Materials and Methods: AHOD0031, a COG study, compares a response adapted treatment paradigm to a standard regimen. Eligibility criteria include patients 0-21 years with newly diagnosed intermediate risk Hodgkin disease. After two chemotherapy cycles, imaging studies are performed at treating institutions. Guided by strict protocol criteria the patient is classified as slow early responder (SER) or rapid early responder (RER). SER patients are randomized to standard or augmented therapy. RER patients receive two more chemotherapy cycles; those in complete response (CR) are then randomized to reduced, no involved field radiation therapy (IFRT) or standard therapy (IFRT). All radiation and imaging data is collected at the Quality Assurance Review Center (QARC). Imaging data, received from over 200 institutions, are identified, reviewed, and archived with digital data virtually replacing hard copy format.

Results: Initially the protocol required the treating institution to assign the SER/RER response after two chemotherapy cycles with only the final determination of CR vs. <CR status for the RER patients after four cycles performed at QARC. It was found that some patients assigned by the institution as RER after two chemotherapy cycles did not achieve CR status on central review after four cycles and had actually been misclassified as RER when in fact they were SER. This suggested a need for earlier centralized response review. Thus the study was amended to verify SER/RER response for all patients in real time at QARC with confirmation sent to COG and the treating institution within 48 hours of data receipt. This real time approach has facilitated accurate category assignment.

Conclusion: Submission and evaluation of real time central review imaging has been outstanding. With more than 1,700 central reviews to date, protocol compliance is >86%. This rapid review increases the proportion of patients eligible to the two study randomizations due to appropriate classification. At trial completion accurate and complete data will be available for analysis to determine treatment regimen efficacy.

10:30 am

077. Multinational Clinical Evaluation of Gadobenate Dimeglumine in Children Referred for Neurologic MR Imaging

Kuhn, M.[1]; Cianciulli, E.[2]; Fonda, C.[3]; Pasowicz, M.[4]; Gao, P.[5]; Mamillapalli, N.[1] 1. Southern Illinois University School of Medicine, Springfield, IL; 2. Santobono Pausillipon Children's Hospital, Naples, Italy; 3. Anna Meyer Pediatric Hospital, Florence, Italy; 4. Krakow Hospital John Paul II, Krakow, Poland; 5. Beijing Tian Tan Hospital, Beijing, China*
Address correspondence to M. Kuhn (mkuhn@st-johns.com)

Objective: The objective was to evaluate the safety and efficacy of gadobenate dimeglumine in pediatric patients referred for neuro-MRI.

Materials and Methods: Ninety-two children (2-17 years) referred for cranial/spinal contrast-enhanced MRI were enrolled at 17 centers in the USA, Europe, or China as part of an open-label clinical study. Enrollment was stratified by age (2-5, 6-10, and 11-17 years). Each received 0.1 mmol/kg gadobenate dimeglumine (2 mL/second) followed by a saline flush. Predose (T1-weighted spin echo [T1wSE], T2-weighted fast spin echo [T2wFSE], and fluid-attenuated inversion recovery [FLAIR]) and postdose (T1wSE) images were evaluated for lesion enhancement, border delineation, and visualization of internal morphology. Lesion-to-brain ratio (LBR) and contrast-to-noise ratio (CNR) were also measured. Safety was assessed in terms of adverse events (AE), changes in vital signs, serial 12-lead ECG, and laboratory findings. All subjects were monitored for AE for 72 hours and followed up at 30 days to determine final diagnosis.

Results: Ninety-two children (45 boys, 47 girls; mean age: 10.6 years [range: 2.0–17.8 yrs]) were enrolled and dosed with 89 children completing all safety evaluations (13 patients 2-5 yrs, 34 patients 6-10 years, and 45 patients were 11-17 years). The mean contrast dose was 8.4 mL (range: 2.0-22.8 mL). A total of nine AE were reported in eight children (8.7%), including three AE in two patients considered possibly related to contrast injection (eyelid edema, abdominal discomfort, and vomiting). All AE were mild or moderate and resolved completely. Headache was reported in two patients with all other reported AE occurring once. No serious AE were reported, and no clinically meaningful changes in vital signs, laboratory values, or ECG were observed. Diagnoses included: 28 (30.4%) nontumor, 60 (65.2%) tumor, and four (4.3%) normal parenchyma. Of the 60 children with tumors, 43 (71.7%) were intra-axial and 17 (28.3%) were extra-axial; 25 (41.7%) were benign and 35 (58.3%) were malignant. In all patients with enhancing lesions, lesion enhancement, border delineation, and visualization of internal morphology were considered good-to-excellent. Lesion-level and patient-level analyses showed predose + postdose images were significantly ($p<0.001$) superior to predose images alone for lesion enhancement, border delineation, and visualization of internal morphology. Quantitative assessments showed gadobenate dimeglumine significantly ($p<0.001$) improved LBR and CNR.

Conclusion: Gadobenate dimeglumine was found to be safe and efficacious for contrast-enhanced MRI of central nervous system lesions in children.

10:40 am

078. Position of Sigmoid Colon in Right Iliac Fossa in Children: A Retrospective Study

Saxena, A.; Tirumani, S.; Mumtaz, H.; Sodhi, K.; Khandelwal, N. Post Graduate Institute of Medical Education and Research, Chandigarh, India*
Address correspondence to A. Saxena (fatakshay@yahoo.com)

Objective: Knowledge of anatomical position of a bowel segment is of crucial importance for evaluation of plain x-rays. Scanty data is available in the literature on the position of the sigmoid colon in right iliac fossa in children.

Materials and Methods: This retrospective analysis was done to asses the frequency of sigmoid colon in right iliac fossa on contrast enema study in children in the settings of a tertiary care centre of a developing country. The study was approved by the ethics committee of our department. During the period of January 1, 2007 to March 1, 2008, 113 contrast enema studies were done at our centre out of which images of 91 studies were available for review and were included in the study. Out of these 91 available studies, 15 were done in the postoperative period. The position of the sigmoid colon was evaluated on an anteroposterior view of the abdomen and categorized as below: *Left lower quadrant*: If most or all of the loops of the sigmoid colon were to the left of the lumbar vertebral bodies; *Right lower quadrant:* if one or more complete loops of sigmoid colon were to the right of the lumbar vertebral bodies; *Midline:* If the sigmoid colon extended superiorly in a vertical orientation, overlying the midline to the level of the second lumbar vertebrae before entering the right or left side of the abdomen; *Indeterminate:* If the position of the sigmoid colon could not be ascertained from available images.

Results: The age range varied from two days to 13 years. The position of sigmoid colon in left lower quadrant, right lower quadrant, midline and indeterminate was 32 (35.16%), 33 (36.26%), 12 (13.19%), and 14 (15.38%) respectively.

Conclusion: Sigmoid colon occupies the right lower quadrant in a large number of children. Awareness of this finding can reduce the likelihood of misinterpreting air in the sigmoid colon as air within the caecum in children suspected of having abnormalities such as intestinal obstruction, intussusception and malrotation.

10:50 am

079. Nonmesiotemporal Sclerosis Causes of Epilepsy in Pediatric Patients

Kanekar, S.; Trescher, W.; Bau, J. Penn State Milton S. Hershey Medical Center, Hershey, PA*
Address correspondence to S. Kanekar (sankan2000@yahoo.com)

Objective: The objective was to investigate the causes and analyze the spectrum of intractable epilepsy in the pediatric age group and to illustrate the neuroimaging spectrum of nonmesiotemporal sclerosis (nonMTS) pathologies leading to intractable epilepsy.

Materials and Methods: We analyzed 225 patients with clinical diagnosis of epilepsy confirmed either clinically, EEG or a combination of two. All patients underwent a routine MRI brain scan along with high resolution 3D spoiled gradient echo sequence and thin 2 mm angled coronal fluid-attenuated inversion recovery and T2-weighted image through the temporal lobe. All the studies were read by two radiologists separately.

Results: Depending on the radiological interpretation patients were classified into mesiotemporal sclerosis (MTS) (56%) and NonMTS (44%) causes. All MTS patients were excluded from this study. NonMTS patients were classified as per their pathology into cortical developmental malformation (11%) (abnormal neuronal and glial proliferation–micro-olissencephaly, hemimegalancephaly, Taylor's dysplasia; abnormal neuronal migration: lissencephaly, double cortex, subependymal heterotopias; abnormal late migration and organization: polymicrogyria, schizencephaly; syndromic: tuberous sclerosis, Sturge Weber syndrome); perinatal hypoxia/ periventricular leukomalacia/cerebral palsy (19%); neoplasm (8%) (astrocytic tumor, ganglioglioma, dysembryoplastic neuroepithial tumor, oligodendroglioma, pleomorphic xanthoastrocytoma); vascular abnormalities (3%) (arteriovenous malformation, cavernoma); miscellaneous (4%) (gliosis [scar epilepsy], trauma, infection [tuberculosis, cysticercosis, abscess, encephalitis]).

Conclusion: Though MTS is one of the most common causes of intractable epilepsy in children there are various nonMTS causes which may cause epilepsy syndrome in children. These abnormalities, especially the developmental malformation of brain, need extra attention. We present a comprehensive review and diagnostic pearls of these cases. NonMTS causes are equally important as compared to MTS causes in intractable epilepsy and should be carefully looked for.

VASCULAR AND INTERVENTIONAL RADIOLOGY PAPERS

Room: 309, Level 3

Tuesday, April 28, 2009, 9:30 am–11:00 am

Abstracts 080-086

Moderators: *J. Lorenz, A. Nemcek*

Keynote Address: Update on Caval Filtration—*J. Lorenz*

10:00 am

080. Safety, Efficacy and Retrievability of the "Optease" Vena Cava Filters: Experience with 71 Patients

Marentis, T.[1]; Jagtiani Sangwaiya, M.[1,2]; Stecker, M.[1,3]; Walker, T.[1,2]; Wicky, S.[1,2]; Kalva, S.[1,2] 1. Harvard Medical School, Boston, MA; 2. Massachusetts General Hospital, Boston, MA; 3. Brigham and Women's Hospital, Boston, MA*

Address correspondence to M. Jagtiani Sangwaiya (mjagtiani@partners.org)

Objective: The objective was to retrospectively evaluate the clinical safety, efficacy and retrievability of Optease vena cava filters (Cordis, Miami, FL).

Materials and Methods: We retrospectively evaluated the clinical and imaging data of patients who had an Optease vena cava filter placed between November 19, 2002 and January 22, 2008 in two institutions. The clinical presentation, indications and procedure-related complications were evaluated. Follow-up CT examinations of the abdomen and chest were evaluated for filter-related complications and recurrent pulmonary embolism (PE) respectively. Follow-up lower extremity studies were evaluated for deep vein thrombosis (DVT).

Results: An Optease vena cava filter was placed in 71 patients (45 males, 26 females; ages: 18-95). Twenty-two patients presented with DVT, 16 with PE, six with both, 16 were trauma patients and the rest presented with other symptoms. Imaging studies for PE were performed in 33 and 17 were positive for PE. Ultrasound and/or CT in 38 patients were positive for DVT in 29. Indications for filter placement were contraindication to anticoagulation (33), failure of anticoagulation (12) and prophylaxis (26). Filters were placed in the infrarenal (64) or suprarenal (seven) position through a femoral (67), jugular (three) and brachial (one) approach. One filter was malpositioned on deployment, repositioning failed and a Tulip filter was deployed proximal to it. Sixty-five patients had clinical followup of 382 days (range 1-1,869). One (1.5%) patient developed symptoms and signs of recurrent PE. Follow-up chest CT done for various clinical indications (23) at a mean of 67 days (range 1-491) showed two (3.1%) postfilter PE. Thirty patients had abdominal CT follow up at a mean of 254 days (range 1-1,686). This showed thrombus in the filter in three, filter fracture in one, inferior vena cava (IVC) thrombosis in one and filter migration in one. Thirty-two patients had DVT imaging follow up. Seven of 32 demonstrated DVT. We attempted to retrieve filters in 16 patients at a mean of 16 days (range 0-48). Twelve filters (75%) were retrieved successfully. Attempts to retrieve were not successful in four cases due to thrombus in the filter in two (13%), intimal hyperplasia in one (6%) and due to procedural difficulties in one (6%).

Conclusion: The Optease IVC filter is effective in the prevention of pulmonary embolism with minimal complications and can be easily retrieved within a two week period. The Optease IVC filter is clinically effective and is associated with minimal complications.

10:10 am

081. Venous Thrombosis in Outpatient Oncology Patients: Distribution, Type, and Comorbidities

Souza, F.[1,2]; Di Salvo, D.[1,2]; Ramayia, N.[2] 1. Brigham and Women's Hospital, Boston, MA; 2. Dana Farber Cancer Institute, Boston, MA*

Address correspondence to F. Souza (ffsouza@partners.org)

Objective: The objective was to examine oncology patients with venous thrombosis (VT) and correlate ultrasound findings with clinical characteristics and outcome.

Materials and Methods: Reports positive for VT were retrospectively reviewed over a 24-month period. Criteria for inclusion were: finalized report available for review and a clinic visit note within three months of the ultrasound visit. Clinical indication, demographics, sonographic findings, comorbidities, and development of pulmonary embolism in these patients were recorded.

Results: Of 509 vascular ultrasounds performed in the interval, 76 studies were positive for VT (44 women, 32 men; mean age 51.2 years; age range: 24-85 years). The most common clinical indication for ultrasound examination was swelling in 44 (58%), pain in 20 (26%) and abnormal prior imaging study in eight (11%). Sixty-four patients had deep venous thrombosis (DVT), while 12 had involvement of the superficial system only. In 57, findings were consistent with acute thrombosis, in 17 with chronic, and in two, findings were consistent with acute thrombosis superimposed on chronic DVT. Forty-five patients had lower extremity VT, while 31 had upper extremity VT. Among studies with lower extremity VT, 21were exclusively above the knee, 14 were exclusively below the knee, and ten were below and above the knee. When VT was seen exclusively below the knee, 11 (76%) were acute, two (14%) chronic, one (10%) was acute superimposed on chronic. In 11 (76%) patients involved the deep venous system and in three (24%) involved the superficial venous system. Among patients with upper extremity VT, 18 (58%) had a central venous catheter (CVC) at the time of diagnosis. Of these, 14 (45%) had DVT while four (13%) had superficial VT. Pulmonary embolism (PE) developed in eight (11%) patients who had lower extremity VT. Of these, seven (88%) had acute and one (12%) had chronic thrombosis. Seven patients (88%) had involvement of the deep system, while one was superficial. PE was seen in two patients on remission, six patients with active disease. Two patients that developed PE were on antiangiogenesis drugs and all eight patients who developed PE were on anticoagulation therapy.

Conclusion: In our cancer population DVT is most commonly acute, involves the lower extremity and the deep venous system above the knee. When DVT involves the upper extremity it is usually associated with CVC. PE is almost exclusively associated with lower extremity and acute DVT and can occur despite anticoagulation therapy.

10:20 am

082. The Use of Contrast-Enhanced Ultrasound in Characterization of Neovascularization in Carotid Atherosclerotic Plaque

Clevert, D.; Saam, T.; Horng, A.; Reiser, M. University of Munich-Grosshadern Campus, Munich, Germany*
Address correspondence to D. Clevert (Dirk.Clevert@med.uni-muenchen.de)

Objective: The objective was to evaluate the use of contrast-enhanced ultrasound in the neovascularization within carotid atherosclerotic plaque.

Materials and Methods: Thirty-three patients with known atherosclerotic plaque in the carotid artery were examined with contrast-enhanced ultrasound to evaluate the features of neovascularization within this plaque. Additionally the plaque was analyzed and correlated with plaque size and echogenicity. For contrast-enhanced ultrasound we injected 2,4 cc of sulphur hexafluoride (Bracco, Diagnostics, Milan, Italy) intravenously. The ultrasound (Acuson, Mountain View, CA) examinations were performed using a 15 MHz or 17 MHz probe and using CPS-software.

Results: There were 41 cases of atherosclerotic plaque, 27 of which (19 soft and eight mixed) enhanced after injection of contrast media. The enhancement occurred from the carotid wall to the center of the plaque with a short-line pattern in 15 cases, whereas 12 cases enhanced from both the carotid wall and the carotid lumen, with just a little spot pattern. The arrival time of contrast was later in the plaque than in the carotid artery and the time to peak was longer in the plaque than in the carotid lumen. Among the 14 cases of unenhanced plaque, four were hard, three were calcified, two were soft, and five were mixed. The unenhanced plaque had a thickness of <2.7 mm.

Conclusion: In our small patient population, contrast-enhanced ultrasound allows the dynamic evaluation of neovascularization within carotid plaque and neovascularization may correlate with plaque morphology.

10:30 am

084. Validation of Fluid Flow Velocity Measurements With Cine Contrast-Enhanced MDCT Imaging

Chu, L.[1]; Prevrhal, S.[1]; Yang, Q.[2]; Sleiman, S.[1]; Wilson, M.[1]; Desai, G.[1]; Yeh, B.[1] 1. University of California-San Francisco, San Francisco, CA; 2. Apollo Medical Imaging Technology, North Melbourne, Australia*
Address correspondence to B. Yeh (ben.yeh@radiology.ucsf.edu)

Objective: The objective was to test a novel dynamic contrast-enhanced MDCT method for measuring fluid flow velocity in a phantom.

Materials and Methods: A water siphon consisting of ½-inch diameter polyethylene tubing looped back and forth through the CT gantry was run at the following seven flow velocities: 54.2, 49.1, 42.4, 38.3, 31.6, 23.5 and 8.6 cm/second. For each flow velocity, a 20 cc bolus of dilute iohexol was injected into the upstream siphon at 10 cc/second after which cine images were obtained at three settings: 1) "optimal" (16 X 2.5 mm thick slices every 0.25 second); 2) "standard" (8 X 5.0 mm thick slices every one second); and 3) "intermittent" (8 X 5.0 mm thick slices every two seconds). Image processing software was used to plot time-attenuation curves for each slice and flow velocity was calculated to be the slope of the trend line of the "mean time" (mean transit time weighted by HU enhancement) of each slice plotted against its distance from the first slice. These velocity measurements were compared to two reference standards: 1) flow velocity derived from volume of water delivered per second divided by the cross-sectional area of tubing, and 2) flow velocity derived from the length of tubing between the proximal and distal portions of siphon imaged in the CT gantry divided by the difference in their times to peak enhancement. Correlation between the three methods was determined by Pearson's correlation, and further analyzed by Bland-Altman plots.

Results: The "optimal" setting gave velocities of 52.2, 44.4, 39.2, 36.2, 28.7, 21.4 and 7.5 cm/second, respectively, yielding errors of 4-13% and 2-11% when compared to the two reference standards, respectively (r=0.9982 and 0.9975, respectively). The "standard" setting gave velocities of 47.3, 47.1, 43.5, 35.4, 27.9, 19.8 and 6.9 cm/second, respectively, yielding errors of 2-19% and 0-16%, respectively (r=0.9884 and 0.9784, respectively). The "intermittent" setting gave velocities of 84.0, 84.7, 48.4, 34.2, 43.3, 19.8 and 12.1 cm/second, respectively, with a lower correlation (r=0.9125 and 0.7547, respectively). The mean time-derived velocities of the "optimal" setting were closer to the velocities of the reference standards, as determined by Bland-Altman plots.

Conclusion: Our novel dynamic contrast-enhanced MDCT accurately estimates flow velocity in a phantom model. While further study is warranted, such physiological blood flow velocity information could complement anatomic findings or provide the basis for table speed settings at CT angiography.

10:40 am

085. Clinical Feasibility of Arterial Phase Dual Energy CT Imaging For Endovascular Aortic Aneurysm Repair

Numburi, U.[1,2]; Greenberg, R.[1]; Saba, O.[3]; Flamm, S.[1]; Halliburton, S.[1,2]; Schoenhagen, P.[1] 1. Cleveland Clinic, Cleveland, OH; 2. Cleveland State University, Cleveland, OH; 3. Siemens Medical Solutions, Malvern, PA*
Address correspondence to U. Numburi (numburu@ccf.org)

Objective: Triple phase (noncontrast, arterial, venous) single energy CT (SECT) scans are often used to monitor patients after endovascular thoracoabdominal aortic aneurysm repair. We investigated the feasibility of replacing noncontrast and arterial phase SECT scans with a single arterial phase dual energy CT (DECT) scan and generating virtual noncontrast images.

Materials and Methods: Twenty-two patients were imaged using a novel DECT protocol on a dual source CT scanner (Siemens Medical Solutions, Forchheim, Germany). Each patient received 120-150 ml of contrast agent Iopromide 370 mgI/ml,

Berlex, Montville, NJ) at 3 ml/second prior to scanning the chest, abdomen and pelvis with the following parameters: tube voltage, 140 kVp (Tube A), 80 kVp (Tube B); tube current-time product, 110 mAs (Tube A), 467 mAs (Tube B) with anatomic-based modulation employed for each tube; gantry rotation time, 500 milliseconds (ms); slice collimation, 14 x 1.2 mm; pitch, 0.6. Both an 80 kVp and a 140 kVp image set were reconstructed (3.0 mm slice thickness, medium smooth kernel [D30f]. Virtual noncontrast images were created from the 80 and 140 kVp images based on a three material decomposition technique for separating iodine from surrounding tissue. Arterial images were created by combining 80 and 140 kVp images in 30:70 ratio. A second scan was performed covering the same range after a five minute delay to capture the venous phase using our standard SECT protocol: tube voltage, 120 kVp; tube current-time product, 270 mAs with anatomic-based modulation, gantry rotation time, 500 ms; slice collimation, 24 x 1.2 mm; pitch, 0.8, slice thickness, 3 mm; medium smooth kernel (B31f). For both SECT and DECT scans, the dose-length product was recorded and noise in the thoracic and abdominal aorta was measured.

Results: Standard noncontrast and arterial phase SECT scans were replaced with a single, novel arterial phase DECT scan in post endovascular aortic stent patients. Virtual noncontrast, arterial, and venous phase images sufficient for diagnostic evaluation were obtained for all patients. Replacement of two of three standard SECT scans with one DECT scan resulted in an overall dose savings of 30%. Noise from DECT compared to SECT images was equivalent in the thoracic aorta ($p=0.068$) but lower in the abdominal aorta ($p<0.001$).

Conclusion: Reconstruction of virtual noncontrast and arterial phase images for evaluation after endovascular thoracoabdominal aortic aneurysm repair is feasible from a single arterial DECT acquisition. In comparison to standard practice using only SECT, the use of DECT is associated with reduced x-ray exposure and lower image noise.

10:50 am

086. Automatic Plaque Removal by Dual Energy CT Angiography: Assessment of Effectiveness and Impact on Quantification of Stenosis-A Phantom Study

Werncke, T.; Meyer, B.; Wolf, K.; Albrecht, T. Charité, Berlin, Germany*
Address correspondence to T. Werncke (Thomas.Werncke@charite.de)

Objective: Dual energy (DE) CT allows automatic removal of calcified plaques from vessel lumen based on different absorption properties of calcium and iodine. The purpose of this phantom study was to evaluate the accuracy of DE CT angiography (CTA) with automatic plaque removal for grading of vascular stenoses.

Materials and Methods: Vessel phantoms of different diameters (3, 5, 8 mm), degrees of stenoses (25-100%), luminal contrast densities (150-450 HU, blood and Iomeprol, Bracco Diagnostics, Milan, Italy) and calcium plaque densities (300-750 HU) were scanned with a dual source CT (Siemens Medical Solutions, Forchheim, Germany) at 80 and 140 kV using the clinical scan protocol for runoff DE CTA. Calcium-subtracted images (luminograms) were generated. The degrees of stenoses on the calcium-subtracted images were correlated with the true stenosis grades using Lin`s concordance correlation (rc). Sensitivity and specificity for detection of relevant stenoses (>50%) were assessed.

Results: A total of 4,130 measurements were performed. Correlation of measured and true stenoses was excellent for 5-8 mm vessel phantoms with 300-450 HU luminal density and 500-750 HU plaque density (rc=0.93-0.97). Moderate correlation was obtained for 5 mm vessels with low lumen and low plaque density (rc=0.65-0.7). Correlation was poor in the smallest vessels regardless of luminal contrast or plaque density (rc=0.3-0.6). Sensitivity was 75% (3 mm vessel) to 99% (8 mm vessel) and specificity 25% (3 mm vessel) to 83% (8 mm vessel) for detection of relevant stenoses.

Conclusion: In our phantom study, automatic plaque removal with dual energy CT showed good results for heavily calcified plaques and high luminal density. Accuracy was limited for low density calcified plaque and low luminal density small vessels mainly due to poor specificity.

CARDIOPULMONARY IMAGING PAPERS

Room: 310, Level 3
Tuesday, April 28, 2009, 1:30 pm–3:00 pm
Abstracts 087-093

Moderators: *G. Reddy, M. Atalay*
Keynote Address: Imaging Evaluation of Cardiac Physiology—*G. Reddy*

1:50 pm

087. Cardiac MR Evaluation of the Influence of Time-to-Reperfusion on the Extent of the Area at Risk, Infarct Size and Microvascular Damage in Patients with ST-Elevated Acute Myocardial Infarction

Algeri, E.; Carbone, I.; Francone, M.; Cannata, D.; Iacucci, I.; Ciolina, F.; Agati, L.; Catalano, C.; Passariello, R. La Sapienza University of Rome, Rome, Italy*
Address correspondence to E. Algeri (emanuela_algeri@yahoo.com)

Objective: Myocardial salvage and limitation of infarct size (IS) expansion are the principal mechanisms by which patients with ST-elevated acute myocardial infarction (STEMI) benefit from reperfusion; current strategies aim to recanalize infarct-related artery as quickly as possible, in order to reduce ischemic window and to save viable myocardium within the risk area. The present study was designed to determine influence of time-to-treatment on the extent of IS, area at risk (RA) and microvascular obstruction (MVO) in patients with STEMI using cardiac MR (CMR) as the reference diagnostic tool.

Materials and Methods: Fifty-eight patients with STEMI targeted for primary or rescue PTCA were enrolled. Patients were divided into four groups according to different time-to-reperfusion intervals: Group A (<90 minutes; n=10); Group B (90-180 minutes; n=23); Group C (3-7 hours; n=16); Group D (7-12 hours; n=9). In all cases a CMR protocol including turbo spin echo T2-weighted short tau inversion recovery (TSE T2w-STIR), 1st-pass and delayed enhancement (DE) sequences after gadobenate dimeglumine (Bracco Diagnostics, Milan, Italy) administration was performed within one week after the acute event. IS and RA were quantified from delayed enhancement (DE) and T2-weighted MRI using a threshold-based manual contouring method; peri-infarction zone was also determined as the difference between RA and IS.MVO was defined as the hypointense zone within the infarcted segments from DE images. Measurements were normalized to left ventricle (LV) mass.

Results: Median time-to-reperfusion was 197 ± 120 minutes. Shorter time-to-reperfusion (group A) was associated with smaller IS (Group A: 9%; Group B: 15%; Group C: 14%; Group D: 18%; group A vs. Group B, C, D p=.044); after 90 minutes, incremental delays in time-to-reperfusion had less impact on IS. Larger RA (Group A: 25%, Group B: 15%; Group C: 16%, Group D: 9%) and peri-infarction zones were also observed in patients treated earlier (<180 minute: Groups A, B vs. C, D p<0.01). Lately reperfused STEMI (Group D) had significantly larger MVO areas (Group D vs. A, B, C p=.041) with higher prevalence of intramyocardial hemorrhage.

Conclusion: Our study suggest that early reperfusion with percutaneous transluminal coronary angioplasty is associated with smaller IS and has a much greater impact within the first 90 minutes, whereas lately reperfused STEMI (7-12 hours) have significantly larger areas of MVO. The peri-infarct zone is also larger in early reperfused STEMI reflecting presence of dysfunctional but salvageable myocardium within the RA.

2:00 pm

088. Quantitative MR Myocardial Perfusion Imaging at Rest and Under Cold Pressor Test

Ritter, C.; Weng, A.; Kowalski, M.; Beer, M.; Hahn, D.; Koestler, H. University of Wuerzburg, Wuerzburg, Germany*
Address correspondence to C. Ritter (ritter@roentgen.uni-wuerzburg.de)

Objective: The response of myocardial blood flow (MBF) to sympathetic stimulation with cold is modulated by endothelium-related factors. It was the aim of this study to establish an MR cold pressor test (MR-CPT) setting for quantitative analysis of myocardial perfusion values and to compare the absolute perfusion values to the myocardial rest perfusion in the same healthy subjects.

Materials and Methods: First-pass perfusion-studies were performed in ten healthy, nonsmoking volunteers (mean age 24 ± 2 years, four females, six males) using a 1.5T MR-scanner (Siemens Healthcare, Forchheim, Germany) with a multislice-steady state free precession (SSFP)-perfusion sequence (true fast imaging with steady state precession [trueFISP]) in prebolus-technique with the following parameters: time of repetition (TR) 2.8 milliseconds (ms), time of echo (TE) 1.1 ms, TI 110 ms, flip angle (FA) 50°, resolution 2.7 x 3.3 mm, slice thickness 8 mm, three slices, 1 cc-4 cc gadobenate dimeglumine, 20 cc saline-flush, flow rate 4 cc/second. An MR-CPT was established using an over head ice-water bath of the left hand. The ice-water bath lasted for two minutes. First perfusion imaging was started after one minute to assure an adequate stimulus. The second imaging series was performed 15 minutes after the cold pressor test (CPT) to examine the perfusion in rest. Perfusion series were motion corrected and segmented with an adapted and automated developer life software tool (Definiens AG, Munich, Germany) to determine myocardial contours. Subsequently the myocardium was divided into eight sectors to determine the MBF. The perfusion in all 480 sectors was quantitatively evaluated after contamination and baseline correction by deconvolving the signal-intensity-time-courses with the arterial input function using an exponential function model as residuum.

Results: The mean myocardial perfusion of the first ten examined volunteers rose from 0.61 ± 0.34 cc/g/minute at rest to 1.16 ± 0.66 cc/g/minute under CPT. All data sets could be evaluated automatically with our adapted software tool.

Conclusion: Quantitative evaluation of myocardial perfusion under MR-CPT is feasible in the MR environment using an over head ice water bath. Perfusion values show a significant increase in cold as physiological sympathetic reaction in healthy volunteers. Further investigations in patients with known impaired endothelium function are necessary to prove the clinical benefit of the method.

2:10 pm

089. Impairment in Aortic Distensibility in Patients with Bicuspid Aortic Valve is Comparable to Marfan Syndrome: A Velocity-Encoded MR Study

Boonyasirinant, T.; Setser, R.; Desai, M.; Flamm, S. Cleveland Clinic, Cleveland, OH*
Address correspondence to T. Boonyasirinant (drthananyaa@yahoo.com)

Objective: Intrinsic pathology of the aortic wall has been reported in patients with bicuspid aortic valve (BAV), as manifested by progressive aortic dilation, aortic aneurysm, and even aortic dissection in at least one-third. Impaired aortic distensibility is well-established in patients with Marfan syndrome, but scant data exists in BAV patients, particularly using velocity-encoded MR imaging (VENC-MRI). Further, despite the increased risk of aortic pathology with BAV and Marfan syndrome, there is no available data directly comparing aortic wall properties in these two patient groups. We sought to assess aortic distensibility using VENC-MRI pulse wave velocity (PWV) measurements in patients with BAV, compared to patients with Marfan syndrome, and normal controls (trileaflet aortic valve without dysfunction, and no aortic aneurysm).

Materials and Methods: VENC-MRI was performed in a total of 60 patients: 20 BAV patients, 20 age and aortic sinus diameter-matched patients with Marfan syndrome, and 20 controls. PWV was determined between the mid ascending and proximal descending aorta. Velocity measurements were made perpendicular to the long axis of the aorta at these two points. The aortic path length between the two locations was directly measured from 3D reconstruction in the oblique sagittal orientation encompassing the aortic arch.

Results: Mean age was not significantly different among BAV patients, Marfan syndrome, and controls (28.4, 28.0, and 31.6 years, respectively; $p=0.50$). Aortic sinus diameter was comparable between patients with BAV and Marfan syndrome (3.6 cm in both groups), but was significantly larger than controls (3.6 vs. 3.0 cm; $p<0.0001$). Both BAV patients and those with Marfan syndrome demonstrated increased PWV compared to controls (8.64 and 8.60 vs. 3.65 m/second; $p=0.001$). There was no difference in PWV between patients with BAV and Marfan syndrome ($p=0.99$).

Conclusion: Diminished aortic distensibility, as indicated by an augmented PWV using VENC-MRI, is present in BAV patients, and is even comparable to the impairment seen in patients with Marfan syndrome. This impairment of aortic wall compliance and distensibility in BAV patients suggests the potential need for heightened surveillance, and potentially altered surgical strategies similar to those implemented in patients with Marfan syndrome.

2:20 pm

090. Evaluation of Valve Dynamics as a New MRI Parameter in the Assessment of Valvular Aortic Stenosis

Weininger, M.; Sagmeister, F.; Herrmann, S.; Weidemann, F.; Ritter, C.; Koestler, H.; Hahn, D.; Beer, M. University Hospital of Wuerzburg, Wuerzburg, Germany*
Address correspondence to M. Weininger (weininger@roentgen.uni-wuerzburg.de)

Objective: The objective was to investigate a noninvasive assessment of the valvular response to the variation of flow during systole in patients with severe valvular aortic stenosis using velocity-encoded phase-contrast MRI (VEC-MRI) in comparison to invasive hemodynamic measurements and transthoracic echocardiography (TTE).

Materials and Methods: Sixteen patients (eight male, eight female; mean age 70 ± 8 years) with severe aortic stenosis (echocardiographic orifice area <1.0 cm^2) were examined using a 1.5T MRI scanner and a standardized scanning protocol consisting of steady-state free precession (SSFP) phase-contrast velocity imaging (VEC-MRI). Temporal changes of the aortic valve area (AVA), determined by manual planimetry of VEC-MRI images, were used to assess the valve dynamics by calculating the time-frame of the ejection period, which the AVAs spent over 85% of the maximal AVA. Calculations were done by dividing the number of frames with AVA over 85% by all frames of the ejection period. Values were expressed as percentages of the total ejection time. MRI results were compared to invasive measurements according to the Gorlin formula (AVA Gorlin) and to the effective orifice area using TTE.

Results: Values for time spent over 85% determined by VEC-MRI were as follows: 34% ± 14%. Mean values of the effective orifice area (TTE) were 0.78 ± 0.14 cm^2 and for the invasively calculated AVA Gorlin 0.79 ± 0.19 cm^2. Comparing the percentages of VEC-MRI to TTE and to AVA Gorlin a significant correlation was found for both: $r=0.61/p<0.05$; $r=0.70/p<0.01$.

Conclusion: In patients with severe aortic stenosis a high correlation was found between MRI measurements and the clinical gold standards (TTE and invasive measurements). Our data indicate that VEC-MRI could provide a new parameter for the quantification of aortic valve dynamics (opening and closing characteristics during systole). In addition it might contribute to the evaluation of the hemodynamic and physiologic severity of the aortic stenosis.

2:30 pm

091. MRI Assessment of Valve Dynamics as a New Predictor of Left Ventricular Mass Regression in Patients with Severe Aortic Stenosis Before and After Valve Replacement Therapy

Weininger, M.; Sagmeister, F.; Weidemann, F.; Ritter, C.; Koestler, H.; Hahn, D.; Beer, M. University Hospital of Wuerzburg, Wuerzburg, Germany*
Address correspondence to M. Weininger (weininger@roentgen.uni-wuerzburg.de)

Objective: The objective was to validate the hemodynamic and clinical relevance of a noninvasive MRI assessment of valvular dynamics in patients with severe aortic stenosis by determining the left ventricular hypertrophy and regression of hypertrophy after valve replacement.

Materials and Methods: Twenty-two patients (13 males, nine females, mean age 68 ± 10 years) with severe aortic stenosis, (echocardiographic effective orifice area, [EOA], <1.0 cm^2) were examined using a 1.5T MRI scanner (steady-state free precession [SSFP] phase-contrast velocity imaging, velocity-encoded [VEC] MRI; SSFP-cine-MRI) before and after valve replacement. Temporal changes of the aortic valve area (AVA), determined by planimetry of VEC-MRI images, were used to assess the valve

dynamics by calculating the time-frame of the ejection period, which AVAs spent over 85% of the maximal AVA. MRI was also used to determine the left ventricular hypertrophy (LVMI) before and after therapy, and the left ventricular mass regression (LVMR). MRI results were compared to EOA and mean transvalvular pressure gradients (PG) determined by transthoracic echocardiography (TTE).

Results: Values for time spent over 85% were 33% ± 16%. Mean MRI values of LVMI before valve replacement were 94 ± 22 g/m², after valve replacement 72 ± 17 g/m². The extent of LVMR was -23 ± 18 g/m² (-24%). Comparing the values of VEC-MRI to the left ventricular hypertrophy significant correlations were found to LVMI before therapy (r=-0.622/p=0.002) and to LVMR (r=0.624/p=0.002). TTE displayed the following mean values before/after therapy: EOA 0.78 ± 0.15 cm²/1.91 ± 0.45 cm²; PG 52 ± 18 mmHg/14 ± 5 mmHg. Compared to TTE the values obtained by MRI significantly correlated to EOA (r=0.482, p=0.023) and PG (r=-0.535, p=0.01) before therapy and to the extent of change of PG before/after therapy (r=0.49, p=0.022).

Conclusion: MRI parameters of aortic valve dynamics are associated with left ventricular hypertrophy and mass regression after valve replacement. MRI values correlate with TTE parameters of hemodynamic severity and their postoperative changes.

2:40 pm

092. Are There Typical Findings in Contrast-Enhanced CT Supporting the Diagnosis of Acute Mediastinitis Following Sternotomy?

Weininger, M.; Schimmer, C.; Ritter, C.; Hahn, D.; Beissert, M. University Hospital of Wuerzburg, Wuerzberg, Germany*

Objective: The objective is to assess if there are typical findings at contrast-enhanced CT in patients with proven acute mediastinitis following median sternotomy.

Materials and Methods: Thirty-two patients (22 male, 11 female, mean age 66 ± 12 years) with clinically proven acute mediastinitis (bacterial culture from mediastinal fluid, blood cultures, surgically obtained inflammatory tissue) received in total 48 examinations using a 64-slice CT scanner and a standardized scanning protocol. Only the initial CT scans were considered (n=32) to evaluate CT findings of acute mediastinitis. These examinations were analyzed by two experienced observers (consensus decision) for the following findings: localized fluid collections with contrast-enhancement pre- (ps) and retrosternal (rs), increased attenuation of fat (ps/rs), free gas (ps/rs), sternal dehiscence/destruction, pleural effusion, pericardial effusion, mediastinal lymph nodes.

Results: Our patients underwent CT an average of 40 ± 41 days after surgery with the earliest scan nine days and the latest 210 days following surgery. CT findings included localized fluid collections with contrast-enhancement (ps, 66%; rs, 94%), increased attenuation of fat (ps, 16%; rs, 41%), free gas (ps, 66%; rs, 53%), sternal dehiscence/destruction (53%), pleural effusion (75%), pericardial effusion (9%), mediastinal lymph nodes (78%). Of the analyzed CT findings statistical significance could only be detected for retrosternally localized fluid collections with contrast-enhancement ($p<0.05$).

Conclusion: Our data indicate that retrosternally localized fluid collections with contrast-enhancement seem to be the key CT finding to diagnose acute mediastinitis. However, the inclusion of the other nonspecific CT findings does increase the level of diagnostic confidence and may help to assess the extent of the disease.

2:50 pm

093. Follow-Up of Coronary Abnormalities in a Pediatric Population with Kawasaki Disease: Coronary MR Angiography vs. Cardiac CT Angiography

Algeri, E.; Carbone, I.; Francone, M.; Cannavale, A.; Ciolina, F.; Cannata, D.; Catalano, C.; Passariello, R. La Sapienza University of Rome, Rome, Italy*
Address correspondence to E. Algeri (emanuela_algeri@yahoo.com)

Objective: Kawasaki disease (KD) is an acute systemic vasculitis, often involving coronary arteries with the development of aneurysms which may evolve to rupture, thrombosis, up to complete occlusion. Since patients with KD need to be periodically followed-up from the time of diagnosis to evaluate the evolution of coronary disease, a noninvasive method is highly desirable. The aim of our study was to compare the ability of coronary MR angiography (MRA) and cardiac CT angiography (CTA) in identifying coronary lesions in patients with KD.

Materials and Methods: Fifteen consecutive patients with a previous diagnosis of KD underwent both a coronary MRA and a cardiac CTA. First a whole heart balanced steady state free precession (bSSFP) acquisition was performed using a 1.5T scanner, then, after the intravenous injection of a bolus of 70 mL of a high-iodine concentration nonionic contrast agent (iomeprol, Bracco Diagnostics, Milan, Italy) CTA acquisition was performed with a 64-slice CT scanner. Results of the two imaging techniques were compared with findings at previously performed selective coronary angiography (SCA).

Results: Coronary MRA produced diagnostic images in 13/15 patients, while CTA in 15/15 patients. Information provided by MRA in the 13 diagnostic exams correlated well with SCA and CTA findings. CTA findings perfectly matched with SCA findings. At CTA, the readers observed four small aneurysms, 15 medium-caliber aneurysms, 13 giant aneurysms, three segments with stenosis, and nine segments with occlusion, six of which were within an aneurysm.

Conclusion: Both coronary MRA and CTA are very useful diagnostic tools for the follow-up of patients with KD. In order to reduce radiation dose the decision to perform a cardiac CTA should be based on MRA findings.

CME credit forms and course evaluations are available online at https://www.directsurv.net/arrs/. Your user name is arrs then your badge number (for example, arrs123456) The password is arrs2009. (Please note that your badge number is also your ARRS ID number.) Please visit this site to claim your CME credit. The site opens on April 26 and will be open through May 16. In an effort to be green, ARRS is not including CME credit forms in your registration packet.

GENITOURINARY/OB/GYN (PELVIS) IMAGING PAPERS

Room: 309, Level 3

Tuesday, April 28, 2009, 1:30 pm–3:00 pm

Abstracts 094-099

Moderators: *C. Menias, E. Sadowski*
Keynote Address: Nephrogenic Systemic Fibrosis: The Impact on Patient Care—*E. Sadowski*

2:00 pm

094. The Role of FDG PET-CT in the Preoperative Staging of Pelvic Lymph Nodes in Carcinoma of the Bladder

Rankin, S.[1]; Barrington, S.[1,2]; Rankin, S.[1]; Chappell, B. [1] 1. Guy's and St. Thomas NHS Foundation Trust, Kent, United Kingdom; 2. King's College, London, United Kingdom*
Address correspondence to S. Rankin (sheila.rankin@gstt.nhs.uk)

Objective: The purpose of the study was to evaluate the value of FDG-PET in the preoperative staging of lymph node involvement in patients with transitional cell carcinoma of the bladder.

Materials and Methods: Thirty-eight patients with transitional cell carcinoma (TCC) of the bladder were included in this retrospective study. All these patients underwent FDG PET-CT prior to surgery. Diagnostic CT (30 patients) or MRI was available in 32 patients. The results of these investigations were compared to the histology of the pelvic lymph nodes obtained from bilateral pelvic lymphadenectomy or from clinical follow up.

Results: Twenty-nine patients underwent surgery and 23 had complete bilateral nodal dissection. In these 23 patients five had lymph node involvement, missed by FDG PET-CT in four. There were no false positives. Diagnostic CT missed lymph node metastases in four patients and there were two false positives. In the remaining nine patients clinical follow up was obtained and PET-CT correctly identified lung cancer in two, bone metastases in three and a lung metastasis in one and nodal metastases in five. CT missed the bone metastases in two patients.

Conclusion: PET-CT has a high positive predictive value for the detection of lymph node metastases and is more specific than diagnostic CT, however the low sensitivity limits its use in preoperative lymph node staging in bladder cancer. It is of value in the detection of distant metastases, which may impact on patient management.

2:10 pm

095. Decreased Uptake of Ferumoxtran-10 in Inguinal Lymph Nodes in Lymphotropic Nanoparticle-Enhanced MRI

Islam, T.[1]; Hahn, P.[2]; Harisinghani, M.[1] 1. Center for Molecular Imaging Research/Massachusetts General Hospital, Boston, MA; 2. Massachusetts General Hospital, Boston, MA*
Address correspondence to T. Islam (Islam.Tina@mgh.harvard.edu)

Objective: Lymphotropic nanoparticle-enhanced MRI (LNMRI) has been shown to cause a homogeneous drop in signal intensity of benign lymph nodes. In patients with primary prostate cancer we evaluated morphological characteristics of inguinal lymph nodes and their signal intensity behavior on LNMRI. This patient population was selected because their inguinal lymph nodes are likely to be benign.

Materials and Methods: Twenty-nine patients with prostate cancer (mean age 63 years) underwent T2-weighted fast spin echo and T2*-weighted gradient echo MR imaging before and 24-36 hours following the intravenous administration of ferumoxtran-10 (AMAG Pharmaceuticals Inc, Cambridge, MA). On the precontrast images shape (oval or round), border contour (well- or ill-defined), hilum status (presence or absence of fatty hilum), signal homogeneity (homogeneous or heterogeneous) were described and nodal short axis diameters were measured for inguinal nodes. On the postcontrast T2*-weighted images the percentage (<30%, 30%-50%, or >50%) of high signal intensity within the benign inguinal nodes were estimated.

Results: A total of 233 inguinal lymph nodes were examined in 29 patients; 93.6% were oval, 57.9% showed a fatty hilum, 90.6% showed a well-defined border, and 92.3% a homogeneous signal. Mean short axis nodal diameter was 0.42 cm (+/- 0.17). Estimated high signal intensity of <30% was found in 31.3% of all groin nodes, indicative of benign differentiation. Estimated high signal intensity region between 30%-50% and >50% was found in 23.2% and 45.5% respectively, mimicking malignant features.

Conclusion: In a patient population with unlikely tumor involvement of inguinal lymph nodes, 68.7% of the presumed benign nodes show a high signal intensity region larger than 30% on LNMRI, similar to that observed in malignant lymph nodes. Benign inguinal lymph nodes take up nanoparticles less avidly than benign deep nodes do. Consequently, different standards must be used in interpreting the appearance of inguinal nodes on LNMRI performed for tumors that typically spread to the groin.

2:20 pm

096. Bladder Cancer Metastases: Assessment with Noncontrast MR and Diffusion-Weighted Imaging

Shaikh, A.[1]; Berggruen, S.[2]; Hammond, N.[2]; Wood, C.[2]; Harmath, C.[2]; Nikolaidis, P.[2] 1. Chicago Medical School, North Chicago, IL; 2. Northwestern University Feinberg, Chicago, IL*
Address correspondence to S. Berggruen (senta.berggruen@nmff.org)

Objective: With nephrogenic systemic fibrosis (NSF), gadolinium restrictions warrant an altered approach to MR imaging in certain patients. Thus, the purpose of this feasibility study was to evaluate the accuracy of nongadolinium enhanced and diffusion-weighted sequences in identifying metastases from bladder cancer.

Materials and Methods: MRI scans performed on 42 patients (two with no bladder malignancy, five localized disease, 13 metastatic disease, and 22 without cancer recurrence) were evaluated retrospectively by a radiologist blinded to gadolinium sequences and diagnoses. The reader reviewed nonenhanced T1-weighted, T2-weighted, and opposed phase imaging of the abdomen and pelvis. Additionally, B-value 500 seconds/mm^2 and b-value 50 seconds/mm^2 were recorded from diffusion-weighted imaging

(DWI) to generate ADC values for identified lesions. The reader then assigned each patient as "negative or no recurrence", "localized malignancy", or "metastatic disease".

Results: Twenty-two of the 24 negative/no recurrence patients were correctly identified (92%). Two of the five localized bladder cancer patients were correctly identified (40%). Eleven of the 13 patients with metastatic disease were correctly identified (85%). The average ADC measurement for metastases was 1.50 (SD 0.3).

Conclusion: While studies have shown restricted diffusion in primary bladder carcinoma, we demonstrate that metastases also have restricted diffusion. However, localized disease was more difficult to identify. Our results suggest that noncontrast MR and DWI MR may serve as an important diagnostic adjunct for evaluation of urinary bladder metastatic disease and surveillance for tumor recurrence, with some limitations.

2:30 pm

097. Pelvic Lymph Node Staging of Gynecological Malignancy with Diffusion-Weighted MRI

Chew, M.[1]; Holalkere, N.[2]; Guimaraes, A.[1]; Hahn, P.[1]; Lee, S.[1] 1. Massachusetts General Hospital, Cambridge, MA; 2. Boston Medical Center, Boston, MA*
Address correspondence to M. Chew (mal_chewbacca@hotmail.com)

Objective: The objective was to evaluate the accuracy of diffusion-weighted imaging (DWI) with apparent diffusion coefficient (ADC) measurements in detecting nodal involvement by tumor.

Materials and Methods: Forty patients with gynecological malignancy and pelvic MRI with DWI over a two-year period were retrospectively reviewed. Standard of reference for lymph node tumor involvement was pathology with no interval therapy or concurrent PET-CT imaging. Nodal specimens were correlated either by nodal station with pathology or node by node with PET-CT. Axial echo planar spin-echo DWI was acquired at 1.5T with field of view=34 x 26 cm, 8/2 mm thickness/gap, 15 slices per 3.5 minute free breathing sequence, TE/TR 50/5,000 milliseconds, matrix 128 x 128, bandwidth + 125 kHz, b=0 and 1,000 seconds/mm^2. Analysis was performed independently by two readers blinded to reference data. Qualitatively, lesions were compared to myometrium or skeletal muscle and considered malignant by displaying restricted diffusion if they were hyperintense on DWI and hypointense on ADC maps. Quantitative analysis involved measuring ADC values of the lesion. ADC<1,000 was considered malignant. Study performance characteristics were calculated for qualitative and quantitative analysis.

Results: Analysis of 47 nodal specimens was performed either by nodal station with a pathologic standard in 32% (15/47) and by node by node with a PET-CT standard in 68% (32/47). Cervical (30/47), endometrial (16/47) and ovarian (1/47) cancer nodal specimens were included. Qualitative analysis for all nodal specimens yielded a sensitivity, specificity, and accuracy of 88% (14/16), 86% (31/36) and 87% (45/52) respectively. Qualitative analysis for pathologically correlated nodal stations yielded a sensitivity, specificity, and accuracy of 100% (4/4), 91% (10/11) and 93% (14/15) respectively. Qualitative analysis for PET-CT correlated nodes yielded a sensitivity, specificity, and accuracy of 89% (8/9), 83% (19/23) and 84% (27/32) respectively. Quantitative analysis for all nodal specimens yielded a sensitivity, specificity, and accuracy of 92% (12/13), 26% (9/34) and 45% (21/47) respectively.

Conclusion: DWI is accurate in discriminating malignant from benign pelvic lymph nodes and should be included in MRI staging of patients with gynecologic malignancy.

2:40 pm

098. Diffusion-Weighted MR Imaging in the Assessment of Tumor Grade in Endometrial Cancer

Bharwani, N.; Narayanan, P.; Sahdev, A.; Reznek, R.; Rockall, A. Barts and The London NHS Trust, London, United Kingdom*
Address correspondence to N. Bharwani (nishatbharwani@gmail.com)

Objective: The objective was to determine if there is a correlation between tumor grade and apparent diffusion coefficient (ADC) in endometrial cancer.

Materials and Methods: Fifteen patients with endometrial cancer underwent diffusion-weighted MR imaging on a 1.5T MR unit, torso phased array coil (Philips Healthcare, Bothell, WA) using six b-values (0, 50, 100, 250, 500, 750). ADC maps were produced and the tumor ADC values were correlated with histological tumor grade obtained at hysterectomy (14 patients) or endometrial biopsy (one patient). MRI images were independently reviewed by two experienced readers and intra- and interobserver variability documented.

Results: The mean ADC value (10^{-3} mm^2/s) of grade 1 (n=6), 2 (n=2) and 3 (n=3) tumors was 0.85 (SD 0.06), 0.94 (SD 0.002) and 0.79 (SD 0.08) respectively. Using linear regression analysis, a good correlation (R=0.60) was obtained between tumor grade and ADC value. There was a significant difference ($p<0.05$) between ADC values of grade 1 and grade 3 tumors. No significant difference was seen between ADC measurements for grade 1 vs. 2 and grade 2 vs. 3 tumors. One patient had benign endometrial hyperplasia, the endometrial ADC value was 1.45.

Conclusion: High tumor grade is an adverse prognostic factor in endometrial cancer. This study is ongoing but preliminary data suggests a good correlation between ADC values and histological grade. Potentially this information, taken in conjunction with a biopsy, may improve preoperative prognostication and thereby optimize patient management.

2:50 pm

099. Image-Guided Drainage of Tubo-Ovarian Abscesses: How Often Do We Succeed?

Levenson, R.[1]; Pearson, K.[1]; Saokar-Rebello, A.[2]; Lee, S.[1]; Mueller, P.[1]; Hahn, P.[1] 1. Massachusetts General Hospital, Cambridge, MA; 2. Boston University Medical Center, Boston, MA*
Address correspondence to R. Levenson (rbl500@yahoo.com)

Objective: Tubo-ovarian abscesses (TOA) that fail conservative management with antibiotics have conventionally been treated with salpingo-oophorectomy. Image-guided TOA drainage offers

an alternative to surgery. We reviewed the etiologies, interventional methodology, and success rate for nonsurgical, image-guided drainage of TOAs.

Materials and Methods: Under IRB approval, we searched our hospital and radiology databases to identify all patients who underwent imaging-guided drainage of TOAs from 2000-2008. Patient history was obtained from the electronic medical record. Imaging approach, needle/catheter manipulation, fluid yield and technical success were determined from PACS images and from radiology and laboratory reports.

Results: Fifty-three TOAs were drained in 46 females (mean age 44.6, 16-95). Thirty (57%) were drained percutaneously using CT guidance and 23 (43%) were ultrasound-guided (21 transvaginal, two transabdominal). Forty-nine cases were drained with catheter(s) left in and four were drained with aspiration alone. Of abscesses drained under CT, 22/30 (73%) were approached from anterior, 7/30 (23%) transgluteal, and one required anterior and transgluteal catheters. A total of 49/53 (93%) cases were technically successful; 9/53 (17%) required redrainage after the initial procedure. Abscess etiologies include pelvic inflammatory disease (PID) (32%), gastrointestinal (GI) related (38%), OB-GYN surgery (19%) and other (11%). GI related causes include diverticulitis (14), appendicitis (4), and Crohn's disease (3). Image-guided drainage avoided salpingo-oophorectomy in 38 cases (72%). Salpingo-oophorectomy was ultimately performed more often in GI-related cases (11/20, 55%) then for all other causes (4/33, 12%, $p<0.001$). After image-guided drainage, mean follow-up time is 44 months (0-107) for those that have not had related surgery. In patients who underwent associated surgery, surgery was performed on average 2.2 months (0.5-5) after initial drainage.

Conclusion: TOAs, especially those of gynecologic origin, can often be successfully treated with image-guided aspiration or catheter drainage. Image-guided drainage/aspiration should be considered as an alternative to salpingo-oophorectomy for the treatment of TOAs.

CARDIOPULMONARY IMAGING PAPERS

Room: 310, Level 3
Tuesday, April 28, 2009, 4:00 pm–6:00 pm
Abstracts 100-107

Moderators: *M. Parker, K. Birchard*
Keynote Address: Radiation Dose Reduction Strategies in Chest CT Scanning—*M. Parker*

4:40 pm

100. Truths and Myths of CT-Guided Thoracic Biopsies: Factors Affecting Complications

Joshi, G.[1]; Javidan-Nejad, C.[2,3]; Pilgram, T.[2,4]; Fattahi, R.[5]; Shaw, H.[6]; Ritter, J.[3,7] 1. University of Missouri Columbia, Columbia, MO; 2. Mallinckrodt Institute of Radiology, St. Louis, MO; 3. Washington University School of Medicine, St. Louis, MO; 4. Electronic Radiology Laboratory, St. Louis, MO; 5. No Institutional Affiliation; 6. University of Maryland School of Medicine, Baltimore, MD; 7. Department of Pathology, St. Louis, MO*
Address correspondence to G. Joshi (joshig@health.missouri.edu)

Objective: The objective was to determine the factors affecting pneumothorax (PTX) rate and severity, chest tube usage, hospitalization, and radiation dose of CT-guided fine needle aspiration of thoracic lesions.

Materials and Methods: This is a retrospective analysis of 627 consecutive CT-guided transthoracic biopsies of 586 patients performed at our center over five years. Records were examined for patient factors (age, sex, prior cancer), pathologic diagnosis and complications (PTX severity, chest tube usage and number of hospitalization days). Images were reviewed for lesion factors (size, location, depth from skin and pleura, presence of cavitation, pleural and chest wall invasion), technique factors (patient position, needle entry site, angle and throw, and radiation dose), and complications (PTX, hemorrhage, and pneumomediastinum). PTX severity was graded by chest radiography description one hour after biopsy as small, moderate and large. Emphysema was graded on CT imaging as none, mild, moderate or severe emphysema.

Results: Of all biopsies, 21% developed pulmonary hemorrhage and 45% developed PTX, 26% of which led to chest tube placement; 18% of all patients were hospitalized after biopsy (2.3 days +/- 2.5, 0.5-14 days). Mean radiation dose was 9,352 mAs (range 1,535-20,677 mAs, STD 4,258). For cases leading to PTX mean lesion diameter was 2.7 cm (range 0.5 - 8.8 cm, STD 1.4) and for those who did not develop PTX the mean was 3.7 cm (0.9 -19.9 cm, 2.2 STD). Of lesions showing pleural invasion (25.4% of all lesions), 17% developed PTX, when compared to a 42% PTX rate of lesions without pleural invasion. No patients with lesions showing chest wall invasion (25/627) developed PTX ($p<0.05$). Lateral/oblique positioning had a higher rate of PTX than other positions ($p<0.05$). The likelihood of developing a PTX was 18% when the lesion abutted the pleura, 38% when 1-10 mm from the pleura, 53% when 11- 40 mm from the pleura, and 60% when > 40 mm from pleura ($p<0.05$). Although presence or severity of emphysema had no correlation with PTX rate, when PTX occurred it resulted in a larger PTX, increased chest tube usage and more hospitalization days ($p<0.05$).

Conclusion: Knowing the factors leading to CT-guided thoracic fine needle aspiration complications helps in appropriate planning of this widely used procedure. Nodule size, depth from pleura, pleural and chest wall invasion, and oblique/lateral patient positioning are associated with increased rate of PTX. Emphysema severity has no correlation with PTX rate, but results in more eventful episodes with greater thoracostomy and hospitalization.

4:50 pm

101. CT-Guided Thoracic Biopsies: A Five-Year Retrospective Study of Outcomes

Joshi, G.[1]; Javidan-Nejad, C.[2,3]; Pilgram, T.[2,3]; Ritter, J.[2,4] 1. University of Missouri Columbia, Columbia, MO; 2. Washington University School of Medicine, Saint Louis, MO; 3. Mallinckrodt Institute of Radiology, Saint Louis, MO; 4. Department of Pathology, Saint Louis, MO*
Address correspondence to G. Joshi (joshig@health.missouri.edu)

Objective: The objective was to determine the accuracy rate and factors associated with reliable diagnosis in patients undergoing percutaneous CT-guided biopsy of thoracic lesions.

Materials and Methods: This is a retrospective chart and image review of 627 consecutive CT-guided fine needle aspiration (FNA) biopsies of pulmonary, mediastinal, and pleural lesions in 586 patients at our center between 2002 and 2006. We categorized pathology reports as diagnostic, indeterminate, and nondiagnostic (non-DX). Diagnostic samples were either confidently negative or positive for malignancy or infection. Indeterminate samples were defined as samples where the pathologist would not conclude a definitive positive or negative diagnosis for cancer or infection. Non-DX samples were defined as those where the sample was deemed unsatisfactory for diagnosis due to hypocellularity, usually due to inadequate sampling. The final outcome of the initial lesions was determined by pathologic and/or microbiologic diagnosis of cancer or infection on eventual surgical resection or follow-up imaging. 37 patients had both FNA and core biopsies (CB) of the same lesions. The pathologic diagnoses by FNA and CB were compared to the final outcome.

Results: Of the 586 patients, initial FNA was positively diagnostic in 381 (65%), negatively diagnostic in 28 (5%), 108 were indeterminate (18%), and 69 were non-DX (12%). Of the 28 negatively diagnostic samples, 11 were found to have cancer (39%). Of the 177 patients with no diagnosis from initial biopsy (non-DX and indeterminate groups), 102 ultimately had cancer (58%). Procedures resulting in no diagnosis had a significant association with increasing radiation dose. Diagnostic samples were correlated with increased number of passes, however after six passes, there was no improvement in rate of diagnosis. Diagnostic samples increased with age, tumor size, and chest wall invasion and had an inverse correlation with depth from pleura. Prone patient position had the highest rate of diagnosis, while oblique and lateral had the lowest rate. Needle throw, entry site, and use of CT-fluoroscopy were not found to be significant in yielding diagnostic samples. Of the lesions biopsied both by FNA and CB, the incidence of indeterminate and non-DX biopsies were not significantly different and CB was falsely negative in 3/28 (10.7%) of the cases with a final outcome of cancer.

Conclusion: Indeterminate and non-DX results of CT-guided biopsy are highly likely to have a final outcome of cancer. Knowing the factors leading to biopsies yielding a more definitive diagnosis is helpful.

5:00 pm

102. Effect of an Externally Applied Custom-Designed Tungsten-Antimony Composite In-Plane Breast Shield on Potential Lesion Conspicuity during Chest CT

Parker, M.[1]; Kelleher, N.[1]; Ellison, E.[1]; Witten, T.[2]; Bennett, S.[1]; Cockrell, C.[1]; Grizzard, J.[1]; Halvorsen, R.[1]; Fatouros, P.[1] 1. Medical College of Virginia Hospitals, Mechanicsville, VA; 2. Virginia Commonwealth University, Richmond, VA*
Address correspondence to M. Parker (msparker@vcu.edu)

Objective: The objective was to determine the potential adverse effects an externally applied custom-designed tungsten-antimony composite breast shield may have on the conspicuity of lung nodules during chest CT and whether the noise created by this shield is diagnostically acceptable.

Materials and Methods: The thorax and chest wall of an adult female was simulated by combining a custom-designed torso phantom with bilateral tissue equivalent breast phantoms. Six sets of custom-designed target lesions of varying diameters (5 mm, 7.5 mm, 10 mm) and attenuations were randomly positioned in the lung tissue equivalent. The phantom was consecutively scanned six times with a 16-detector CT employing three different imaging parameters: *V1 (pulmonary embolus CT angiography protocol)*; *V2 (standard chest protocol)*; and *V3 (low dose protocol)*. The first set of scans was performed without shielding. The second set of scans was performed with the custom-designed breast shield applied. Four different blinded radiologists reviewed the scans and were asked to: (1) identify as many lesions as possible; (2) estimate the lesion diameter; (3) estimate the attenuation of identified lesions; and (4) grade the level of noise generated by the shield.

Results: A total of 96% of target lesions were identified; 58.3% of lesion diameters were estimated correctly; 34.6% overestimated and 3.2% underestimated. Accurate lesion attenuation estimation was problematic; 85/156 target lesions were mischaracterized for a 54.5% error rate. A total of 65/108 benign lesions were mischaracterized as indeterminate for a 60% error rate and 8/48 indeterminate lesions were mischaracterized as benign for a 16.7% error rate. Smaller diameter lesions had more errors in attenuation estimates. There were 49 errors with 5 mm diameter lesions (error rate 68.1%); (49/72). A total of 29/40 5 mm benign lesions were mischaracterized as indeterminate (error rate 72.5%). Noise scores were rated as *none* or *mild* by all radiologists in run *V1* except for one *moderate* score. Noise scores were rated as *none* or *mild* by radiologists two, three, and four on run *V2*. The *least noise* was recorded on run *V1* and the *most* on run *V3*. No *moderate-severe noise* scores were recorded.

Conclusion: This breast shield design does not adversely effect the identification or quantification of small target pseudonodules in phantoms. However, the shield does adversely effect the estimation of a lesion's attenuation precluding confident differentiation of benign and indeterminate lesions. The noise generated by the shield's application is acceptable amongst tested radiologists.

5:10 pm

103. Use of Computer-Aided Detection in Overlooked Lung Cancer on Chest Radiography

Chen, J.; Flukinger, T.; Jeudy, J.; White, C. University of Maryland Medical Center, Baltimore, MD*
Address correspondence to J. Chen (josephjschen@gmail.com)

Objective: Missed lung cancer continues to be a serious challenge for radiologists. We analyzed a computer-aided detection (CAD) system using updated software to identify lung cancer not recognized by the radiologist on initial interpretation of the chest radiograph.

Materials and Methods: Between 1995 and 2006, 3,000 patients who were diagnosed with lung cancer from an institutional registry were identified. Two radiologists reviewed all chest radiographs prior to the discovery of the lung cancer to determine if a lesion was present retrospectively. The size and location of missed lesions were documented. The radiographs containing the missed lesions were analyzed by a chest radiography CAD system (Riverain Medical, Miamisburg, OH) in three different sensitivity settings (reduced false positive, default setting, higher sensitivity).

Results: A total of 112 radiographs with missed lung cancer were found among 88 patients (38-86 years of age, mean age of 65 years, 79 men, nine women). Lesions ranged in size from 0.4-5.5 cm (mean size - 1.8 cm) and were most common on the right (55%) lung, in the periphery (75%) and in the upper lobes (79%). The reduced false positive, default setting, and higher sensitivity CAD identified 51 (45%), 56 (50%) and 62 (55%) of the nondetected lesions on a per-film basis, respectively; 38 (44%), 42 (48%), and 47 (54%) on a per-patient basis. False positive rate per chest radiograph was 2.6, 3.2 and 3.6, respectively. There was a significant difference found in the location of the nodules detected by CAD and those that were not detected ($p<0.01$-0.05). However, no statistical difference was found in nodule size.

Conclusion: Chest radiographic CAD shows potential to detect many lesions overlooked by radiologists. The use of CAD in different operating points gives radiologists a preference in trade-off between sensitivity and false positives in the detection of subtle lung cancers.

5:20 pm

104. Visual Semiquantitative Approach to Scoring Lung Cancer Treatment Response Using CT: A Pilot Study

Gottlieb, R.[1]; Kumar, P.[1]; Loud, P.[1]; Klippenstein, D.[1]; Raczyk, C.[1]; Tan, W.[1]; Lu, J.[1]; Ramnath, N.[2] 1. Roswell Park Cancer Institute, Williamsville, NY; 2. University of Michigan, Ann Arbor, MI*
Address correspondence to R. Gottlieb (radwize@aol.com)

Objective: Our objectives were to compare a newly developed semiquantitative visual scoring (SVS) method with the current standard, the Response Evaluation Criteria in Solid Tumors (RECIST) method, in the categorization of treatment response and reader agreement for patients with metastatic lung cancer followed by CT.

Materials and Methods: The 18 subjects (five women, 13 men, mean age=62.8 years) were from an institutional review board approved phase II study that evaluated a second line chemotherapy regimen for metastatic nonsmall cell lung cancer. Four radiologists, blinded to patient outcome and each other's reads, evaluated the change in patient tumor burden from the baseline to the first restaging CT scan using either the RECIST or SVS method. We compared the numbers of patients placed into the partial response (PR), stable disease (SD), and progressive disease (PD) categories (Fisher's exact test) as well as observer agreement (kappa statistic).

Results: Requiring concordance of three of four readers resulted in RECIST placing 17/17 patients (100%) in the SD category compared with SVS placing 9/15 patients (60%) in the PR, 5/15 patients (33%) in the SD, and 1/15 patients (6.7%) in the PD categories ($p<0.0001$). Interobserver agreement was higher for readers using the SVS method (kappa statistic=0.54, $p<0.0001$) compared with the RECIST method (kappa statistic=-0.01, $p=0.5378$).

Conclusion: Using the SVS method readers more finely discriminated between patient response categories with superior agreement compared with the RECIST method, which could potentially result in large differences in early treatment decisions for advanced lung cancer.

5:30 pm

105. Effect of Computer-Aided Diagnosis on Radiologists' Detection Performance of Subsolid Pulmonary Nodules on CT: Initial Results

Godoy, M.[1]; Ko, J.[1]; Kim, T.[2]; Naidich, D.[1]; Bogoni, L.[3]; Florin, C.[3]; De Groot, P[1].; White, C. [4]; Vlahos, I.[1]; Park, S.[3]; Salganicoff, M.[3] 1. New York University, New York, NY; 2. Seoul National University Bundang Hospital, Seongnam–si, Korea; 3. Siemens Medical Solutions, Malvern, PA; 4. University of Maryland Medical Center, Baltimore, MD*
Address correspondence to M. Godoy (migbarco@gmail.com)

Objective: The objective was to establish the sensitivity of a computer-aided detection (CAD) prototype developed for detection of subsolid and solid pulmonary nodules on CT, and to evaluate CAD's effect on radiologists' detection of pulmonary nodules.

Materials and Methods: Forty-six chest MDCT scans with known subsolid nodules were selected by report from a pool of cases with lung nodules from two institutions. These CT scans had not been previously used for CAD development/training. Four chest radiologists independently reviewed 1.0 mm sections for each case; marking all lung nodules and rating their confidence (scale 1-4). Nodules were characterized by maximum diameter and attenuation, which included pure ground-glass (GG), part-solid (PS), and solid nodules (SN). CAD marks for each CT were generated by a prototype CAD device. All four radiologists subsequently reviewed CAD results for each case. Discrepancies between readers for the presence or characterization of the nodules were resolved by a fifth experienced chest radiologist.

Results: A total of 279 nodules were adjudicated as ground-truth. After exclusion of nodules <4 mm and GG nodules <6 mm, a total of 118 nodules were evaluated (median maximum diameter 5.5 mm, range 4.0-27.5 mm), including 62 SN, 20 PS and 36 pure GG nodules. The sensitivity of CAD was 79% (overall), 87% (SN), 85% (PS) and 61% (GG). CAD increased reader sensitivity in all subgroups. The range of the sensitivity of the readers (minimum-maximum, mean sensitivity) improved as follows: from 62%-85%, 68% before the use of CAD to 74%-99%, 83% with CAD for overall nodules; from 48%-71%, 60% to 77%-100%, 85% for SN; from 65%-95%, 80% to 95%-95%, 95% for PS; from 50%-94%, 75% to 72%-100%, 86% for GG. The overall impact of CAD was significant for all four readers ($p<0.001$). CAD false positive rate ranged from 0-9 per scan (median 2). The use of CAD did not increase the number of false positives for any of the readers.

Conclusion: CAD positively impacts the detection of both solid and subsolid nodules without significant increase in false positive rates. Radiologists' detection performance improves with the use of CAD as a second reader for all nodule types including pure GG and PS nodules, usually not detected by previous CAD systems, yet of clinical significance since they are often indicative of adenocarcinoma and its premalignant forms.

5:40 pm

106. Value of Lateral View in Routine Screening Chest Radiographs of Purified Protein Derivative Positive Patients

Eisenberg, R.; Romero, J.; Bankier, A.; Boiselle, P.; Litmanovich, D. Beth Israel Medical Center, Boston, MA*
Address correspondence to R. Eisenberg (rleisenb@bidmc.harvard.edu)

Objective: In screening individuals with positive purified protein derivative (PPD) for suspected tuberculosis, many employee health centers routinely obtain posteroanterior (PA) and lateral radiographs. Because restriction to a single PA radiograph can potentially reduce patient irradiation and examination costs and increase throughput, we tested the hypothesis that the lateral projection adds no clinically relevant information to the PA view and can be eliminated in this setting.

Materials and Methods: All adults with positive PPD results referred from our employee health service during 2007 underwent routine screening PA and lateral chest radiographs. Two radiologists retrospectively and independently interpreted each study for evidence of abnormalities suggestive of acute or chronic tuberculous infection. For each case, the PA radiograph was initially reviewed. The lateral projection was then analyzed to determine how frequently it demonstrated an abnormality not apparent on the PA view or changed the interpretation of any abnormalities seen on the PA projection. When the two readers disagreed, the final decision was made by a third radiologist serving as an arbitrator. Radiation doses for PA and lateral chest radiographs were obtained from hospital annual survey data.

Results: The study cohort comprised 875 individuals (483 women, 392 men), ranging in age from 18 to 63 (median, 35 years). Of the 91 individuals with positive PPD who had radiographic abnormalities, the most commonly observed findings were: calcified lymph node or granuloma in 36 (39.6%); apical pleural thickening in 24 (26.4%); noncalcified nodule(s) in 23 (25.3%); and fibrous scarring in 11 (12.1%). The PA view demonstrated the abnormalities in all 91 individuals with positive radio-

graphs. The lateral view demonstrated abnormalities in only 16 (17.6%). All abnormalities demonstrated on the lateral projection were also seen on the PA view. When abnormalities were detected on both projections, in no case did the information provided by the lateral view change the interpretation made on the PA view alone. Based on calculated radiation doses for PA and lateral chests radiographs in our institution of 10 mrad and 75 mrad, respectively, eliminating the lateral projection would reduce the overall radiation exposure per examination by about 88%.

Conclusion: In an occupational health setting, a single PA view is sufficient for tuberculosis screening of individuals with positive PPD results and will substantially reduce radiation exposure to this population.

5:50 pm

107. MDCT of Forced Expiratory Tracheal Collapsibility: Comparison of Tracheal Morphology and Measurements Between Healthy Volunteers and Patients with Tracheomalacia

Boiselle, P.; O'Donnell, C.; Ernst, A.; Millett Pollock, M.; Potemkin, A.; Loring, S. Beth Israel Deaconess Medical Center, Boston, MA Address correspondence to P. Boiselle (pboisell@bidmc.harvard.edu)*

Objective: The objective was to compare changes in tracheal morphology and measurements between inspiration and forced expiration on paired inspiratory-dynamic expiratory CT in healthy volunteers (HVs) and patients with bronchoscopically proven tracheomalacia (TM).

Materials and Methods: We prospectively studied 51 HVs (25 males, 26 females) with a mean age of 50 (range 25 -75), normal spirometry and no history of smoking or risk factors for tracheomalacia. All participants were imaged according to a standard protocol using a 64-detector-row scanner with active respiratory coaching and spirometric monitoring of acquisitions at both total lung capacity and during forced exhalation with 40 mAs, 120 kVp, and 0.625 mm detector collimation. We retrospectively identified a comparison cohort of 17 patients (five males, 12 females) with mean age of 54 (range 36-78) with bronchoscopically proven TM who were imaged using a similar protocol without spirometric monitoring. For each examination, a thoracic radiologist determined the tracheal shape and measured the sagittal and coronal diameters of the trachea 1 cm above the aortic arch at both end-inspiration and dynamic expiration. The tracheal index (ratio of coronal to sagittal diameter) was calculated at end-inspiration and expiration for the HVs and patients with TM.

Results: All HVs and 16 (94%) of 17 TM patients demonstrated a normal tracheal configuration (round, oval, horseshoe, or inverted pear) at end-inspiration. One (6%) of 17 TM patients had an abnormal lunate configuration. At forced exhalation, HVs demonstrated the following changes in the posterior membranous wall: flattening, n=2 (4%); slight anterior bowing, n=10 (20%); mild to moderate anterior bowing with broad anterior convexity, n=17 (33%); mild to moderate anterior bowing with narrow anterior convexity, n=19 (37%); and severe anterior bowing with crescenteric configuration (also referred to as the "frown sign"), n=1 (2%). The frown sign was also observed in nine (53%) of 17 patients with TM at forced exhalation, resulting in a sensitivity of 53% and a specificity of 98% for TM. End-inspiratory tracheal index was 0.93 in HVs compared to 1.1 for TM patients. Forced expiratory tracheal index was 1.2 in HVs compared to two for patients with TM.

Conclusion: Inspiratory tracheal morphology is similar between healthy volunteers and tracheomalacia patients. Although a range of expiratory tracheal configurations may be observed in health and disease, the expiratory frown sign has a high specificity for tracheomalacia.

GASTROINTESTINAL (COLON) IMAGING PAPERS

Room: 309, Level 3
Tuesday, April 28, 2009, 4:00 pm–6:00 pm
Abstracts 108-118

Moderators: *A. Dachman, D. Caroline*
Keynote Address: The Future of Virtual Colonoscopy: Training and Maintaining—*A. Dachman*

4:20 pm

108. Should We Recommend Follow-Up Colonoscopy for Patients Under 50 Diagnosed with Diverticulitis on CT?
Nikolaidis, P.[1,2]; Kim, J.[1]; Miller, F.[1,2]; Berggruen, S.[1,2]; Hammond, N.[1,2]; Hoff, F.[1,2]; Gabriel, H.[1,2]; Yaghmai, V.[1,2]; Dhand, S.[1]; 1. Northwestern University, Feinberg School of Medicine, Chicago, IL; 2. Northwestern Memorial Hospital, Chicago, IL*
Address correspondence to P. Nikolaidis (p-nikolaidis@northwestern.edu)

Objective: The need for colonoscopy following the diagnosis of diverticulitis on CT in younger patients has not been established. The objective of this study is to assess the incidence of colorectal carcinoma and other important colonic lesions in patients aged 49 or younger diagnosed with acute diverticulitis on MDCT.

Materials and Methods: Following institutional review board (IRB) approval, we identified 340 patients less than 50 years of age with a CT diagnosis of diverticulitis, following a search of the radiology report database at our institution. Patients presented either at the emergency department or as outpatients between January 2, 2004 and August 14, 2008 with a variety of abdominal symptoms, most notably left lower quadrant pain. A total of 138 patients had a follow-up colonoscopy at our institution (83 males; 55 females). The average age of our study population was 40 years (median: 42, mode: 49, range 19-49). All colonoscopy procedure notes and histopathologic reports were reviewed. Images were reviewed on a PACS workstation by two fellowship-trained body imagers, specific CT findings including extent of diverticulosis, wall thickening, degree of surrounding fat stranding, adenopathy, presence of perforation were recorded.

Results: The majority of colonoscopies (99/139, 71%) revealed only diverticulosis and benign findings such as hemorrhoids. There was only one patient with malignancy discovered on colonoscopy, an adenocarcinoma, in a different location than the site of diverticulitis. Additional findings included 16 adenomatous polyps (all tubular adenomas) in 14 patients (10%), which were more prevalent in the 45-49 age group (11/14, 79%). One patient had an inflammatory polyp. Twenty-four other patients had other benign polyps, including hyperplastic polyps in 16, and seven pseudopolyps (lymphoid aggregates).

Conclusion: The majority of patients under 50 with a CT diagnosis of diverticulitis have benign findings on colonoscopy. Follow-up colonoscopy in this population may not be necessary, particularly in those younger than 45 years of age with no other suspicious findings, such as significant bowel wall thickening or adenopathy.

4:30 pm

109. Intrapatient Comparison of Low Dose Techniques at CT Colonography
Robbins, J.; Pickhardt, P.; Kim, D.; Ranallo, F. University of Wisconsin, Madison, WI*
Address correspondence to J. Robbins (jrobbins@uwhealth.org)

Objective: The objective was to compare patient dose and image quality using a static mA technique vs. bimodal tube current modulation at CT colonography (CTC).

Materials and Methods: Intrapatient static mA and tube current modulation techniques (GE Healthcare, Milwaukee, WI) were prospectively compared in 88 consecutive patients (mean age, 58 years) undergoing CTC evaluation. The static mA level was selected based on body mass index (BMI) and ranged from 100-300 mA with kVp=120. Smart-mA parameters included noise index=70, mA range=30-150, and kVp=140. Each patient was imaged with both techniques, randomly assigned to either the supine or prone acquisition. Effective dose and image noise for each series was calculated.

Results: Mean patient BMI was 27.8 (range, 16-45). Mean intrapatient dose reduction for tube current modulation vs. static mA technique was 28.4% (SD ± 18.5%). Dose reduction did not correlate with BMI or patient position. Mean effective dose for modulated and static mA series were 2.7 mSv and 3.8 mSv, respectively ($p<0.01$). Although objective image noise measurements were increased for the tube current modulation technique, all studies were of diagnostic quality by subjective assessment.

Conclusion: By utilizing tube current modulation at CTC, substantial reductions in radiation dose can be achieved without sacrificing diagnostic quality.

4:40 pm

110. Positive Predictive Value for Polyps Detected at Screening CT Colonography: Effect of Polyp Size, Morphology, and Diagnostic Confidence
Wise, S.; Pickhardt, P. University of Wisconsin School of Medicine and Public Health, Madison, WI*
Address correspondence to S. Wise (swise@uwhealth.org)

Objective: The objective was to determine the positive predictive value (PPV) for polyps equal to 6 mm detected at screening CT colonography (CTC) and to assess factors affecting the PPV.

Materials and Methods: A total of 639 (12.5%) of 5,124 consecutive adults undergoing CTC screening at a single institution were prospectively called positive for polyps equal to 6 mm, consisting of 958 total lesions. A total of 479 patients with 739 CTC-detected lesions were evaluated at subsequent optical colonoscopy (OC) or surgery; the remaining 219 lesions were enrolled in short-term CTC surveillance or did not undergo OC for other reasons and were necessarily excluded from analysis. PPV was derived from OC and surgical findings: CTC true positive equaled matched finding at OC (or surgery); false positive equaled not found at OC. PPV was further analyzed in terms of polyp size at CTC (6-9 mm vs. equal to 10 mm), morphology (pedunculated, sessile, flat, carpet [nonpolypoid equal to 3 cm], and invasive

mass), and diagnostic confidence of the CTC finding (3=most confident, 1=least confident).

Results: The overall PPV for CTC-detected lesions equal to six was 91.6% (677/739). PPV according to size was 90.1% (410/451) for 6-9 mm lesions and 92.7% (267/288) for lesions equal to 10 mm (p=0.4). PPV for sessile, pedunculated, flat, carpet, and invasive mass morphology was 92.4% (441/477), 97.2% (139/144), 76.8% (73/95), 100% (10/10), and 100% (14/14), respectively. Sessile or pedunculated morphology more often yielded a matching lesion than flat morphology (93.5% [580/620] vs. 76.8% [73/95]; p< 0.0001). PPV according to diagnostic confidence was 94.7% (554/585) for highest confidence (score=3), 83.4% (106/127) for intermediate confidence (score=2), and 63% (17/27) for least confidence (score=1). Level 2 or 3 confidence more often yielded a matching lesion at OC than level 1 confidence (92.7% [660/712] vs. 63% [17/27]; p<0.0001).

Conclusion: High concordance for CTC-detected lesions at subsequent OC results in an overall PPV >90% for our CTC screening program. Increased diagnostic confidence and a polypoid (nonflat) morphology correlate with a higher likelihood of finding a matching lesion at OC. Polyp size alone (6-9 mm vs. equal to 10 mm) had little effect on PPV, being >90% for both size categories.

4:50 pm

111. Flat (Nonpolypoid) Lesions at CT Colonography: Imaging and Histologic Characteristics Using a New Morphologic Definition

Robbins, J.; Pickhardt, P.; Kim, D. University of Wisconsin, Madison, WI*
Address correspondence to J. Robbins (jrobbins@uwhealth.org)

Objective: The objective was to assess the histology and morphologic definition of flat (nonpolypoid) lesions equal to 6 mm detected at CT colonography (CTC).

Materials and Methods: Results from CTC screening in 5,107 consecutive adults were reviewed for polyps prospectively categorized as flat (nonpolypoid). Lesion histology was compared against polypoid lesions (sessile and pedunculated) of similar size. Advanced histology was defined by presence of villous component, high-grade dysplasia, or cancer. Carpet lesions (laterally spreading tumors) were defined as flat lesions equal to 3 cm in size. Maximal lesion height with respect to the surrounding normal mucosa was measured to assess morphologic definition.

Results: A total of 125 flat lesions in 106 adults were prospectively identified. Mean size was 12.7 mm (range, 6-80 mm), including 73 lesions 6-9 mm, 42 lesions 10-29 mm, and 10 carpet lesions. All ten carpet lesions were neoplastic and nine (90%) were histologically advanced. Of 92 flat lesions <3 cm evaluated at colonoscopy, 23 (25.0%) were neoplastic, five (5.4%) were histologically advanced, and none was malignant. In comparison, polypoid lesions <3 cm were more likely to be neoplastic (60.3%; 363/602; p<0.001), histologically advanced (12.1%; 73/602; p=0.07), and malignant (0.5%; 3/602; NS). Nine flat lesions were seen only at colonoscopy (CTC false negative); of these none was histologically advanced and only two were neoplastic (tubular adenomas). For flat lesions <3 cm, maximal lesion height averaged 2.2 mm, with 85.2% (98/115) measuring equal to 3 mm. The mean ratio of height:width for all 125 flat lesions was 0.24 ± 0.1 and was equal to 0.40 for 92.8% (116/125) and equal to 0.33 in 86.4% (108/125).

Conclusion: Flat colorectal lesions <3 cm in size are histologically benign, rarely advanced, and often non-neoplastic, whereas large carpet lesions (equal to 3 cm) are almost always histologically advanced. Polypoid lesions <3 cm are significantly more likely to be neoplastic and histologically advanced. A maximal height:width ratio of 0.33 or 0.40 appears to be a reasonable definition for flat lesions, regardless of size.

5:00 pm

112. Feasibility of Remote CT Colonography at Two Rural Native American Medical Centers

Friedman, A.; Kilian, C.; Downing, D.; Chino, J.; Lance, P. University of Arizona, Tucson, AZ*
Address correspondence to A. Friedman (arnief51@yahoo.com)

Objective: Fort Defiance Indian Hospital and Tuba City Indian Medical Center are two rural hospitals with limited availability of screening optical colonoscopy (OC). We interpret most of their imaging via a teleradiology VPN and wanted to expand this service to include screening CT colonography (CTC). The goal is to determine whether adequate exams can be obtained with remote supervision after brief on-site instruction.

Materials and Methods: One of the authors traveled to Fort Defiance and gave a one-hour presentation on CTC for colorectal cancer screening (indications, preparation, technique, anatomy, basic pathology) to representatives from both hospitals. He conducted one CTC exam on a volunteer. Bowel preparation was with magnesium citrate, bisacodyl and barium fecal tagging. Insufflation was by a CO_2 pump. Scanning was performed at 120 kVp on either a 16 or a 32 slice MDCT in supine (50 mAs) and prone (25 mAs) positions. Data were transmitted to our local teleradiology server (10-20 minutes) and then uploaded to a CTC workstation (five minutes). Subjects were 58 females and 28 males scanned between May 21, 2008 and September 25, 2008. Mean age was 60.8 years with a range of 37-88. Indications included screening (71), heme + stool (three), iron deficiency anemia (one) and miscellaneous (11).

Results: Studies were graded for quality on a five-point scale (five being excellent, one being poor) by one author evaluating residual stool, residual fluid, and degree of distention. Residual stool assessment: 43 patients 5/5, 20 patients 4/5, 18 patients 3/5, one patient 2/5, three patients 1/5 (one of which did not take prep), one patient failed (could not retain gas). Residual fluid assessment: 37 patients 5/5, 27 patients 4/5, 16 patients 3/5, two patients 2/5, three patients 1/5, one patient failed. Distention assessment: 36 patients 5/5, 11 patients 4/5, 13 patients 3/5, 17 patients 2/5, eight patients 1/5, one patient failed. Additional technical problems encountered included vaginal insufflation (two), partial splenic flexure (two) or rectal (three) cutoff on prone images, respiratory motion artifacts (seven), photopenia hindering interpretation (two), dense iodinated contrast in stomach causing artifact (one). Eight patients were C0, 67 patients were C1, three patients were C2 (two with polyps), seven patients were C3, and one patient failed. OC referral rate was 9%. Twenty-five patients were E1, 51 were E2, three were E3 and six were E4 and one patient failed.

Conclusion: CTC can be introduced with minimal effort to rural underserved communities, adequately performed locally and then interpreted remotely by an expert.

5:10 pm

113. Comparison of High-Volume PEG Lavage with Low-Volume CT Colonography Bowel Preparations Utilizing Oral Contrast at Optical Colonoscopy

Lawrence, E.[1,2]; Pickhardt, P.[1] 1. University of Wisconsin, Madison, WI; 2. Albert Einstein College of Medicine, Bronx, NY*
Address correspondence to P. Pickhardt (pj.pickhardt@hosp.wisc.edu)

Objective: The objective was to compare the fidelity of low-volume CT colonography (CTC) bowel preparation using oral contrast with standard PEG lavage.

Materials and Methods: The study group consisted of 300 consecutive adults (mean age, 58.3 years) who underwent colonoscopy immediately after positive CTC. Bowel preparation for the study group was <1 liter in total volume, consisting of osmotic cathartic (sodium phosphate [n=266] or magnesium citrate [n=34], in conjunction with oral contrast (2% barium and diatrizoate). A control group of 300 adults (mean age, 58.3 years) underwent primary colonoscopy following standard 4-liter PEG lavage without oral contrast. The prospective preparation quality rating by the endoscopist served as the reference standard. A rating of poor/marginal was considered inadequate and adequate/good/excellent was considered diagnostic.

Results: The frequency of inadequate bowel preparation was 4.3% (13/300) in the study group vs. 12.3% (37/300) for the control group ($p<0.001$). Specifically, preparation was poor or marginal in 10 and three cases in the CTC cohort and in 29 and eight cases in the PEG cohort, respectively. Preparation quality was rated as excellent in 32% (96/300) in the CTC cohort and 23.3% (70/300) in the PEG cohort ($p<0.05$). Magnesium citrate led to fewer inadequate preps (n=1) compared with sodium phosphate (n=13).

Conclusion: At colonoscopy, low-volume bowel preparations utilizing both saline laxatives and oral contrast are more effective than high-volume PEG lavage. Beyond improvements in quality, the low-volume preparation would presumably improve patient compliance and would allow for immediate CTC if colonoscopy is incomplete, without the need for additional oral contrast tagging.

5:20 pm

114. Incidental Carcinoid Tumors of the Appendix: Imaging Appearance at Preoperative CT

Coursey, C.[1]; Nelson, R.[1]; Dodd, L.[1]; Moreno, R.[2]; Patel, M.[1]; Vaslef, S.[1] 1. Duke University Medical Center, Cary, NC; 2. Triangle Surgical Associates, Cary, NC*
Address correspondence to C. Coursey (cours002@mc.duke.edu)

Objective: The incidental detection of a carcinoid tumor of the appendix in an appendectomy specimen can be an unpleasant surprise for both the surgeon and the patient as right hemicolectomy is the definitive treatment for appendiceal carcinoid tumor depending on tumor size. The ability to prospectively identify these tumors at CT would therefore help with preoperative planning. The purpose of this project was to determine the frequency and preoperative CT imaging characteristics of appendiceal carcinoid tumors.

Materials and Methods: A surgical database search performed using the current procedural terminology codes for appendectomy and colectomy yielded 1,366 patients who underwent appendectomy (n=925 urgent, 387 incidental, 40 interval and 14 elective) and 1,761 patients who underwent colectomy from January, 1998 through September, 2007 and were at least 18 years of age at time of surgery. Pathology reports were reviewed to identify those patients in whom an appendix was removed (n=2,108) and a classical appendiceal carcinoid tumor was found (n=23). CT reports for studies that took place within the two months preceding surgery were reviewed. CT images were reviewed to determine if intravenous or oral contrast media was administered, the type of CT scanner used (4-, 16-, or 64-slice), slice thickness, and if coronal images were obtained. Medical records were reviewed to determine whether patients underwent additional treatment for carcinoid tumor.

Results: Twenty-three classical carcinoid tumors (1.1%; 15 women (65.2%), eight men (34.8%); average age 54 years (range 23-86)) were identified. The average reported tumor size was 6.1 mm (range 1.5 to 15.0 mm, n=18), and a tip or distal location was reported for all tumors for which a location was given (n=15). Eleven patients underwent preoperative CT, and CT images were available for nine of these patients. CT studies were obtained with IV and oral contrast (n=7), IV contrast only (n=1), and oral contrast only (n=1). Four studies included coronal reformations from isotropic voxels. Studies were acquired with 16- (n=8) and 4- (n=1) slice CT scanners. No tumors were identified prospectively. No patients underwent additional surgery. All patients were without evidence of recurrent disease (mean follow-up 35 months, range 0.75-81 months).

Conclusion: Classical carcinoid tumors occurred in 1.1% of appendix specimens. These tumors were small (mean size 6.1 mm, range 1.5 to 15.0 mm), located in the distal appendix or tip, and difficult to identify prospectively at CT.

5:30 pm

116. Taking Advantage of Chemical Shift Artifact: Using Out-of-Phase Imaging to Locate the Normal Appendix on MR

Horowitz, J.; Nikolaidis, P.; Hammond, N.; Gabriel, H.; Wood, C.; Miller, F. Northwestern University, McGaw Medical Center, Chicago, IL*
Address correspondence to J. Horowitz (jhorowitz77@gmail.com)

Objective: The objective was to determine if out-of-phase sequence imaging, with the chemical shift artifact, can assist in locating the normal appendix on pelvic MR exams.

Materials and Methods: Fifty consecutive adult pelvic MR exams were retrospectively reviewed by a board certified radiologist. Axial and coronal T2 half-Fourier acquisition single-shot turbo spin-echo (HASTE), axial T1 in-phase and out-of-phase, and axial postcontrast T1-weighted sequences were examined to locate the appendix.

Results: The appendix was identified on the axial and/or coronal T2 sequence in 29/50 cases (58%). In 24/50 cases (48%), the appendix was identified on the out-of-phase sequence in addition to a T2 sequence. In 11/50 patients (22%), the appendix was especially conspicuous on the out-of-phase sequence, increasing confidence in localization. In 16/50 patients (32%), the out-of-phase sequence had a characteristic appearance, with the chemical shift artifact outlining both the relatively smooth base of the cecum and a small nubbin of the base of the appendix, giving it a "button nose" appearance.

Conclusion: The out-of-phase T1 sequence can increase confidence in localizing the normal appendix on MR. This has important implications in diagnosing and excluding appendicitis, especially in populations such as pregnant, pediatric, and renal failure patients.

5:40 pm

117. MDCT in Adults Suspected of Acute Appendicitis: Impact of Oral and Intravenous Contrasts at Standard-Dose and Simulated Low Dose Techniques

Keyzer, C.[1]; Tack, D.[2]; De Maertelaer, V.[3]; Bohy, P.[2]; Gevenois, P.[1]*
1. Erasme Hospital, Brussels, Belgium; 2. Réseau Hospitalier de Médecine Sociale Baudour, Baudour, Belgium; 3. Institut de Recherche Interdisciplinaire en Biologie Humaine et Moléculaire, Brussels, Belgium
Address correspondence to C. Keyzer (caroline.keyzer@erasme.ulb.ac.be)

Objective: The objective was to prospectively investigate and compare the performance of MDCT with and without oral and/or intravenous contrast material at standard and low radiation dose in adults suspected of acute appendicitis.

Materials and Methods: In this ethical committee-approved study, 131 consecutive patients (80 women, 51 men; age range, 18-87 years; mean age, 37 years) suspected of appendicitis were randomly assigned to either ingest or not ingest iodinated contrast. Thereafter, all patients of these two groups underwent IV unenhanced and enhanced abdominopelvic MDCT with 4x2.5 mm collimation at 120 kVp and 100 effective mAs. Dose reduction corresponding to 30 effective mAs was simulated. Two radiologists independently read scans during separate sessions, and coded the following: appendix visualization, gas or contrast in its lumen, appendicolith, periappendiceal fat stranding, and abscess or phlegmon. They also measured the appendiceal diameter and proposed a diagnosis (appendicitis or alternative) with a score of confidence. Data were compared with definite diagnosis based on surgical findings or clinical follow-up using exact Pearson's and Fisher tests. Inter-reader agreements were assessed by statistics.

Results: With oral contrast, there were fewer misclassified signs ($p=<0.001$-0.012), higher appendix visualization ($p=0.003$) and higher reader's confidence in alternative diagnosis ($p=0.040$) than without oral contrast. Sensitivity, specificity, positive predictive value, negative predictive value, and accuracy for diagnosing appendicitis were not statistically significantly influenced by dose, IV contrast and readers in each randomized group ($p=0.195–0.969$). In addition, the proportions of misclassified diagnosis as compared with the definite diagnosis were not statistically different between CT protocols, groups and readers ($p=0.321—1.000$). Inter-reader agreements in the diagnosis of appendicitis were good to excellent (values ranging from 0.67 to 0.91; $p<0.001$), whatever the radiation dose and the use of oral and/or IV contrast.

Conclusion: Appendix visualisation and reader's confidence in alternative diagnosis are higher with than without oral contrast. No influence of radiation dose and contrast enhancement could be demonstrated on the diagnostic performance and on the misclassification rate of the reader's diagnosis. For diagnosing appendicitis at CT in clinically suspected patients, radiation dose could be reduced to 30 mAs. Contrast enhancement is not mandatory but improves reader's confidence.

5:50 pm

118. CT Findings of Sigmoid Volvulus

Den, E.[1]; Levsky, J.[2]; Wolf, E.[2]; Dubrow, R.[2]; Rozenblit, A.[2] 1. Albert Einstein College of Medicine, Bronx, NY; 2. Montefiore Medical Center, Bronx, NY*
Address correspondence to E. Den (eden@aecom.yu.edu)

Objective: The purpose was to evaluate features of sigmoid volvulus (SV) on CT scanograms and cross-sectional images.

Materials and Methods: This IRB-approved, HIPAA-compliant study retrospectively reviewed 21 cases of SV (15 men, six women, ages 33-93). Three radiologists evaluated scanograms and cross-sectional images for several classical and two novel imaging signs of volvulus (crossing sigmoid transitions / the "X-marks-the-spot" sign and folding of the sigmoid wall by partial twisting/ the "split-wall" sign). A general impression was assigned for scanograms and cross-sectional images. CT findings suggesting bowel compromise were compared with pathologic and endoscopic findings. Sensitivities were calculated, including subgroup analyses of cross-sectional imaging features for classical and nonclassical scanograms.

Results: The most sensitive scanogram findings were absent rectal gas (19/21, 90%) and an inverted-"U" shaped distended sigmoid (18/21, 86%), followed by the "coffee bean" sign and disproportionate sigmoid enlargement (both 16/21, 76%). The most sensitive cross-sectional findings were a sigmoid colon transition point (20/21, 95%) and disproportionate enlargement of the sigmoid (18/21, 86%). The "X-marks-the-spot" and "split-wall" signs were present in 9/21 (43%) and 11/21 (52%) patients, respectively, but one of the two signs was present in 18/21 (86%). Classic radiographic and definitive cross-sectional findings were seen in 11/21 (52%) and 16/21 (76%), respectively. Findings suggesting bowel compromise correlated poorly with clinical ischemia.

Conclusion: SV has a spectrum of imaging findings and a classic appearance is absent in approximately half of scanograms and one quarter of CT scans. New signs modeling the pathophysiology of volvulus ("X-marks-the-spot" sign for more complete twisting and "split-wall" sign for less severe twist) may improve diagnostic confidence.

Scientific Session 16

Breast Imaging Papers

Room 309, Level 3

Wednesday, April 29, 2009, 8:00 am–9:30 am

Abstracts 119-125

Moderators: *A. Nees, T. Stephens*
Keynote Address: We Have Come a Long Way: A Reflective Perspective of Breast Imaging—*L. Salkowski*

8:20 am

119. Comparison of Elastographic Parameters and Sonographic Features in Assessment of Breast Lesions

Sim, L.; Leong, L.; Lee, Y.; Wan, C. Singapore General Hospital, Singapore, Singapore*
Address correspondence to L. Sim (gdrssj@sgh.com.sg)

Objective: The objective was to compare the clinical performance of parameters used in elastography with conventional ultrasound features in distinguishing benign and malignant breast lesions.

Materials and Methods: Ninety-nine women with 110 sonographically visible breast lesions were evaluated independently with conventional ultrasound, elastography and combined ultrasound and elastography (CUSEI). Images were acquired with a conventional ultrasound unit and BIRADS scores were assigned to standardize ultrasound interpretation. The elastogram was classified as benign, malignant or equivocal; based on the strain pattern, the length and area ratios. By correlating with histopathology, the sensitivity, specificity, positive predictive value, negative predictive value and accuracy of ultrasound, elastography and CUSEI were obtained. Receiver operating characteristic curves were plotted using the BIRADS scores and elastogram ratios and the area under the curve compared to assess diagnostic performance. The optimal length and area ratios to distinguish benign and malignant lesions on elastography were derived. The performance of each elastographic parameter and ultrasound feature was compared.

Results: Of the 110 breast lesions, 26 were malignant and 84 were benign on histology. The sensitivity, specificity and accuracy of ultrasound was 88.5%, 42.9% and 53.6% respectively. The sensitivity, specificity and accuracy of elastography was 100%, 76.2% and 81.8% respectively, and that of CUSEI was 84.6%, 81% and 81.8% respectively. Elastography and CUSEI achieved significantly better results than conventional ultrasound ($p<0.0005$). The optimal length and area ratios to distinguish benign and malignant lesions on elastography were both 1.1. The elastographic parameters and ultrasound features were rated in order of best to worst performance as follows: elastogram area ratio, elastogram distance ratio, shape, orientation, margin, Doppler vascularity, posterior acoustic feature, elastogram grey scale, calcifications, and echo pattern.

Conclusion: Breast elastography has a higher sensitivity, specificity and accuracy than conventional ultrasound. CUSEI gives higher specificity and accuracy but reduces sensitivity, relative to elastography alone. Area and distance ratios on elastography are superior to every sonographic feature in distinguishing benign and malignant breast lesions. A combined algorithm consisting of both elastographic parameters and ultrasound features enables a more accurate diagnosis of breast cancer. This can be used in a computer-aided diagnosis program for analysis of breast lesions.

8:30 am

120. Preprogrammed Protocol for Survey Breast Ultrasound: Does it Promote Workflow Efficiency?

Marshall, H.; Dimitrijevic, E.; Mendelson, E.; Weber, S. Carle Clinic/Mills Breast Institute, Urbana, IL*
Address correspondence to E. Mendelson (emendelson@nmff.org)

Objective: In diagnostic breast imaging, ultrasound (US) evaluation is frequently the cause of delays in patient throughput, causing the backup in radiologists' schedules and prolongation of patient time from exam commencement to completion. This study was undertaken to assay the efficacy of a formal protocol for breast survey scanning to improve workflow efficiency.

Materials and Methods: A scanning template was installed in an ultrasound system (Philips Healthcare; Bothell, WA) as a software upgrade. This template for a user-selected protocol comprises a set of preannotated views which follow in automated sequence as a view is completed and captured. Time for completion of the study was compared with that of routine US scanning, each view annotated manually by the operator. Thirty patients were scanned twice, once using the protocol and a second time with routine techniques, order of studies randomized. The protocol's sequence of views is stored in the system, and called up for a particular user. The protocol is paused for a finding so that the usual techniques of lesion characterization can be applied, orthogonal views recorded, and measurements taken.

Results: Thirty women (49 breasts) were studied. An automated protocol saved an average of one minute, 44 seconds per case compared with routine techniques. Time to complete the study using the protocol ranged from two minutes, 30 seconds to ten minutes for a unilateral exam and from three minutes, 38 seconds to ten minutes for a routine exam. For two patients, protocol scan time equaled or was longer than for the routine exam. Time to complete a bilateral study on protocol ranged from five minutes, 14 seconds to 35 minutes compared with routine bilateral survey scanning: five minutes, four seconds to 37 minutes. Interrupting the protocol view sequences to evaluate a finding lengthened scan time. The survey scan was interrupted for 26 of 30 patients; four women had no pauses recorded; in 13 women, the study was paused once; in six, the exam was paused twice; three pauses were recorded in three patients, four in two patients, and five in one case. Eight pauses (multiple benign masses) occurred in one case.

Conclusion: Use of a scanning template shortened survey breast US exam time with a measurable increase in workflow efficiency. If survey scanning were performed in 15 patients a day, the savings in time, a total of 26 minutes on average, would allow one additional patient to be scanned per day or five in a work week. In addition, use of an automated protocol with preprogrammed annotations for each view enables the operator to focus on the patient and the acquired images on the monitor rather than on the keyboard or touchscreen.

8:40 am

121. Interpretation Times in Dual Modality Breast Imaging Using Automated Ultrasound With Digital Tomosynthesis Mammography

Roubidoux, M.; Jeffries, D.; Joe, A.; Klein, K.; Pinsky, R.; Patterson, S.; Sinha, S.; Hadjiiski, L. University of Michigan Health Systems, Ann Arbor, MI*
Address correspondence to M. Roubidoux (roubidou@umich.edu)

Objective: The objective was to measure reading times in dual modality breast imaging using automated ultrasound (AUS) with digital tomosynthesis mammography (DTM).

Materials and Methods: A prototype GE DTM and whole breast ultrasound system with GE Logiq 9 ultrasound (US) was developed with General Electric Global Research that allows DTM and sonographic breast imaging during a single breast compression with motorized transducer carriage for automation of the US. DTM images were obtained by acquiring approximately 21 projections over a 60 degree range / < 8 seconds, in the CC or lateral position; images are reconstructed at 1 mm intervals, resulting in approximately 60 DTM images per view (CC or LAT); AUS was performed in either the CC or lateral (LAT) position, depending on optimal positioning for the location of the mass of concern. Thirty patients with BIRADS 4/5 masses underwent research DTM and AUS imaging prior to biopsy. At a dedicated workstation six radiologists independently reviewed case sets consisting of DTM and AUS image volumes. The DTM images volumes (CC and lateral) of the breast with the suspicious mass were each reviewed and readers identified the most suspicious mass in each image volume by digitally placing a box surrounding it. The time for this action was digitally measured for each image volume. Readers also rated conspicuity of the mass on a scale of 1-10 and the BIRADS mammogram density classification (not timed). Subsequently readers reviewed the corresponding AUS image volume and, assisted by registration software, identified the most suspicious area corresponding to the DTM finding, digitally drawing a box around it, this time also digitally measured. Readers were experienced academic breast radiologists, blind to histologic outcomes and clinical images. Cases sets were randomized.

Results: The mean time for reader interpretation for each of the two image volumes (CC or Lateral) of DTM = 47 seconds. (range 36-64 seconds/reader). There was no correlation between time to interpret the DTM image volumes and mass conspicuity (correlation coefficient .11) or BIRADS density (correlation coefficient .00). Mean time for identifying the suspicious mass in the AUS volume was 55 seconds.

Conclusion: Dual modality imaging with AUS and DTM and image registration demonstrated reasonable radiologist reading times. There was no correlation between reader times in DTM and mammogram density or mass conspicuity. Supported by USPHS grants CA91713 (a partnership with GE Global Research) and CA95153.

8:50 am

122. Digital Screening Mammography Soft Copy Interpretation Times: Normal is Quicker

Whitman, G.; Wang, J.; Atkinson, E.; Geiser, W.; Yang, W.; Lane, D.; Stephens, T.; Santiago, L.; Haygood, T. The University of Texas M. D. Anderson Cancer Center, Houston, TX*
Address correspondence to G. Whitman (gwhitman@mdanderson.org)

Objective: The main purpose of this study was to compare digital screening mammography soft copy interpretation times (IT) for cases classified as BIRADS 0, 1, and 2. The second aim was to determine how often the mammographers utilized additional information (AI) while interpreting screening mammograms such as radiology reports (RR), pathology reports, and other images, including older mammograms. The third aim was to determine if the use of AI correlated with IT and BIRADS category.

Materials and Methods: In this prospective study, six experienced mammographers interpreted 333 screening mammograms obtained with a digital mammography unit (Hologic, Bedford, MA) using a workstation (Philips Medical Systems; Foster City, CA). One designated timer recorded the IT, including the time needed to complete a report using a mammography reporting and tracking system (MagView, Burtonsville, MD) and noted if the mammographer utilized AI.

Results: A total of 177 cases were classified as BIRADS 1, 116 cases were classified as BIRADS 2, and 40 cases were classified as BIRADS 0. The average IT, including the time to generate a report, was 198.9 seconds. For BIRADS category 1 reports, the average IT was 156.7 seconds. For BIRADS category 2 reports, the average IT was 215.5 seconds. For BRADS category 0 reports, the average IT was 337.2 seconds.

When the average IT for BIRADS category 1 and 2 cases were compared, the average IT for BIRADS 1 was significantly faster than that for BIRADS 2 ($p<0.001$). When the average IT for BIRADS category 1 and 0 cases were compared, the average IT for BIRADS 1 was significantly faster than that for BIRADS 0 ($p<0.001$). When the average IT for BIRADS category 2 and 0 cases were compared, the average IT for BIRADS 2 was significantly faster than that for BIRADS 0 ($p<0.001$).

The most commonly utilized AI was additional mammograms (AM) on the workstation in 162 cases, paper mammography reports (PMR) in 60 cases, and workstation RR in 22 cases. The use of AI was associated with increased IT ($p<0.0001$ for PMR and workstation RR and $p= 0.0017$ for AM on the workstation). The use of AI was associated with BIRADS assessment for PMR, the workstation RR, and AM on the workstation.

Conclusion: BIRADS 1 cases were interpreted more quickly than BIRADS 2 and 0 cases. BIRADS 2 cases were interpreted more quickly than BIRADS 0 cases. An average BIRADS 0 case took more than twice as long to interpret as an average BIRADS 1 case. The use of AI was associated with increased IT and BIRADS category.

9:00 am

123. Improving Excision of Intraductal Lesions: Clip Placement at Time of Ductography

Woodward, S.; Daly, C.; Patterson, S.; Joe, A.; Helvie, M. University of Michigan Health System, Ann Arbor, MI*
Address correspondence to C. Daly (cpdaly@med.umich.edu)

Objective: The objective was to describe an accurate method of grid coordinate clip placement for patients with abnormal ductogram findings occult on sonography and to compare the success of grid coordinate clip placement with ductogram guided wire localization (WL).

Materials and Methods: Following IRB approval, a retrospective search identified all patients with nipple discharge referred for ductography from January, 2001 to May, 2008. The number of successful ductograms, reasons for failure, patients with abnormal ductograms, and those who underwent clip placement at time of ductography were recorded. Patients referred for ductogram guided WL, pathology results and clinical follow-up were also recorded. Routine work-up of nipple discharge included mammography and subareolar ultrasound. Ductography was performed if requested by the clinical service, often in cases of negative routine work-up. Image guided WL was usually requested for distal ductal abnormalities which may not be excised by routine subareolar dissection. Toward the end of the study period, five patients with abnormal ductograms underwent clip placement in consultation with the surgical service for later excision. Our method used grid coordinate technique with an 18 gauge biopsy clip device to mark the abnormality on ductography.

Results: A total of 183 patients ages 23-88 years comprised the study population; 34 patients had more than one exam. Of 225 referrals for ductography, 140 (62%) were successful; 85/140 (61%) ductograms were positive. Positive abnormalities included duct cut-off, duct irregularity, and filling defects (1-15 mm). Sixteen patients were referred for ductogram guided WL, of which nine (56%) were successful. Seven patients failed ductogram WL: four had no discharge, one was negative, one was technically infeasible and one opacified a different duct on the day of surgery. Five of five (100%) patients with grid coordinate clip placement underwent successful WL and excision of the clip. A total of 129 surgeries were performed; ten (8%) cancers; 67 (52%) papillomas; eight (6%) high risk lesions. Pathology results for the five patients with clip placement included three papillomas, one papillary intraductal hyperplasia, and one fibrocystic change.

Conclusion: Grid coordinate clip placement at the time of initial abnormal ductogram provides an accurate method of localizing sonographically occult distal ductal abnormalities, thus facilitating future WL. Clip placement obviates the need for repeat ductogram on the day of surgery (which may be unsuccessful) and ensures surgical removal of the ductogram abnormality.

9:10 am

124. Can Some Patients with Atypical Ductal Hyperplasia Found at Stereotactic Vacuum-Assisted Breast Biopsy Avoid Surgical Excision?

Kohr, J.[1,2]; Eby, P.[1,2]; Allison, K.[1]; DeMartini, W.[1,2]; Gutierrez, R.[1,2]; Lehman, C.[1,2] 1. University of Washington, Seattle, WA; 2. Seattle Cancer Care Alliance, Seattle , WA*
Address correspondence to P. Eby (preby@u.washington.edu)

Objective: Prior research suggests that upgrade to ductal carcinoma in situ (DCIS) or invasive carcinoma does not occur when 11- or 14-gauge stereotactic breast biopsy reveals atypical ductal hyperplasia (ADH) in less than three ducts. Our goal was to determine if upgrade occurs in patients when stereotactic 9- or 11-gauge vacuum-assisted breast biopsy (VABB) yields ADH in less than three ducts and all mammographic calcifications are removed.

Materials and Methods: Following IRB approval, we retrospectively reviewed 991 consecutive 9- or 11-gauge stereotactic VABB procedures from February, 2001 through June, 2006 to identify all cases performed for suspicious mammographic calcifications with a histologic diagnosis that included any type of atypia. Patients with a diagnosis of cancer at the time of biopsy or as a result of the biopsy were excluded. The search yielded 147 cases. A single pathologist performed a blinded review of and confirmed ADH in 112. Each large duct or terminal duct-lobular unit containing ADH was defined as a focus and the foci were counted for each case. Ten cases without surgical follow-up were excluded leaving 102 in the analysis set. Postbiopsy mammograms were reviewed to assess if the calcifications had been entirely removed. Upgrade was determined from excisional biopsy pathology reports. The upgrade rates, as a function of number of foci and presence or absence of residual calcifications, were calculated and compared with Chi-Square test.

Results: Upgrade occurred in 20/102 (19.6%) study cases. ADH was present in one focus in 25 (24.5%), two foci in 24 (23.5%), three foci in 15 (14.7%) and four or more foci in 38 (37.3%) cases. Upgrade was significantly more likely in cases with three or more foci (15/53, 28.3%) compared with less than three foci (5/49, 10.2%, p=0.02). Post-biopsy mammograms were available for review in 87 of 102 cases. The upgrade rate associated with removal of all mammographic calcifications (8/42, 19.0%) was not significantly different than in cases with residual calcifications (9/45, 20.0% p=0.91). Upgrade occurred in 2/17 (11.8%) cases with less than three foci of ADH and all calcifications removed.

Conclusion: The risk of upgrade is significantly higher when ADH is present in three or more ducts. Although the upgrade rate is low, surgical excision is still recommended for patients when ADH involves less than three ducts and all mammographic calcifications are removed.

9:20 am

125. Lobular Neoplasia Identified at Image-Guided Core Biopsy of the Breast: Is Surgical Excision Indicated?

Leung, J.[1]; Denny, M.[1,2]; Margolin, F.[1]; Ching, B.[1,3] 1. California Pacific Medical Center, San Francisco, CA; 2. Washington University in St. Louis, St. Louis, MO; 3. National Cancer Center of Singapore, Singapore, Singapore*
Address correspondence to J. Leung (leungjw@sutterhealth.org)

Objective: The objective was to analyze the outcomes of lobular neoplasia identified at image-guided core biopsy and to determine whether surgical excision is indicated for such lesions.

Materials and Methods: We retrospectively identified 57 lesions which contained lobular neoplasia (atypical lobular hyperplasia [ALH] or lobular carcinoma in-situ [LCIS]) as the highest-risk lesion among 8,089 breast core biopsies performed over a 10-year period at a single institution. Cases with concomitant high-risk lesions including atypical ductal hyperplasia, radial scar, or papillary lesion were excluded. Thirty-four (60%) of the 57 lesions were biopsied with stereotactic guidance (30 using an 11-gauge vacuum-assisted device; four using a 14-gauge automated needle). Twenty-three (40%) lesions were biopsied with ultrasound guidance (19 using a 16-gauge and 14 using a 14-gauge automated needle). For stereotactic-guided biopsies, the median lesion size was 6 mm (range 2-20 mm) and median number of core samples was eight (range 6-17). For ultrasound-guided biopsies, the median lesion size was 8 mm (range 4-18 mm) and median number of core samples was four (range 3-6). Mammograms, sonograms, MR images, and pathology reports were reviewed. Concordance with surgical pathology findings was assessed.

Results: The incidence of lobular neoplasia at core biopsy without a concomitant high-risk lesion was 0.7% (57/8,089). Among these 57 cases, 36 (63%) were ALH and 21 (37%) were LCIS. Forty-four (77%) of the 57 lesions were detected at screening mammography (32 calcifications, seven masses, four masses associated with calcifications, one architectural distortion). Eight (14%) presented as palpable findings, while five (9%) were initially seen at MRI. No suspicious change was identified in 13 lesions with imaging follow-up of two years or longer. The remaining 44 lesions were surgically excised; malignancy was identified in ten (one ductal carcinoma in-situ, four invasive ductal carcinomas, five invasive lobular carcinomas). Hence, the underestimation rate was 18% (10/57). Underestimation was mostly likely when imaging finding was a mass, discordance between imaging and pathology was present, or LCIS (rather than ALH) was initially identified. We did not find a correlation between disease underestimation and the number or size of core samples.

Conclusion: Given the underestimation rate of 18% in our series, we believe that all core biopsies showing lobular neoplasia as the highest-risk lesion should be surgically excised.

BREAST IMAGING PAPERS

Room 310, Level 3

Wednesday, April 29, 2009, 10:00 am–12:00 noon

Abstracts 126-134

Moderators: *C. Comstock, L. Salkowski*
Keynote Address: Breast MRI: Screening and Diagnosis—*G. Newstead*

10:30 am

126. The Value of Second Look Ultrasound as a Confirmatory Method for Incidental Enhancing Lesions Found on Breast MRI

Luciani, M.; Pediconi, F.; Dominelli, V.; Cagioli, S.; Martino, V.; Catalano, C.; Passariello, R. University of Rome La Sapienza, Rome, Italy*
Address correspondence to F. Pediconi (federica.pediconi@uniroma1.it)

Objective: The objective was to evaluate the role of second look high resolution ultrasound (US) for the identification of incidental enhancing lesions detected on preoperative breast MRI that have no x-ray mammographic or palpable correlate.

Materials and Methods: Between January, 2004 and March, 2006, 182 patients aged 35 to 72 years, with confirmed breast cancer based on conventional x-ray mammography or US underwent breast MRI with 0.1 mmol/kg gadobenate dimeglumine for breast cancer staging. Patients with additional incidental lesions on breast MRI thereafter underwent a second look high resolution US examination directed specifically at the site of the incidental finding. Both MR and US images were analyzed by two radiologists in consensus and a comparison between the two imaging modalities was performed.

Results: Breast MRI detected 55 additional enhancing lesions in 46/182 (25.3%) patients that were not seen on x-ray mammography or first look US. Of these 55 additional lesions, 43 (78.2%) corresponding lesions were subsequently detected on second look US. US-guided biopsy or US-guided wire localization followed by excisional biopsy subsequently confirmed that 19 of these 43 lesions were malignant. Treatment planning was altered for four patients with multicentric cancer and seven patients with multifocal cancer based on combined breast MRI and US findings. The 12 lesions detected on breast MRI for which a corresponding lesion was not detected on second look US were evaluated on MR-guided biopsy or were reassessed by breast MRI after three months. One of these 12 lesions was confirmed as malignant.

Conclusion: At our facility, direct second look US is a feasible confirmatory method for incidental findings at breast MRI. The likelihood of carcinoma is markedly higher for lesions with a US correlate than for lesions without a US correlate.

10:40 am

127. Utility of Targeted/Second Look Ultrasound after Breast MRI

Lee, J.; Mercado, C.; Moy, L.; Toth, H. New York University Clinical Cancer Center, New York, NY*
Address correspondence to J. Lee (JIYON_L@hotmail.com)

Objective: The purpose was to evaluate the frequency and efficacy of targeted or "second-look ultrasound" (US) for lesions detected on MRI of the breast.

Materials and Methods: We retrospectively reviewed 889 breast MRI examinations performed within a 24-month period. Of 889 breast MRI exams, 178 (20%) studies led to a recommendation for targeted/second-look ultrasound (US) for lesions detected on MRI. The frequency of targeted US recommendation and yield of US correlates were assessed.

Results: The 178 MRI exams were performed in 178 patients. There were 263 mammographically-occult MRI-detected lesions recommended for targeted US. The clinical indications for MRI in the 178 patients were for evaluation of extent of disease in 58 (33%), high risk screening in 82 (46%), and problem solving in 38 (21%). Lesion types were nodules/masses in 213 (81%) with a mean lesion size of 8.6 mm, and nonmass-like enhancement lesions (NMLE) in 50 (19%) with a mean lesion size of 2.1cm. US was performed for evaluation of 124 MRI-detected lesions in 91 of 178 patients (51%). US correlate was found in 59 lesions (57 masses and 2 NMLE) (48%). Biopsy of 54 lesions revealed 38 benign and 16 malignant/high risk lesions. Twenty-two of the 38 benign lesions were confirmed to be stable or resolved on follow up MRI.

Conclusion: Targeted US recommendation was found to be helpful for less than half of the lesions (48%) seen on breast MRI; more useful for masses and less so for nonmass-like enhancement lesions. These findings suggest that the recommendation for targeted US for MRI-detected breast lesions may be used more selectively, given the higher rate of ultrasound detection of mass lesions.

10:50 am

128. Second-Look Ultrasound in Assessing MRI-Detected Breast Lesions: Can Absence of a Sonographic Correlate Be Used to Exclude Cancer?

Ching, B.[1,2]; Leung, J.[1]; Margolin, F.[1]; Denny, M.[1,3] 1. California Pacific Medical Center, San Francisco, CA; 2. National Cancer Center of Singapore, Singapore, Singapore; 3. Washington University in St. Louis, St. Louis, MO*
Address correspondence to J. Leung (leungjw@sutterhealth.org)

Objective: The objective was to determine the usefulness of second-look ultrasound in assessing MRI-detected breast lesions and to determine the incidence of cancer in MRI-detected breast lesions that are sonographically occult.

Materials and Methods: Among 762 breast MRI studies performed over a 20-month period at a single institution, we retrospectively identified 207 (27%) MRI-detected breast lesions in which second-look ultrasound was prospectively recommended and performed as the next imaging step. Mammograms, sono-

grams, MR images and pathology reports were reviewed. A correlative finding was identified at second-look ultrasound in 126 (61%) of 207 cases. A total of 120 of these 126 sonographic lesions were sampled using ultrasound-guided core biopsy. Six sonographic correlative lesions were not biopsied because they showed features representative of benign intramammary nodes. No sonographic correlate was seen in the remaining 81 (39%) cases. Of these 81 cases, MRI-guided core biopsy using a vacuum-assisted device was performed in ten, surgical excision in five and imaging follow-up (range 6-32 months) in 66.

Results: Thirty-six cancers (30%) were diagnosed among the 120 MRI-detected lesions in which second-look ultrasound revealed a correlative finding that was not a benign intramammary node. Among these 36 cancers, there were 24 invasive ductal carcinomas (IDC), three invasive lobular carcinomas (ILC), eight cases of ductal carcinoma in situ (DCIS), and one intramammary node containing metastatic tumor. Seven cancers (9%) were diagnosed among the 81 MRI-detected lesions that had no sonographic correlate (three IDC, two DCIS, one ILC, and one mucinous carcinoma). Among the remaining 74 lesions that had no sonographic correlate, seven were benign at MRI-guided core biopsy. One of the 74 lesions had no sonographic correlate but appeared as architectural distortion at mammography; histology at stereotactic-guided core biopsy and subsequent surgical excision was atypical ductal hyperplasia. Fifty-one showed no interval change at imaging follow-up, five decreased in size and nine resolved. One lesion is awaiting MRI-guided core biopsy as it increased at follow-up MRI.

Conclusion: Second-look ultrasound was useful in showing a correlative finding for MRI-detected breast lesions in the majority (61%) of cases. The positive predictive value (PPV) of malignancy when a sonographic correlate was present was 30%. Although the probability of malignancy was lower when there was no sonographic correlate, the 9% PPV in such instances is still sufficiently high to warrant biopsy using MRI-guidance.

11:00 am

129. Diffusion-Weighted Imaging and Apparent Diffusion Coefficients Mapping for Characterization of Focal Breast Lesions at 3T

El-Khouli, R.[1]; Jacobs, M.[2]; Macura, K.[2]; Barker, P.[2]; Bluemke, D.[1,2] 1. National Institutes of Health, Bethesda, MD; 2. Johns Hopkins University School of Medicine, Baltimore, MD*
Address correspondence to R. El-Khouli (elkhoulir@cc.nih.gov)

Objective: The objective was to evaluate the role of diffusion-weighted imaging (DWI) and apparent diffusion coefficient (ADC) mapping in characterizing benign from malignant breast lesions at high field 3T scanner, and to evaluate the added value of ADC normalization.

Materials and Methods: A total of 550 consecutive patients referred for clinical breast MRI underwent bilateral diagnostic breast MRI, including DWI, on a 3T MR system (Philips Healthcare, Bothell, WA) using a dedicated breast coil. Study inclusion criteria included a pathology proven benign or malignant diagnosis, or at least one follow-up scan demonstrating stability of the lesion as proof of benignity. DWI was acquired in the sagittal or axial planes using an echo planar sequence with fat suppression (SPAIR) and b values of 0 and 600 seconds/mm^2. ADC maps were constructed. Regions of interest were drawn on the lesions and normal appearing glandular tissue. Ratios of lesion ADC to glandular tissue ADC (L/GT) were calculated. Logistic regression was used to determine statistical parameters and significance was set with $p<0.05$. Receiver operating curve (ROC) analysis was performed to assess the diagnostic accuracy of each parameter. Different cutoff points were tested by creating different datasets for both the absolute ADC value and the L/GT ratio. ROC curve analysis was performed to determine the optimal cutoff point (resulting in the best accuracy).

Results: Inclusion criteria were fulfilled in 80 patients with 85 lesions, (25/85 [29.4%] benign and 60/85 [70.6%] malignant). There was no difference observed in benign and malignant ADC and L/GT ratio between pre- and postmenopausal women. The ADC value of benign lesions ranged from 0.7 to 3.3 x 10^{-3} mm^2/second (mean 2 + 0.76) while for malignant lesions it ranged from 0.4 to 1.9 x 10^{-3} mm^2/second (mean 1.1 + 0.37) ($p<0.05$). For L/GT ratio, benign lesions ranged from 0.5 to 1.7 (mean 1.1 + 0.39) and malignant lesions from 0.28 to 0.98 (mean 0.53 + 0.15) ($p<0.05$). The area under the ROC curve for the ADC values was good (0.84) while it was excellent for L/GT ratio (0.92).

Conclusion: Diffusion-weighted imaging coupled with ADC mapping of focal breast lesions with normalization relative to glandular tissue has potential to improve the accuracy of breast MRI for lesion characterization.

11:10 am

130. Apparent Diffusion Coefficient Values for Discriminating Benign and Malignant Breast MRI Lesions: Masses vs. Nonmass-Like Enhancement

Mullins, C.[1,2]; Partridge, S.[1,2]; DeMartini, W.[1,2]; Kurland , B.[3]; Eby, P.[1,2]; White, S.[1,2]; Lehman, C.[1,2] 1. University of Washington, Seattle, WA; 2. Seattle Cancer Care Alliance, Seattle, WA; 3. Fred Hutchinson Cancer Research Center, Seattle, WA*
Address correspondence to S. Partridge (spartrid@seattlecca.org)

Objective: The objective was to determine if diffusion-weighted imaging (DWI) apparent diffusion coefficient (ADC) values can distinguish benign from malignant breast MRI masses and nonmass-like enhancement (NMLE).

Materials and Methods: Following IRB approval, retrospective review of all MRI exams performed between October, 2005 and November, 2006 identified 141 consecutive exams with masses or NMLE with a BIRADS assessment of 3, 4, or 5. DWI was acquired in 113 exams as part of the standard breast MRI and incorporated an EPI sequence with diffusion gradients applied in six directions and b=0 and 600 s/mm^2. DWI images were reviewed and ADC calculated for each lesion. A benign or malignant outcome for each lesion was determined by histology, MRI follow-up, or linkage with the Cancer Surveillance System registry with minimum follow-up of 12 months. Mean ADC values for benign and malignant masses and NMLE were compared by t-test. Positive predictive values (PPV) of recommendation to biopsy with and without DWI information were compared for both masses and NMLE.

Results: Of the 113 exams, 15 were excluded due to technical problems, yielding a final cohort of 98 exams in 93 women with 126 breast lesions (75/126 masses, 51/126 NMLE). Eighteen of

75 (24%) masses and 14/51 (27%) NMLE were malignant. For masses, the mean ADC was significantly lower for malignant (1.20 ± 0.30 x10^{-3} mm²/second) than for benign lesions (1.70 ± 0.50 x10^{-3} mm²/second, p<0.001). The mean ADC was also lower for malignant NMLE (1.34 ± 0.30 x10^{-3} mm²/second) compared to benign NMLE (1.59 ± 0.33 x10^{-3} mm²/second, p=0.015), though the difference was smaller than for masses. All malignancies had ADC=1.81 x10^{-3} mm²/second. Applying this ADC cutoff to achieve 100% sensitivity resulted in both up and downgrading of lesions, and the PPVs for both masses and NMLE with and without DWI information were comparable (DCE alone PPV: 31% for masses, 33% for NMLE; DCE with DWI PPV: 33% for masses, 33% for NMLE).

Conclusion: DWI shows promise in distinguishing benign from malignant breast MRI lesions, both for masses and NMLE. However, overlap in ADC values limits its clinical utility at this time and further study to assess the added diagnostic value of DWI and appropriate use in clinical practice is needed.

11:20 am

131. Contrast-Enhanced MR Mammography: Improvement in Breast Lesion Detection and Characterization with Gadobenate Dimeglumine Compared to Gadopentetate Dimeglumine

Dominelli, V.; Pediconi, F.; Catalano, C.; Padula, S.; Roselli, A.; Cagioli, S.; Passariello, R. University of Rome La Sapienza, Rome, Italy*
Address correspondence to F. Pediconi (federica.pediconi@uniroma1.it)

Objective: The objective was to prospectively and intraindividually compare 0.1 mmol/kg doses of gadobenate dimeglumine and gadopentetate dimeglumine for contrast-enhanced breast MRI.

Materials and Methods: Forty-seven women (mean age: 50.8 ± 12.9 years) with breast lesions classified as BIRADS 3, 4 or 5 for suspicion of malignancy underwent two identical MR examinations at 1.5T separated by 48–72 hours. T1-weighted gradient-echo images were acquired predose and at two minute intervals after the randomized injection of gadopentetate dimeglumine or gadobenate dimeglumine at 2 ml/second. Two blinded readers evaluated randomized image sets for lesion detection and differentiation as benign or malignant compared to histology. McNemar's Exact test and the Generalized Estimating Equation (GEE) were used to compare lesion detection rates and diagnostic performance in terms of sensitivity, specificity, accuracy and positive and negative predictive values (PPV and NPV).

Results: Histopathology data were available for 78 lesions. Significantly more lesions overall (75/78 [96%] vs. 62/78 [79%]; p=0.0002) and significantly more malignant lesions (49/50 [98%] vs. 38/50 [76%]; p=0.0009) were detected with gadobenate dimeglumine. All detected malignant lesions were correctly diagnosed with both agents. More detected benign lesions were correctly diagnosed with gadobenate dimeglumine (20/26 [77%] vs. 17/24 [71%], respectively). Differentiation of lesions was significantly (p=0.0001) better with gadobenate dimeglumine. Significantly better diagnostic performance was noted with gadobenate dimeglumine for sensitivity (98.0% vs. 76.0%; p=0.0064), accuracy (88.5% vs. 69.2%; p=0.0004), PPV (86.0% vs. 76.0%; p=0.0321) and NPV (95.2% vs. 57.1%; p=0.0003).

Conclusion: Lesion detection and malignant/benign differentiation is significantly better with 0.1 mmol/kg gadobenate dimeglumine compared to 0.1 mmol/kg gadopentetate dimeglumine. Gadobenate dimeglumine at a standard dose of 0.1 mmol/kg bodyweight is potentially the contrast agent of choice for breast MRI.

11:30 am

132. Dynamic MRI of the Breast: Quantitative Method for Kinetic Curve Shape Assessment

El-Khouli, R.[1]; Macura, K.[2]; Barker, P.[2]; Jacobs, M.[2]; Kamel, I.[2]; Bluemke, D.[1] 1. National Institutes of Health, Silver Spring, MD; 2. Johns Hopkins University/School of Medicine, Baltimore, MD*
Address correspondence to R. El-Khouli (elkhoulir@cc.nih.gov)

Objective: The type of wash-out curve (persistently enhancing, plateau, wash-out) for dynamic contrast-enhanced (DCE) breast MRI is predictive of malignancy. Qualitative assessment of the shape of the curve is most commonly used. The purpose of this study was to evaluate qualitative and quantitative methods for determining the type of DCE-MRI curve.

Materials and Methods: Ninety-one patients underwent DCE breast MRI. The shape of the DCE-MRI wash-out curve was assessed qualitatively by three radiologists on two occasions. For quantitative assessment, average wash-out slope and absolute wash-out percentage enhancement difference were calculated. Kappa statistics were used to determine inter- and intraobserver agreement for the qualitative method. Matched sample (MS) tables, extended McNemar test and receiver operating characteristic statistics were used to compare quantitative vs. qualitative methods for establishing or excluding malignancy.

Results: Seventy-eight patients (77.2%) had malignant lesions and 23 (22.8%) patients had benign lesions. Good intra- and interobserver agreement was suggested (kappa range, 0.74-0.88), with area under the curve of 0.73-0.77 for qualitative assessment. Using the quantitative method, the highest accuracy was obtained using 0.03% per second average wash-out slope and 5% absolute percentage enhancement difference as cutoff points. Using this method, there were significantly higher accuracies (AUC=0.87 and 0.87 respectively) compared to qualitative assessment (p<0.01).

Conclusion: Quantitative assessment of the kinetic curve shape resulted in significantly higher diagnostic performance when compared to the standard qualitative method.

11:40 am

133. Surgical Outcome of High-Risk Lesions at MRI-Guided 9-Gauge Vacuum-Assisted Breast Biopsy

Elias, K.; Mercado, C.; Lee, J.; Toth, H.; Moy, L. New York University Medical Center, New York, NY*
Address correspondence to K. Elias (krelias@yahoo.com)

Objective: The objective was to determine the frequency of high-risk lesions at MRI-guided 9-gauge vacuum-assisted breast biopsy and to review the surgical outcome of these lesions.

Materials and Methods: We performed a retrospective review of 100 consecutive lesions detected at MRI and subsequently biopsied under MRI guidance during a 12-month period. Underestimation was defined as cancer at surgery. Indications for breast MRI, imaging features, biopsy technique and histology findings were reviewed.

Results: Among the 100 women, the clinical indications for breast MRI were: assessment of extent of disease in 36 (36%), high-risk screening in 42 (42%), and problem solving in 22 (22%). The median age of the patients was 55 years (range, 37-82 years). Histologic analysis yielded 23 high-risk lesions in 22 patients: atypical ductal hyperplasia (ADH) in 11 (11%), lobular-carcinoma-in-situ (LCIS) in four (4%), flat cell atypia in three (3%), atypical lobular hyperplasia (ALH) in three (3%), and papilloma in two (2%) of 100 lesions. Among 23 MRI lesions, six (26%) were mass lesions and 17 (74%) were nonmass-like enhancement. Median lesion size was 1.1 cm (range 0.7-5.2 cm). Median number of core specimens obtained was 12 (range 6-18). Surgical excision was performed on 21 lesions yielding four malignancies (19%). All were ductal carcinoma in-situ at surgical pathology and ADH on initial biopsy. Ten (47%) were high-risk lesions at surgery: seven of 11 ADH, two of four LCIS, one of three flat cell atypia. Of these ten lesions, five were ADH without other high-risk lesions, three were ADH and papilloma, and two were ADH and LCIS. All cases of ALH and papilloma were benign on subsequent surgery. Review of the MR findings demonstrated no specific imaging features among the four malignancies based on lesion size, lesion type, morphology, and enhancement pattern.

Conclusion: The underestimation for malignancy when a high-risk lesion is diagnosed at MRI biopsy in our series was 19%. No specific imaging features were seen in cases upgraded to a malignancy. Surgical excision is recommended for all high-risk lesions at MRI-guided vacuum-assisted breast biopsy, especially in cases of ADH.

11:50 am

134. Cancelled MRI-Guided Interventional Procedures of the Breast: Outcomes on Followup MR Imaging

McOsker, J.[1]; Andrejeva, L.[2]; Philpotts, L.[2] 1. New York Medical College, Valhalla, NY; 2. Yale University School of Medicine, New Haven, CT*

Address correspondence to L. Andrejeva (liva.andrejeva@yale.edu)

Objective: The objective was to determine the reasons for cancellation of MRI-guided interventional procedures of the breast and the outcome of the cancelled cases on followup MR imaging.

Materials and Methods: We examined the imaging record of 53 patients whose MRI-guided interventional breast procedure was cancelled. For these cancelled cases, patient characteristics—age, pre- or postmenopausal status, risk stratification—were determined; the type and size of the MRI abnormality detected on the diagnostic breast MRI, reason for cancellation, and outcome on follow up imaging were also documented. The relationship between patient characteristics, the characteristics of the breast lesions, and the reasons for cancellation were examined.

Results: From 736 MRI-guided interventional procedures of the breast scheduled at the Yale New Haven Hospital between October, 2003, and February, 2008, 53 (7%) procedures were cancelled. In 48 (91%) of the 53 cancelled procedures, the reason for cancellation was nonvisualization of the target lesion. Other reasons for cancellation included patient intolerance of the procedure, suboptimal location of the lesion, and confirmation of the presence of a biopsy marking clip within the abnormality. Of the 48 nonvisualized lesions, 34 (71%) were determined to be benign based on MRI follow up, and five underwent subsequent biopsy: two (4%) diagnosed as benign high-risk lesions and two (4%) diagnosed as malignant. No followup information was available on the remaining ten (21%). Nonvisualization of the lesion was more likely to occur in premenopausal patients (33 of 34 patients) than in postmenopausal patients (13 of 17 patients). Most of the lesions that were not visualized were smaller than 1 cm in size (32 vs. 16). Both cases of cancer were diagnosed in high-risk patients whose initial diagnostic MRI revealed masses smaller than 1 cm. The reasons for cancellation of these cases will be reviewed in detail.

Conclusion: The main reason for cancellation of MRI-guided procedures of the breast in our institution is nonvisualization of the lesion at the time of the attempted biopsy. Premenopausal patients and patients with lesions that are smaller than 1 cm are more likely to experience cancellation. For these patients, careful imaging follow-up is necessary. If the abnormality is again visualized and retains a suspicious appearance, a reattempt at MRI-guided interventional procedure is recommended in order to avoid missing cancer.

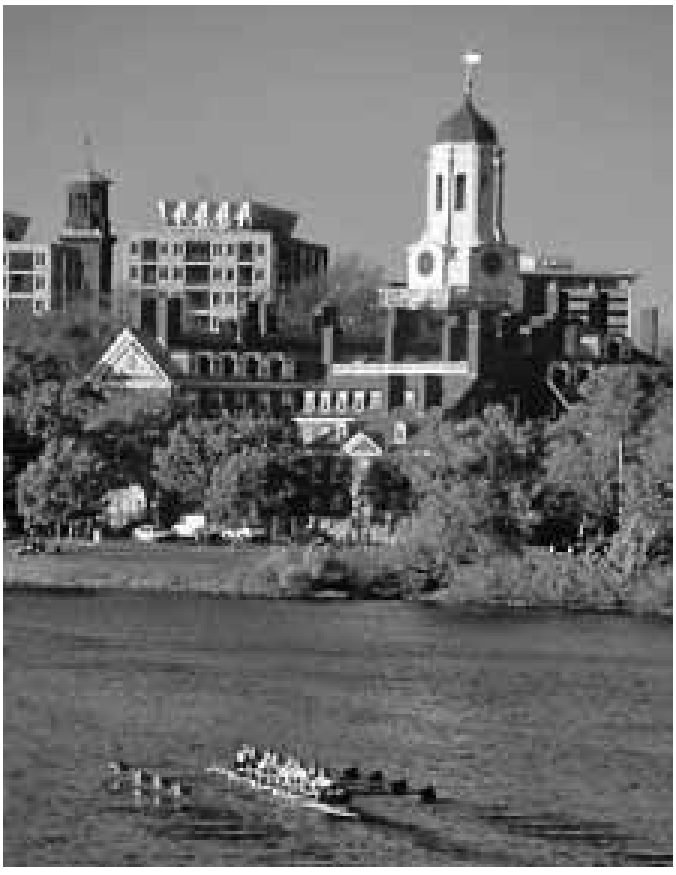

MUSCULOSKELETAL (PELVIS/LOWER EXTREMITY) IMAGING PAPERS

Room: 207, Level 2

Wednesday, April 29, 2009, 10:00 am–12:00 noon

Abstracts 135-146

Moderators: S. Smith, A. Zoga

10:00 am

135. MR Appearance of the Proximal Hamstring Origin in Symptomatic and Asymptomatic Individuals

Alsheik, N.; Blankenbaker, D.; De Smet, A.; Lindstrom, M.*
University of Wisconsin School of Medicine and Public Health, Madison, WI
Address correspondence to D. Blankenbaker (dg.blankenbaker@hosp.wisc.edu)

Objective: The objective was to evaluate the MR appearance of the proximal hamstring origin (PHO) in patients with and without hamstring symptoms and physical findings.

Materials and Methods: IRB approval was obtained for this retrospective review of consecutive pelvis MRI examinations from 2005-2007. Patients included were all evaluated by physicians in orthopedics, rheumatology, sports medicine or rehabilitation medicine. Those with history of inflammatory arthropathy, fracture, total hip arthroplasty, infection and pelvic tumor were excluded. A total of 118 pelvis MR exams (236 PHO) were analyzed by two musculoskeletal radiologists blinded to symptoms and physical findings. The PHO was evaluated at four consecutive axial locations for: number of tendons, size, internal signal intensity (SI) (0=normal, 1=equal to muscle, 2=fluid), ischial tuberosity edema, fluid around the PHO, shape of the surrounding fluid (feathery, crescentic, round), fluid location (subtendinous, superficial) and presence of PHO tear. Correlation was made to clinical symptoms and physical examination. Statistical analysis included Fisher's exact test, Chi square test, t test and nonparametric t test.

Results: The study group consisted of 68 females and 50 males (mean age 41 years). Twenty-one patients had symptoms referable to the PHO. Mean length and width of the PHO at the four locations was not statistically different in symptomatic versus asymptomatic patients (p=0.086). More than 70% of patients had increased T1 and T2 signal within the PHO, which did not correlate with symptoms (p>0.1); 11/236 (4%) had tuberosity edema. Tuberosity edema correlated with physical exam findings (p=0.0087), symptoms (p=0.0103) and younger age at presentation (mean age 27, p=0.0071); 43-72% of patients had fluid signal about the PHO at the four axial locations without correlation with symptoms. Most commonly, fluid was crescentic in shape and occurred superficially. There were nine (4%) hamstring tears which correlated with symptoms (p=0.0040).

Conclusion: Increased SI is commonly seen within and around the proximal hamstring origin and does not correlate with symptoms or physical examination findings. Tuberosity edema and PHO tears are significantly associated with hamstring symptoms.

10:10 am

136. Patterns of Bone and Muscle Injury After High Risk Vaginal Delivery Compared to Caesarian Section: Acute and Chronic Appearance of the Pubic Bone

Brandon, C.; Miller, J.; Jacobson, J. University of Michigan, Ann Arbor, MI*
Address correspondence to C. Brandon (catbrand@umich.edu)

Objective: The objective was to better define pubic bone changes and levator ani muscle injury arising from childbirth, especially comparing vaginal delivery and caesarian section.

Materials and Methods: In this ongoing study 28 primiparous postpartum women have been enrolled, 18 with vaginal delivery factors associated with pelvic floor damage and ten with C-section. All were imaged at 4-6 weeks, 16 have had 6-7 month followup imaging, 11 are awaiting follow-up, one dropped. MR was a 3T with cardiac coil, intermediate and intermediate with fat saturation sequences, 4 mm and 2 mm sections. Bone marrow edema, stress fractures and muscle tears were graded as to location, extent and severity.

Results: Bone marrow edema was present in 22/28 women (14/18 vaginal, 8/10 C-section) initially, all decreased or resolved on follow-up. For vaginal delivery all foci were at or near insertion of levator ani muscles along posterior inferior pubic cortex. Most were focal and moderate to intense (5/18 unilateral, 6/18 asymmetrical) only 3/18 were mild and symmetrical. Only two C-section had moderate signal, and most were diffuse and anterior in the pubic bone (4/10 symmetrical, 3/10 unilateral diffuse, 1/10 asymmetric diffuse). Stress fracture was seen in 8/28 (7/18 vaginal, 1/10 C-section), all had marrow edema and were at or near the posterior inferior portion of pubic symphysis. All were focal but one, a displaced fracture extended into the inferior pubic ramus. Six stress fractures had bilateral muscle tears, five with contralateral higher grade tears. Stress fractures without tears were seen in one vaginal and one C-section woman. Muscle tears were seen in 10/28 (10/18 vaginal, 0/10 C-section) with nine cases of marrow edema and six stress fractures. All tears involved the anterior pubic portion of levator ani muscle. One woman had complete bilateral tears, another's tear extended into rectum and lateral levator ani fibers.

Conclusion: Two trauma patterns are seen in at risk women. Vaginal delivery has focal, intense bone marrow edema at or near the levator ani insertion on posterior inferior pubic cortex, often associated with anterior levator ani muscle tears and small stress fractures into the pubic symphysis opposite side from higher grade tears. C-section has diffuse, mild, bilateral bone marrow edema with more anterior pubic location, no muscle tears and occasional stress fracture. Unexpected findings included one pubic stress fracture in a C-section patient who pushed for two hours.

10:20 am

137. Hip Abductor Strain at the Level of the Iliac Tubercle: A Unique Entity Demonstrated by MRI

Sher, I.[1]; Umans, H.[1,2,3]; Arora, R.[2]; Tobin, K.[2]; Olson, T.[3]; Downie, S.[3] 1. Jacobi Medical Center, Bronx, NY; 2. Lenox Hill Radiology and Imaging Associates, New York, NY; 3. Albert Einstein College of Medicine, Bronx, NY*
Address correspondence to H. Umans (hilary.umans@gmail.com)

Objective: The objective was to describe the clinical and imaging features of abductor strain at the level of the iliac tubercle.

Materials and Methods: All MRI studies of the bony pelvis from the period of October, 2006-September, 2008 demonstrating abductor strain, appearing as bright T2 signal at the enthesis along the inferior margin of the iliac tubercle, were identified by three musculoskeletal radiologists at a single imaging center using either a 1.5T or 3T MRI unit. History and patient demographics were reviewed. Literature review was performed, focusing on hip abductor injuries. Cadaveric dissection was performed to delineate the anatomy of the abductor origin at the iliac tubercle.

Results: All six individuals identified with hip abductor strain at the level of the iliac tubercle were women (34–56 years old). Three reported onset of pain with running, one while playing tennis. One 50-year old nonathlete could not recall the etiology of the symptoms. A 56-year old nonathlete underwent treatment for lymphoma of the contralateral iliac bone prior to nontraumatic onset of pain. All four athletes experienced pain in the region of the iliac tubercle, which was worse with activity, for 1-2 months. Radiographs obtained in two of six were normal. For one, normal hip MRI was initially performed, followed by pelvis MRI. In five, MRI demonstrated thinning and fraying with partial tear near the origin of the gluteus medius (GM) tendon adjacent to the iliac tubercle, with peritendinous edema seen best on fat suppressed T2-weighted images. In one nonathlete there was only minor thickening of the tendon origin with mild peritendinous edema along the enthesis.

There are no imaging reports in the literature describing abductor strain at the level of the iliac tubercle. The majority of reports describe injury at the level of the greater trochanter of the hip, either in runners or in an elderly, primarily female population. Anatomic dissection shows the GM and tensor fasica lata (TFL) originating both from the iliac tubercle. The TFL overlies the GM and the two are intimately related in the region of the iliac tubercle. The superior gluteal nerve courses just deep and close to the origin of the GM.

Conclusion: Abductor strain at the level of the iliac tubercle is a distinct entity, separate from insertional strains which have been reported at the level of the greater trochanter. Imaging of this entity must include the iliac tubercle, which is excluded in standard hip MRI. This appears to primarily affect women, and is most commonly a stress injury related to running.

10:30 am

138. Posterior Tibial Tendon and Spring Ligament Abnormalities and the Development of Osteoarthritis and Ankle Deformity on Follow-Up MRI

Long, S.[1]; Morrison, W.[1]; Zoga, A.[1]; Gopez, A.[1]; Siegler, S.[2] 1. Thomas Jefferson University Hospital, Philadelphia, PA; 2. Drexel University, Philadelphia, PA*
Address correspondence to S. Long (suzanne.long@mail.tju.edu)

Objective: The objective was to evaluate patients with various degrees of posterior tibial tendon (PTT) abnormality over time by MRI to determine the frequency of patients with spring ligament abnormality, development of osteoarthritis (OA), onset/progression of deformity, and abductor digiti minimi (ADM) atrophy.

Materials and Methods: MRI of 33 ankles (eight males/25 females, age 48 years average, range 23–67 years) showing PTT abnormality (including tenosynovitis, tendinosis and/or tear) were evaluated by two musculoskeletal radiologists in consensus and compared with follow-up MRI (average follow-up 32 months, range 12-105 months). The presence or absence of PTT tenosynovitis, hypertrophy/atrophy, tear, subtendinous edema and the appearance of the spring ligament (thinned/thickened/torn) was noted as well as subtalar, ankle joint, and talonavicular osteoarthritis. Ankle deformity including arch depression, hindfoot valgus, pes planus, overpronation and fibular-calcaneal abutment were evaluated as well as ADM atrophy.

Results: On the initial MRI, PTT tenosynovitis was seen in all 33 ankles; PTT hypertrophy in 15 (45.5%)/atrophy in ten (30.3%); PTT tear in 16 (48.5%). Spring ligament abnormality including tear, thinning, thickening, and/or edema was seen in 19 (57.6%). Osteoarthritis was seen in 12 (36.4%) on the initial study.

Of the initial 33 ankle MRI exams, 14 had normal spring ligaments initially; three developed new or progressive osteoarthritis (21%; average follow-up 21 months) and 2 (14%; average follow-up 25 months) developed new deformity. Five had a thickened spring ligament; one (20%; 23 month follow-up) showed new or progressive osteoarthritis and none developed new deformity. Eleven initially had a thinned spring ligament; six developed new or progressed osteoarthritis (55%; average follow-up 40 months). Eleven developed new deformity (100%; average follow-up 48 months)

Conclusion: A thinned spring ligament in the setting of PTT abnormality appears to be associated with increased risk of progressive arthritis and deformity over a relatively short period of time. MRI provides potentially useful clinical information in the setting of PTT abnormality and concomitant spring ligament abnormality that may predispose to development of OA and deformity. MRI could potentially be used to better stage patients with PTT symptoms to determine which may require more aggressive surgical intervention.

10:40 am

139. Delayed Gadolinium-Enhanced MR Imaging of Cartilage After Anterior Cruciate Ligament Tear

Tung, G.; Mehan, W.; Portnoy, R.; Fadale, P.; Hulstyn, M.; Bowers, M.; Oskendahl, H.; Fleming, B. The Warren Alpert Medical School of Brown University/Rhode Island Hospital, Providence, RI*
Address correspondence to W. Mehan (wmehan01@hotmail.com)

Objective: Delayed gadolinium-enhanced MR imaging of cartilage (dGEMRIC) is a molecular imaging technique used to study glycosaminoglycan (GAG) content of articular cartilage. The objective of this study is to compare dGEMRIC indices of femoral and tibial articular cartilage in both the anterior cruciate ligament (ACL)-injured and uninjured knee. We hypothesize that dGEMRIC indices will be lower in the ACL-injured knee, and that imaging order will not affect the dGEMRIC index.

Materials and Methods: dGEMRIC was performed on a 1.5T system. Each subject received 0.2 mmol/kg of gadopentetate dimeglumine (Bayer HealthCare Pharmaceuticals, Montville, NJ), and after 90 minutes, a series of five turbo inversion recovery sequences in the mid-sagittal plane of medial femoral condyle

were acquired in the injured and uninjured knees sequentially. The order was alternated such that the injured knee was scanned first in the odd-numbered subjects.

Results: Subjects included five men and seven women (mean age, 33 years; range, 20-49) with unilateral ACL tear and no prior history of knee injury. The median time between injury and dGEMRIC was 67.5 days. The pooled dGEMRIC index of the ACL-injured knees (419 ± 53; mean ± SD) was significantly less than that of uninjured knees (460.4 ± 72; p=0.01). When the injured knee was imaged first, there was no significant difference in the dGEMRIC indices between ACL-injured and uninjured knees for either the femur (p=0.19) or tibia (p=0.39). However, when the injured knee was imaged second (100 minutes after contrast administration), there was a significant difference in dGEMRIC indices for both the femur (p=0.04) and tibia (p=0.008). The dGEMRIC indices for uninjured knees were not affected by imaging order: femur, 460.8 ± 58 vs. 460.0 ± 58; tibia, 429.5 ± 58 vs. 430.8 ± 58.

Conclusion: dGEMRIC reveals significantly lower GAG content in the femoral and tibial articular cartilage of ACL-deficient-knees. dGEMRIC indices of ACL-injured knees were sensitive to imaging order since it takes longer for equilibrium to be established between gadopentetate dimeglumine concentration in synovial fluid and articular cartilage when GAG content is abnormal.

10:50 am

140. Accuracy of Radiographs for the Detection of Hip and Pelvic Fractures in Patients Presenting in an Emergency Department Setting

Kirby, M.; Spritzer, C. Duke University Medical Center, Durham, NC*
Address correspondence to M. Kirby (matthew.kirby@duke.edu)

Objective: Our study seeks to evaluate the accuracy of radiographs of the hip and/or pelvis in patients who present in an emergency department (ED) setting with complaints of pain and who ultimately receive an MR examination.

Materials and Methods: All 128 MRI exams of the lower extremity or pelvis ordered by the ED from July, 2005 to June, 2008 were retrospectively reviewed by two musculoskeletal (MSK)-trained radiologists in consensus. Thirty patients were excluded: three pediatric patients; five who were not MSK protocols; two had no plain films; one patient's records could not be located; 15 imaged the knee or foot; and one patient's MR was obtained seven days after his plain films. All 94 remaining patients received radiographs of the pelvis, a single hip, bilateral hips, and/or the femur within one day of their MR study. All 94 patients had their plain films and MR reviewed and evaluated in regards to age, sex, MR protocol, site of fracture, fracture identification, other possible pain generators, as well as for unexpected findings. Four patients received bilateral studies for a total of 98 exams.

Results: Our patient population had an elderly and female bias, average age 70.4 (range 18-99) with 77 women and 17 men. Twelve patients had fractures identified by MR only. In addition, seven patients had their plain films interpreted as possible fracture and of these, four were positive for fracture on MR and three were negative. Eight patients who had their radiographs interpreted as positive were subsequently negative on MR. MR identified a total of 51 more fractures than plain films. MR demonstrated multiple fractures in nine patients (range 2-5) and demonstrated other potential etiologies of pain ranging from gluteal tendinopathy to muscle or hamstring injury in 33 patients. MR also demonstrated four cases of metastatic disease not identified on radiographs.

Conclusion: Elderly females are often osteopenic and constitute the majority of patients requiring MR after presenting to the ED with complaints of pelvic or hip pain. These patients often present a diagnostic challenge when plain films do not detect a fracture or an equivocal interpretation is offered. Our study demonstrates a 12.7 % rate of fracture identification on MR in this population after negative plain film evaluation and an overall plain film accuracy of 75.7%, excluding equivocal reads. Thus, in the elderly female ED population, clinical management based solely on negative plain films should be performed with caution and MR should be strongly considered given its higher rate of fracture detection and ability to identify additional pain generators.

11:00 am

141. MRI of Isolated Anterior Tibial Eminence Fractures in Adults

Feldman, F. Columbia Presbyterian Medical Center, New York, NY*
Address correspondence to F. Feldman (friedafeldman@hotmail.com)

Objective: The objective was to emphasize that anterior tibial eminence fractures which have heretofore been considered to predominantly occur in children may also occur in adults and particularly in older age groups.

Materials and Methods: Fifty adults 18-60 years old who presented with anterior tibial eminence fractures were imaged with radiographs and/or CT and MRI. MRI examinations utilized 1.5 or 3T magnets (GE Healthcare, Milwaukee, WI) with dedicated knee coils and multiple sequences in multiple planes.

Results: Isolated anterior tibial eminence fractures were often overlooked particularly on radiographs and CT. When subtle or occult they were considered tibial spine fractures or due to degenerative disease in older patients. When detected and particularly on MRI increased fragmentation and displacement increased with patients' age. A high incidence of associated soft tissue damage as well as the extent of both bony and soft tissue injuries were either not well defined or unappreciated in all age groups unless documented by MRI.

Conclusion: Anterior eminence fractures of the knee are not uncommon and should be considered in older patients as well as in children along with their differing mechanisms of injuries. MRI is the imaging modality of choice for the more complete documentation of associated injuries particularly due to the extent and degree of soft tissue damage which occurs in more than 80% of patients. These findings will be illustrated and discussed since the most complete extent of this injury particularly in adults as definite with MRI is associated with the best clinical outcome.

11:10 am

142. Tibial Plateau Cysts at the Meniscal Root Insertions: Incidence and Association with Meniscal Pathology

Didolkar, M.; Vinson, E. Duke University Medical Center, Durham, NC*
Address correspondence to M. Didolkar (manjiri.didolkar@duke.edu)

Objective: Small cysts in the bone marrow of the tibial plateau at the meniscal root insertions are often present on knee MRI examinations. The purpose of this study is to identify a possible relationship between tibial plateau cysts occurring at the meniscal root insertions and meniscal pathology, including meniscal tears and intrameniscal cysts.

Materials and Methods: One musculoskeletal-trained radiologist and a fourth year radiology resident retrospectively reviewed 200 consecutive knee MRI examinations obtained for clinical purposes at our institution for the presence or absence of tibial plateau cysts at the meniscal root insertion sites. The cysts were categorized as to location. Associated meniscal pathology, including meniscal tears and intrameniscal cysts, were also noted in each case.

Results: Of the 200 knee examinations, 83 (41.5%) demonstrated medial meniscal pathology and 47 (23.5%) demonstrated lateral meniscal pathology. Twenty-one (10.5%) of the 200 knee MRI examinations demonstrated cysts in at least one of the described locations; two knees had cysts in two separate locations each. Four (2%) of the examinations had cysts at the anterior horn medial meniscal root insertion, and all four (100%) of these had medial meniscal pathology. Eleven (5.5%) of the examinations demonstrated cysts at the posterior horn medial meniscal root insertion, and eight (72.7%) of these had associated medial meniscal pathology. Five (2.5%) of the studies demonstrated cysts at the anterior horn lateral meniscal root insertion, and one (20%) of these had associated lateral meniscal pathology. Two (1%) of the studies demonstrated cysts at the posterior horn lateral meniscal root insertion, and one (50%) of these had associated lateral meniscal pathology.

Conclusion: Tibial plateau cysts at the meniscal root insertions are often seen on knee MRI examinations. These cysts often correlate with meniscal pathology in the adjacent meniscus; this is particularly true of cysts located at the insertions of the anterior and posterior horns of the medial meniscus.

11:20 am

143. Obturator Externus Bursa: Prevalence of Communication with the Hip Joint and Associated Intra-Articular Findings in 200 Consecutive Hip MR Arthrograms

Kassarjian, A.[1,2]; Llopis, E.[3]; Bencardino, J.[4]; Schwartz, R.[5] 1. Corades, S.L., Majadahonda, Spain; 2. Massachusetts General Hospital, Harvard Medical School, Boston, Spain; 3. Hospital de la Ribera, Alzira, Spain; 4. New York University, New York, NY; 5. Longwood MRI Specialists, Brookline, MA*
Address correspondence to A. Kassarjian (akassarjian@partners.org)

Objective: The objective was to demonstrate the prevalence of communication between the hip joint and the obturator externus bursa at hip MR arthrography.

Materials and Methods: Following institutional review board approval, 200 hip MR arthrograms were retrospectively reviewed by two musculoskeletal radiologists. The presence or absence of communication between the hip joint and the obturator externus bursa was recorded. Communication between the hip joint and the obturator externus bursa was defined as gadolinium entering the obturator externus bursa. The status of the acetabular labrum and articular cartilage were recorded.

Results: A total of 200 hip arthrograms in 196 subjects were independently reviewed by two musculoskeletal radiologists. Discrepancies were resolved by adjudication. The obturator externus bursa was seen to communicate with the hip joint in 11 of 200 hip MR arthrograms. Of these, six were men and five were women. The age range was 15-63 years old with a mean age of 34 years. All 11 patients had labral tears. Eight of the 11 had mild degenerative changes including cartilage thinning/defects and subchondral marrow changes.

Conclusion: The obturator externus bursa can be seen to communicate with the hip joint in 5.5% of hip MR arthrograms. Associated intra-articular lesions are common.

11:30 am

144. Spontaneous Anterior Cruciate Ligament Repair

Steinbaker, R.; Patel, H.; Helms, C.; Taylor, D. Duke University, Durham, NC*
Address correspondence to R. Steinbaker (csteinba@gmail.com)

Objective: The anterior cruciate ligament (ACL), while essential for stability and movement of the knee, is one of the most frequently torn ligaments. ACL reconstruction is currently performed over 250,000 times per year in the U.S. Although it has been reported, spontaneous healing of a complete ACL tear is thought to be a rare occurrence. Five cases will be presented showing healing of complete ACL tears with clinical, MRI and surgical proof.

Materials and Methods: Retrospective review of five patients with MRI findings of a complete ACL tear were evaluated. All five were scheduled for ACL reconstruction by a single orthopedic surgeon who found immediately preoperatively that they had a negative Lachman's test. Repeat MRI was performed in three patients and two proceeded to arthroscopy. Three of the patients were females and two males. Age at presentation ranged from 22-64. Three of the patients received follow-up MRI exams between 3-102 months after their initial MRI and two patients went to arthroscopy. On follow-up physical exam all patients demonstrated a negative Lachman's test.

Results: All patients presented following an injury and physical exam findings which were concerning for an ACL tear. This was confirmed with MRI in all patients. All patients were scheduled for surgery but demonstrated a negative Lachman's test preoperatively. Subsequent MRI demonstrated an intact ACL in three cases. Two patients proceeded to arthroscopy which demonstrated a normal ACL.

Conclusion: In a certain subset of patients there is evidence to support that a nonoperative course may be of benefit to regain ACL function. Very few reports have documented spontaneous healing of a torn ACL. While extremely rare, this report is the first

to show clinical, MRI and surgical proof of spontaneous ACL healing. Although no criteria have been developed to suggest which patients might undergo spontaneous ACL healing, radiologists should be aware that this may be encountered.

11:40 am

145. Assessment of Tibial Plateau Fracture Healing: Precise Evaluation Using an Advanced CT Workstation

Choplin, R.[1]; Persohn, S.[1]; Ricci, W.[2]; Watson, T.[3]; Weber, T.[4]; Borrelli, J.[5]; White, R.[6]; Batts, J.[6] 1. Indiana University School of Medicine, Carmel, IN; 2. Washington University School of Medicine, St. Louis, MO; 3. St. Louis University Health Science Center, St. Louis, MO; 4. Orthopedics Indianapolis, Indianapolis, IN; 5. University of Texas Southwestern Medical Center, Dallas, TX; 6. Wright Medical Technology, Inc., Arlington, TN*
Address correspondence to R. Choplin (rchoplin@iupui.edu)

Objective: Assessment of reduction of tibial plateau fractures is performed by radiography using specific measures. Little has been written about using multichannel CT (MCCT) with multiplanar reformations (MPRs) for this task. We describe a method of using MCCT for assessment of fracture reduction and healing.

Materials and Methods: All patients were being evaluated for fracture reduction and healing using a synthetic bone graft substitute as an adjunct to screw-plate internal fixation. Radiographs (anteroposterior, oblique, and lateral) and a MCCT scan of the knee were obtained at the time of the initial injury, within seven days of the initial surgical repair, at 12 weeks and 24 weeks. Fractures were classified using the Arbeitsgemeinschaft fur Osteosynthesefragen-Orthopedic Trauma Association Classification of Tibial Plateau Fractures. The MCCT data was loaded onto a postprocessing workstation that allows up to four separate studies to be presented side-by-side. Axial, coronal and sagittal MPR were precisely aligned so that all measurements are made at nearly identical geometric positions. When possible, the data were evaluated as 1 mm thick sections. Measurements included depth of fracture depression, length of fracture, and width of fracture gaps. The volume of depression of the tibial plateau was measured in patients with subsidence > 2 mm. Comparison was made between serial radiographic measurements and CT measurements. The first postoperative scan served as baseline for evaluation of subsidence.

Results: Twenty-seven patients were enrolled at three institutions. There were eight B type fractures and 15 C type fractures. On radiographs, most patients had vertical or lateral decentering of the tibial plateau making measurement of depression unreliable. On the first post operative MCCT, 7/23 patients had restoration of the tibial plateau to normal, 15/23 patients had the tibial plateau depressed > 2.0 mm, 1/23 patients had the tibial plateau elevated > 2.0 mm. On 24 week MCCT, 3/23 patients had developed subsidence of the fracture > 2.0 mm. The volumes of subsidence were 2.1, 3.9, and 17.9 mm^3.

Conclusion: Assessment of reduction of tibial plateau fractures is unreliable by radiography. MCCT and use of an advanced postprocessing workstation allows for precise alignment and measurement of fracture reduction for longitudinal evaluation. Subsidence can be identified and a volumetric calculation can be performed.

11:50 am

146. Complications of Anterior Cruciate Ligament Reconstruction: MRI Evaluation

Pierre-Jerome, C.[1,2]; Albastaki, U.[1]; Kakarala, A.[2]; Gothlin, J.[1]; Terk, M.[2] Banerjee, S[2] 1. Sahlgrenska-Molndal University Hospital, Gothenborg, Sweden; 2. Emory University Hospital, Atlanta, GA
Address correspondence to C. Pierre-Jerome (cpierrejerome@msn.com)

Objective: Persistent symptoms following anterior cruciate ligament (ACL) reconstruction are usually suggestive of graft failure. The purpose of this study was to evaluate the findings associated with ACL graft dysfunction applying MRI.

Materials and Methods: The study was HIPPA and IRB compliant. We did a retrospective database search from two institutions for patients with symptoms following ACL reconstruction. There were 15 patients with symptoms referable to ACL reconstruction failure. Seven (46.6%) were operated on using an absorbable material (DePuy Mitek, Piscataway, NJ) Six (40%) underwent partial meniscectomy at the time of the ACL reconstruction. Symptoms were correlated to specific complications. Imaging was performed three weeks to three years following surgery. The MR images were acquired with spin echo sequences with and without fat saturation in all examinations. Gradient echo water excitation and in-and-out of phase images were added to some studies.

Results: There were five categories of complications: 1) Graft discontinuity 2) Inappropriate position of femoral and/or tibial tunnel 3) Hardware failure 4) Infection 5) Intra-articular arthrofibrosis. All 15 (100%) knees had some degree of joint effusion, as osteoarthritic changes were present in seven (46.6%) knees.

Conclusion: MRI accurately detected the causes of surgical failure and persistent pain following ACL reconstruction.

SCIENTIFIC SESSION 19

GENITOURINARY/OB/GYN (FEMALE GENITOURINARY) IMAGING PAPERS

Room: 309, Level 3

Wednesday, April 29, 2009, 10:00 am–12:00 noon

Abstracts 147-155

Moderators: *K. Andresen, P. Ramchandani*
Keynote Address: Female Pelvic Imaging: An Update—*P. Ramchandani*

10:40 am

147. Adenomyosis: New Observations on Sonohysterography with MRI Correlation

Verma, S.[1]; Lev-Toaff, A.[2]; Baltarowich, O.[1]; Bergin, D.[3]; Verma, M.[1]; Mitchell, D.[1] 1. Thomas Jefferson University Hospital, Philadelphia, PA; 2. Hospital of the University of Pennsylvania, Philadelphia, PA; 3. Galway University Hospital, Galway, Ireland*
Address correspondence to S. Verma (medskv@yahoo.com)

Objective: The objective was to describe features of adenomyosis on sonohysterography (SHG) with MRI correlation, including a previously unreported feature.

Materials and Methods: A three-year database search was performed to identify 26 women (mean age 45; age range, 25-64 years) who underwent SHG and pelvic MRI within six months and in whom either modality suggested adenomyosis. Indications for SHG included abnormal bleeding (n=22); infertility (n=3) and tamoxifen use/abnormal transvaginal sonography (TVS) (n=1). Twenty-three of 26 (88%) women had SHG findings suggestive of adenomyosis and three (12%) had adenomyosis identified on MRI performed after SHG. MRI and static SHG images were retrospectively evaluated by two radiologists in consensus. These radiologists reviewed the images and suggested adenomyosis based on one or more of these findings on SHG: asymmetric thickening of myometrium and heterogenous echo-texture, fluid tracking from the endometrial cavity into "myometrial cracks," myometrial cysts, appearance of air bubbles in myometrium and indistinct endometrial-myometrial junction.

Results: Among 23 women with adenomyosis on SHG, findings were: asymmetric myometrial thickening and heterogeneous echo-texture (n=14, 61%), "myometrial cracks" (n=6, 26%), myometrial cysts (n=6, 26%), indistinct endometrial-myometrial junction (n=5, 22%), myometrial air (n=3, 13%), combination of two (n=9, 39%). MRI confirmed the diagnosis of adenomyosis in 22/23 (96%). In 3/23 (13%) SHG suggested adenomyosis because of the appearance of myometrial echo-densities, presumably air bubbles during SHG, but MRI did not confirm adenomyosis in the same location.

Conclusion: When SHG findings suggested adenomyosis, MRI confirmed the diagnosis in 96% of cases. Intravasation of air into the myometrium in our small series did not correlate with focal adenomyosis by MRI in the same location as the air bubbles. A previously unpublished sign of adenomyosis on SHG is "myometrial cracks."

10:50 am

148. The Use of Transposterior Fornix Scanning in Patients with Uterus in Neutral Position

Yeh, H.; Shapiro, R.; Simpson, W. Mount Sinai Hospital, New York, NY*
Address correspondence to H. Yeh (hsu-chong.yeh@mountsinai.org)

Objective: The objective was to evaluate the advantages of transposterior fornix scanning (TPFS) technique in the examination of uterus when the details of uterus are not well visualized because of unfavorable position, e.g., neutral position.

Materials and Methods: Twenty-one patients found to have uteruses not well visualized on endovaginal scanning due to neutral position or incomplete anteverted position are included in the study. The tip of the transducer was repositioned into the posterior fornix and an appropriate pressure was applied on the transducer to convert the uterus into retroverted position in order to better visualize the details of the uterus.

Results: Among 21 uteruses studied, 11 uteruses were in neutral and straight position, six in neutral and slightly retroflex or slightly anteflexed position, two in incomplete anteverted anteflexed position and two in neutral and anteflex position. TPFS technique was completely successful in visualizing the details of the uterus in 71.4% of the cases, partially successful in 14.3% of the cases and failed in 14.3% of the cases. Incidentally, some uteruses changed from anteverted to various degree of retroverted positions or vise versa or changed to neutral position during the course of follow up examinations without manipulation. This may be called flip-flop uterus.

Conclusion: TPFS technique is very useful for improving visualization of uteruses in most patients when the uteruses were in unfavorable positions that prevented good visualization. The pliability of the uterus renders success for the TPFS technique and also resulted in flip-flop phenomenon in some patients. This technique was not useful when the uterus is too stiff or when the posterior fornix is too shallow.

11:00 am

149. Sonohysterography: The Utility of Diagnostic Criteria Sets

Bhaduri, M.; Glanc, P.; Khalifa, M.; Tomlinson, G. University of Toronto, Toronto, Canada*
Address correspondence to M. Bhaduri (bhmous@gmsil.com)

Objective: The purpose of this study was to determine if applying specific diagnostic criteria to the interpretation of a sonohysterogram would improve the diagnostic power of the interpretation.

Materials and Methods: This is a retrospective study of patients who underwent both a sonohysterogram and a procedure which resulted in a positive pathological diagnosis. The initial read (reader one) was performed by senior radiologists, each with more than ten years of experience, at the time of the examination. Subsequently, the sonohysterograms were interpreted by a reviewer (reader two) with limited expertise, blinded to both the original medical imaging report and the associated pathology

diagnosis. Reader two utilized a designated set of diagnostic criteria to determine the following diagnoses: endometrial hyperplasia, endometrial polyp, endometrial carcinoma or submucosal leiomyoma. These results were compared to the initial diagnostic report (reader one) and the final pathological findings.

Results: A total 60 patients were reviewed. The comparison of reader one to reader two using the pathology diagnosis as the gold standard was as follows: 66.7% polyps by reader one vs. 68.3 % polyps by reader two (kappa=0.81); 10% hyperplasia and 5% cancer identified by both reader one and reader two (kappa=0.81, 0.3, respectively). The overall concordance with pathology was 84.5% for reader one and 91.7% for reader two.

Conclusion: Sonohysterography performs well in the diagnosis of common endometrial pathologies. Using specific diagnostic criteria added to diagnostic accuracy in the identification of endometrial polyps and hyperplasia, even in the hands of a reviewer with limited experience.

11:10 am

151. Treatment Response with Ca-125 in Ovarian Cancer Patients: Comparison among RECIST, WHO, Tridimensional and 3D Volumetric Criteria

Oliveira, G.[1]; Zondervan, R.[2]; Harris, G.[2]; Hodge, S.[2]; Harisinghani, M.[2] 1. University of Washington, Seattle, WA; 2. Massachusetts General Hospital, Boston, MA*
Address correspondence to G. Oliveira (grachid@u.washington.edu)

Objective: The purpose of our study was to compare RECIST (1D), WHO (2D) and two different volumetric techniques (3M and 3D) for the evaluation of treatment response in ovarian cancer patients.

Materials and Methods: Ninety-seven lesions, from 37 patients enrolled in six different ovarian cancer clinical trials were independently evaluated using one-dimensional (1D), bidimensional (2D), tridimensional (3M) and 3D volumetry by a radiologist and an extensively trained image analyst. The measurements were summed across lesions to obtain the overall patient response. All patients had CT scans and blood level of the tumor marker Ca-125 every two months with at least six months follow-up.

Results: The correlation between methods was assessed using Pairwise Correlations. RECIST vs. 2D, r(141)=0.93; RECIST vs. 3M=r(141)=0.85, RECIST vs. 3D=r(141)=0.76, all of them with p<.0001. When comparing 2D vs. 3M, r(141)=0.95; 2D vs. 3D r(141)=0.88, in both, p<.0001. 3M vs. 3D, the r(141)=0.91, p<.0001. The Ca-125 demonstrated a poor correlation with all four methods with r(141)=0.272 (p<.001), 0.324 (p<.0001), 0.24 (p<.003) and 0.326 (p<.0001) when compared with 1D, 2D, 3M and 3D respectively. The responses were categorized as stable disease (SD), partial response (PR) and progressive disease (PD) for each criteria used. The percent agreement was calculated using kappa (k) statistic. RECIST agree to 2D in 84/104 (80%), k=0.64 (SE=0.068). With 3M the agreement was 79 of 104 (75%) k=0.55 (SE=0.074), and with 3D was 85/104 (81%) k=0.63 (SE=0.072). 2D agree to 3M in 88/104 (84%), k=0.73 (SE=0.06), and with 3D the agreement was 87/104 (83%) k=0.71 (SE=0.063). 3M agree to 3D in 87/104 (83%), k=0.71 (SE=0.063).

Conclusion: The results suggest a strong correlation between RECIST, 2D, 3M and 3D criteria when evaluating tumor response in patients in ovarian cancer patients without statistically significant difference. However Ca-125 didn't show correlation statistically significant when compared with any of the size criteria utilized. The level of agreement demonstrated to be full to almost perfect agreement, with the exception of a moderate agreement showed between 2D and 3M. RECIST is the most common method used to assess therapeutic effects in oncology clinical trials, and when compared with other criteria, it doesn't show a statistically significant difference.

11:20 am

152. MRI Diagnosis of Pelvic Organ Prolapse: Puboccocygeal Line and Midpubic Line Compared With Clinical Examination

Pannu, H.[1]; Scatarige, J.[2]; Eng, J.[2] 1. Harvard Medical School, Boston, MA; 2. Johns Hopkins Medical Institutions, Baltimore, MD*
Address correspondence to H. Pannu (hpannu@bidmc.harvard.edu)

Objective: The objective was to compare MRI diagnosis of pelvic organ prolapse relative to pubococcygeal line (PCL) and midpubic line (MPL) with clinical exam.

Materials and Methods: Dynamic MRI exams done in 88 women (with rectal contrast n=39, noncontrast n=49) were evaluated by two readers. The PCL was drawn from inferior pubis to the last coccygeal joint. The MPL was drawn along the long axis of the pubis. Organ descent below PCL, bladder <3 cm above MPL, vagina <5 cm above MPL, anterior rectal bulges >/=3 cm defined as abnormal. Clinical exam reviewed (bladder n=77 patients, vagina n=65, rectum n=80).

Results: Overall percentage of patients positive for abnormality: cystocele-clinical 82%, MPL 99%, PCL 82%; vaginal prolapse-clinical 75%, MPL 78%, PCL 60%; rectocele-clinical 82%, MRI 38%. Rectal contrast MRI agreement with clinical: cystocele-85% for MPL, 79% for PCL (p=0.17); vaginal prolapse-59% for MPL, 50% for PCL (p=0.2); rectocele-61% with imbalance in disagreements (p=0.02). Noncontrast MRI agreement with clinical: cystocele-78% for MPL, 67% for PCL (p=0.19); vaginal prolapse-71% for MPL, 58% for PCL (p=0.1); rectocele-40% with imbalance in disagreements (p<0.001).

Conclusion: There was agreement with clinical exam similar for MPL and PCL for cystocele and vaginal prolapse. There was significant disagreement between clinical exam and MRI for rectoceles, especially for noncontrast MRI.

11:30 am

153. Comparison of Sagittal T2-Weighted BLADE and Fast Spin Echo MR Imaging of the Female Pelvis for Motion Artifact and Lesion Detection

Lane, B.; Qureshi, F.; Oz, R.; Irwin, E.; McMillan, A.; Wong-You-Cheong, J. University of Maryland School of Medicine, Baltimore, MD*
Address correspondence to B. Lane (blane@umm.edu)

Objective: The purpose of this study is to compare conventional sagittal T2-weighted fast spin echo MR imaging of the female

pelvis with a novel PROPELLER-based sequence, for the presence of artifacts and for image quality.

Materials and Methods: A total of 26 female patients underwent both sagittal T2-weighted BLADE and fast spin echo (FSE) MR imaging of the pelvis using a 1.5 T magnet (Siemens Healthcare, Malvern, PA). Following data randomization, three abdominal radiologists, blinded to the sequences, independently reviewed the studies on a PACS workstation. A modified Likert scale was used to evaluate artifacts (bowel motion, respiratory motion, radial artifact and aliasing), anatomic detail (junctional zone, fibroid detection and ovaries/follicles), and overall image quality. Scores for each radiologist and imaging sequence were analyzed statistically with a linear mixed model, adjusting for correlation within radiologist and within patient. Quantitative comparison was also conducted to investigate changes in signal uniformity (coefficient of variation) from multiple regions of interest.

Results: Image quality was superior with a PROPELLER-based sequence. There were fewer respiratory motion, bowel motion and aliasing artifacts with a PROPELLER-based sequence. With the exception of bowel motion, these were highly statistically significant ($p<0.001$). A PROPELLER-based sequence introduced radial artifact which was absent in the FSE sequence, although this did not affect overall image quality. A PROPELLER-based sequence was superior for evaluation of the junctional zone ($p=0.0019$), ovaries ($p= 0.0001$) and fibroids (when present), ($p=0.0218$). Quantitative analysis revealed mean coefficients of variation for a PROPELLER-based sequence and FSE in the uterus to be 28.6% and 29.5%, respectively. For fat, the mean coefficients of variation were 6.1% and 11.5%, indicating significantly ($p=0.00027$) less variation in the PROPELLER-based sequence images. The mean time for acquisition of the PROPELLER-based sequence was 4:31 minutes, compared to 3:46 minutes for the FSE sequence.

Imaging of uterine junctional zone anatomy, ovaries, and fibroids was superior with a PROPELLER-based sequence compared to FSE T2. Common artifacts were reduced with a PROPELLER-based sequence. Radial artifacts introduced by the PROPELLER-based sequence and slightly longer imaging time are offset by improved image quality.

Conclusion: A sagittal PROPELLER-based sequence can replace FSE in imaging of the female pelvis, resulting in reduction of artifacts and improved image quality, with only minimal increase in acquisition time.

11:40 am

154. Early First Trimester Fetal Radiation Dose Estimation in 16- and 64-MDCT: a Multivendor Trial

Jaffe, T.; Neville, A.; Yoshizumi, T.; Toncheva, G.; Anderson-Evans, C. Duke University Medical Center, Durham, NC*
Address correspondence to T. Jaffe (jaffe002@mc.duke.edu)

Objective: The objective was to corroborate the relationship between estimated absorbed fetal dose (FD) derived by directly measured uterine doses in early first trimester and the volume CT dose index (CTDIvol) for 16- and 64-channel MDCT scans of the maternal chest, abdomen and pelvis.

Materials and Methods: Estimated absorbed FD was measured using a metal oxide semiconductor field effect transistor (MOSFET) dosimeter that was placed in the uterus of an adult female anthropomorphic phantom. The phantom was scanned on a 16- and 64-channel MDCT scanner (Siemens Medical Solutions, Forchheim, Germany) as well as a 64-channel scanner (GE Healthcare, Milwaukee, WI) using a trauma chest-abdomen-pelvis protocol and an abdomen and pelvis protocol. Beam energy was selected based on scanner options and automated tube current modulation (ATCM) was used on all scanners. Three different settings for ATCM were applied to the trauma chest, abdomen and pelvis protocol, for a total of four protocols for each scanner. Absorbed uterine dose was measured directly from the MOSFET detector. Each protocol was performed three times and mean uterine dose was calculated. CTDIvol for each protocol was recorded from the scanner console. Correlation between mean uterine dose and CTDIvol was tested with a goodness of fit model.

Results: Mean absorbed uterine dose ranged from 9.25 to 37.7 mGy. Absorbed FD in the early first trimester correlated with the CTDIvol via a linear regression equation. For the 16-detector scanner at 130 kVp, FD (mGy) =2.091*CTDIvol (mGy)- 9.489 . For the 64-channel scanner at 120 kVp, FD (mGy) = 1.113*CTDIvol (mGy) +1.773. For the 64-channel scanner at 140 kVp, FD (mGy) = 2.451*CTDIvol (mGy)-5.696 and at 120 kVp, FD(mGy)= (1.408 ± 0.1190)*CTDIvol (mGy)-1.044. The goodness of fit (R^2) for the above equations is 0.97, 0.98, 0.89 and 0.98, respectively.

Conclusion: Absorbed fetal dose from a first trimester is linearly associated with the CTDIvol and may be calculated from scanner console data, regardless of beam energy, detector configuration, or scanner manufacturer. This corroborates earlier data obtained on a 16-channel scanner.

11:50 am

155. What is the Impact of MRI in Fetuses with Ventriculomegaly and Intracranial Hemorrhage?

Sansgiri, R.[1]; Levine, D.[1]; Estroff, J.[2]; Robertson, R.[2]; Poussaint, T.[2]; Robson, C.[2]; Mehta, T.[1]; Barnewolt, C.[2] 1. Beth Israel Deaconess Medical Center, Boston, MA; 2. Children's Hospital, Boston, MA*
Address correspondence to R. Sansgiri (rsansgir@bidmc.harvard.edu)

Objective: The objective was to compare ultrasound (US) and MRI diagnosis of intracranial hemorrhage (ICH) in fetuses with ventriculomegaly (VM).

Materials and Methods: Medical records of 383 fetuses enrolled in a prospective study of US and MRI for VM over a five year period were reviewed for the diagnosis of ICH. Prenatal and postnatal US and MR were independently interpreted by seven radiologists. Types of bleed were intraventricular, subependymal, parenchymal, subdural, or other. Presence of any bleed and specific type of bleed were tallied. Consensus diagnosis was reached after prospective reads were tallied. Gestational age ranged from 20-36 (mean 28) weeks. Reference standards were postnatal US (n=9) and MRI imaging (n=13), and autopsy (n=3).

Results: Twenty-one cases were coded by at least one reviewer as having ICH. One patient declined prenatal MRI after enrollment. There were seven terminations of pregnancy, one stillbirth and 13 live births; 16 cases had reference standard (three autopsies and 13 postnatal imaging). Of these, 13 were positive and three were negative for intracranial bleed. In 3/10 cases all US reviewers agreed on the presence on bleed, but in only 1/10 cases did they agree on the location. In 7/20 cases all MR reviewers agreed on the presence on bleed, but in only 1/20 cases did they agree on the location. Prenatal US consensus diagnosis detected 8/13 positive cases and 2/3 negative cases. Prenatal MRI detected 9/10 positive cases and 1/5 negative cases. Prenatal US findings were consistent with reference standard findings for the presence of bleed in 7/8 cases but only in 5/8 for location of bleed. Prenatal MRI findings were consistent with reference standard for presence of bleed in 7/13 and location of bleed in 2/13. Prenatal US and MRI were in agreement for the type of bleed in four cases. MRI changed the type of bleed in 2 and added another bleed type in two cases. MRI showed additional findings not seen on US of septal dysplasia (n=1), infarction (n=7), defects in the corpus callosum (n=3), cerebellar hypoplasia (n=1) and porencephaly (n=5). US detected one bleed and one hypoplasia of corpus callosum which were not seen on MRI. Postnatal imaging showed new findings of periventricular leukomalacia (n=4), septal dysplasia (n=1), infarctions (n=2), callosal abnormalities (n=3), migrational abnormalities (n=3) and porencephaly (n=2).

Conclusion: Disagreements are common in diagnosis of fetal ICH. MRI is a valuable complementary tool in detecting and characterizing ICH in fetuses with VM. This is important in patient counseling.

BREAST IMAGING PAPERS

Room 310, Level 3

Wednesday, April 29, 2009, 12:30 pm–2:30 pm

Abstracts 156-164

Moderators: *J. Leung, S. Patterson*
Keynote Address: Triple Negative Breast Cancer: Current Concepts—*G. Whitman*

1:00 pm

156. Breast Tuberculosis in a Developing Country

Shah, S.; Walvekar, V.; Parekh, K.; Goswami, K. Gujarat Cancer and Research Institute, Ahmedabad, Gujarat, India*
Address correspondence to S. Shah (swatishah_73@yahoo.co.in)

Objective: Breast tuberculosis is rare in developed countries. The incidence, however, shows a rising trend in developing countries owing to drug resistant strains. The aim is to study the mode of different presentations of breast tuberculosis in developing countries. This study also aims at studying mammographic and sonographic features of breast tuberculosis.

Materials and Methods: We performed mammographic examinations with craniocaudal and oblique views after explaining the procedure to the patient. All the patients underwent mammosonographic evaluation with high resolution 7.5 MHz probe. All the cases were confirmed with pathological diagnosis by fine needle aspiration cytology (FNAC), Mantoux test or blood chemistry.

Results: We studied nine case of breast tuberculosis in five years. Total incidence is 0.09%. The majority of patients were between 30 and 40 years. However cases also were found at a minimum age of 18 years and maximum of 48 years. The most common presenting symptom was painless lump (55%), followed by pus discharging sinus (44%). A history of low grade fever was found in two patients. Five cases (55.55%) were known cases of tuberculosis with secondary involvement of breast while four cases had no history of Koch's elsewhere in the body (44.44%). Mammographic findings showed ill-defined soft tissue density with nonspecific features in seven cases while two cases did not show the lesion by virtue of its location. Ultrasound showed cystic lesion with internal echoes with well defined wall and multiple side tracks extending into adjacent parenchyma.

Conclusion: Incidence of breast tuberculosis is still high in developing countries. Mammography is not specific for its detection. Clinical features like painless swelling, recurrent swelling, cutaneous fistulous track should raise high suspicion of tubercular breast. Secondary breast involvement is more common than primary breast tuberculosis. Ultrasound may be of great help in characterizing the lesion and locating it. Doppler shows peripheral vascularity along the margins of the lesion.

1:10 pm

157. Imaging Findings of Triple Negative Breast Carcinoma

Vieira, C.; Guth, A.; Moy, L.; Lee, J.; Toth, H.; Cangiarella, J.; Mercado, C. NYU Cancer Institute, New York, NY*
Address correspondence to C. Mercado (cecilia.mercado@nyumc.org)

Objective: Although much has been reported about the clinical features and the therapeutic management of triple negative breast (TNB) carcinoma, few studies have reported on the imaging findings. The purpose of this study is to describe the imaging characteristics of TNB tumors and correlate them with the histopathologic findings.

Materials and Methods: The records of 43 women with 57 triple negative breast cancers (TNBC) from June, 1996 to April, 2007 with available imaging studies were reviewed retrospectively. TNBC were defined as those with immunohistochemical staining negative for estrogen receptor, progesterone receptor, and HER2 negative. One woman had metachronous bilateral breast cancer and two had synchronous bilateral breast cancer. The clinical presentation, imaging features, and histopathologic findings were reviewed.

Results: The 57 TNBCs occurred in 43 women with mean age of 54 years (range, 28-84 years). Forty-six TNB tumors were index lesions for which initial imaging was performed. Eleven additional TNBCs were identified on histopathology specimens at surgery and were occult clinically and on imaging. A palpable mass was present in 63% of index lesions (29/46). Mean lesion size of index lesions was 16.7 mm (range, 3-80 mm). Mammography was available for 40 of 43 patients. Mammographic findings of 43 index TNBCs in 40 patients were mass in 20, focal asymmetry in three, architectural distortion in three, calcifications in four, and mass and calcifications in six. Seven index lesions were mammographically occult. Sonographic findings available for 33 index lesions all showed a mass. In total 18 of 54 (33%) TNBCs were mammographically occult. Histopathology revealed 47 lesions were infiltrating ductal carcinomas (IDC) (82%), four infiltrating lobular carcinomas (ILC) (7%), two medullary carcinomas (4%), two tubular carcinomas (4%), one metaplastic (2%), and one was mixed IDC/ILC (2%). Thirty-nine of the 47 IDC cases (83%) were poorly differentiated, seven (15%) were moderate, and one (0.2%) was well. Of the18 mammographically occult lesions, 14 were IDC, one was ILC, and three other (two tubular, and one metaplastic). Ductal carcinoma in situ (DCIS) was seen in association with the TNBC in 49/57 lesions (86%).

Conclusion: Less than half (48%, 26/54) of the TNBCs appeared on mammography as a mass without or with calcification. One-third (33%) of all TNB tumors imaged in our series were mammographically occult. Despite 86% of TNBCs having an associated DCIS component on histopathology, only 19% (10/54) appeared as calcifications on mammography.

1:20 pm

158. Frequency of Associated Ductal Carcinoma In Situ in Triple Negative Breast Cancers

Mercado, C.; Vieira, C.; Guth, A.; Moy, L.; Lee, J.; Toth, H.; Cangiarella, J. NYU Cancer Institute, New York, NY*
Address correspondence to C. Mercado (cecilia.mercado@nyumc.org)

Objective: Recent histopathologic studies have indicated that triple-negative breast (TNB) cancers typically are poorly differentiated tumors that have little or no associated ductal carcinoma in situ component. It is hypothesized that TNB tumors may directly progress to invasive carcinoma without an in-situ phase due to their rapid growth. The purpose of this study was to determine

how often DCIS was seen in TNB cancers and to correlate these with the tumors histologic type and grade.

Materials and Methods: The records of 128 women with 145 triple negative breast lesions defined as those with estrogen receptor negative, progesterone receptor negative and HER2 negative by immunohistochemistry were identified and reviewed retrospectively. The mean patient age was 54.9 years (range, 27 to 94 years). The presence of a DCIS component associated with the TNB lesions was evaluated and correlated with the histologic type and grade of these tumors.

Results: A total of 62% (90/145) of TNB cancers had an associated DCIS component. The histologic type of the TNB cancers containing a DCIS component was ductal type in 80 (89%) cases, lobular in two (2%), mixed-ductal/lobular in three (3%), metaplastic in two (2%), invasive apocrine in two (2%), invasive papillary in one (1%). There were no medullary carcinomas. The tumor grades of the TNB cancers were 68 (76%) high grade, 17 (19%) moderate, and five (6%) low. The DCIS component was high grade in 66 cases (73%), intermediate grade in 15 (17%) and low grade in nine (10%).

Conclusion: A large percentage (62%) of TNB cancers has an associated DCIS component. The majority of TNB cancers with associated DCIS are high grade invasive ductal carcinomas with a DCIS component which is high grade in the majority of cases (73%).

1:30 pm

159. Computerized Assessment of Mammographic Breast Density

Saenz, N.[1]; Huo, Z.[2]; Foos, D.[2]; Lao, Z.[2]; Siegel, E.[1,3] 1. University of Maryland School of Medicine, Baltimore, MD; 2. Carestream Health, Inc, Rochester, NY; 3. Veteran Affairs Maryland Health Care System, Baltimore, MD*
Address correspondence to N. Saenz (njsaenz@gmail.com)

Objective: Increased mammographic density is associated with an increased risk for breast cancer. Breast composition, primarily determined by the relative amount of dense breast tissue on a mammogram, is evaluated visually and subjectively in current practice. We have developed a method to automatically assess breast density on mammograms. We are not aware of any previous quantitative techniques to evaluate breast density on a mammogram. The method could provide a more consistent and accurate measure of breast density.

Materials and Methods: The algorithm automatically 1) segments the breast region from its background, 2) removes the pectoral muscle, and 3) clusters breast tissue into two categories, dense or fatty. The percentage of tissue over the region of the breast that is dense, excluding the pectoral muscle, is calculated and is referred to as MDP (mammographic density percentage). We employed an unsupervised clustering technique, known as "fuzzy c-means (FCM) clustering", to classify the pixels in the breast region as "dense" or "fatty". The performance of the method was evaluated on 200 standard mammograms from 50 patients. Three radiologists reviewed four mammograms from each patient and provided a visual estimation of MDP to the nearest 5%. They also ranked the accuracy of computer estimates of breast density as within a difference of +5, +10, +15%, or beyond in comparison with their visual assessment.

Results: We assessed the correlations on MDP ratings. The correlation coefficients ( ) between the three readers are 0.88, 0.89, and 0.92, respectively. The computer ratings (average of four mammograms) also yielded a strong correlation (γ=0.86) with the readers' overall ratings (average of the three readers). Of the 50 cases, 38 cases were ranked by at least one reader as "within a +5% difference in agreement". The correlation between the computer and readers' overall ratings increased to γ=0.90 on these 38 cases. Our analysis also showed that the individual reader's MDP ratings tended to agree better with the computer for fatty than for dense breasts. Of the cases that were ranked as "within a +5% difference in agreement", the actual reader's MDP's were on average 2.5% and 35% higher than the computer for the fatty (MPD< 20%) and dense (MPD>50%) breasts, respectively.

Conclusion: Our automated computer assessment of MPD correlates strongly with overall reader assessment. This suggests that the algorithm could be utilized to provide an objective assessment of breast density and change over time.

1:40 pm

160. Breast Mass Density: An Important Predictor of Breast Cancer?

Woods, R.[1]; Salkowski, L.[1]; Sisney, G.[1]; Shinki, K.[2]; Burnside, E.[1] 1. University of Wisconsin School of Medicine and Public Health, Madison, WI; 2. University of Wisconsin-Madison, Madison, WI*
Address correspondence to R. Woods (rwoods@uwhealth.org)

Objective: Prior research has not demonstrated a significant association between noncalcified solid breast masses and breast malignancy. The purpose of this study was to determine if breast mass density is predictive of malignancy and to evaluate the interobserver agreement for assessing breast mass density.

Materials and Methods: Between October, 2005 and December, 2007, we gathered BIRADS descriptor data for all noncalcified solid breast masses undergoing biopsy. We collected mass density, shape, margin, and overall breast density descriptor data prospectively using a mammography reporting system (PenRad, Minnetonka, MN). In order to have complete mass density descriptor data for all solid masses and compare these descriptors between radiologists, we assessed mass density (and size when not previously collected) in a retrospective reader study. The masses were randomized and three subspecialty trained mammographers, blinded to biopsy results, evaluated each mass. A forward stepwise binary logistic model evaluated the relative contribution of mass density and size, overall breast density, and age to benign or malignant outcome. We calculated a kappa statistic to determine interobserver agreement on the subset of masses that had mass density evaluated both prospectively and retrospectively.

Results: Our data set consisted of 359 solid masses in 328 women age 31-95 (mean 54.9, SD 13.4). There were 236 benign masses with an average size of 12.8 mm (SD 8.4), and 123 malignant masses with an average size of 15.2 mm (SD 8.6, $p<0.001$). Only breast mass density ($p<0.0001$) and age ($p=0.001$) were predictive of malignancy in our logistic model, while size and overall breast density were removed from the model because they did not significantly improve prediction accuracy. On a subset of 187 masses, the interobserver agree-

ment between prospective and retrospectively measured breast mass density was k=0.447, reflecting moderate agreement.

Conclusion: We found that high breast mass density is a significant predictor of malignancy. Though moderate interobserver agreement between prospective and retrospective assessment of breast mass density may indicate it is difficult to consistently evaluate, breast mass density is in fact predictive of malignancy.

1:50 pm

161. Sonographic Evaluation of Internal Mammary Adenopathy

Ojeda-Fournier, H.; Comstock, C.; Gardner, C. University of California, San Diego, San Diego, CA*
Address correspondence to H. Ojeda-Fournier (ojeda-lowy@sbcglobal.net)

Objective: Silicone-induced lymphadenopathy is a complication of silicone implant rupture or silicone gel-bleed. We report two cases of patients status postmastectomy and reconstruction with silicone implants presenting with new internal mammary and axillary lymphadenopathy.

Materials and Methods: Evaluation of the axillary lymph nodes is standard, and the classic "snowstorm" appearance by ultrasound is pathogneumonic for a benign process. We report the technique for ultrasound evaluation of the internal mammary lymph nodes and describe a new sign in radiology that is noted in patients with silicone-induced lymphadenopathy in the internal mammary lymph node chain: the pleural interruption sign.

Results: Patient one: BRCA positive with history of ovarian cancer, prophylactic mastectomies and silicone implant reconstruction. Patient two: history of breast cancer and mastectomy with silicone implant reconstruction. Routine CT of the chest in both patients found internal mammary and axillary lymphadenopathy. Ultrasound of the axillary lymph nodes demonstrated classic appearance of silicone lymphadenopathy. Ultrasound of the internal mammary lymph node was then performed and revealed a solid echogenic mass with distinctive interruption of the pleural line as a result of snowstorm shadowing.

Conclusion: In patients with silicone implants placed after breast reconstruction, the presence of axillary or internal mammary lymphadenopathy is concerning for recurrence of breast cancer. While silicone is generally considered an inert compound, it is important to realize that any female with silicone implants, including those with a history of breast cancer, may develop an inflammatory, immune reaction to silicone microparticulates, especially in the context of implant rupture or leakage that can manifest as silicone-induced adenopathy. Silicone lymphadenopathy may involve the axillary, intramammary, supraclavicular, and internal mammary regions. In such situations, ultrasound and/or MR can be used to further evaluate and characterize definitively the appearance of causal silicone-induced lymphadenopathy, hereby avoiding unnecessary biopsies and surgical procedures.

2:00 pm

162. Can Preoperative Axillary Ultrasound Exclude Stage N2 and N3 Metastatic Breast Cancer?

Neal, C.; Daly, C.; Nees, A.; Helvie, M. University of Michigan, Ann Arbor, MI*
Address correspondence to C. Neal (hawleyc@med.umich.edu)

Objective: The objective was to report the accuracy of preoperative axillary ultrasound to exclude N2/N3 metastatic disease in breast cancer patients. Preoperative distinction between N1 and N2/N3 disease may be clinically relevant to reduce morbidity and guide treatment protocols.

Materials and Methods: Following IRB approval, retrospective search of radiology records at our National Comprehensive Cancer Network (NCCN) designated site between January 1, 2006 and December 31, 2007 identified 449 breast cancer patients with preoperative axillary ultrasound (AUS). Of these, 218 had negative AUS with correlative surgical lymph node data (216 patients, 3 males). Indications for AUS were invasive cancers >1 cm or as requested by the referring clinician. The criteria used for abnormal lymph nodes included diffuse or focal cortical thickening and replacement or compression of the fatty hilum. The original radiology report was used to document negative or positive studies. All AUS were performed by MQSA dedicated academic breast imagers. Axillary status was determined by surgical pathology reports. Patient age, sex, tumor type, grade, size and hormone receptor status (ER/PR/HER2/neu) were documented from medical records.

Results: Patient age range was 25-88 years (mean=55). 151/218 (69%) of the cancers were invasive ductal, 47/218 (22%) were lobular or mixed ductal/lobular, 15/218 (7%) were other invasive carcinomas and 5/218 (2%) were ductal carcinoma in situ (DCIS). Of 218 cases with negative AUS, 13/218 (6%) had final node staging of N2/N3; 11/218 (5%) were N2 stage and 2/218 (1%) were N3 stage. N2/N3 patients were all female. Of the patients with N2/N3 disease, 8/13 (62%) had lobular histology and 5/13 (38%) had ductal histology. The false negative rate for N2/N3 disease was 3% (5/151) for invasive ductal cancer and 17% (8/47) for invasive lobular cancer ($p<0.01$).

Tumor size was: T0 5/218 (2%), T1 134/218 (62%), T2 71/218 (33%), T3 5/218 (2%) and T4 3/218 (1%). Seven of 13 (54%) N2/N3 patients were T1, 5/13 (39%) N2/N3 patients were T2 and 1/13 (7%) were T3. None of the N2/N3 disease arose from T0 or T4 size tumors. Nodal status for the study population was: N0 164/218 (75%), N1 41/218 (19%), N2/N3 13/218 (6%). Two of 30 (7%) HER2/neu positive cancers had N2/N3 disease. Zero of 38 (0%) triple negative hormone tumors were N2/N3.

Conclusion: AUS did not exclude N2/N3 disease. For women with invasive ductal breast cancer, the false negative rate was very low (3%). However, the false negative rate for lobular cancer was significantly ($p< 0.01$) higher (17%).

2:10 pm

163. Mammographic Findings of Partial Breast Irradiation vs. Whole Breast Irradiation in Patients Who Underwent a Segmental Mastectomy for Invasive Ductal Carcinoma

Kuzmiak, C.; Zeng, D.; Cole, E.; Pisano, E. University of North Carolina, Chapel Hill, NC*
Address correspondence to C. Kuzmiak (Cherie_Kuzmiak@med.unc.edu)

Objective: The objective was to determine if patients who underwent a segmental mastectomy followed by partial breast irradiation had fewer mammographic changes on the first post-treatment mammogram than patients who underwent a segmental mastectomy followed by whole breast irradiation.

Materials and Methods: Subjects enrolled in our institution's IRB-approved partial breast irradiation therapy after a segmental mastectomy study (IORT) plus a random sample of patients who underwent a segmental mastectomy but followed by conventional whole breast radiation therapy (WBRT) were identified through our institution's breast cancer database from March, 2003 through February, 2006. A radiologist, specializing in breast imaging, reviewed and recorded each patient's pretreatment mammogram for the breast density and location of tumor, and the first post-treatment mammogram obtained within the first year of treatment for three common types of mammographic change seen after breast surgery and radiation treatment (breast edema, skin thickening, and surgical scar), which when severe, make it difficult to use mammography for continuing follow-up of the conserved breast. The extent of mammographic change was noted by the radiologist as minimal, moderate, or marked. The data was entered into a database and statistical analysis was conducted using logistic regression models and Chi-square test. The effect of breast density on mammographic change was also assessed.

Results: The severity of edema was lower with decreasing breast density ($p<0.006$). There was no apparent effect of breast density on the severity of skin thickening. The extent of surgical scarring decreased as the amount of density in the breast increased ($p<0.026$). Analysis of the data from the cumulative logistic regression models demonstrated that even after controlling for breast density, WBRT patients had significantly more edema ($p=0.003$), skin thickening ($p=0.003$), and surgical scar than the IORT group ($p<0.001$).

Conclusion: Patients have a higher probability of having fewer post-treatment mammogram changes after a segmental mastectomy followed by partial breast irradiation than after whole breast irradiation.

2:20 pm

164. Breast Cancer in the Young Patient Aged 25 Years and Under

Blane, C.; Joe, A.; Daly, C. University of Michigan Health System, Ann Arbor, MI*
Address correspondence to C. Blane (cblane@umich.edu)

Objective: The objective was to describe imaging and histopathology of breast cancer in the young patient.

Materials and Methods: This was an IRB approved study. From 1998–2007, ten of 1,103 patients (0.9%) aged 25 years and under were diagnosed with breast cancer. Demographics, histopathology and ultrasound (US) appearance of the cancers were compiled. Age range was 15–25 years (mean 22 years).

Results: Invasive ductal carcinoma (IDC) was found in seven patients (70 %), five of whom also had ductal carcinoma in situ (DCIS). There was one malignant phyllodes tumor, one secretory carcinoma and one patient had lymphoblastic lymphoma. All US were BIRADS 4, suspicious. There were no false negatives. The IDC and secretory carcinomas were hypoechoic with lobulated and/or indistinct margins. The lymphoma and phyllodes had additional cystic components. In the seven patients with IDC, six were ER/PR positive and five of these were HER2/neu positive. One IDC patient and the phyllodes patient had a strong family history. The patient with lymphoblastic lymphoma is deceased. All nine remaining patients (90 %) are alive 0–8 years since diagnosis (mean survival 2.3 years). Two of the nine survivors had lumpectomy initially, one of whom had a mastectomy after local recurrence. Six had initial mastectomy, two of whom had local recurrence. One patient sought treatment elsewhere.

Conclusion: Breast cancer at age 25 or younger is uncommon, 1 % of our breast imaging studies for patients in this age range. Though 70% are invasive ductal carcinoma there is a spectrum of neoplasia in this age group. The majority (86%) of IDC were hormone responsive. US evaluation was suspicious in every case with no false negative studies. Treatment in this age group is usually mastectomy with reconstruction since postlumpectomy radiation carries a much higher risk. US remains an excellent screening tool in this population since treatment is usually mastectomy. MRI may have a limited role in those few patients who do not elect bilateral mastectomy. US should be the primary imaging modality in patients 25 years of age and under.

GASTROINTESTINAL (PANCREAS/BILIARY) IMAGING PAPERS

Room: 309, Level 3

Wednesday, April 29, 2009, 12:30 pm–2:30 pm

Abstracts 165-175

Moderators: *C. Sirlin, M. Macari*
Keynote Address: Epidemiology and Imaging of Pancreas Cancer—*M. Macari*

12:40 pm

165. Calculating Growth Rate of Pancreatic Adenocarcinoma on MDCT Based on RECIST and Volumetry

Rezai, P.; Tochetto, S.; Yaghmai, V. Northwestern University, Chicago, IL*
Address correspondence to V. Yaghmai (v-yaghmai@northwestern.edu)

Objective: The objective was to predict treatment response on MDCT of patients with pancreatic adenocarcinoma treated with chemotherapy and radiation by quantifying changes in tumor growth rate using RECIST diameter and volumetry.

Materials and Methods: Fifteen patients with localized pancreatic adenocarcinoma were evaluated by contrast-enhanced abdominal MDCT before and after being treated with chemotherapy and radiation. Tumor volumes and RECIST diameter were measured on the baseline and follow-up studies. Tumor volume doubling times based on RECIST diameter (RVDT) and volume (TVDT) were calculated. Doubling times based on RECIST diameter for untreated patients (RVDT no Tx) were obtained from the literature. For comparisons, doubling times were converted into growth rate. Growth rates based on RECIST diameter (GRr) and volume (GRv) in patients who received treatment were compared with growth rate based on RECIST diameter in patients who received no treatment (GRr no Tx); ;<0.05 was considered significant.

Results: Median GR based on tumor volume and RECIST diameter changes after treatment were -0.81 (95 CI, -2.45 to 1.82) and -1.46 (95% CI, -5.32 to 2.17). Median GRr no Tx was 2.39 (95% CI, 1.51 to 4.25). There was a significant difference between GRr no Tx and both GRr and GRv ($p<0.05$, in both instances).

Conclusion: Our preliminary data suggest that the growth rate of pancreatic adenocarcinoma decreases with treatment. Its quantification on MDCT might be of value in monitoring response to treatment.

12:50 pm

166. Analysis of Pancreatic Adenocarcinoma Morphology on MDCT Before and After Treatment with Chemotherapy and Radiation

Rezai, P.; Tochetto, S.; Yaghmai, V. Northwestern University, Chicago, IL*
Address correspondence to V. Yaghmai (v-yaghmai@northwestern.edu)

Objective: The objective was to evaluate the change in morphology of pancreatic adenocarcinoma in patients with localized disease after treatment with chemotherapy and radiation.

Materials and Methods: Contrast-enhanced abdominal MDCT scans of 16 patients with localized pancreatic adenocarcinoma were evaluated with semiautomated segmentation software. Patients had been treated with chemotherapy and radiation treatment after the baseline CT. Tumor volumes (ml), RECIST diameter (mm), volume equivalent sphere diameter (VESD) (mm) maximum 3D diameter (M3DD) (mm) and elongation value were obtained. RECIST diameter, VESD, M3DD and elongation values of the tumors at baseline and follow-up were compared to determine differences. The significance level was set at $p<0.05$.

Results: Mean volume, RECIST diameter, VESD, M3DD and elongation for baseline vs. follow-up studies were 23.12 ml vs. 19.43 ml ($p>0.05$), 41.86 mm vs. 39.35 mm ($p>0.05$), 33.14 mm vs. 32.1 mm ($p>0.05$), 51.76 mm vs. 51.73 mm ($p>0.05$) and 0.67 vs. 0.76 ($p>0.05$) respectively. There was a significant difference at baseline and follow-up between RECIST diameter, VESD and M3DD ($p<0.05$, in all instances).

Conclusion: Our results suggest that pancreatic adenocarcinomas are not spherical in shape and become more elliptical after treatment.

1:00 pm

167. Quantitative Perfusion and Diffusion-Weighted MR Imaging of Pancreatic Adenocarcinoma at 3T: A Pilot Study

Morgan, D.[1]; Kim, H.[1]; Ng, T.[1]; Christein, J.[1]; Eloubeidi, M.[1]; Posey, J.[1]; Pednekar, A.[2] 1. University of Alabama at Birmingham, Birmingham, AL; 2. No Institutional Affiliation*
Address correspondence to D. Morgan (dmorgan@uabmc.edu)

Objective: The objective was to evaluate feasibility of obtaining quantitative physiologic parameters using MR imaging in patients with naïve pancreatic adenocarcinomas.

Materials and Methods: Newly diagnosed biopsy proven pancreatic cancer patients were enrolled prospectively after IRB-approved informed consent. Physiologic MRI consisted of routine pancreatic protocol plus diffusion-weighted and dynamic contrast-enhanced MRI on a 3T system using 6-channel phased array torso coil with diffusion-weighted single shot echoplanar images: (b values 0, 700), TR/TE 7000/70 milliseconds, matrix 256/256, field of view 375×375 cm, slice thickness 4 mm 0 gap, number of slices 10; and dynamic contrast-enhanced MRI: T1-weighted 3D fast field echo sequence using TR/TE of 5/2.3 milliseconds, 15° flip, matrix 192×192, SENSE factor 2, temporal resolution 2.1 seconds for 120 cycles during injection of 0.1 mmol/kg gadoteridol administered IV with 20-ml saline flush at 2 ml/seconds. Calculation of apparent diffusion coefficient (ADC) averaging three orthogonal values, and K^{trans} (two compartment model) was performed on downloaded DICOM raw data.

Results: Eleven patients (mean age 64.5 years, six males, five females) entered into the study thus far. Mean ± SD ADC ($1x10^{-3}mm^2$/second) and K^{trans} (ml/ml/minute) values for pancreatic tumor, normal pancreas, liver metastases and normal liver were, respectively: 1.7114 ± 0.5897, 1.6917 ± 0.5469, 1.4097 ±

0.3495, 1.1104 ± 0.3514, and 1.1288 ± 0.5679, 0.9775 ± 0.6229, 0.8132 ± 0.3549, 0.7842 ± 0.3986. When liver metastases were present, the difference between pancreatic tumor ADC and normal pancreas was greater, and K^{trans} of normal liver was nearly doubled compared to livers without metastases.

Conclusion: Quantitative physiologic MRI of pancreatic adenocarcinoma is feasible at high field strengths. There is variability among lesions that may be related to tumor differentiation or stage at diagnosis.

1:10 pm

168. Comparison of Tumor Growth Rate Estimated from RECIST Diameter, Volume and CA 19-9 Level in Patients with Localized Pancreatic Adenocarcinoma Treated with Chemotherapy and Radiation

Rezai, P.; Tochetto, S.; Yaghmai, V. Northwestern University, Chicago, IL*
Address correspondence to V. Yaghmai (v-yaghmai@northwestern.edu)

Objective: The objective was to compare tumor growth rate estimated from RECIST diameter and volume change (GR*r* and GR*v*, respectively) on MDCT with the estimated growth rate obtained from changes in CA 19-9 (GR*c*) levels in patients with localized pancreatic adenocarcinoma treated with chemotherapy and radiation.

Materials and Methods: Baseline and follow-up RECIST diameter and tumor volume were measured by segmentation software (Siemens Medical Solutions, Forchheim, Germany) on contrast-enhanced MDCT of 15 patients before and after receiving chemotherapy and radiation. Corresponding CA 19-9 levels were also obtained. Tumor volume doubling time based on change in RECIST diameter (DTr) was calculated using the following equation: DT*r*= t×log2 / 3 ×log (fu/bl) where t, fu and bl represent the time interval between studies in days and RECIST diameter on the follow-up and baseline studies, respectively. Tumor volume doubling time based on change in volume (DT*v*) and CA19-9 levels (DT*c*) were calculated using the equation: DT= (t× log 2)/ [log (fu/bl)] where t is the time interval in days and fu and bl represent corresponding measurements on the follow-up and baseline studies. Using the formula GR=365/DT, doubling time was converted into growth rate. Comparison between GR*r*, GR*v* and GR*c* was made; $p<0.05$ was considered significance.

Results: Median DT*r*, DT*v* and DT*c* between the baseline and follow-up exams were -55 days (95% CI, -111.6 to 164.2), -51.3 days (95% CI, -213.8 to 273.8) and -25 days (95% CI, -85.2 to -17.1), respectively. Median GR*r*, GR*v* and GR*c* between the baseline and follow-up exams were -1.46 (95% CI, -5.32 to 2.17), -0.81 (95% CI, -2.45 to 1.82) and -10.14 (95% CI, -15.87 to -2.28), respectively. There was not a significant difference between GR*r* and GR*v* ($p>0.05$). However, GR*r* and GR*v* were significantly different than GR*c* ($p<0.05$).

Conclusion: Our results suggest that estimated tumor growth rates based on tumor volume and RECIST diameter on MDCT are significantly different results compared to those estimated from CA 19-9 levels.

1:20 pm

169. Can Dimensions of the Pancreatic Duct or Cyst Communication Stratify Intraductal Papillary Mucinous Neoplasms into Branch Duct Type from Combined?

Sainani, N.; Fritz, S.; Mino-Kenudson, M.; Fernandez-del Castillo, C.; Sahani, D. Massachusetts General Hospital, Boston, MA*
Address correspondence to N. Sainani (drnisainani@gmail.com)

Objective: The objective was to evaluate value of dimensions of main pancreatic duct (MPD) and cyst communication in differentiating side-branch (SB) from combined (C) intraductal papillary mucinous neoplasms (IPMN)s.

Materials and Methods: Preoperative MDCT (n=75) and MR (n=8) in 83 patients (M:F 42:41, age range 42-92 years) with 97 pathological confirmed SB or C IPMNs were reviewed. Size of cystic lesion, largest dimension of communicating channel and MPD and presence of mural nodule in cyst or MPD were recorded. Predictive value of these features for subtype diagnosis was calculated. Relationship of communicating channel (CC)/MPD ratio with a subtype diagnosis was analyzed. Incidence of malignancy in each subtype was calculated. Positive predictive value (PPV) of cystic lesion size, MPD/channel dimension and mural nodule for malignancy was calculated.

Results: On pathology, 66/97 (68%) lesions were C IPMNs, 31/97 (32%) were SB IPMNs. Accuracy of imaging for IPMN subtype categorization was 69%. PPV of MPD and channel dimension of =5 mm for C IPMN was 65% and 32%, of MPD and channel < 5 mm for SB IPMN was 85% and 90% respectively. For communicating channel /MPD ratio <1 and > 1, the PPV for SB IPMNs were 45% and 55%. Incidence of malignancy (invasive and carcinoma in situ [CIS]) in SB and C IPMN with MPD < 5 mm was 15% and 22%, in SB and C IPMN with MPD=5 mm was 60% and 63%, in SB and C IPMN with channel < 5 mm was 14% and 28% and in SB and C IPMN with channel = 5 mm was 66% and 90% respectively. PPV for malignancy for MPD dimension =5 mm was 77%.

Conclusion: In patients with cystic pancreatic lesions and prominent PD, the smaller MPD and channel diameter (<5mm) favors a diagnosis of SB IPMN. Nevertheless there is no such association of either of diagnosis with larger dimensions =5 mm. Though imaging categorization of IPMNs into subtypes relies on ductal dimensions, pathological diagnosis depends on growth of the papillary epithelium in the cystic lesion or main duct, which can exist regardless of ductal dimensions. Incidence of malignancy is higher in IPMNs with larger MPD or channel dimensions (=5 mm) irrespective of subtype. It is hence rational to approach IPMNs with larger ductal dimensions more aggressively than to attempt to distinguish them into subtypes. Dimensions of MPD and communicating channel can thus influence the management strategy of IPMNs irrespective of subtype diagnosis on imaging.

1:30 pm

170. Experience with Percutaneous Image-Guided Pancreatic Biopsy in 124 Solid and Cystic Lesion

Ma, X.; Sahani, D.; Arellano, R.; Gervais, D.; Hahn, P.; Mueller, P. Massachusetts General Hospital, Boston, MA*
Address correspondence to X. Ma (xma@partners.org)

Objective: The objective was to assess the performance of percutaneous image-guided biopsy for solid and cystic lesions in the pancreas, and to evaluate the accuracy of fine needle aspiration (FNA) and core biopsy (CB) for establishing the diagnosis.

Materials and Methods: This single center retrospective study was HIPPA compliant and IRB approved. Between 2000 and 2007, 124 patients (M:F=70:54; age=66 ± 14) underwent image-guided percutaneous pancreatic lesion biopsies for 99 solid and 25 cystic lesions. The procedure included both CB and FNA in 115, CB alone in three and FNA alone in six. Chi-Square tested accuracy among combined core biopsy and FNA, core biopsy alone, and FNA alone in solid masses and cystic lesions respectively. Negative biopsies without subsequent histological information were followed over six months.

Results: A total of 100 malignant and 24 benign lesions were confirmed. The overall accuracy of biopsy was 94.4%. The accuracy of combined CB and FNA, CB alone, and FNA alone in solid lesions were 93.9%/82.8%/85.6% respectively ($p>0.05$) and for cystic lesion it was 96%/95.7%/75% ($p<0.05$) respectively. In the malignant and benign groups, the accuracy was 94%/85.4%/88.8% ($p>0.05$) and 95.8%/100%/60.9% ($p<0.001$) respectively. The accuracy was 94.8% and 88.9% for CT and US guidance respectively ($p>0.05$). Thirteen complications included five hematomas, four biopsy-induced pancreatitis, moderate abdominal pain in three, and fever, nausea and vomiting in one.

Conclusion: Percutaneous pancreatic lesion biopsy is a highly accurate alternative method for the diagnosis of pancreatic disease when biopsy including cores and FNA. Core biopsy improves the diagnostic accuracy in the cystic lesions and for benign pancreatic masses.

1:40 pm

171. 64-Slice MDCT as a Surrogate End Point for the Postoperative Evaluation of Laparoscopic and Natural Orifice Transluminal Endoscopic Distal Pancreatectomy in a Porcine Model

Kambadakone Ramesh, A.; Singh, A.; Willingham, F; Gee, D.; Sylla, P.; Mino-Kenudson, M.; Rattner, D.; Brugge, W.; Sahani, D.*
Massachusetts General Hospital, Boston, MA
Address correspondence to A. Kambadakone Ramesh (akambadakone@partners.org)

Objective: As novel minimally invasive surgeries of pancreas transitions to human trials, MDCT will play a critical role in planning treatment and evaluation of outcome of these techniques and is likely to serve as a surrogate endpoint. The objective of our study was to evaluate the accuracy of 64-slice CT in depicting the postoperative anatomy and complications following laparoscopic and endoscopic transgastric distal pancreatectomy in a porcine model.

Materials and Methods: Twenty-six swine (body weight: range-32-56 kg, mean—38kg) underwent unenhanced and enhanced MDCT examination following laparoscopic or endoscopic transgastric distal pancreatectomy as part of a surgical trial. The CT images were evaluated for pancreatic size, pancreatic abnormalities, status of postoperative site, focal fluid collections, status of adjacent organs and vasculature. The animals underwent autopsy and histopathological examination within 24 hours following CT.

Results: The postoperative anatomy and the preserved splenic vasculature was accurately (100%) evaluated in all the animals. CT detected pancreatic resection margin abnormalities measuring less than 1 cm in 9/26 (34.6%) of cases of which seven had necrosis of mean size 1.3 cm on histopathology giving CT a sensitivity of 85.7%, specificity of 80.95% and accuracy of 88.46%. CT had a 100% accuracy in the detection of focal postoperative site collections [4/26(15.4%)] and in the evaluation of adjacent organ integrity.

Conclusion: 64-slice MDCT was accurate in the evaluation of the postoperative anatomy, focal fluid collections, pancreatic resection margin abnormalities and adjacent organ and vascular integrity and can act as a surrogate endpoint in the postoperative evaluation of minimally invasive surgeries of the pancreas.

1:50 pm

172. Utility of Gadobenate Dimeglumine-Enhanced MR Cholangiography in the Diagnosis of Acute Cholecystitis: Preliminary Report

Akpinar, E.; Turkbey, B.; Balli, O.; Akkapulu, N.; Balas, S.; Tirnaksiz, B.; Akata, D.; Karcaaltincaba, M.; Akhan, O. Hacettepe University School of Medicine, Ankara, Turkey*
Address correspondence to B. Turkbey (bturkbey@yahoo.com)

Objective: The objective was to investigate the feasibility of the use of gadobenate dimeglumine -enhanced T1-weighted MR cholangiography (MRCP) in diagnosis of acute cholecystitis.

Materials and Methods: This prospectively designed IRB approved HIPAA compliant study was done between January, 2007 and November, 2007. Eleven patients (seven males, mean age 59 years) presented to the emergency room with acute right upper quadrant pain with equivocal physical examination and/or ultrasound findings were included. All patients underwent contrast-enhanced (CE) MR cholangiography examinations. CE-MR cholangiography was performed on a 1.5T magnet using 3D T1-weighted high resolution isotrophic volume examination (THRIVE) obtained at 90^{th} minute after intravenous injection of gadobenate dimeglumine. Imaging features detected on CE-MR cholangiography were correlated with operative and histopathologic findings.

Results: On MRCP, gallstones were present in nine patients (eight in gallbladder, seven in cystic duct). Hydropic gallbladder, significant wall thickening and pericholecystic free fluid were detected in seven, seven and six patients, respectively. On delayed phase CE-MR cholangiography, significant enhancement of gallbladder wall was seen in ten patients and contrast agent excretion into gallbladder was absent in all patients. Surgery was performed in ten patients and cholecystostomy was done in one patient. Surgery and histopathology findings were consistent with cholecystitis in all patients.

Conclusion: Besides anatomical assessment, gadobenate dimeglumine-enhanced MR cholangiography can provide functional evaluation similar to hepatobiliary iminodiacetic acid (HIDA) scintigraphy in diagnosing acute cholecystitis in patients with acute right upper quadrant pain and equivocal findings.

2:00 pm

173. Gadolinium-Labeled Pineapple Juice vs. Ferumoxsil as a Negative Oral Contrast Agent in Secretin-Enhanced MR Cholangiopancreatography

Restaino, G.; Missere, M.; Occhionero, M.; Cucci, E.; Ciuffreda, M.; Sallustio, G. Catholic University of Sacred Heart, Campobasso, Italy*
Address correspondence to G. Restaino (gennares@hotmail.com)

Objective: The quality of secretin-enhanced MR cholangiopancreatography (S-MRCP) images is frequently degraded by high signal from the gastrointestinal tract. Suspensions of superparamagnetic particles, like ferumoxsil, are commonly used to overcome this problem, but they are not widely available, they are expensive and rather unpalatable. Pineapple juice, thanks to its high manganese content, shortens the T2 relaxation time of a solution and has been proposed as negative oral contrast agent in MRCP. The aim of this study is to prospectively compare Gadolinium-labeled pineapple juice (Gd-PJ) and ferumoxsil as an oral negative contrast agent in S-MRCP.

Materials and Methods: Between May, 2007 and May, 2008 100 consecutive patients, referred for S-MRCP with a clinical suspicion of pancreatic disease, were prospectively examined after ingestion of 180 ml of ferumoxsil (group one: 50 patients) or 180 ml of PJ labeled with 1 ml Gd-DOTA (group two: 50 patients). A palatability score evaluation was obtained from each patient (1 unacceptable - 2 bad - 3 acceptable - 4 good) and registered. Images were evaluated qualitatively by one radiologist (GR) with five years experience in MRCP reading who scored the ability of contrast agent to cancel signal intensity in stomach, duodenum and jejunum (1 null - 2 minimal - 3 partial - 4 total), the quality of visualization of main pancreatic duct (MPD) in head, body and tail (1 null - 2 poor - 3 suboptimal - 4 excellent) and the overall diagnostic quality of the examination (1 nondiagnostic - 2 poor - 3 suboptimal - 4 excellent). Average results for each field in the two groups were compared using Student's t test (significant threshold value of $p<0.01$).

Results: Palatability score resulted significantly higher for Gd-PJ than for ferumoxsil (3.8 vs. 2.9, $p<0.01$). Signal cancellation in stomach, duodenum and jejunum and quality of visualization of MPD in head, body and tail didn't show significant differences in the two groups. Overall quality of the examination resulted slightly, but not significantly, better with ferumoxsil than with Gd-PJ (3.8 vs. 3.7, $p>0.01$).

Conclusion: PJ labeled with gadolinium constitutes an efficient and palatable negative oral contrast agent for S-MRCP combining availability, palatability, and low cost and may be proposed as an alternative to ferumoxsil.

2:10 pm

174. Superior Mesenteric Artery Syndrome: A Misdiagnosed Cause of Recurrent Pancreatitis and Pancreatitis-Like Abdominal Complaints? A Retrospective Study With Secretin-Enhanced MR Cholangiopancreatography Toward the Hypothesis of a Duodenopancreatic Functional Unit

Restaino, G.; Missere, M.; Occhionero, M.; Cucci, E.; Ciuffreda, M.; Sallustio, G. Catholic University of Sacred Heart, Campobasso, Italy*
Address correspondence to G. Restaino (gennares@hotmail.com)

Objective: Superior mesenteric artery (SMA) syndrome is a relatively rare condition caused by obstruction of the third portion of the duodenum between the SMA and aorta. Its estimated incidence rates are from 0.01% to 0.33%. Typical clinical presentation includes long lasting epigastric pain, postprandial vomiting, and distension. An aortomesenteric distance (AOD) < 8 mm on axial sectional images is considered as a 100% sensitive and specific cut-off for CT diagnosis of the disease. The purposes of this study were to assess the prevalence of this finding in patients referred for pancreatic-type clinical signs and to find a new more functional imaging diagnostic criterion with secretin-enhanced MR cholangiopancreatography (S-MRCP).

Materials and Methods: We retrospectively reviewed 313 S-MRCP examinations performed at our institution between 2004 and 2008. All the studies were performed with a 1.5T scanner according the same extended protocol which included a complete morphologic study of the upper abdomen with gadolinium administration and dynamic S-MRCP sequential evaluation after IV administration of secretin (0.1 CU/Kg). In all patients we measured the AOD at the point where the third duodenum passes between the vessels and the largest diameter of second and third duodenum after secretin stimulation.

Results: The AOD was < 8 mm in 56/313 patients (18%); in six of these patients, images after secretin stimulation showed a progressive dilatation of second and third duodenum (>40 mm) with abrupt vertical narrowing of the 3rd portion and a typical "flute-beak" appearance on axial slices. No other common causes of pancreatic disease where found, like pancreas divisum, biliopancreatic maljunction, papillary stenosis or intraductal papillary mucinous neoplasia. All these patients complained of postprandial abdominal discomfort, dyspepsia and fullness.

Conclusion: S-MRCP can directly and dynamically demonstrate duodenal obstruction and distension in SMA syndrome and can therefore delineate new diagnostic functional imaging criteria of SMA syndrome. AOD < 8 mm cannot be considered as sole diagnostic marker of this condition, but a severe dilatation of second and third duodenum after secretin stimulation must be observed. SMA syndrome, at least in mild form must be included in the differential diagnoses of pancreatitis or pancreatitis-like symptoms. Further insights into this subject are advisable, in order to enlighten the anatomo-functional relationship between the duodenum and the pancreas.

2:20 pm

175. Application of an Adaptive Nonlinear Postprocessing Filter for Improving the Image Quality of Low Radiation Dose CT: A Double Blinded Comparative Study

Singh, S.[1]; Kalra, M.[1]; Sjöberg, J.[2]; Sahani, D.[1]; Blake, M.[1] 1. Massachusetts General Hospital, Boston, MA; 2. SharpView AB, Linköping, Sweden*
Address correspondence to S. Singh (ssingh6@partners.org)

Objective: Although image filters have been shown to reduce noise, they also decreased lesion conspicuity and image contrast. The purpose of our double-blinded study was to evaluate the effect of a new adaptive nonlinear image postprocessing filter on image quality of abdominal CT acquired at low radiation dose.

Materials and Methods: Thirty-one subjects (mean age=72, M:F 15:16) underwent abdominal CT on a four-row MDCT. After standard of care CT, two series of images were acquired immediately at an identical z-position with standard (160-220 mAs) and with 50% reduced (80-110 mAs) radiation dose, with remaining parameters held constant. DICOM images were exported to adaptive filter software (SharpView, Linköping, Sweden) for improving quality of low dose CT images with applications of two levels of noise reduction. The resulting two sets of postprocessed images were randomized with original standard and reduced dose images (n=124 image series) and presented to two radiologists for independent assessment of image noise, contrast, conspicuity of small soft tissue structures less than 5 mm in size, diagnostic acceptability and presence of artifacts on a five point scale (1=excellent; 5=unacceptable). Regions of interest were drawn in the liver to measure CT numbers and quantitative image noise. Statistical analysis was performed with Wilcoxon signed rank test.

Results: There was a strong interobserver agreement between the two radiologists (kappa=.8; $p<.01$). Postprocessed low dose images had significantly lower image noise and superior visibility of small structures ($p<.001$). Of the 24 CT examinations graded as unacceptable or with suboptimal noise on low dose CT images, adaptive filtration resulted in acceptable noise in 21 CT exams, with no significant change in image contrast or image artifacts ($p>.5$). There was no significant change in HU numbers with the use of adaptive filters ($p>.8$), but mean quantitative image noise improved from 21.5 for low dose CT to 17.1 and 14.9 respectively, with adaptive filtering at two strengths (p=.02-.006).

Conclusion: Contrary to previously reported studies of prior versions, new adaptive nonlinear filters can help reduce abdominal CT radiation dose by up to 50% without compromising image contrast or conspicuity of small structures.

MUSCULOSKELETAL (UPPER EXTREMITY) IMAGING PAPERS

Room: 210, Level 2

Wednesday, April 29, 2009, 12:30 pm–2:30 pm

Abstracts 176-186

Moderators: *H. Umans, D. Blankenbaker*

Keynote Address: Sonographic Imaging of Digital Nerve Injury in the Context of Penetrating Trauma—*H. Umans*

12:40 pm

176. Ultrasound of the Hands and Feet: Effect on Rheumatologists' Diagnostic Confidence and Patient Management

Harish, S.[1]; Zia, P.[1]; Matsos, M.[1]; Ioannidis, G.[2]; Ho, Y.[2]; Chow, A.[3]; Khalidi, N.[1] 1. St. Joseph's Healthcare/McMaster University, Burlington, Canada; 2. McMaster University, Hamilton, Canada; 3. Credit Valley Hospital, Mississauga, Canada*

Address correspondence to S. Harish (harishsrinivasan@yahoo.com)

Objective: The purpose of our study was to quantify the impact that ultrasound (US) of the hands and feet have on rheumatologists' diagnosis and diagnostic confidence and on patient management.

Materials and Methods: A prospective controlled observational study was performed with 62 consecutive referrals from two rheumatologists to a teaching hospital for sonography of the hands and/or feet. Measurements of diagnostic confidence for both specific clinical findings (synovitis, erosion, enthesitis, tenosynovitis, other/osteophytosis) as well as overall diagnosis (rheumatoid arthritis, seronegative arthropathy, inflammatory osteoarthritis [OA], OA, gout, septic arthritis, normality, other diagnoses) using a Likert scale were made both before and after the US examination in each case. Certainty was defined as 'very unlikely' or 'definite' on the Likert scale. Proposed management (intra-articular steroids, parenteral steroids, oral steroids, disease-modifying antirheumatic drug (DMARD), surgical referral, nonsteroidal anti-inflammatory drug (NSAID)/ review at outpatients, physiotherapy, and discharge) was also recorded before imaging and then with benefit of the US result. The McNemar test was performed to test for differences in diagnostic certainty and proposed management before and after US.

Results: The proportion of physician certainty for specific clinical findings increased for synovitis (9.7 vs. 38.7%; $p<0.001$), tenosynovitis (9.7 vs. 46.8%; $p<0.001$), erosions (1.6 vs. 58.1%; $p<0.001$), enthesitis (50.0 vs. 83.9%; $p<0.001$), and other/osteophytosis (53.2 vs. 77.4%; $p= 0.003$). The physician certainty for overall diagnosis increased for seronegative arthropathy (46.8 vs. 61.3%; $p= 0.049$), inflammatory OA (46.8 vs. 87.1%; $p<0.001$), OA (46.0 vs. 73.0%; $p=0.002$). A total of 88.7% of patients had DMARD as a proposed management option before US vs. 48.4% after US ($p<0.001$). In addition, 4.84% of patients had NSAID/ review as outpatients as a proposed management option before US vs. 45.26% after US ($p<0.001$).

Conclusion: Sonography of the hands and/or feet significantly influences the rheumatologists' diagnostic confidence in specific clinical findings and management plans.

12:50 pm

177. 3T MR Imaging of the Shoulder: Is MR Arthrography Necessary?

Magee, T., NSI, Merritt Island, FL*

Address correspondence to T. Magee (tmageerad@cfl.rr.com)

Objective: We report our experience in diagnostic sensitivity of 3T conventional MR vs. MR arthrography of the shoulder in the same patient population.

Materials and Methods: One hundred fifty consecutive conventional shoulder MR and MR arthrography exams performed on patients age 50 or under who went on to arthroscopy were reviewed retrospectively by consensus reading of two musculoskeletal radiologists. All patients selected for arthroscopy had abnormal clinical exams and abnormal MR and/or MR arthrography exams. All 150 patients were referred from one orthopedic group. All patients consented to have both MR and MR arthrograms performed. None had prior shoulder surgery. Full or partial thickness supraspinatus tendon tears, superior labral anterior posterior (SLAP) tears and anterior or posterior labral tears were assessed.

Results: Three full thickness and nine partial thickness supraspinatus tendon tears, seven SLAP tears, six anterior labral tears and two posterior labral tears were seen on MR arthrography but not on conventional MR. All additional MR arthrography findings were confirmed at arthroscopy. On conventional MR exam sensitivities and specificities as compared to arthroscopy were as follows: anterior labral tear (83% sensitivity, 100% specificity), posterior labral tear (84%, 100 %), SLAP tear (83%, 99%), supraspinatus tendon tear (92%,100%), partial thickness articular surface tear (68%,100%), and partial thickness bursal surface tear (84%,100%). On MR arthrography sensitivities and specificities as compared with arthroscopy were as follows: anterior labral tear (98%, 100%), posterior labral tear (95%, 100%), SLAP tear (98%, 99%), supraspinatus tendon tear (100%, 100%), partial thickness articular surface tear (97%, 100%), and partial thickness bursal surface tear (84%, 100%). MR arthrography demonstrated a statistical improvement in sensitivity ($p< .05$) for detection of partial thickness articular surface supraspinatus tears, anterior labral tears and SLAP tears at 3T.

Conclusion: In this series, MR arthrography demonstrates statistically significant increased sensitivity for detection of partial thickness articular surface supraspinatus tears, anterior labral tears and SLAP tears compared with conventional MR at 3T. Based on the above findings, we perform 3T MR arthrograms on patients for which anterior labral tears, SLAP tears and partial thickness supraspinatus tendon tears are suspected clinically.

1:00 pm

178. High Frequency Sonography of the Normal Volar Digital Nerves of the Hand

Kessler, J.[1]; de la Lama, M.[1]; Negron, J.[1]; Umans, H.[1,2] 1. Jacobi Medical Center, Bronx, NY; 2. Albert Einstein College of Medicine, Bronx, NY*

Address correspondence to H. Umans (hilary.umans@gmail.com)

Objective: The objective was to describe our technique for high frequency sonography of the volar digital nerves, and define the course, caliber and morphology of the normal volar digital nerve.

Materials and Methods: Digital nerves of five male and five female (ages 26-46) volunteers were imaged using an ultrasound system (Toshiba Medical Systems, Tochigi-ken, Japan) with a 12 MHz linear array hockey stick transducer by a single sonographer under direct radiologist supervision. Height, weight, glove size, and hand dominance were recorded. All nerves were imaged in long axis, found paracentral to flexor tendons by slight translation of the probe. Color Doppler was used as needed to locate nerves superficial to vessels. Each radial and ulnar nerve was divided into four segments (proximal, deep proximal, middle, distal), for a total of 760 segments. Segment thickness and depth were measured using digital calipers. Student's t test, analysis of variance, analysis of covariance, and linear regression were used for data analysis with alpha=0.05.

Results: All nerves demonstrated a smooth trilaminar appearance, located paracentral to flexor tendons and superficial to digital vessels, without aberrance. Mean nerve thickness (NT) was 1.3 mm for proximal, 1.2 mm for deep, 1.2 mm for middle, and 0.8 mm for distal segments. Nerves were thickest proximally and thinnest distally (mean NT 1.1 mm) ($p<0.0001$). Mean nerve depth (ND) was 3.6 mm for proximal, 3.2 mm for deep, 2.6 mm for middle, and 1.8 mm for distal segments with differences between all segments ($p<0.0001$). Mean ND was 2.8 mm (range 0.7 mm-6.8 mm). Student's t-test revealed no difference between radial and ulnar digital NT and ND. Mean NT by finger ranged from 1.1-1.2 mm. Mean NT was greater in the third compared to the first or fifth digits and in the second and fourth digits compared to the fifth. Regression analysis identified a positive correlation between height and NT (p=0.0077). Nerves were thicker in males (1.2 mm) vs. females (1.1 mm) (p=0.0002), but males were taller than females (p<0.0001). There was no correlation between NT or ND measurements and weight, age, body mass index or glove size. Dominance had no effect on NT. ND was greater in dominant right hands (p=0.0002), but not in the one dominant left hand.

Conclusion: High frequency sonography permits high resolution imaging of the volar digital nerves which follow a predictable course and demonstrate a trilaminar morphology which is distinctly different from the deeper digital vessels and the surrounding integument. Nerve caliber and depth vary predictably by segment.

1:10 pm

179. MRI Findings Associated with Luxatio Erecta Humeri

Krug, D.; Vinson, E.; Helms, C. Duke University Medical Center, Durham, NC*
Address correspondence to D. Krug (dkkrug@yahoo.com)

Objective: Luxatio erecta humeri is a rare type of inferior glenohumeral dislocation, and has been associated with fractures, rotator cuff tears, inferior capsular and ligamentous injuries, and neurovascular pathology. To date, there are no studies in the radiology literature describing the MRI findings associated with this dislocation. The purpose of this study is to describe the incidence of associated MRI findings in patients with prior luxatio erecta.

Materials and Methods: Two musculoskeletal trained radiologists retrospectively reviewed four shoulder MRI exams from patients with clinical and radiographic evidence of prior luxatio erecta. Three exams were obtained using conventional MRI protocol, and one exam was obtained using MR arthrography. The MRI exams were evaluated for the presence of rotator cuff and biceps tendon pathology (tendinosis, partial tear, or full thickness tear); glenoid labrum pathology (irregularity, tear, or detachment); joint capsule and glenohumeral ligament injury; fractures and bone marrow contusions; articular cartilage injury; and joint effusions.

Results: Rotator cuff tears were present in 3/4 exams including tears of the supraspinatus (SS) (3/4), infraspinatus (IS) (3/4), and subscapularis (SC) (1/4). These included massive full thickness tears of both SS and IS (2/4), small full thickness tears of SS (1/4) and SC (1/4), and partial thickness tear of IS (1/4). The biceps tendon was torn in 1/4 exams. All four exams showed labral tears including tears of the anterior, posterior and superior labrum. All four exams showed injury to the inferior glenohumeral ligament (IGHL) including intrasubstance tears of both anterior and posterior bands (1/4), tear of anterior band at labrum and injury to posterior band (1/4), humeral avulsion of posterior band with injury to anterior band (1/4) and injury to both anterior and posterior bands (1/4). One exam showed a bone marrow contusion in superolateral humeral head and a different exam showed an impaction fracture of superolateral humeral head.

Conclusion: To our knowledge, this is the first report in the radiology literature describing the MRI findings associated with luxatio erecta. Common MRI findings in patient with a prior luxatio erecta humeri dislocation include rotator cuff tears, injury to the glenoid labrum and injury to both the anterior and posterior bands of the inferior glenohumeral ligament. These findings are compatible with the mechanism of dislocation in luxatio erecta.

1:20 pm

180. MR Imaging of Annular Ligament Injuries of the Elbow: The Overlooked Isolated Annular Ligament Tear

Brouha, S.; Cardoso, F.; Pathria, M.; Resnick, D.; Chung, C. University of California San Diego, San Diego, CA*
Address correspondence to S. Brouha (sharonbrouha@gmail.com)

Objective: In this study, we review the normal MR appearance of the annular ligament and describe the MR appearance of annular ligament injuries.

Materials and Methods: We reviewed all 336 elbow MR imaging reports from two institutions performed between January, 2006 and March, 2008 and one institution during 2007 to identify cases with annular ligament pathology. The selected cases were reviewed by two musculoskeletal-trained radiologists for elbow pathology. In addition, the patient histories were reviewed to evaluate for symptoms including snapping of the elbow.

Results: We identified 15 MRI elbow studies in 14 patients with annular ligament pathology. Five studies in four patients demonstrated isolated annular ligament injuries without concurrent ligamentous injuries of the elbow. All these patients encountered either posterior elbow pain or snapping elbow. Pathology encountered includes one patient with bilateral partial tears of the annular ligament; two patients with isolated annular ligament injuries, including a rupture of the posterior band of the annular ligament; and one patient with subluxation of the annular ligament to the level of the radiohumeral articulation. In ten cases, the annular ligament injury was associated with other ligamentous and/or osseous injuries within the elbow.

Conclusion: Isolated annular ligament injuries may occur more frequently than reported in the literature. The posterior attachment of the annular ligament is most susceptible to injury. Furthermore, isolated annular ligament injuries may be demonstrated by MRI of the elbow and possibly to better advantage with MR arthrography. Reports of isolated annular ligament tears without concomitant elbow pathology are rare in the radiology and orthopedic literature. In all but one reported case the annular ligament injury was not identified at the time of MRI but at subsequent arthroscopy. These lesions should be suspected in patients who present with snapping or clicking of the elbow. Recognition of this entity and its clinical presentation may enable diagnosis at the time of imaging and potentially impact management.

1:30 pm

181. The Sternoclavicular Joint: Can Imaging Differentiate Infection from Degenerative Change?

Johnson, M.; Jacobson, J.; Fessell, D.; Kim, S.; Brandon, C.; Caoili, E. University of Michigan, Ann Arbor, MI*
Address correspondence to M. Johnson (mrkjohn@med.umich.edu)

Objective: The purpose of this study was to determine if there are any imaging findings that can differentiate a septic from degenerative sternoclavicular joint.

Materials and Methods: Search of radiology reports from 2000–2007 revealed 460 subjects with imaging of the sternoclavicular joint, of which 38 had aspiration or biopsy. The final study group consisted of nine subjects with unequivocal pathologic proof of sternoclavicular joint infection and ten subjects with pathologic and clinical findings excluding infection and consistent with degenerative change. Available ultrasound, CT, and MR images were retrospectively reviewed recording echogenicity, capsular distention, erosions, cysts, hyperemia or enhancement, and bone marrow signal. Clinical data was also reviewed.

Results: With ultrasound, those with infection showed joint distention as hypoechoic (40%) or isoechoic (60%) with cortical irregularity (100%) and hyperemia (100%); those with degeneration showed joint distention as hypoechoic (86%) or isoechoic (14%) with cortical irregularity (71%) and hyperemia (86%). With CT, those with infection showed erosions (67%) and osteophytes (22%); those with degeneration showed erosions (43%), subchondral cysts (57%), and osteophytes (57%). There were no subjects with joint subluxation. With MRI, fluid signal joint distention with enhancement was present in all subjects with infection or degeneration. Fluid signal bone marrow replacement was only seen with infection (100%). With infection, the average joint distention was 14 mm (range 10-20) and extended over the sternum and clavicle in 60%, compared to 5 mm (range 3–8) in those with degeneration and only extended over the clavicle. With infection, 78% had fever, 100% had elevated c-reactive protein (CRP) and erythrocyte sedimentation rate (ESR), and 44% had elevated white blood cell count; with degeneration, none had fever, and three had elevated CRP and ESR (possibly from another source). With infection, 33% were female with average age of 52 years; with degeneration, 90% were female with average age of 54 years.

Conclusion: Although there was overlap of the imaging findings with both sternoclavicular joint infection and degeneration (erosions, hyperemia, enhancement), findings that indicate infection include joint distention 10 mm or greater, extension over the clavicle and sternum, and adjacent fluid signal bone marrow replacement.

1:40 pm

182. Sonographic Assessment of the Lateral Ulnar Collateral Ligament of the Elbow in Cadavers and Asymptomatic Volunteers

Stewart, B.[1]; Harish, S.[2]; Popowich, T.[2]; Oomen, G.[1]; Wainman, B.[1]; Moro, J.[2] 1. McMaster University, Hamilton, Canada; 2. St. Joseph's Hospital, Hamilton, Canada*
Address correspondence to B. Stewart (briang.stewart@utoronto.ca)

Objective: The objective was to assess the ability of high-resolution sonography in identifying and characterizing the size and echogenicity of the lateral ulnar collateral ligament (LUCL) of the elbow in cadavers and asymptomatic volunteers.

Materials and Methods: The lateral ulnar collateral ligament of four cadaveric elbows was imaged with a high-resolution linear array transducer. Upon localization, the ligament was injected with 0.1% methylene blue using sonographic guidance. To confirm accurate identification of the ligaments, the elbows were then immediately dissected, revealing the exact location of the dye. The bilateral ligaments in 35 asymptomatic adult volunteers are to be subsequently imaged.

Results: Surgical dissection confirmed injection of methylene blue into all four cadaveric ligaments. The LUCL was identified overlying the radial head bilaterally in all 35 asymptomatic volunteers with a mean thickness of 1.2 mm in both females and males. The proximal attachment of the LUCL to the humerus was well visualized bilaterally in 91% of volunteers, with a mean thickness of 1.7 mm in females and 1.6 mm in males. The distal attachment on the ulna was well visualized bilaterally in 86% of volunteers. The LUCL was echogenic in all 35 volunteers. Differences in ligament measurements with regard to age, sex, weight, height, and hand dominance were not significant.

Conclusion: High-resolution ultrasound can accurately identify and measure the normal lateral ulnar collateral ligament. Given this, ultrasound could prove valuable in assessing the abnormal ligament.

1:50 pm

183. Sleep Position and Rotator Cuff Disease

Yochim, S.[1]; Clifford, P.[2]; Arheart, K.[2]; Infante, J.[2] 1. Jackson Memorial Hospital, Miami, FL; 2. University of Miami Miller School of Medicine, Miami, FL*
Address correspondence to S. Yochim (seyochim@gmail.com)

Objective: Controlling factors that contribute to rotator cuff disease could prevent the disease or keep patients with mild disease from progressing to a more extensive, symptomatic disease state. The purpose of this study is to determine if sleep position is a factor in the development of degenerative rotator cuff disease.

Materials and Methods: Institutional review board approval and informed consent were obtained for this retrospective study. One hundred fifty-two consecutive patients who had a shoulder MR at the University of Miami were eligible and 69 patients participated (mean age, 49.8 years; range 17-84 years), including 32 men (mean age, 47.1 years; range, 17-84 years) and 37 women (mean age, 52.2 years; range 20-84 years). Participants answered a questionnaire that assessed demographic, occupational, recreational, and medical risk factors for rotator cuff disease The

patients selected their preferred sleep position prior to symptom onset. Sleep positions, as defined in the published literature, were categorized as side, supine, and abduction external rotation (ABER—on the back or stomach with hands above the shoulders). A blinded musculoskeletal radiologist (PC) retrospectively reviewed the MR studies using a standardized data collection sheet. Age-adjusted logistic regression was performed and p-values less than or equal to 0.05 were considered significant.

Results: The prevalence of full-thickness tears trended lower in the ABER vs. side and supine sleep positions (18% vs. 35% and 33%, respectively; p=0.65). The prevalence of all tears (partial and full thickness) also trended lower in the ABER position (46% vs. 78% and 75%, respectively; p=0.16). These findings were not statistically significant due to a small sample size and a large number of confounding variables. A down-sloping acromion (p=0.03) and a low-lying acromion (p=0.05) were significantly associated with a decreased prevalence of tears.

Conclusion: This study suggests a decreased prevalence of rotator cuff tears in those who sleep with their arms abducted, compared with those who sleep supine or on their side. ABER sleep position could thus be used to prevent development or progression of rotator cuff disease in those at risk. Additionally, a lower prevalence of rotator cuff tears was noted in patients with a down-sloping or low-lying acromion, anatomical factors said to predispose to rotator cuff disease according to impingement theory.

2:00 pm

184. MR Arthrography of the Shoulder: Does Gadolinium Improve the Diagnosis of Rotator Cuff and Labral Pathology?

McGonegle, S.; Whiteside, M.; Vinson, E.; Helms, C. Duke University Medical Center, Durham, NC*
Address correspondence to S. McGonegle (shane.mcgonegle@duke.edu)

Objective: While reviewing shoulder MR arthrograms, we have observed that T2-weighted (T2W) images are primarily used to assess rotator cuff and labral pathology. T1-weighted (T1W) images with intra-articular gadolinium appear to offer no additional diagnostic information. This study evaluated the utility of performing shoulder MR arthrography with saline-only distention of the joint.

Materials and Methods: Our database was reviewed for 100 consecutive shoulder MR arthrograms performed between January, 2007 and December 2007. Patient information was blinded and images were reviewed at a dedicated workstation by at least one radiology fellow and one radiology attending, each with musculoskeletal training (four total evaluators). Our protocol includes fat-suppressed T1W and T2W images in the axial, coronal oblique, and sagittal oblique planes, with non fat-suppressed T1W images in the sagittal oblique plane. If arthrography could be performed with saline alone, several image series could be eliminated. We reviewed T2W images in isolation to simulate saline-only arthrography. After a three to four week delay, the full study was reviewed. These were evaluated for rotator cuff and labral pathology. If there was a significant discordance between the two reads, the study was again reviewed to reach a consensus. A significant discordance was defined as a difference in identifying a labral or rotator cuff tear, or describing a partial vs. full thickness cuff tear between the two assessments.

Results: There were 98 patients reviewed, 64 male and 34 female (average age 36.2 years). Two had bilateral MR arthrograms. Out of the 100 arthrograms, 55 showed concordance and 45 showed discordance between the isolated T2 and full study assessments. Review of these 45 cases again in consensus showed that T1W and T2W images displayed labral and cuff pathology similarly. These discordances were therefore attributed to intraobserver variability.

Conclusion: Our data suggests that shoulder MR arthrography can be performed adequately with saline alone. Eliminating gadolinium and fat-suppressed T1W imaging offers a financial and time savings with a small reduction in allergy risk.

2:10 pm

185. Noncontrast MRI Diagnosis of Adhesive Capsulitis

Kim, J.[1]; Zoga, A.[2]; Saaty, H.[1]; Morrison, W.[2] 1. Loma Linda University Medical Center, Loma Linda, CA; 2. Thomas Jefferson University Hospitals, Philadelphia, PA*
Address correspondence to J. Kim (jxk009@gmail.com)

Objective: This was a prospective study on noncontrast MRI diagnosis of adhesive capsulitis of the shoulder. A noncontrast MR protocol is the standard of care for shoulder impingement syndrome, the most common indication for shoulder MRI, in the 40-70 year old group. Scarce information has been published about diagnosing adhesive capsulitis on noncontrast MRI. We hypothesized that clinical adhesive capsulitis can be reliably predicted with noncontrast MRI.

Materials and Methods: A triad of findings is proposed for the diagnosis of adhesive capsulitis on noncontrast MRI: thickening of the coracohumeral ligament greater than 2 mm, subcoracoid fatty infiltration, and inferior glenoid injury or thickening of the joint capsule in the axillary recess. A database search was performed to obtain 16 patients: 38-72 years old with mean age of 56 years, six males and ten females, who already had noncontrast, nonarthrographic, shoulder MRI exams using keywords "adhesive capsulitis" and "frozen shoulder" as part of their history. Additional age-matched control studies were also obtained for those who underwent noncontrast MRI studies for reasons other than those deemed suspicious for adhesive capsulitis, which numbered 15 in total. Studies were blinded and presented to an musculoskeletal fellowship trained radiologist for review.

Results: One patient with suspected history of adhesive capsulitis was excluded due to significant concomitant findings of large joint effusion and traumatic labral tear. Comparing MRI findings to the reference standard of adhesive capsulitis by clinical suspicion, sensitivity was 67% and specificity was 73%. For patients who met the MRI criteria for adhesive capsulitis but were not clinically suspected, the radiologist's average confidence level was found to be 3.2/5, compared to overall average of 3.5/5.

Conclusion: Although adhesive capsulitis is reliably diagnosed on direct MR arthrography, noncontrast MRI of the shoulder is a noninvasive method for assessing patients presenting with a common complaint of shoulder pain. Often clinically suspected, strict criteria for diagnosis and confirmation of adhesive capsulitis has not been previously established for noncontrast MRI of the shoulder. Based on the findings from this study, a reliable triad of findings has been proposed in making the diagnosis with

increased confidence. However, further investigation will be conducted to refine the criteria to achieve even greater concordance of radiographic and clinical diagnoses of adhesive capsulitis.

2:20 pm

186. Sonographic Assessment of Suture Artifact Obscuring Visualization of the Digital Nerve

de la Lama, M.[1]; Kessler, J.[1]; Magge, K.[1]; Negron, J.[1]; Umans, H.[1,2] 1. Jacobi Medical Center, Bronx, NY; 2. Albert Einstein College of Medicine, Bronx, NY*
Address correspondence to H. Umans (hilary.umans@gmail.com)

Objective: The objective was to grade and compare the severity of sonographic artifact produced by four commonly used suture materials and determine whether these artifacts affect visualization of the digital nerve.

Materials and Methods: A fresh pig foot model was selected due to similarities between porcine and human skin subcutaneous tissues. A 17g percutaneous needle was placed subcutaneously to mimic the depth and caliber of a normal volar digital nerve. Longitudinal incisions superficial to the needle were closed with four different skin suture types using interrupted stitch technique. The following sutures were used: 5-0 Nylon (N), a synthetic nonabsorbable monofilament suture; 5-0 Chromic (C), an absorbable suture made of surgical gut; 5-0 Vicryl (V), a braided multifilament absorbable suture; and 5-0 Prolene (P), a nonabsorbable monofilament suture. One plastic surgery fellow performed all incisions and sutures.Ultrasound was performed using an ultrasound system (Toshiba Medical Systems, Tochigiken, Japan) with a 12 MHz hockey stick transducer. Twenty radiology residents and attendings were surveyed to grade severity of artifact and nerve obscuration related to suture material on a four-point ordinal scale (none, mild, moderate, severe) and ten-point numerical scale (1-10). Each was asked to separately evaluate the severity of suture artifact and nerve obscuration. Two image types were shown: one suture type per image and a composite image of each suture type evenly spaced and adjacent to each other. Data was analyzed using the Student's t test setting alpha=0.05.

Results: Severity of nerve obscuration from most to least was: on the composite image using the numerical scale, P=V=N>C; on the composite image using the ordinal scale, P=V=N>C; on the individual images using the numerical scale, P>V>N>C; on the individual images using the ordinal scale, P>N>V>C. Severity of artifact from most to least was on the composite image using the numerical scale, V=N>P>C; on the comparison image using the ordinal scale, V= N>P>C; on the individual image using the numerical scale, P>N>V>C; on the individual image using the ordinal scale, P>N>V>C.

Conclusion: Although all four suture materials produced sonographic artifact, only chromic produced mild artifact which did not significantly obscure visualization of the nerve model. If preoperative sonographic imaging assessment of volar digital nerve injury is contemplated in the context of penetrating trauma, chromic sutures should be selected for wound closure.

GASTROINTESTINAL (DIFFUSION/PERFUSION) IMAGING PAPERS

Room: 310, Level 3

Wednesday, April 29, 2009, 3:00 pm–5:00 pm

Abstracts 187-197

Moderators: *E. Merkle, C. Santillan*

Keynote Address: DWI and DCE-MRI of the Liver: The Basics—*E. Merkle*

3:10 pm

187. Comparison of ADC Values in Normal Liver Across Different Software Versions and Between Different Magnet Strength

Yousaf, A.; Pandey, T.; Kaushik, C.; Malak, S.; Jambhekar, K.; Viswamitra, S. University of Arkansas for Medical Sciences, Little Rock, AR*

Address correspondence to T. Pandey (drtarunpandey@hotmail.com)

Objective: There is an increasing body of literature that suggests using ADC values to characterize lesions. However, there is also variability in the ADC values. The software used to calculate the ADC has also been improved by vendors in the last three years. This study aimed to evaluate if the calculated ADC was dependent on field strength and software version improvements.

Materials and Methods: All imaging was performed using a 1.5T (Siemens Medical Solutions, Erlangen, Germany) and 3T (Siemens Medical Solutions, Erlangen, Germany) MRI scanner. Diffusion-weighted images (DWI) were obtained using single-shot echo planar sequence (repetition time [TR]/echo time [TE] 4200/ 82 milliseconds, matrix 124 x 192, b-values 0/50/400/800 and 1,000 mm^2/second). Direct measurements of ADC values of these lesions were obtained on a workstation (Siemens Medical Solutions, Erlangen, Germany). The mean and standard deviation of the ADC values was calculated. Statistical analysis was performed using analysis of variance (ANOVA). Forty-six normal subjects consisting of 30 subjects scanned on the 3T and 19 on the 1.5T magnets, were studied. The software versions for 1.5T included B13 (12 patients), B11 (seven patients) and for the 3T were B15 (19 patients) and B12 (eight patients).

Results: Comparing the different software versions in patients scanned on 3T between 2006/ 2007 (version B12) and 2008 (version B15), the mean ADC values (x 10^{-3} mm^2 /second) were 0.12 and 0.96 respectively with a p value of 0.01. Among 1.5 T subjects scanned between 2006 (version B11) and 2007/2008 (version B13) the mean ADC values were 0.124 and 1.117 respectively with a statistically significant difference ($p<0.001$). No statistically significant difference was noted among subjects scanned between the 1.5T and 3T magnets using any of the software versions.

Conclusion: There is statistically significant difference seen in ADC values in normal liver between different versions of the software used on the same magnet with no significant difference seen in normal livers scanned between different magnet strengths.

3:20 pm

188. Qualitative Effect of Gadolinium on Diffusion-Weighted MR Imaging of the Liver, Spleen, Pancreas and Kidney at 3T

Wang, C.; Dale, B.; Neville, A.; Boll, D.; Samei, E.; Merkle, E. Duke University, Durham, NC*

Address correspondence to C. Wang (kaerolynlee@yahoo.com)

Objective: The objective was to retrospectively assess the effect of intravenous gadolinium-based contrast on the diffusion-weighted imaging (DWI) qualitative appearance of the liver, spleen, pancreas and kidneys.

Materials and Methods: This HIPAA-compliant, IRB approved retrospective study evaluated 50 consecutive patients (25 male; mean age 59.4 years) who underwent contrast-enhanced abdominal MRI (Siemens Medical Solutions, Forchheim,Germany). Patients received either gadobenate dimeglumine (Bracco Diagnostics, Princeton, NJ) (n=46) or gadopentetate dimeglumine (Bayer HealthCare Pharmaceuticals, Montville, NJ) (n=4). DWI was acquired prior to and after contrast administration, using single-shot echo planar imaging with b-values of 50 and 800 s/mm^2. Pre- and postgadolinium DWI images of the liver, spleen, pancreas, and kidneys were analyzed by three expert readers for the best diffusion-weighted appearance. Statistical analysis included the binomial test to determine if precontrast was preferred more than 50% of the time (i.e. more than flipping a coin) for each of the organs specified. Intraobserver and interobserver agreement was determined using Cohen's kappa statistics.

Results: Mean time interval between the initiation of contrast and acquisition of post-contrast DWI was 642 ± 164 seconds. The expert readers preferred the precontrast DWI images of the liver in 52% ($p=0.623$) of the cases, of the spleen in only 49% ($p=0.801$) of the cases, and of the pancreas in 58% ($p=0.065$); none of which were statistically significant. There was statistical significance in the DWI appearances of the kidneys with precontrast images being preferred in 83% ($p<0.001$) of the cases. No significant interobserver or intraobserver agreement was noted in any of the organs tested, with a Cohen's kappa of <0.262 in all cases.

Conclusion: Intravenous gadolinium administration does not make a statistically significant difference in the qualitative appearance of the liver, spleen, or pancreas in the DWI when comparing precontrast to postcontrast DWI. This may allow DWI sequences, which may improve liver lesion detection, to be performed either before or after contrast administration as needed.

3:30 pm

189. Characterization of Normal, Cirrhotic Livers and Focal Liver lesions on 3T MRI Using Apparent Diffusion Coefficient Values

Pandey, T.; Jambhekar, K.; Kaushik, C.; Yousaf, A.; Malak, S.; Viswamitra, S. University of Arkansas for Medical Sciences, Little Rock, AR*

Address correspondence to T. Pandey (drtarunpandey@hotmail.com)

Objective: Apparent diffusion coefficient (ADC) values have been used in characterization of liver lesions with varying successes,

predominantly on 1.5T systems. We evaluated the efficacy of ADC values in characterization of liver lesions on a 3T MRI. ADC values were also obtained in normal and cirrhotic livers.

Materials and Methods: Direct measurement of ADC values were obtained on a workstation (Siemens Medical Systems, Erlangen, Germany) on 75 patients (38 males and 37 females, age range 19 to 84) scanned on a 3T scanner (Siemens Medical Systems, Erlangen, Germany) using diffusion-weighted single-shot echo planar sequence (DW-SS-EPI). B-values used were 0/50/400/800 or 1,000 mm^2 /s. These included 32 benign liver lesions (13 cysts, four hemangiomas, seven adenomas, seven focal nodular hyperplasias [FNH] and one abscess) in 20 patients and 34 malignant lesions (18 hepatocellular cancers [HCC], 15 metastatic lesions and one cholangiocarcinoma) in 20 patients. Measurements were also obtained in 25 cirrhotic and 19 normal livers. Lesion size varied from 0.5-10 cm for benign and 1.0-18 cm for malignant lesions. Students-t test and analysis of variance (ANOVA) was performed to detect the differences between the various mean ADC values.

Results: Mean ADC value (x 10^{-3} mm^2 /s) was 0.96 and 0.87 for normal and cirrhotic livers respectively; 2.5 for cysts, 1.6 for hemangiomas, 1.2 for FNH and 1.2 for adenomas. The ADC values were 0.88 for HCC, 0.78 for noncarcinoid metastatic deposits and 0.57 for carcinoid metastases. There was no significant difference between the ADC values of normal and cirrhotic livers. Statistically significant difference ($p< 0.001$) was however seen between the ADC values of primary liver tumor (HCC) versus benign hepatocellular lesions (FNH and adenomas). While HCC could not be differentiated from secondary deposits, statistically significant difference in ADC values was seen between carcinoid metastases as a group and other metastases ($p<0.01$) as well as HCC ($p<0.001$).

Conclusion: ADC values can differentiate HCC from benign hepatocellular lesions like FNH or adenoma on 3T MRI. Cysts and hemangiomas afford differentiation due to high ADC values. FNH and adenomas cannot be differentiated from each other due to similar ADC values. No significant difference in ADC values is noted in normal and cirrhotic livers or between primary and secondary liver lesions except carcinoid metastases which showed significantly less ADC values than other malignant lesions.

3:40 pm

190. MR Imaging Compared with In-111-Labeled Pentetreotide Scans for Neuroendocrine Tumor: Is MR Diffusion-Weighted Imaging Helpful?

Horowitz, J.; Gabriel, H.; Spies, W.; Miller, F.; Yaghmai, V.; Nikolaidis, P. Northwestern University, McGaw Medical Center, Chicago, IL*
Address correspondence to J. Horowitz (jhorowitz77@gmail.com)

Objective: The objective was to determine if abdominal MR diffusion-weighted imaging (DWI) increases detection of neuroendocrine tumors compared with conventional MR and In-111-labeled pentetreotide scans, or increases confidence in characterizing lesions as malignant.

Materials and Methods: Fifteen patients who underwent abdominal MR with DWI and In-111-labeled pentetreotide scans with SPECT, and who had pathologically proven neuroendocrine tumor, were retrospectively reviewed. Axial T2 half fourier acquisition single-shot turbo spin echo (HASTE), arterial gadolinium-enhanced T1 fat saturated (FS), B0/B50 and B500, and apparent diffusion coefficient maps were reviewed, analyzing a total of 23 lesions. Lesions were considered positive, equivocal, or negative on MR and In-111-labeled pentetreotide scans. It was determined whether the DWI increased the conspicuity and increased the confidence in characterizing lesions as malignant.

Results: Eleven of 23 lesions (48%) demonstrated restricted diffusion. Restricted diffusion increased confidence that the lesion was neoplastic in 10/15 patients (67%). The lesions showed increased conspicuity on B500 in 5/15 patients (33%). DWI both increased the confidence in diagnosing neoplasm and showed increased conspicuity of lesions in 3/15 patients (20%). DWI was not helpful in 3/15 patients (20%). The In-111-labeled pentetreotide scans detected the neuroendocrine tumor as positive in 9/15 patients (60%), equivocal in 5/15 patients (33%), and negative in 1/15 patients (7%).

Conclusion: MR DWI is helpful in detecting and characterizing neuroendocrine tumors, by increasing the conspicuity of lesions and confidence that a lesion is neoplastic.

3:50 pm

191. Analysis of Apparent Diffusion Coefficient Values of the Spleen in Patients with Suspected Iron Overload on In- and Out-of-Phase MR Imaging

Jambhekar, K.; Pandey, T.; Yousaf, A.; Kaushik, C.; Malak, S.; Viswamitra, S. University of Arkansas for Medical Sciences, Little Rock, AR*
Address correspondence to T. Pandey (drtarunpandey@hotmail.com)

Objective: Splenic parenchymal signal dropout on in phase versus out-of-phase images secondary to increased susceptibility due to iron overload. We assessed if apparent diffusion coefficient (ADC) values of the splenic parenchyma could be used as an additional tool to evaluate iron overload. We also aimed to propose a threshold ADC value to differentiate normal vs. spleen with iron overload.

Materials and Methods: ADC values were obtained in 35 subjects consisting of 22 patients suspected of iron overload based on in-phase and out-of-phase MR imaging and 13 controls with no MR evidence of iron overload. The 22 patients with evidence of iron overload on T1W in-and out-of-phase images were diagnosed with multiple myeloma, had received multiple blood transfusions and had no evidence of extramedullary disease. The 13 patients forming the control group were patients with normal scans and no evidence of splenic pathology. All patients were scanned on a 1.5T scanner (Siemens Medical System, Erlangen, Germany). Multi-breathhold 2D-flash T1W in-and out-of-phase images were obtained (5/1mm slice thickness, TR/TE 165/ 2.38, 4.97 ms, matrix of 256 x 256). Signal intensity was quantified using mean pixel value of a standard circular measurement tool on the PACS (Sectra Medical Systems, Linkoping, Sweden) workstation. Diffusion-weighted images (DWI) were obtained using single-shot echo planar sequence (TR/TE 4200/ 82ms, matrix 124x192, b-values 0/ 50/ 400/ 800 mm^2 /s). Direct measurements were obtained from the spleen on the ADC maps processed on the workstation (Siemens Medical System, Erlangen,

Germany). For the purpose of uniformity an average of three measurements were obtained. Statistical analysis using student's t-test was performed.

Results: The study subjects included 21 males and 14 female patients with an age range of 17 to 85 years. The mean ADC value (x 10^{-3} mm^2 /s) of the spleen was 0.6 ± 0.3 in the patients with iron overload compared to 1.3 ± 0.4 in the control group. These values were statistically different ($p<0.001$). We propose a threshold ADC value of 1.0 to differentiate patients with iron overload versus normal splenic parenchyma with 95.5% sensitivity, 69.2% specificity, 90.0% negative predictive value and 84% positive predictive value. The absolute mean difference between in/out-of-phase pixel values was significantly greater among cases compared to controls (33.1 vs. 15.5; $p<0.05$)

Conclusion: ADC values are helpful in assessment of iron overload in the spleen and can be used as an adjunct to the in-and-out of phase images.

4:00 pm

192. Evaluation of Liver Fibrosis with Diffusion-Weighted Imaging in Nonalcoholic Fatty Liver Disease: The Affect of Analysis Location on Histopathologic Correlation

Qayyum, A.; Nystrom, M.; Noworolski, S.; Chu, B.; Westphalen, A.; Vigneron, D. University of California, San Francisco, San Francisco, CA*
Address correspondence to A. Qayyum (aliya.qayyum@radiology.ucsf.edu)

Objective: The purpose was to determine the affect of apparent diffusion coefficients (ADC) measurement location on histopathologic correlation in nonalcoholic fatty liver disease.

Materials and Methods: Committee on Human Research approval and patient consent were obtained, and the study was in compliance with HIPAA. Diffusion-weighted images were reviewed in ten patients with grade 1 steatosis due to nonalcoholic fatty liver disease (three men and seven women) with a mean age of 52 years (range, 43-67). ADC were measured from multiple regions of interest placed peripherally in the liver in the right lobe and medial segment of the left lobe on three consecutive axial slices centered at the portal vein. The mean total liver ADC and mean right lobe ADC were calculated as from nine and six measurements, respectively. The ADC was also measured in the right lobe at the mid-axillary line in the mid axial level of the liver to approximate liver biopsy location. Spearman's correlation was used to determine the correlation of ADC from the expected biopsy location, right lobe, and total liver with histopathologic fibrosis stage.

Results: The number of patients with stages 0, 1, 2, 3 and 4 fibrosis were three, five, one, zero and one, respectively. A significant inverse correlation was observed between ADC and fibrosis stage ($p<0.05$). The greatest correlation between ADC and fibrosis was observed at the expected biopsy location ($R^2= 0.78$), compared to the mean ADC of the right lobe ($R^2=0.71$) or the mean ADC of both right and left lobes ($R^2=0.65$).

Conclusion: Liver apparent diffusion coefficient values are inhomogeneous and measurements in the expected region of liver biopsy correlate the most with histopathologic fibrosis.

4:10 pm

193. Apparent Diffusion Coefficient: An Indicator of Improvement of Extramedullary Lesions on Treatment in Multiple Myeloma

Viswamitra, S.; Jambhekar, K.; Pandey, T.; Kaushik, C.; Yousaf, A.; Malak, S. University of Arkansas for Medical Sciences, Little Rock, AR*
Address correspondence to T. Pandey (drtarunpandey@hotmail.com)

Objective: The aim of our study was to evaluate the statistical significance of apparent diffusion coefficient (ADC) in evaluating response to treatment of extramedullary lesions in patients with multiple myeloma.

Materials and Methods: Six patients with multiple myeloma having a total of seven extramedullary lesions were included in our study. Five lesions were located in liver, one in muscle and one in perinephric region. All patients were male and were in the age range of age range of 50-71 years. All imaging was performed using 1.5T MRI scanner (Siemens Medical Solutions, Erlangen, Germany). Diffusion-weighted images (DWI) were obtained using single-shot echo planar sequence (repetition time [TR]/echo time [TE] 4200/82 milliseconds, matrix 124x192, b-values 0/50/400/800 mm^2 /second). Direct measurements of ADC values of these lesions were obtained on a workstation (Siemens Medical Solutions, Erlangen, Germany). The mean and standard deviation of the ADC values was calculated. Statistical analysis was performed using paired sample t-test.

Results: The extramedullary lesions had a mean ADC of 0.9 x 10^{-3} mm^2/second, SD ± 0.4 prior to the treatment compared to a mean ADC 1.3 x 10^{-3} mm^2/second, SD ± 0.4 after treatment. The paired mean difference is 330.5 which is statistically significant ($p<0.005$).

Conclusion: Increase in ADC is significant after treatment and is suggestive for response to treatment.

4:20 pm

194. CT Perfusion Parameters Obtained from Routine Dynamic Contrast-Enhanced CT Timing Bolus Reflects Severity of Liver Disease

Sleiman, S.; Wang, Z.; Schneider, J.; Aslam, R.; Chu, L.; Yeh, B. University of California, San Francisco, San Francisco, CA*
Address correspondence to B. Yeh (ben.yeh@radiology.ucsf.edu)

Objective: The objective was to determine whether CT perfusion parameters obtained from routine timing bolus images correlate with liver disease.

Materials and Methods: We routinely perform timing bolus examinations by imaging the abdomen using low dose technique (40 mA at 100 kVp) every other second after a 30 ml bolus of intravenous contrast material in order to determine CT scan delays for multiphase abdominal examinations. We identified 150 consecutive patients (84 men and 66 women, mean age of 59 years) who had timing bolus examinations and processed the images using a CT perfusion workstation (Apollo Medical Imaging Technology, North Melbourne, Australia) to determine the following hepatic perfusion parameters: arterial, portal and total blood

flow, arterial fraction, mean transit time, and distribution volume. We reviewed all patient medical records to determine the Model for End-Stage Liver Disease (MELD) score, history of partial hepatectomy, and whether cirrhosis or portal hypertension was present and correlated these with the perfusion parameters using t-tests and the Pearson correlation coefficient.

Results: A significantly higher mean hepatic arterial blood flow and hepatic arterial fraction was seen in the 35 patients with cirrhosis (26.7 mL/minute/100 grams and 21%) than the 99 without cirrhosis (18.7 mL/minute/100 grams and 15.2%, respectively, $p<0.0001$ for both). Similarly, a significant correlation was found between a more severe MELD score and a higher hepatic arterial blood flow ($r=0.46$, $p<0.0005$) and hepatic arterial fraction ($r=0.40$, $p<0.005$). In contrast, the presence or absence of cirrhosis did not correlate with the total hepatic blood flow, portal blood flow, mean transit time, nor distribution volume. In the 16 patients who had prior partial hepatectomy, a higher mean portal blood flow was seen (153 mL/minute/100 grams) than in the 134 patients without (111 mL/minute/100 grams, $p<0.05$).

Conclusion: Hepatic arterial blood flow and hepatic arterial fraction derived from routine low dose timing bolus CT images correlate with the severity of diffuse liver disease. Potentially, such physiological perfusion parameters may be obtained as a quantitative and adjunctive evaluation of liver disease at routine CT.

4:30 pm

195. Quantification of Wash-out of Hepatocellular Carcinoma at Contrast-Enhanced Ultrasound: Usefulness of a Semiquantitative Index

Cabassa, P.; Gavazzi, E.; Gatti, E.; Morone, M.; Narbone, M.; Maroldi, R. University of Brescia, Brescia, Italy*
Address correspondence to P. Cabassa (paolocab@libero.it)

Objective: The objective was to quantify wash-out of hepatocellular carcinoma (HCC) using a semiquantitative index during portal phase with contrast-enhanced ultrasound (CEUS).

Materials and Methods: Forty-three consecutive histologically proven HCCs were prospectively studied with CEUS. CEUS was performed with 2.4 ml of sulphur hexafluoride with dedicated software (contrast coherent imaging). Real time B mode scanning was performed during arterial portal and late phases. One significant frame (in bitmap format) of portal phase was chosen for each lesion and analyzed by software (AdobePhotoshop 7.0). Two circular defined regions of interest (ROI) for each image were drawn encompassing the lesion and the adjacent normal parenchyma. Sonography videotape intensity (VI) was measured in gray-scale levels (0-255) through histogram analysis for each ROI. Background VI was set at the same level for each image. A semiquantitative index (VItumor–VIliver/VIliver) was therefore calculated. Results were divided according to grading type and also compared with other benign and malignant liver lesions.

Results: HCCs showed a median index value of –0.37 (SD 0.24). The index significantly correlates with the HCC grading ($p<0.05$). The index correlates with pathology but an overlap with benign lesions (regenerative nodules) was noted. The main reason was the relatively isoechogenicity compared to the surrounding parenchyma of well differentiated HCCs during portal phase.

Conclusion: The wash-out during portal phase was quantified. The correlation with grading could help in patient staging and treatment options.

4:40 pm

196. Intraindividual Comparison of Hepatic Venous Phase and Delayed Phase for the Detection of Wash-Out Contrast-Enhancement Pattern of Hepatocellular Carcinoma at MDCT of the Liver

Furlan, A.[1]; Brancatelli, G.[2]; Marin, D.[3]; Palermo Patera, G.[2]; Ronzoni, A.[4]; Lagalla, R.[2]; Bazzocchi, M.[1]; Vanzulli, A.[4] 1. Università degli Studi di Udine, Udine, Italy; 2. University of Palermo, Palermo, Italy; 3. Università la Sapienza, Roma, Italy; 4. A. O. Niguarda Ca Granda, Milan, Italy*
Address correspondence to A. Furlan (ali.furlan@gmail.com)

Objective: The objective was to retrospectively compare the hepatic venous phase (HVP) with the delayed phase (DP) for the detection of washout contrast-enhancement pattern of hepatocellular carcinoma (HCC) lesions at MDCT of the liver.

Materials and Methods: The study cohort comprised 30 cirrhotic patients (25 men, five women; mean age, 57 years, range, 36-66) who underwent multiphasic 64-slice MDCT of the liver within 90 days before liver transplantation. CT was performed immediately before contrast medium administration (2 mL/Kg body weight of iomeprol, 350 mgI/mL at 3.5-4.0 mL/second) and during the hepatic arterial dominant phase, HVP, and DP, obtained respectively at, 12, 55, and 120 seconds after the trigger threshold (120 HU at the level of the abdominal aorta) using automatic bolus tracking. Two radiologists qualitatively evaluated the CT images during the HVP and DP, for the detection of tumor wash-out contrast-enhancement pattern. Additionally, tumor-to-liver contrast-to-noise ratio (CNR) was measured for each lesion at both phases.

Results: At pathologic examination of explanted livers, 61 HCCs (mean size, 1.6 cm; range, 0.8-4.2 cm) were confirmed in 27 patients. Forty-seven (77%) of 61 HCCs were detected at MDCT. A significantly higher number of tumors demonstrated a wash-out contrast-enhancement pattern during the delayed phase (DP) (19 of 47, 40%) compared to the HVP (12 of 47, 26%) ($p<0.0001$, McNemar's test). Lesion-to-liver mean CNR increased significantly during the DP (-2.07 ± 1.2) compared to the HVP (-1.33 ± 1.4) ($p=0.0003$, Student's t-test).

Conclusion: The DP is superior to the HVP for the detection of wash-out contrast-enhancement pattern of HCC at multiphasic 64-section MDCT of the liver.

4:50 pm

197. Optimization of Contrast Material Dose for Abdominal MDCT: Predicting Patient Lean Body Weight by Using Preliminary Axial CT Images

Marin, D.[1]; Ho, L.[1]; Guerrisi, A.[2]; Toth, T.[3]; Nelson, R.[1] 1. Duke University Medical Center, Durham, NC; 2. University of Rome Sapienza, Rome, Italy; 3. GE Healthcare, Milwaukee, WI Address correspondence to D. Marin (danielemarin2@gmail.com)*

Objective: Compared to total body weight (TBW), contrast material dose based on measured lean body weight (LBW) has been shown to yield more consistent aortic and liver enhancement in patients undergoing abdominal MDCT. The purpose of this study was to determine whether a fat-fraction derived from preliminary axial CT images can be used to estimate lean body weight (eLBW), in anticipation of using this metric as the basis for determining the dose and rate of contrast material during abdominal MDCT.

Materials and Methods: Using a commercially available body composition analyzer scale (Tanita, Arlington Heights, IL) the measured lean body weight (mLBW) was determined in 12 patients (for men, eight women; age ranges, 28-72 years) prior to contrast-enhanced abdominal MDCT examination. CT image data of the abdomen and pelvis was processed using computer-assisted, vendor-specific software (GE Healthcare, Milwaukee, WI) which calculated a fat-fraction for each transverse image. The fat-fraction was automatically measured by the software as the number of fat pixels (-200 to -50 HU) divided by the total number of pixels having an attenuation value equal or greater than -200 HU. By averaging data over multiple contiguous sections, the fat-fraction was individually assessed for the upper, mid, and lower abdomen (upper pelvis). For each anatomical region, eLBW was calculated by multiplying TBW by (1—fat-fraction). Correlation between mLBW and eLBW was calculated by linear regression analysis.

Results: The average mLBW for all patients was 50 ± 9 kg (range, 38-64 kg). For the upper, mid, and lower abdominal regions respectively, eLBW values were 52 ± 9 kg (range, 37-65 kg), 51 ± 9 kg (range, 35-64 kg), and 50 ± 10 kg (range, 36-66 kg). The regression coefficients between mLBW and eLBW demonstrated excellent correlation for the mid and lower abdomen (r=0.76 and 0.90, respectively), and good correlation for the upper abdomen (r=0.66).

Conclusion: Estimated lean body weight derived directly from preliminary axial CT images can accurately predict measured lean body weight without need for a time consuming body composition analysis. Using estimated lean body weight as the basis for determining the dose and rate of contrast material has the potential to improve consistency of vascular and parenchymal enhancement during abdominal MDCT.

MUSCULOSKELETAL IMAGING (AND TREATMENT INNOVATIONS) PAPERS

Room: 207, Level 2

Wednesday, April 29, 2009, 3:00 pm–5:00 pm

Abstracts 198-208

Moderators: *K. Schreibman, W. Morrison*
Keynote Address: Pitfalls in the Human Visual System—*K. Schreibman*

3:10 pm

198. Percutaneous Sonographically-Guided Achilles Tendon Debridement: Preliminary Results and Ultrasound Findings

Grant, T.[1]; Ionita, J.[1]; Omar, I.[1]; Ahmed, M.[2]; Kelikian, A.[1] 1. Feinberg School of Medicine, Northwestern, Chicago, IL; 2. Loyola University Chicago, Maywood, IL*
Address correspondence to J. Ionita (j-ionita2@md.northwestern.edu)

Objective: Achilles tendinosis is associated with hind foot pain, swelling, and loss of ankle motion. Overuse, calf weakness, excessive ankle pronation, and poor footwear can cause the condition. Conservative therapy includes stretching, nonsteroidal anti-inflammatory drugs, physical therapy, and immobilization. Surgery is reserved for patients with refractory symptoms. Percutaneous sonographically-guided Achilles tendon debridement is an emerging option for patients who fail conservative therapy. This procedure offers patients a minimally invasive treatment option. Few studies have looked at the patient response following this procedure, and the goal of our study is to examine its effectiveness.

Materials and Methods: Seventeen consecutive patients (ten women, seven men, age 28 to 74 with mean age 50) with clinical and ultrasound documented Achilles tendinosis were included. All had at least six months of pain unresponsive to conservative management. The procedure was performed using a 20-gauge spinal needle that is placed into the Achilles tendon under ultrasound guidance. Approximately 50 to 60 to and fro movements are made into the abnormal tendon. Six months to three years after the procedure, a modified American Orthopaedic Foot and Ankle Society Ankle and Hindfoot Functional Survey was given to the patients to determine the effectiveness of the procedure. Questions in the survey ask patients to rate pain, symptoms, and activity limitations before and after the procedure.

Results: Of the 17 patients surveyed, ten reported improvement in their symptoms and satisfaction with the procedure. Improvement in symptoms involved pain resolution, ease in walking and climbing stairs, and less activity restrictions. Symptoms improved from one month to one year after the procedure. Of the seven patients who reported no improvement, none reported worsening in symptoms. Three of the seven underwent surgery with improvement in symptoms. Ultrasound findings after the procedure ranged from slight improvement in the appearance of tendinosis to complete resolution of the abnormal findings.

Conclusion: The preliminary results of this study suggest percutaneous sonographically-guided Achilles tendon debridement may be helpful in patients with Achilles tendinosis who fail conservative management. Of the patients in this small study group, 59% reported improvement in symptoms. There were no procedural complications and none of the patients reported worsening in symptoms.

3:20 pm

199. Sonographically-Guided Percutaneous Needle Release of the Carpal Tunnel: Preliminary Experience

Austin, A.[1]; Nazarian, L.[1]; McShane, J.[2] 1. Thomas Jefferson University Hospital, Philadelphia, PA; 2. McShane Sports Medicine, Villanova, PA*
Address correspondence to L. Nazarian (levon.nazarian@jefferson.edu)

Objective: Patients who fail conservative management for carpal tunnel syndrome (CTS) may need surgical release. We evaluated our initial experience performing carpal tunnel release using a sonographically (US) guided, minimally invasive, percutaneous needle technique.

Materials and Methods: IRB approval was obtained for retrospective review of nine consecutive patients who underwent US-guided percutaneous needle release of the carpal tunnel between January 2005 and August 2008. The patient population consisted of eight women and one man, mean age 51.7 years (range 37-69 years). All patients had presented with clinical diagnosis of CTS, failed conservative management, and were now considered surgical candidates. After 1% lidocaine was administered subcutaneously, under US guidance a 22-gauge hypodermic needle was used to repeatedly fenestrate the transverse carpal ligament at the site of median nerve compression, in a proximal to distal approach. The procedure was concluded when the ligament palpably softened and median nerve compression visibly lessened. 0.5 cc (20 mg) of triamcinolone acetonide was then injected directly into the ligament. The needle was withdrawn, and hemostasis achieved. Each patient participated in a telephone questionnaire at a mean follow-up time of 29.4 months (range 4-42 months) after the procedure. Nineteen questions pertained to severity of CTS, both before and after the procedure. Answers were evaluated using a paired Student's t-test.

Results: Significant ($p<0.05$) improvement in symptoms and/or function was seen for the following: pain at night waking the patient ($p<0.0001$), numbness or tingling waking the patient ($p=0.0004$), pain during daytime ($p=0.0004$), frequency of daytime pain ($p=0.0007$), daytime numbness or tingling ($p<0.001$), muscle weakness ($p=0.007$), writing ($p=0.01$), gripping a telephone handle ($p=0.01$), opening jars ($p=0.005$), household chores ($p=0.02$), carrying grocery bags ($p=0.003$), and bathing and dressing ($p=0.03$). There were no major complications. A total of 89% (8/9) of patients gave the procedure the highest score on a four-point scale, and felt that there was little to no room for improvement. The ninth patient eventually needed surgical release. All nine of the patients stated that they would refer a friend or relative for the procedure.

Conclusion: US-guided percutaneous needle release of the carpal tunnel may be a safe and effective minimally invasive alternative to surgery. A randomized controlled study is required to compare this procedure to existing therapies.

3:30 pm

200. Quantitative Molecular Characterization of Musculoskeletal Lesions by Proton MR Spectroscopy

Fayad, L.[1]; Salibi, N.[2]; Jacobs, M.[1]; Ouwerker, R.[1]; Okollie, B.[1]; Eng, J.[1]; Weber, K.[1]; Barker, P.[1]; Bluemke, D.[1,3] 1. Johns Hopkins University, Baltimore, MD; 2. No Institutional Affiliation; 3. National Institutes of Health, Bethesda, MD*
Address correspondence to L. Fayad (lfayad1@jhmi.edu)

Objective: The objective was to demonstrate the feasibility and potential utility of proton MR spectroscopy (MRS) for measuring the absolute concentration of the metabolite Choline (Cho) in benign and malignant musculoskeletal (MSK) abnormalities at 3T.

Materials and Methods: At 3T, in vivo Cho concentrations were measured by means of MRS examinations in 10 subjects with MSK abnormalities at 12 sites with a method which uses water as an internal reference compound, previously validated and optimized for the MSK system by our group. Utilizing a surface coil for signal reception, a 2 x 2 x 2 cc single voxel was positioned in the most suspicious portion of each MSK abnormality identified by routine conventional MR imaging and a PRESS sequence (repetition time 2s; echo time 144 ms; 128 acquisitions; water presaturation) performed. MSK abnormalities were one-Ewing's sarcoma, one neurofibroma, one cellular neurofibroma with nuclear atypical, one stress fracture, one abscess, one hematoma, one degenerative cyst, three postoperative fibrosis in history of chordoma/MFH/liposarcoma that was stable for 24/16/18 months respectively, one postoperative pigmented villonodular synovitis stable for 12 months and one incidental signal abnormality in a patient with osteosarcoma that resolved at three month follow-up. The presence or absence of a discrete Cho signal peak was recorded for each abnormality and the Cho concentration was calculated. Descriptive statistics for the concentrations of the MSK abnormalities were reported.

Results: Good quality spectra were obtained in all cases. A discrete Cho peak was identified in one malignant (Ewing's sarcoma), one borderline malignant (neurofibroma with atypia) and two benign MSK abnormalities (neurofibroma, postoperative fibrosis with history of chordoma). All other benign abnormalities showed no evidence of a discrete Cho peak. The Cho concentrations in the malignant and borderline malignant lesions were 1.49 and 0.28 mmol/kg respectively. The Cho concentrations in the two benign abnormalities were 0.19 and 0.11 mmol/kg. In all other benign abnormalities, the Cho concentration was zero. The average Cho concentration in benign abnormalities was 0.03 mmol/kg with standard deviation of 0.07.

Conclusion: This is the first report regarding the measurement of absolute metabolite concentration by proton MRS in MSK tumors. The results provide a quantitative basis for studies of metabolic alterations in diseases of the MSK system and show that benign and malignant abnormalities may potentially be differentiated by MRS.

3:40 pm

201. MR Arthrography of the Second and Third Metatarsophalangeal Joints for the Detection of Tears of the Plantar Plate and Joint Capsule

Kier, R.[1,2]; Abrahamian, H.[2]; Caminear, D.[3]; Eterno, R.[4]; Feldman, A.[2]; Abrahamsen, T.[5]; Rice, A.[5]; Davis, D.[2] 1. Advanced Radiology Consultants, Trumbull , CT; 2. Bridgeport Hospital, Bridgeport, CT; 3. Connecticut Orthopaedic Specialists, Hamden, CT; 4. St. Vincent's Hospital, Bridgeport, CT; 5. Norwalk Hospital, Norwalk, CT*
Address correspondence to R. Kier (ruben.kier@adrad.com)

Objective: Tears of the plantar plate and joint capsule of the metatarsophalangeal joint (MTPJ) are under-recognized causes of lesser metatarsalgia. Attempts to detect these tears have employed either conventional arthrography of the MTPJ or non-contrast MR imaging. The current study evaluated MR arthrography for evaluation of this condition.

Materials and Methods: Forty-one patients (27 women, 14 men, ages 18-71) with pain at the second or third MTPJ were referred for MR arthrography of 45 joints (25 right, 20 left). The procedure was performed at the second MTPJ only in 35 patients, at both the second and third MTPJ in four patients, and at the third MTPJ only in two patients. Joints were injected using a 5/8 inch 25-gauge hypodermic needle under fluoroscopic guidance with 1-2 cc of a dilute solution of Gadolinium-DTPA, nonionic iodinated contrast media, and lidocaine. MR imaging was begun within 30 minutes of injection, using dedicated extremity coils on 1.5T magnets. Pulse sequences included axial and sagittal T1-weighted images both with and without fat saturation, and coronal T1-weighted and gradient echo images. Slice thickness was 2 mm with field-of-view of 8 cm. Images were evaluated prospectively for integrity of the plantar plate, MTPJ capsule, and dorsal interosseous tendons. Capsular tears were considered partial if contrast entered the capsule and complete if contrast extravasated into adjacent tissues.

Results: The plantar plate remained grossly intact in 39 of 45 joints. Contrast media entered the second flexor tendon sheath in six patients, suggesting a plantar plate tear that was difficult to distinguish from an adjacent capsular tear. Forty capsular tears were seen, including 37 of 39 second MTPJs and three of six third MTPJs. Capsular tears were complete in 26 and partial in 14. No capsular tear was seen in five joints. Capsular tears were centered at the distal lateral border of the plantar plate in 22 complete tears and 13 partial tears, and at the distal medial border of the plantar plate in five complete tears. The dorsal interosseous tendon showed a complete tear in seven, a partial tear in 14, and tendinosis in five.

Conclusion: We conclude that capsular tears at the MTPJ are far more common than plantar plate tears. Most capsular tears occur at the distal lateral border of the plantar plate. Many of these tears are associated with pathology of the adjacent dorsal interosseous tendon. MR arthrography of the MTPJ clearly delineates capsular tears and associated pathology.

3:50 pm

202. Metal Artifact Suppression on CT--Preliminary Results Using a New Postprocessing Technique

Ramirez, I.[1]; Northington, A.[2]; Brown, K.[1]; Buckwalter, K.[2] 1. No Institutional Affiliation; 2. Indiana University, Indianapolis, IN*
Address correspondence to K. Buckwalter (kbuckwal@iupui.edu)

Objective: The objective was to assess of a new postprocessing algorithm to correct artifacts on MDCT images of patients with orthopedic hardware.

Materials and Methods: CT studies of different body regions from seven different patients with orthopedic hardware were processed using an image-based metal correction algorithm (Philips Medical Systems, Bothell, WA). This algorithm identifies regions within CT images containing metal artifacts. The algorithm creates a correction image which is added to the original image to compensate for the artifact. Unlike prior algorithms which require raw image data for processing, the algorithm is applied after CT image reconstruction and can be applied to archived images when the raw image data is no longer available.

Hardware assessed included shoulder, hip, and knee prostheses, an intramedullary nail, spinal fusion hardware, and malleable fixation plates. The postprocessed image sets were compared to the original images in a nonblinded fashion. Image sets were scored using a five-point scale (1=definitely better, 2=somewhat better, 3=no change, 4=somewhat worse, and 5=definitely worse). The parameters graded included the visualization of bone and soft tissues within 1 cm and 5 cm from the metal components, reduction of artifacts from metal, and improvement in the diagnostic quality of the scans. Readers assessed for new artifacts produced by the processing and for new anatomy revealed on the postprocessed images.

Results: The mean scores for the image set comparisons were as follows: visualization of bone within 1 cm of metal, 1.57; visualization of soft tissues within 1 cm of metal, 2.29; visualization of bone within 5 cm of metal, 2.0; visualization of soft tissues within 5 cm of metal, 2.43. The mean score for improvement in diagnostic quality was 1.57. Six of the seven cases had new artifacts, and 6 of the 7 cases had new anatomy revealed on the postprocessed images.

Conclusion: This preliminary study demonstrates the usefulness of a new algorithm to correct for artifacts present on CT images of patients with orthopedic hardware. The most significant improvement in image quality occurred in the immediate vicinity of the metal hardware, typically the region of greatest artifacts. Although some artifacts were introduced by the algorithm, the mean score for improvement in diagnostic quality of the processed images was 1.57. This processing algorithm is significant because it does not require raw image data unlike prior techniques and it can be applied retrospectively.

4:00 pm

203. MR Arthrography of the Hip: Comparison of a Dedicated IDEAL Sequence with Standard MR Sequences in the Detection of Cartilage Lesions

Ullrick, S.; Blankenbaker, D.; Kijowski, R.; De Smet, A.; Lindstrom, M.; Keene, J. University of Wisconsin, Madison, WI*
Address correspondence to S. Ullrick (ullrickmd@yahoo.com)

Objective: The objective was to compare the diagnostic performance of a dedicated cartilage MR sequence (iterative decomposition of water and fat with echo asymmetry and least squares estimation [IDEAL]) with standard MR arthrogram sequences in grading cartilage abnormalities of the hip.

Materials and Methods: Forty-one consecutive hip MR arthrograms (11 males/30 females; mean age 36 years) were independently retrospectively reviewed by three musculoskeletal radiologists. Each articular surface was graded on MR using a modified Noyes classification. The IDEAL and routine MR sequences were read separately. The location of cartilage lesions were recorded as anteromedial (AM), anterosuperior (AS), posteromedial (PM), and posterosuperior (PS) in the femoral head and as anterosuperior (AS) and posterosuperior (PS) in the acetabulum. The arthroscopic maps of cartilage lesions made by the orthopedic surgeon using the Noyes classification were used as the gold standard for calculating sensitivity, specificity and accuracy of the IDEAL sequence and the standard MR sequences. Inter-reader variability was calculated using kappa values.

Results: Of the 246 (41 arthrograms x 6 locations per arthrogram) possible locations for cartilage defects, there were 72 cartilage lesions. For the IDEAL sequence, the accuracy for grade 2B or higher lesions within the four femoral quadrants (AM, AS, PM, PS) was 0.92, 0.85, 0.9, and 0.9, respectively. For the standard MR arthrogram sequences, the accuracy for the four femoral quadrants was 0.95, 0.9, 0.92, and 0.88. For the IDEAL sequence, the accuracy for grade 2B or higher lesions within the two portions of the acetabulum (AS, PS) was 0.85 and 0.92 while it was 0.9 and 0.92 using the standard MR sequences. When considering all grade 2B lesions or higher, IDEAL sensitivity and specificity was 0.75 and 0.92, while standard MR arthrogram sensitivity and specificity was 0.71 and 0.97. None of these differences were statistically significant. There were a total of 17 grade 2A lesions at arthroscopy. Using IDEAL, the readers identified a cartilage abnormality in the corresponding quadrant 51% (26/51) of the time, compared to only 31% (16/51) of the time using standard MR sequences (p=0.007). The inter-reader variability was moderate for IDEAL (0.62) and for standard MR (0.61).

Conclusion: The 1 mm thick IDEAL cartilage sequence images do not improve detection of grade 2B or higher cartilage lesions of the hip when compared to standard MR arthrogram sequences. However, detection of shallower 2A lesions was improved when using the IDEAL sequence.

4:10 pm

204. Imaging of Chronically Draining Sinuses in the Musculoskeletal System by 'Ultrasonosinography': A Useful Diagnostic Procedure

Nath, A.; Sethu, A. Khoula Hospital, Muscat, Oman*
Address correspondence to A. Nath (akn20j@gmail.com)

Objective: The objective was to study the efficiency of ultrasonography of chronically draining sinuses in the musculoskeletal system and compare with contrast sinography.

Materials and Methods: Thirty patients with chronically draining sinuses in the musculoskeletal system underwent plain x-rays of the affected part, sonography of the affected and contralateral normal part with 7.5 MHz phased array linear transducer followed by contrast sinography using iopromide (Bayer HealthCare Pharmaceuticals, Montville, NJ).

Results: Plain x-rays were useful in illustrating radiopaque foreign bodies in two cases but ten nonradiopaque foreign bodies were missed; bony changes of osteomyelitis in 12 patients. Ultrasound showed one; all 12 foreign bodies both nonradiopaque and radiopaque with exact localization, depth and size; complete sinus tract in 30 patients along with alternate channels, and soft tissue abscesses in six cases. Evidence of osteomyelitis and subperiosteal abscesses with precise extent in 12 patients. Contrast sinography delineated the complete sinus tract in 25 patients but in five patients the complete sinus tract could not be outlined, possibly because of obstruction to contrast due to debris and alternate channels. All foreign bodies were missed. The extent of soft tissue abscesses and subperiosteal abscesses could not be exactly evaluated.

Conclusion: Ultrasound is useful in providing details of chronically draining sinuses in the musculoskeletal system along with all its causes. Ultrasound imaging of chronically draining sinuses musculoskeletal system may be termed as ultrasonosinography.

4:20 pm

205. Accuracy of 1T Extremity Knee MR Imaging for Meniscal Tears, Anterior Cruciate Ligament Tears and Cartilage Lesions

Harsha, A.[1]; Petchprapa , C.[1,2]; Sherman , O.[1,2]; Gidumal , R.[1,2]; Schweitzer , M.[1,2] 1. New York University, New York , NY; 2. Hospital for Joint Diseases-Orthopaedic Institute, New York , NY*
Address correspondence to A. Harsha (harsha01@med.nyu.edu)

Objective: Increasing constraints on medical costs create a potential advantage to lower field and dedicated MR imaging. Consequently we sought to evaluate the accuracy of dedicated 1T extremity MR for internal derangements of the knee.

Materials and Methods: The records of 99 consecutive patients undergoing knee MR on a dedicated extremity 1T scanner were assessed for menisci, ligaments, and cartilage derangements with arthroscopic confirmation. The sensitivity, specificity, accuracy, positive predictive values (PPV) and negative predictive values (NPV) were reported for the detection, location and severity of injury to these structures.

Results: Regarding detection of lesions: *medial meniscus:* accuracy, sensitivity, and specificity of 96%, 95%, and 98% (PPV 98%; NPV 93%); *lateral meniscus:* accuracy, sensitivity, specificity of 92%, 77%, 100% (PPV 100%; NPV 91%); *anterior cruciate ligament:* accuracy, sensitivity, specificity of 95%, 85%, 100% (PPV 100%; NPV 93%); *medial-compartment cartilage:* accuracy, sensitivity, specificity of 79%, 54%, and 96% (PPV 84%, NPV 84%); *lateral-compartment cartilage:* accuracy, sensitivity, and specificity of 84%, 42%, and 94% (PPV 62%; NPV 87%); *patello-femoral cartilage*: accuracy, sensitivity, and specificity all 88%. Regarding lesion location for *medial and lateral menisci*: accuracy, sensitivity, and specificity of 91%-89%, 86%-67%, and 98%-100% respectively; lesion location and severity for *articular cartilage:* 82%-80%, 62%-55%, and 93%-92% respectively; lesion severity for *anterior cruciate ligament*: accuracy, sensitivity, and specificity of 94%, 82%, 100% (PPV 100%; NPV 92%).

Conclusion: The diagnostic performance of dedicated extremity MR for menisci and ligaments is comparable to higher field strengths. Surprisingly, extremity MR exceeds the accuracy of conventional sequences at higher fields for cartilage and may prove a cost-effective alternative to whole body knee imaging.

4:30 pm

206. Dynamic Ultrasonography in Evaluation of Muscular Trauma

Nath, A.[1]; Bouras, R.[2]; Shiabullah, M.[2] 1. Khoula Hospital, Muscat, Oman; 2. Sultan Qaboos Sports Complex, Muscat, Oman*
Address correspondence to A. Nath (akn20j@gmail.com)

Objective: The objective was to describe the role of dynamic ultrasonography in muscular trauma.

Materials and Methods: Fifty male football players of the age group 20 to 30 years, presenting with clinical muscular trauma in the thigh and calf region were evaluated in this study. Dynamic ultrasonography of both the affected and contralateral normal part, using 7.5 to 11 MHz phased array linear transducer in sagittal, coronal and angulated axis was performed, both without contraction and with contraction of the muscles. Needle aspiration of suspected hematomas was performed for diagnosis and treatment. All muscles tears and hematomas were studied and followed up after 72 hours, until complete healing.

Results: Forty-six of the total 50 patients had muscle tears and or hematomos in the thigh and calf region. Four patients had no abnormality; 32 patients had clear-cut complete muscle tears appearing as echogenic retracted portions surrounded by hematomas ranging from highly reflective mass to complete echo poor areas on followup. The remaining 14 patients had partial tears, appearing as hypoechoic subtle lesions with relaxed muscle and looking like pseudotumors on contraction because of bunching together of partially broken muscle fibers, which was diagnostic for partial tears. Healed tears appeared as highly reflective scar tissue.

Conclusion: Ultrasonography is very useful in diagnosis, management, and followup of muscle tears and hemotomas. Dynamic ultrasonography is essential for diagnosis of partial tears.

4:40 pm

207. Rapid Assessment of Disease Severity in Osteoarthritis Research Studies Using Vastly Undersampled Isotropic Projection Steady-State Free Precession Imaging

Lafita, V.; Kijowski, R.; Rabago, D.; Woods, M.; Klaers, J.; Block, W. UW Hospital and Clinics, Madison, WI*
Address correspondence to V. Lafita (vaishalilafita@yahoo.com)

Objective: MR protocols in osteoarthritis (OA) research studies typically consist of a 3D sequence for measuring cartilage volume and multiple 2D fast spin-echo (FSE) sequences for providing comprehensive joint assessment. This study was performed to determine whether an isotropic resolution vastly undersampled isotropic projection steady-state free precession (VIPR-SSFP) sequence could be used to provide rapid cartilage volume analysis and comprehensive knee joint assessment for OA research studies.

Materials and Methods: The study group consisted of 20 consecutive patients with knee OA enrolled in a clinical trial evaluating the efficacy of a newly developed OA therapy. All patients were evaluated at 3T using a five minute isotropic resolution VIPR-SSFP sequence and a 30 minute MR protocol consisting of axial fat-saturation (fat-sat) T2-FSE, coronal fat-sat proton density-weighted fast spin-echo (PD-FSE), sagittal fat-sat T2-FSE, sagittal PD-FSE, and sagittal spoiled gradient recalled-echo (SPGR) iterative decomposition of water and fat with echo asymmetry and least-squares estimation (IDEAL) sequences. Cartilage volume measurements were performed using the IDEAL-SPGR and VIPR-SSFP sequences. Two radiologists independently performed comprehensive knee joint assessment twice at separate sittings using the entire 30 minute MR protocol and a ten minute MR protocol consisting of VIPR-SSFP and sagittal fat-sat T2-FSE sequences. Comprehensive knee joint assessment was performed using the whole-organ magnetic resonance (WORM) system in which numerical values are used to estimate the overall severity of OA and the severity of each individual feature of OA (i.e. cartilage loss, osteophytes, subchondral bone marrow edema, subchondral cysts, meniscal tears, ligament tears, joint effusions, etc.) Correlation coefficients were used to compare WORM scores obtained using the ten minute and 30 minute MR protocols.

Results: The average random error between cartilage volume measurements performed using VIPR-SSFP and measurements performed using IDEAL-SPGR was 1.3%. There was a strong correlation (r=0.992) between the overall WORM scores obtained using the ten minute and 30 minute MR protocols. There was also a strong correlation between the WORM scores obtained using the 10 minute and 30 minute MR protocols for each individual feature of OA (ranging between r=0.859 for lateral meniscal tears to r=1.00 for ACL tears).

Conclusion: A ten minute MR protocol consisting of isotropic resolution VIPR-SSFP and a sagittal fat-sat T2-FSE sequence can provide rapid cartilage volume analysis and comprehensive knee joint assessment for OA research studies. This may allow more time for physiologic cartilage imaging sequences such as T2 and spin-lattice relaxation in the rotating frame (T1-rho) mapping to be incorporated into research MR protocols.

4:50 pm

208. Improved Fat Suppression Using Multipeak Reconstruction for IDEAL Chemical Shift Fat-Water Separation: Application with Fast Spin Echo Imaging

Kijowski, R.[1]; Woods, M.[1]; Lee, K.[1]; Yu, H.[2]; Shimakawa, A.[2]; Brittain, J.[2]; Reeder, S.[1] 1. University of Wisconsin, Madison, WI; 2. GE Healthcare MR Global Applied Science Lab, Menlo Park, CA*
Address correspondence to R. Kijowski (rkijowski@uwhealth.org)

Objective: The objective was to demonstrate improvements in the quality of fat suppression for fast spin-echo (FSE) imaging of the knee using multi-peak fat spectral modeling and IDEAL fat-water separation.

Materials and Methods: T1-weighted and T2-weighted FSE sequences with IDEAL fat-water separation and two frequency-selected fat-saturation methods (GE Healthcare, Milwaukee, WI, "classic fat-sat" and "dark fat-sat) were performed at 3T in ten knees of five asymptomatic volunteers. The IDEAL images were reconstructed using a conventional single-peak method and a multipeak method that more accurately model the nuclear magnetic resonance spectrum of fat. Signal-to-noise ratio (SNR) and contrast-to-noise ratio (CNR) were measured in various tissues for all sequences. Student t-tests were used to compare SNR and CNR values. T2-weighted FSE sequences with "classic fat-sat", single-peak IDEAL, and multipeak IDEAL were performed at 3T on the knees of ten patients with acute post-traumatic bone marrow contusions. Two fellowship-trained musculoskeletal radiologists ranked the sequences according to the following subjective criteria of image quality: 1) quality of fat-suppression, 2) overall tissue contrast, and 3) conspicuity of bone marrow edema. Exact binomial tests were used to compare the ranks given to each sequence.

Results: Multipeak IDEAL had significantly greater ($p<0.05$) suppression of signal of subcutaneous fat and bone marrow than "classic fat-sat", "dark fat-sat", and single-peak IDEAL for both T1-weighted and T2-weighted FSE sequences. For T1-weighted FSE sequences, multipeak IDEAL had between 66% and 84% greater suppression of signal of subcutaneous fat and bone marrow. For T2-weighted FSE sequences, multipeak IDEAL had between 21% and 81% greater suppression of signal of subcutaneous fat and bone marrow. On subjective analysis, T2-weighted FSE sequence with multipeak IDEAL was ranked significantly higher ($p<0.05$) than T2-weighted FSE sequences with "classic fat-sat" and single-peak IDEAL for quality of fat-suppression, overall image quality, and conspicuity of bone marrow edema.

Conclusion: Multipeak IDEAL fat-water separation provides improved fat-suppression for T1-weighted and T2-weighted FSE imaging of the knee when compared to single-peak IDEAL and two widely used frequency-selected fat-saturation methods.

CME credit forms and course evaluations are available online at https://www.directsurv.net/arrs/. Your user name is arrs then your badge number (for example, arrs123456) The password is arrs2009. (Please note that your badge number is also your ARRS ID number.) Please visit this site to claim your CME credit. The site opens on April 26 and will be open through May 16. In an effort to be green, ARRS is not including CME credit forms in your registration packet.

SCIENTIFIC SESSION 25

VASCULAR AND INTERVENTIONAL RADIOLOGY PAPERS

Room: 309, Level 3

Wednesday, April 29, 2009, 3:00 pm–5:00 pm

Abstracts 209-217

Moderators: *R. Murthy, S. Zangan*
Keynote Address: Use of Novel Guidance Systems for Planning and Performing Percutaneous Procedures—*S. Solomon*

3:30 pm

209. Comparison Between Conventional CT-Guided and MDCT Fluoroscopic-Guided Lung Biopsy: Procedure Time, Complication Rates, and Diagnostic Yield

Sarwani, N.; Tappouni, R.; Chamarthi, S. Penn State Milton Hershey Medical Center, Hummelstown, PA*
Address correspondence to N. Sarwani (doctor@nabeelsarwani.com)

Objective: The objective is to determine the benefit of MDCT fluoroscopy over conventional CT guidance in percutaneous lung mass biopsies. This retrospective study examines the time to perform the procedure, complication rate and diagnostic yield, before and after the routine use of MDCT fluoroscopy.

Materials and Methods: The study was approved by the hospital's institutional review board. The biopsy services database procedure log was reviewed. Fifty lung biopsies using conventional, single slice CT scan (Picker) were compared with 50 cases using MDCT fluoroscopy (Siemens Healthcare, Malvern, PA). Total procedure time and complication rates as determined from the radiology information system, diagnostic yield, and rebiopsy rates were obtained. Complications were defined as any pneumothorax and/or hemorrhage, regardless of size. Information regarding needle caliber and lesion size and location were also recorded.

Results: Total procedure time using single slice and MDCT fluoroscopy were 48 minutes and 44 minutes respectively. Complication rate using single slice and MDCT fluoroscopy were 25/50 (50%) and 19/50 (38%). Using conventional CT, three patients required chest tubes for treatment of pneumothorax, compared with only one using MDCT. The number of satisfactory biopsies using single slice and MDCT fluoroscopy were 48/50 (96%) and 50/50 (100%) respectively. The rebiopsy rates for single slice and MDCT fluoroscopy were 2/50 (4%) and 1/50 (2%) respectively. Smallest pulmonary lesion biopsied using conventional CT was 9 mm, compared with 5 mm using MDCT fluoroscopy.

Conclusion: The use of MDCT fluoroscopy to guide percutaneous lung biopsies reduced the total procedure time, decreased complications rate and increased the diagnostic yield compared with conventional CT guidance. This has resulted in the effective sampling of smaller, sub centimeter pulmonary nodules. The use of MDCT fluoroscopy in lung biopsies is justified by reduced patient morbidity and increased resource utilization.

3:40 pm

210. C-Arm CT Based Electromagnetic Navigation for Percutaneous Drainage Procedures

Wacker, F.[1,2]; Peter, O.[2]; Wolf, K.[2]; Meyer, B.[2] 1. Johns Hopkins University, Baltimore, MD; 2. Charite, Berlin, Germany*
Address correspondence to F. Wacker (fwacker1@jhmi.edu)

Objective: The objective was to evaluate the value of an electromagnetic field-based navigation system using C-arm CT images for abscess drainage.

Materials and Methods: Five patients with pelvic, abdominal and thoracic fluid collections were included in the study. Images were acquired using a C-Arm CT (Siemens Medical Solutions, Forchheim, Germany). An electromagnetic navigation system (CAS Innovations, Erlangen, Germany), consisting of a workstation, an electromagnetic field generator, and a needle was used for puncture. After defining the target on CACT images, the needle position was electromagnetically tracked and interactively visualized in the 3D CACT dataset and on top of fluoro images during puncture. After reaching the fluid collections, the needle position was verified using a CACT dataset. Subsequently a drainage catheter was inserted. The puncture duration was recorded and errors were calculated (user error=distance between target and visualized needle tip position; system error=distance between visualized and real needle tip position).

Results: The interactive needle visualization using real-time MPR of the CACT dataset facilitated safe and reliable puncture guidance, leading to an average skin-to-target time of 65 seconds (range, 35–98 seconds). The targeted puncture was successful in all cases with a mean user error of 6 mm (range, 3-10 mm) and a mean system error of 5 mm (range, 3-6 mm). The total puncture time ranged from 3 to 10 minutes, including trajectory planning. The average scan-to-scan time (from achieving the preprocedural CACT to the control CACT) was 24 minutes.

Conclusion: In this clinical pilot trial on abscess drainage procedures, electromagnetic needle tracking in combination with C-arm CT images provided safe and reliable real-time puncture guidance leading to a correct needle placement and successful drainage in all patients. If the results can be confirmed in a larger study population, this technique might allow for higher patient throughput because transferring patients between CT and C-arm fluoroscopy and the use of ultrasound in combination with a C-arm can be avoided.

3:50 pm

211. Musculoskeletal Abscess: Effectiveness of Percutaneous Catheter Drainage

Cronin, C.; Hahn, P.; Gervais, D.; Arellano, R.; Guimaraes, A.; Levis, D.; Mueller, P. Massachusetts General Hospital, Boston, MA*
Address correspondence to C. Cronin (carmelcronin2000@hotmail.com)

Objective: The objective was to retrospectively evaluate the effectiveness of percutaneous catheter drainage in the treatment of musculoskeletal fluid collections and to identify any factor that may be predictive of a poor clinical outcome.

Materials and Methods: This HIPAA-compliant study was approved by the institutional review board; informed consent was waived. The details of percutaneous catheter drainage and microbiologic findings were recorded. The technical success (ability of catheters placed to drain collections treated) and the clinical success (ability of patients to recover fully without surgery) of percutaneous catheter drainage were determined. Safety was evaluated on the basis of complications. Multifactorial logistic regression analysis was used to identify predictors of a poor clinical outcome; age, sex, history of diabetes, history of acquired immunodeficiency syndrome, history of malignancy, history of solid-organ transplantation, steroid therapy, chemotherapy and/or radiation therapy, complexity of collection and bone involvement.

Results: Collections were drained in 39 patients. The origins of the musculoskeletal abscesses included postoperative fluid collection (n=11), in the setting of malignancy and chemotherapy (n=9), systemic infection (n=5), Crohn's, pancreatitis, cholecystitis, diverticulitis (n=10) and others (n=4). The abscesses were 4–15 cm in diameter. The volume of the aspirate was 5–260 mL. There were no complications and no procedure-related mortality. Size and complexity of collection, history of malignancy were associated with a poor clinical outcome and recurrence. The technical success rate was almost 100%, however 12.8% (5/39) recurred requiring repeat drainage and surgery was required in 5% (2/39).

Conclusion: Percutaneous image-guided musculoskeletal drainage is clinically useful, safe and effective for draining complex fluid collections, aids treatment of joint infections and osteomyelitis, with most patients avoiding surgery.

4:00 pm

212. Incidence of Infectious Complications Following Ultrasound-Guided Intervention

Cervini, P.; Hesley, G.; Thompson, R.; Sampathkumar, P.; Knudsen, J. Mayo Clinic, Rochester, MN*
Address correspondence to P. Cervini (patrickcervini@gmail.com)

Objective: We conducted a large retrospective review to determine the incidence of postprocedure infectious complications of common ultrasound (US)-guided procedures including: biopsy, fine needle aspiration (FNA), drain placement, paracentesis and thoracentesis.

Materials and Methods: Infection Prevention and Control (IPAC) Mayo Clinic, Rochester, conducts surveillance through a review of microbiology records to identify infections related to a radiology procedure. Each infection identified by this process is reported back to the department of radiology as soon as possible; summaries of this data are reviewed jointly by IPAC and radiology staff at periodic intervals. Similarly, the department of radiology prospectively follows all ultrasound-guided biopsies for complications at 24 hours, three months and 12 months. We reviewed two years of data from both these sources to determine the incidence of infections following common US-guided procedures.

Results: We performed 13,857 US guided procedures from January, 2006 to December, 2007. There were 11 likely and three possible procedure-related infections for an overall incidence of 0.1% (14/13,857). The infections consisted of five abscesses, four bloodstream infections, four cases of peritonitis, and one urinary tract infection. The highest incidence of infections occurred following ultrasound-guided biopsy (0.2%, 10/4,355), with pancreatic transplant biopsy having the highest incidence (0.9%, 1/110). No infections occurred following thoracentesis and FNA despite the high number of procedures performed (2,489 and 2,335 respectively).

Conclusion: The incidence of an infectious complication following US-guided intervention is low. This information is helpful in better understanding the actual risk of infection from ultrasound guided percutaneous procedures. Radiologists can use this data to provide more accurate information for consent prior to procedures and reassure their patients.

4:10 pm

213. Fluoroscopy-Guided Punctures in a Flat Detector C-Arm System: Preclinical Evaluation of Stereoscopic Needle Tracking Based on Cone Beam CT Images

Meyer, B.[1]; Brost, A.[2]; Lewin, J.[3]; Wacker, F.[3] 1. Charité - University Medicine, Campus Benjamin Franklin, Berlin, Germany; 2. Universität Erlangen-Nürnberg, Erlangen, Germany; 3. Johns Hopkins Medical School, Baltimore, MD*
Address correspondence to B. Meyer (b.meyer@marleben.de)

Objective: The objective was to evaluate the accuracy and feasibility of a C-Arm CT (CACT) based fluoroscopic needle guidance tool for percutaneous punctures in phantoms and animals.

Materials and Methods: The study was performed in a CACT using a prototype navigation tool (NT). After determining the skin entry point and the target in a previously acquired CACT, NT overlays the needle path on any fluoroscopic image. The needle is advanced using intermittent fluoroscopy to align the needle and superimposed path. For the phantom study, plastic rings (diameter 7 mm) were used as targets. Twenty punctures were performed by two operators. In the animal experiments, 21 double-oblique punctures were performed (three pigs, three operators). Final needle position was assessed in both in a postprocedural CACT.

Results: In the puncture phantom, the 7 mm ring targets were hit in all cases with a needle placement error from the center of the rings of 5.2 ± 2.0 mm. In the animal study, the targeted puncture was successful in all 21 punctures. The mean needle placement error for the three user was 4.8 mm ± 2.1 mm (maximum 6.9 mm), 5.1 mm ± 2.5 mm (maximum 9.0 mm), and 4.5 mm ± 1.9 mm (maximum 8.2 mm) respectively. Mean skin-to-target puncture time in the animal study was 10:46 minutes.

Conclusion: The CACT-based fluoroscopic puncture guidance tool facilitates CT like punctures in an angio suite. It proved to be accurate and useful for needle navigation in both, the phantom punctures as well as the animal experiments. Double oblique punctures that are often challenging with CT, can easily be performed.

4:20 pm

214. Recognition of Isolating and Nonisolating Biliary Obstructions by CT Prior to Biliary Drainage

Thornton, R.; Getrajdman, G.; Brown, K. Memorial Sloan Kettering Cancer Center, New York, NY*
Address correspondence to R. Thornton (thorntor@mskcc.org)

Objective: Complex patterns of malignant bile duct obstruction are often recognized for the first time during biliary drainage, sometimes following contamination of undrained segments of the biliary tree. This can lead to ongoing cholangitis, suboptimal bilirubin reduction and need for additional drainage. Our purpose was to determine how accurately we could predict the level of bile duct obstruction and presence of isolation of right and left sides using preprocedure CT in oncology patients undergoing biliary drainage.

Materials and Methods: A retrospective review of an IRB-approved biliary drainage database identified 100 consecutive biliary drainages between November, 2004 and November, 2006 of which 85 procedures in 80 oncology patients (41 male, 39 female; median age 65, range 41-85) had contrast-enhanced abdominal CT scans within 30 days of biliary drainage. Indications for drainage were to lower bilirubin for chemotherapy administration (34), cholangitis (28), pruritus (22), preoperative (3) and for diversion of bile leak (3). Two interventional radiologists retrospectively examined each sector of the liver on 5 mm collimation portal phase CT, predicted the level of obstruction by consensus, and determined if optimal drainage would be achieved from the left or the right. True levels of obstruction and isolation, determined by review of the drainage cholangiogram and postprocedure CT scans, were organized into three functional categories: Nonisolating obstruction of the common duct or surgical anastomosis, where the entire liver would be drained by a single catheter (Group 1); isolation at the primary biliary confluence, where only a hemiliver would be drained by a single catheter (Group 2); and isolation extending to a secondary confluence, where only sectors or segments of a hemiliver would be drained by a single catheter (Group 3).

Results: Twenty-nine of 33 (88%) Group 1, one of two (50%) Group 2, and 49 of 50 (98%) Group 3 obstructions were correctly predicted. Overall predictive accuracy was 93%. In 25 of the 36 Group 3 livers containing both lobes, a higher level of obstruction was recognized in one lobe, prompting a preference for drainage of the contralateral hemiliver.

Conclusion: Even complex patterns of biliary obstruction can be ascertained by careful study of the pre-procedure CT, providing important prognostic information, allowing precise planning for optimal drainage and potentially improving patient outcomes

4:30 pm

215. Percutaneous Sacroplasty as a Successful Treatment for Sacral Insufficiency Fractures: Retrospective Review of Eleven Cases Performed at Northwestern Memorial Hospital

Aghaei Lasboo, A.; Walker, M.; Hurley, M.; Shaibani, A. Northwestern University, Chicago, IL*
Address correspondence to A. Aghaei Lasboo (a-lasboo@northwestern.edu)

Objective: The objective was to evaluate the efficacy of percutaneous sacroplasty using both computed tomographic (CT) and fluoroscopic guidance in treatment of sacral insufficiency fractures (SIFs) with respect to pain relief and overall functional capacity.

Materials and Methods: After obtaining approval from the institution's review board, we retrospectively studied eleven consecutive patients treated by percutaneous sacroplasty in a single center from 2003 to 2008. All included patients had back pain causing restriction of activities of daily living. Using a numerical rating scale (zero ("no pain") to ten ("worst pain imaginable"), pain assessment was performed before and after the procedure to score their pain.

Results: Eleven patients underwent sacroplasty for SIFs, with a female to male ratio of 10:1. All patients presented with back pain and limited activities of daily living (ADLs). Imaging studies included CT spine (n=7), MRI spine (n=5) and whole body bone scan (n=5), with an SIF demonstrated in each case. Plain radiographs were only performed in two patients and failed to reveal the fractures in both cases. SIF was bilateral in eight and unilateral in three cases. All patients had a period of analgesic use before the procedure with no symptomatic improvement. Sacroplasty or percutaneous injection of synthetic bone cement into the fractured sacrum using CT guidance for needle placement and fluoroscopy to monitor the polymethylmethacrylate (PMMA) injection was performed in all cases. Ten patients underwent a single percutaneous sacroplasty procedure and one patient required a repeat procedure. All patients were followed up, with a median interval of 12.6 months (range of three weeks-4.6 years). Pain scores ranged from zero to seven with a mean of 2.86 (2.86 +/-2.03), comparing favorably to pretreatment baselines which ranged from three to ten with a mean of 7.45 (7.45 +/- 2.1). On average, results revealed a 60% decline in the pain score. Four patients reported discontinuation of analgesics with the remainder dependent upon a smaller and less frequent dose. Most importantly, all patients experienced a significant improvement in their ADLs. All patients who were bed-ridden prior to treatment were able to return to ambulation (with assist devices or alone) and conduct basic ADLs such as independent use of the rest room.

Conclusion: Sacroplasty can be reliably and safely performed by a combination of CT and fluoroscopic guidance. In selected patients, pain relief is usually profound and expedites patient rehabilitation.

4:40 pm

216. Minimally Invasive Management by Interventional Radiologic Techniques of Urinary Tract Fistulae (Outcome Study)

Lang, E.[1]; Hanano, A.[1]; Bizzell, C.[2]; Auster, M.[2]; Allaf, M. [2]; Thomas, R. [3]; Rudman, E.[1]; Myers, L. [3]; Colon, I. [1] 1. SUNY Downstate Medical Center, Brooklyn, NY; 2. Johns Hopkins Medical Institute, Baltimore, MD; 3. Tulane University Medical Center, New Orleans, LA*
Address correspondence to E. Lang (erich.lang@downstate.edu)

Objective: The objective was to evaluate the indications for and outcome of minimally invasive radiologic techniques such as percutaneous nephrostomy (PCN), drainage, antegrade stenting and

percutaneous ureteroneocystostomies in the management of urinary tract fistulae.

Materials and Methods: A retrospective analysis of treatment results was carried out in 522 patients (47 patients were censored because of incomplete follow-up data) deemed suitable for treatment of urinary tract fistulae by interventional radiologic techniques. A total of 347 were male, 171 female and four children, ages 11-88 years. Material collected from LSU Medical Center, New Orleans Veterans Administration Hospital, Tulane Health Science Center, SUNY Downstate Medical Center, Johns Hopkins Bayview Center from 1985-2007. Selection criteria were: dehiscences of urinary tract due to trauma, inflammatory or neoplastic disease without compromise of vascular supply or excessive separation of margins.

Results: Four of 13 fistulae from bowel or pancreas to the renal collecting system closed when they were managed minimally invasively by PCN, antegrade stent with or without drainage. Likewise, 145 of 197 traumatic fistulae of ureter and bladder without vascular compromise nor significant separation of margins closed when treated by PCN, antegrade stent, with or without drainage. Conversely, only 51 of 104 such fistulae with compromise of their vascular supply closed under treatment by PCN, antegrade stent, sometimes drainage and antegrade uereteroneocystostomy. Fifty-nine of 132 fistulae attributable to underlying neoplastic disease responded satisfactorily to such radiologic management, as did 37 of 80 fistulae caused by inflammatory disease. In 12 patients interventional radiologic techniques failed and surgical urologic correction had to be instituted. In another 197 patients PCN often with drainage was successfully used as a temporizing measure until definitive urologic intervention could be carried out. In eight patients the follow-up period was inadequate.

Conclusion: Minimally invasive radiologic techniques definitively treated 60% (317 of 522) of select urinary tract fistulae, and moreover proved useful in temporizing conditions in another 197 patients awaiting definitive urologic intervention. The minimally invasive nature and attendant lower cost and reconvalescence period recommend use of this modality.

4:50 pm

217. Body Interventional Procedures in Patients With Coagulation Abnormalities: A Retrospective Study of Pathological Results Obtained

Chintapalli, K.; Choudhary, S.; Prasad, S.; Ojili, V.; Sunnapwar, A.; Freckelton, M. University of Texas Health Science Center at San Antonio, San Antonio, TX*
Address correspondence to A. Nagar (arpitnagar@hotmail.com)

Objective: Nonvascular body interventions (NVI) in radiology are commonly performed in contemporary medicine. Many times these patients have abnormal coagulation profiles and the urgent need for nonvascular interventions for both diagnostic and therapeutic procedures. We conducted this retrospective study to determine the frequency of the procedures in such patients and clinical significance of the results achieved in a tertiary care hospital.

Materials and Methods: A retrospective review of the nonvascular intervention database from November 9, 2005 to September 11, 2008 was performed. Of a total of 1,665 patients, 99 patients with coagulation abnormalities were identified. An interventional procedure was performed following an attempt at the correction of the coagulation problem: stoppage of medication, administration of fresh frozen plasma or platelets. Patient profiles, indications, procedures performed, needle or gun used and pathological diagnosis were reviewed. Ninety-seven patients were studied (age range: 4-83 years). There were 57 male patients and 40 females. The pathological results from these procedures were divided into three groups. 1. Significant pathology. 2. Not significant and 3. Unsatisfactory specimen for diagnosis.

Results: The pathology in 35/97 (36.1%) patients was classified as demonstrating significant abnormality (altering clinical management). In 60 (61.85%) patients findings were not significant and in two (2.06%) patients tissue samples were unsatisfactory.

Conclusion: The indications for nonvascular intervention are showing a steady rise over the years as the number of patients with coagulation abnormalities continue to rise. In spite of coagulation abnormalities due to multiple drug regimes including antiplatelet and antithrombotic drugs, nonvascular interventional procedures were helpful in 36% of these patients, which made a significant impact on the patient's management. We routinely perform these procedures after correcting the coagulation abnormality using reasonable precautions.

GASTROINTESTINAL (BOWEL/PERITONEUM) IMAGING PAPERS

Room: 207, Level 2

Thursday, April 30, 2009, 10:00 am–12:00 noon

Abstracts 218-228

Moderators: *T. Jaffe, D. Katz*

Keynote Address: Crohn's Imaging in the 21st Century: Where We Are Going—*T. Jaffe*

10:10 am

218. Evaluation of Diffusion-Weighted MR Imaging for Detection of Bowel Inflammation in Patients with Crohn's Disease: A Pilot Study

Oto, A.; Zhu, F.; Kulkarni, K.; Karczmar, G.; Turner, J.; Rubin, D.*
University of Chicago, Chicago, IL
Address correspondence to A. Oto (aoto@radiology.bsd.uchicago.edu)

Objective: The objective was to determine the feasibility of diffusion-weighted MR imaging (DWI) in detection of bowel inflammation and investigate the changes in apparent diffusion coefficient (ADC) values in the inflamed bowel in Crohn's disease.

Materials and Methods: Eleven patients who had undergone MR enterography (including DWI) for known or suspected Crohn's disease and had colonoscopy or surgery within four weeks of MR examination were recruited. DWI images with b=600 seconds/mm^2 were obtained using parallel imaging. For analysis purposes, the bowel was divided into six segments. Two radiologists retrospectively evaluated DWI images and ADC maps for inflammation in each segment using a grading scale of four based on DWI findings and artifacts. Quantitative analysis involved calculation of ADC values from the wall of each segment by averaging two measurements performed by two radiologists. Endoscopy, surgery and pathology results were reviewed to determine the presence of inflammation in each segment. Bland-Altman analysis was used to calculate the interobserver agreement in ADC values. Receiver operating characteristic (ROC) curve was constructed for ADC values.

Results: Of the 34 normal bowel segments, DWI detected 28, yielding a specificity of 82.4%. Six normal bowel segments in four patients were characterized as inflamed by DWI without surgical, endoscopic or pathologic confirmation, therefore were classified as "false positive". Of the 19 inflamed segments, DWI detected 18 (grading score 2 or 3), yielding a sensitivity of 94.7%. Inflammation could not be detected (grading score 1) in one rectosigmoid segment (patient one). Artifacts were either minimal or not present in 10/11 patients (90.9%) and were moderate in one patient. Correlation coefficient was 0.81 for the two measurements by two radiologists suggesting good interobserver variability. The mean ADC values of proven inflamed bowels was 1.59 ± 0.45 x 10^{-3} mm^2/second (range: 0.46–2.50), compared to 2.74 ± 0.68 x 10^{-3} mm^2/second (range: 1.44–4.03) in normal bowel segments ($p<0.0001$). The area under the ROC curve was 0.938 (95% confidence interval: 0.873–1.000). Using 2.0 x 10^{-3} mm^2/second as the cut-off point, the sensitivity of low ADC values for detecting inflamed bowels was 84% and the specificity of high ADC values for ruling out inflamed bowels was 91%.

Conclusion: DWI with parallel imaging is a feasible technique for detection of inflammation in patients with Crohn's disease. ADC values are decreased in the inflamed bowel segments indicating restricted diffusion.

10:20 am

219. Modified Small Bowel CT for Evaluation of Recurrent Crohn's Disease

Kielar, A.[1]; Tao, H.[1]; McKeever, C.[1]; Taljaard, M.[2] 1. University of Ottawa, The Ottawa Hospital, Barrie, Canada; 2. University of Ottawa, Ottawa, Canada*
Address correspondence to A. Kielar (aniakielar@gmail.com)

Objective: Crohn's disease is an idiopathic, transmural inflammatory condition affecting the gastrointestinal tract. Cross-sectional imaging may identify involved segments, degree of inflammation or stricture and associated complications. Patients usually present between the ages of 15-30 years old with recurrent flare-ups. Their young age predisposes them to more risk from radiation exposure. Thus, we have developed a low-radiation-dose unenhanced CT (MBCT) scan to evaluate the small bowel using hyperdense (9% ioxitalamic acid) oral contrast, viewed using "bone windows". Radiation dose is 2-5 times less than conventional CT enterography.

Materials and Methods: The MBCT was investigated for use in patients with previously pathologically-proven Crohn's disease. After ethics approval, 98 consecutive patients with new symptoms were retrospectively evaluated with MBCT. The images were independently reviewed by two radiologists. To determine reproducibility of MBCT, kappa values of interobserver agreement were calculated for characteristics such as obstruction, bowel segment involved, active inflammation vs. chronic stricture, as well as ancillary findings such as abscess formation, fistulas and skip lesions. In this group, 54 underwent surgery, colonoscopy or repeat imaging within four months as confirmation of findings.

Results: Kappa was 0.84 regarding the presence of an abnormality vs. a normal exam. Kappa for differentiating active inflammation from stricture was 0.89. Level of agreement regarding the specific bowel segments involved varied between 0.53-1.0. Level of agreement for presence of skip areas, abscess formation and fistula was 0.62, 0.75 and 0.78 respectively. In the subset of patients with follow-up, there was 85% agreement. In eight cases, gold-standard tests revealed a different finding compared to the original MBCT report.

Conclusion: MBCT is a low-radiation technique used to determine the involved bowel segments, presence of obstruction and degree of disease activity in patients with known Crohn's disease. Kappa values for these parameters were considered good or very good. Further investigation is required in the form of a prospective study in order to further refine parameters of disease activity compared to CT enterography and small bowel follow-through.

10:30 am

220. Quantitative Dynamic Contrast-Enhanced MRI for Assessment of Bowel Inflammation in Crohn's Disease

Oto, A.; Fan, X.; Mustafi, D.; Kulkarni, K.; Zhu, F.; Karczmar, G.; Turner, J.; Rubin, D. University of Chicago, Chicago, IL*
Address correspondence to A. Oto (aoto@radiology.bsd.uchicago.edu)

Objective: The objective was to evaluate the feasibility of quantitative analysis of dynamic contrast-enhanced (DCE)-MRI data in detection of bowel inflammation in patients with Crohn's disease.

Materials and Methods: Eleven patients who had undergone MR enterography (including DCE-MRI) for known or suspected Crohn's disease and had colonoscopy or surgery within four weeks of MR examination were recruited. 3D coronal dynamic contrast-enhanced MRI images were acquired using a 1.5T scanner with temporal resolution of 5-12 seconds for approximately five minutes. For analysis purposes, the bowel was divided into six segments (distal ileum, cecum, ascending, descending, transverse and rectosigmoid colon). Region of interests (ROI) were placed on the aorta and bowel wall of each segment. The contrast concentration curves were calculated for each ROI and signal from the aorta was used for arterial input function. The two-compartment model was used to analyze the data to obtain the volume transfer constant (K^{trans}) between blood plasma and the extravascular extracellular space (EES), and the volume of EES per unit volume of tissue (v_e). Endoscopy, surgery and pathology results were reviewed to determine the presence of inflammation in each segment. The differences in perfusion parameters between normal and inflamed bowel were compared using student t-test. Goodness of fitting parameter was calculated for the two-compartmental model.

Results: Based on endoscopy and surgery results, 53 segments (19 with inflammation, 34 normal) were included in the analyses. Due to motion artifacts, noise and/or low contrast uptake, the ROIs for two normal segments could not be obtained in one patient to generate usable signal intensity curves. The mean values of K^{trans} (1.47 min-1) and v_e (0.66) for inflamed bowels were significantly higher ($p<0.05$) than the corresponding values of K^{trans} (0.90 min-1) and v_e (0.45) for normal bowels. The goodness of fitting parameter R2 indicated that TCM fitted the curves fairly well (R^2 value of 0.78).

Conclusion: DCE-MR with analysis using two compartmental model is a feasible method for detection of bowel inflammation in Crohn's disease. Analyses show significantly increased value of K^{trans} and v_e in inflamed bowel that may reflect increased angiogenesis and permeability.

10:40 am

221. Is it Possible to Classify Crohn's Disease Based on CT Findings? An Interobserver Variability Study

Brady, C.[1]; Jaffe, T.[1]; Haystead, C.[1]; Neville, A.[1]; Zink, S.[2]; Paulson, E.[1] 1. Duke University Medical Center, Durham, NC; 2. St. Francis Hospital and Medical Center, Hartford, CT*
Address correspondence to C. Brady (christopher.brady@notes.duke.edu)

Objective: The purpose of this study was to test the hypothesis that it is possible to classify active Crohn's disease into subtypes based on CT findings.

Materials and Methods: From 2002 to 2006, 100 consecutive patients (38 men and 62 women; mean age, 39 years) underwent helical CT for evaluation of Crohn's disease. All scans were performed after the administration of a positive oral contrast agent and 150 mL iopamidol. Scans were reconstructed at 5 mm thickness. All reconstructed images were anonymized and reviewed on a workstation (GE Healthcare, Waukesha, WI). Five independent blinded reviewers with subspecialty training in abdominal imaging were trained in the imaging features for the three subtypes of Crohn's disease (fibrostenotic, fistulizing/perforating, and inflammatory). Each reader was also given two peer-reviewed articles describing Crohn's disease subtype classification. For each case, a data sheet was completed regarding the presence or absence of findings of acute Crohn's disease: small bowel or colonic involvement, hypervascularity, mural hyperenhancement, wall thickening, presence of fistula or extraluminal collection, and luminal narrowing. Reviewers classified each case of Crohn's disease by most likely subtype. Cohen's kappa coefficient was used to assess for interobserver agreement.

Results: Interobserver agreement for findings of acute Crohn's disease was fair with regard to the presence of small bowel and colonic involvement (k=0.471, 0.421, respectively), and presence of interloop fistula or collection (k=0.471, 0.546, respectively). There was slight interobserver agreement regarding appearance of wall thickening (k=0.306-0.315), luminal narrowing (k=0.202) and prestenotic dilatation (k=0.263). Poor interobserver agreement was found with regard to presence of hypervascularity (k=0.168), and mural hyperenhancement (k=0.141). For subtype classification of Crohn's disease patients, there was fair interobserver agreement (k=0.391).

Conclusion: Despite published results to the contrary, it is difficult to subtype Crohn's disease based on CT findings, even for experienced abdominal radiologists.

10:50 am

222. Differentiation of Small Bowel Crohn's Disease from Lymphoma Based Upon Morphologic Appearance at MR Small Bowel Follow-Through

Cronin, C.; Lohan, D.; Alhajeri, N.; Roche, C.; Murphy, J. University College Hospital Galway, Galway, Ireland*
Address correspondence to C. Cronin (carmelcronin2000@hotmail.com)

Objective: The objective of our study is to describe the morphologic appearances of small-bowel Crohn's disease and small bowel lymphoma (SBL) at MR small bowel follow through/enterography, determining key morphologic traits that may be capable of noninvasively distinguishing these two conditions which often present with subacute or chronic nonspecific symptomatology.

Materials and Methods: During a period from September, 2003 to February, 2008, 280 MR small bowel follow-through (MRSBFT) examinations were performed at a single institute. Sixty-four patients in all met inclusion criteria. The studies of 53 patients with Crohn's disease involving 58 small bowel segments and 11 patients with small bowel lymphoma involving 20 segments

were retrospectively and independently evaluated by two blinded reviewers. Studies were quantitatively and qualitatively assessed for a variety of potentially distinguishing morphological features.

Results: Crohn's disease occurs at a significantly younger age than SBL (33.5 ± 13.2 years vs. 61.2 ± 13.3 years). Involved Crohn's disease segments were long (mean 17.9 cm), narrowed (0.68 cm), concentric lesions without eccentric components or mesenteric fat infiltration compared to SBL which were significantly shorter (mean 10.3 cm) and more dilated (mean 1.68 cm), concentric lesions with eccentric components and mesenteric fat infiltration. There was no significant difference in signal intensity or relative signal intensity of the lesion, nor was jejunal or ileal location determined as being a discriminating factor. Significantly more Crohn's disease segments involved the terminal ileum.

Conclusion: We have identified and described key morphologic traits capable of distinguishing these two, often insidious-onset conditions at MRSBFT. In so doing it is intended that the radiologist may have a greater role to play in the noninvasive characterization of Crohn's disease and SBL.

11:00 am

223. Assessment of Motility Function of the Small Bowel with Cine-MR Imaging Using Balanced Steady-State Free Precession Imaging (FIESTA Sequence): Preliminary Study in Healthy Volunteers

Wakamiya, M.[1]; Furukawa, A.[1]; Kanasaki, S.[1]; Kono, N.[1]; Maeda, K.[2]; Sasaki, T.[2]; Murata, K.[1]; Sakamoto, T.[1] 1. Shiga University of Medical Science, Otsu, Japan; 2. Kusatsu Sougou Hospital, Kusatsu, Japan*
Address correspondence to M. Wakamiya (wakamiya@belle.shiga-med.ac.jp)

Objective: The purpose of the study is to evaluate the potential of cine-MR imaging using balanced steady-state free precession imaging (FIESTA sequence) to monitor and assess the motility function of the small bowel. Amplitude and frequency of small bowel peristalsis are measured in a healthy population to establish parameters for the assessment of bowel motility.

Materials and Methods: Eight healthy volunteers without abdominal symptoms were included in this study. MR imaging was performed after eight hours of fasting and 1500mL of a non-absorbable fluid was administered orally in 20 minutes prior to initiation of scanning. Cine-MR imaging was performed with a 1.5T MR machine using an 8-channel body array coil. FIESTA sequence (repetition time/echo time [TR/TE]=3.4/1.2 millisecond, flip angle=75 degree, acquisition time per image=0.5 second) was utilized and the area of 45 cm x 45 cm was imaged to cover the entire loops of the small bowel. Three 10 mm-thick coronal images were obtained to cover the small bowel loops in the ventral and dorsal directions. At each plane, cine-MR imaging was obtained for 90 seconds. Obtained images were assessed on a monitor to measure the caliber of two representative bowel loops, one at the left upper abdomen (LUA) and the other at the right lower abdomen (RLA). Measurement was performed at every 0.5 seconds for 90 seconds and the results were put on graphs.

Results: The small bowel peristalsis was clearly demonstrated on cine-MR images in all cases. Frequency and amplitude of the peristalsis was uneven depending on the level of small bowel loops. Particularly, strong and frequent peristalsis were initiated with the arrival of the intraluminal content. The average frequency and amplitude of the small bowel peristalsis was 5.9/minute (range: 0-11.3), and 13.0 mm (range: 0-31.6), respectively. Appearance of the peristalsis (the frequency and amplitude) of each segment of the small bowel was not even and changed with time during the observation.

Conclusion: The potential of cine-MR imaging with FIESTA sequence to monitor the small bowel peristalsis was demonstrated. Amplitude and frequency of the peristalsis are calculated from the cine-MR imaging and these parameters should be useful for assessing the motility function of the small bowel in various conditions.

11:10 am

224. Accuracy of MDCT Diagnosis of Blunt Bowel and Mesenteric Injury

Yu, J.; Fulcher, A.; Cockrell, C.; Wooten, K.; Mohiuddin, S.; Malhotra, A.; Halverson, R.; Turner, M. Virginia Commonwealth University, Richmond, VA*
Address correspondence to J. Yu (jyu1@vcu.edu)

Objective: The objective was to determine the accuracy of MDCT detection of bowel and mesenteric injury following blunt abdominal trauma.

Materials and Methods: Patients (n=18) with surgically proven blunt bowel and/or mesenteric injury were identified from the registry of a Level I trauma center for a two-year period (2005-2006). These patients were matched by age and injury severity score with blunt trauma patients (n=76) who did not have bowel or mesenteric injury. All 94 patients had MDCT scans performed within six hours of admission. Two abdominal radiologists independently reviewed the CT scans in a blinded fashion. The CT scan assessment included presence, location and extent of intraperitoneal fluid; extraluminal air or oral contrast; mesenteric hematoma; fat stranding; IV contrast extravasation; bowel wall thickening; and bowel wall discontinuity. The interpretations were correlated with surgical or final clinical diagnoses.

Results: From 94 CT scans, bowel and mesenteric injury was found in 17 of 18 surgically proven patients by reader one and by reader two, with a sensitivity of 94.4% for both readers. For reader one and reader two, specificity was 96.1% and 94.7%, respectively. The accuracy was 95.7% for reader one and 94.6% for reader two (k=0.76). The CT features of bowel and mesenteric injury in 18 positive patients included presence of free air (n=5); free fluid in patients without solid organ injury (n=4); oral contrast extravasation (n=1); mesenteric hematoma (n=8); fat stranding (n=7); mesenteric IV contrast extravasation (n=4); bowel wall thickening (n=7); and bowel wall discontinuity (n=2). For reader one, the false negative case demonstrated extensive liver and spleen injury with a large amount of hemoperitoneum. For reader two, the false negative case demonstrated a small amount of pelvic free fluid in a suboptimal CT scan due to motion artifact.

Conclusion: MDCT has a high accuracy in detecting bowel and mesenteric injury. However, no single CT feature is highly sensitive in the presence of bowel and/or mesenteric injury.

11:20 am

225. Radiological Manifestations of Recurrent Malignant Peritoneal Mesothelioma

Souza, F.[1,2]; Ramaiya, N.[2]; Johnston, C.[2]; Jagannathan, J.[2]; Ros, P.[2] 1. Brigham and Women's Hospital, Boston, MA; 2. Dana Farber Cancer Institute, Boston, MA*
Address correspondence to F. Souza (ffsouza@partners.org)

Objective: The aim of this study is to describe the CT imaging findings of recurrent malignant peritoneal mesothelioma in patients who underwent debulking surgery.

Materials and Methods: The history, clinical and laboratory data, and imaging studies of 14 patients with histologically proven diagnosis of malignant peritoneal mesothelioma (MPM) and their recurrence following cytoreductive surgery were retrospectively reviewed. CT studies were reviewed for the following findings: presence of ascites; peritoneal, mesenteric and omental involvement, presence of solid abdominal viscera involvement, gastrointestinal involvement, presence and location of enlarged lymph nodes and extra-abdominal sites of involvement.

Results: The study population consisted of 14 patients (eight women, six men; mean age 52 years; age range: 16-81 years). Two patients had prior history of asbestosis exposure. The most common radiological finding at the time of initial recurrence was ascites, seen in six patients. Peritoneal thickening was seen in five patients with a nodular (n=3) or smooth (n=2) appearance; diffuse sheet like infiltration of the peritoneum was seen in one patient and low density implants mimicking pseudomyxoma peritonei was seen in another patient. None of the peritoneal implants showed calcification. Three patients had large discrete masses in the omentum and/or peritoneum. The mesentery was involved in five patients. Multifocal serosal implants were seen in four patients; one had low grade small bowel obstruction which was managed conservatively. Three patients had evidence of intrathoracic disease seen as soft tissue pericardial mass (n=1) and malignant pleural effusions (n=2).

Conclusion: CT findings of recurrent malignant peritoneal mesothelioma may mimic metastatic or granulomatous diseases and may show a different pattern of peritoneal involvement as opposed to the appearance of the disease at presentation. Even though it appears confined to the abdominal cavity at presentation, recurrence may be seen at extra-abdominal sites.

11:30 am

226. Delayed Enhancement of Ascites Following Intravenous Contrast Material Administration at CT: Time Course and Clinical Correlation

Benedetti, N.[1]; Aslam, R.[2]; Joe, B.[2]; Yeh, B.[2] 1. Stanford University School of Medicine, Los Altos, CA; 2. University of California San Francisco, San Francisco, CA*
Address correspondence to N. Benedetti (nancyjb@stanford.edu)

Objective: The objective was to determine the prevalence, time course and clinical predictors of delayed contrast enhancement of ascites.

Materials and Methods: We retrospectively identified 132 consecutive patients with ascites and repeated abdominopelvic CT scans done within seven days of each other. These patients included 112 patients who received and 20 who did not receive intravenous contrast material at the initial CT scan. For each scan, we recorded the CT attenuation of the ascites. For the followup scan, we recorded the presence of delayed enhancement of ascites, defined as an increase in CT attenuation greater than 10 Hounsfield units (HUs) over baseline. We used the Fisher's exact test, unpaired t-test and logistical regression to determine predictors of delayed enhancement.

Results: Delayed enhancement of ascites occurred only when prior intravenous contrast was given, and occurred in 15 of these 112 patients (13%). For such patients scanned less than one day apart, 10 of 16 patients (63%) showed delayed enhancement of ascites. Delayed enhancement was observed up to 2.6 days after contrast administration. The mean serum creatinine was higher in patients with than without delayed enhancement of ascites (2.4 vs. 1.2 mg/dL, $p=0.006$). Multivariate logistical regression showed that a short time interval between scans ($p<0.001$), increased serum creatinine ($p<0.001$) and loculated ascites ($p<0.05$) were independent predictors of the magnitude of delayed enhancement of ascites.

Conclusion: Delayed contrast enhancement of ascites occurs commonly after recent prior intravenous contrast material administration and should not be mistaken for intraperitoneal catastrophe.

11:40 am

227. Diffusion-Weighted MR Imaging for the Diagnosis of Anal Fistula

Hori, M.; Oto, A.; Orrin, S.; Suzuki, K.; Baron, R. The University of Chicago, Chicago, IL*
Address correspondence to M. Hori (mhori@radiol.med.osaka-u.ac.jp)

Objective: Contrast-enhanced MRI is known to improve the diagnosis of anal fistulae; however, administration of gadolinium (Gd) may be contraindicated in some patients. The purpose of this study was to retrospectively determine the additional value of diffusion-weighted MRI to T2-weighted images in the evaluation of anal fistulae and compare its added value with Gd-enhanced MRI.

Materials and Methods: Twelve patients with 18 anal fistulae who underwent MRI were included. The patients had a mean age of 34.3 years (range, 20-61 years). Six patients (50%) were men and six (50%) were women. MRI was performed using a 1.5T superconducting unit. The MRI protocol consisted of fat-suppressed T2-weighted fast spin-echo, diffusion-weighted single-shot echo-planar (b=800), and Gd-enhanced fat-suppressed T1-weighted 3D gradient echo sequences. MR images were retrospectively reviewed by two radiologists. First, they evaluated fat-suppressed T2-weighted images of each patient and recorded the location of possible fistulae by consensus. Then, they scored each possible fistula by consensus in terms of the presence of anal fistulae using a four-point scale: 1, probably not a lesion; 2, a possible lesion; 3, a probable lesion; and 4, a definite lesion. After the evaluation of T2-weighted images, the radiologists evaluated T2-weighted images together with diffusion-weighted images and then with Gd-enhanced images in two different ses-

sions two weeks apart from each other using the same methodology. The results were compared with reference standard based on radiological, surgical, and clinical records.

Results: Sixteen fistulae (89%) were detected on T2-weighted images, and 17 (94%) and 17 (94%) were detected on T2-weighted images and diffusion-weighted images combined and on T2-weighted images and Gd-enhanced images combined, respectively (p>.5; McNemar test). Confidence scores with T2-weighted images and diffusion-weighted images combined or those with T2-weighted images and Gd-enhanced images combined were significantly greater than those with T2-weighted images alone (p=.0027 and .014, respectively; Wilcoxon signed-rank test). There was no significant difference in confidence scores between T2-weighted images and diffusion-weighted images combined and T2-weighted images and Gd-enhanced images combined (p=.26).

Conclusion: Diffusion-weighted MRI is a useful sequence for detection of anal fistulae and shows additional value to fat-suppressed T2-weighted imaging mainly by improving the level of confidence in their diagnosis.

11:50 am

228. The Cisterna Chyli: Prevalence, Characteristics and Predisposing Factors

Feuerlein, S.; Kreuzer, G.; Brambs, H.; Pauls, S. Ulm University, Ulm, Germany*
Address correspondence to S. Feuerlein (sfeuerlein@yahoo.com)

Objective: The objective was to determine the prevalence and characteristics of the cisterna chyli (CC) in a large 3,000 patient cohort and to identify potential predisposing factors for the development of a CC.

Materials and Methods: The local institutional review board approved the study and waived the requirement for obtaining informed consent. 3,000 consecutive contrast-enhanced CT examinations (1,261 women, 1,739 men, mean age 61 years) of the chest and/or abdomen were included in this retrospective study. Imaging characteristics of the CC (size, attenuation, location) were documented as well as clinical information (malignant disease, tumor type, pattern of metastasis).

Results: A CC was found in 16.1% of the patients. The average diameter was 6.2 mm, the average length 13.1 mm, resulting in an average volume of 0.302 ml. The mean attenuation was 4.8 Hounsfield Units (HU). A total of 20% of the CC showed CT densities of 15 HU and higher. The most common location was on the level of T12/L1. Patients with malignancies showed a significantly (p<0.001) higher prevalence for a CC (340/1,757, 19.4%) than patients with benign conditions (144/1,243, 11.6%). Especially the finding of a large CC (>1 ml) represents an elevated relative risk for malignancy of 1.7 (p=0.0017). A few tumors could be identified that showed a higher prevalence of a CC compared to the baseline prevalence in the malignant cohort of 19.4%. This group includes: hepatocellular carcinoma (35.3%, p=0.197), lymphoma (25.0%, p=0.410) and pancreatic carcinoma (24.6%, p=0.368).

Conclusion: We found a significant association between malignant disease and the presence and size of a cisterna chyli. Especially a large CC represents a relative risk of malignancy of 1.7 in our cohort. Identifying the continuity between the CC and the thoracic duct is a safer method to distinguish a CC from retrocrural lymph nodes than near-water CT attenuation alone.

NUCLEAR MEDICINE PAPERS

Room: 309, Level 3

Thursday, April 30, 2009, 10:00 am–11:30 am

Abstracts 229-234

Moderators: *H. Jacene, D. Yoo*

Keynote Address: Quantification in PET: Getting the Most Mileage from SUVs—*T. Wong*

10:30 am

229. Usefulness of Delayed Whole Body Tc-99m Methylene Diphosphonate Bone Scan Imaging Following Directed Three-Phase Examinations

Davenport, M.; Brown, R.; Frey, K. University of Michigan, Ann Arbor, MI*

Address correspondence to M. Davenport (matdaven@med.umich.edu)

Objective: The objective was to determine the usefulness of delayed whole body Tc-99m methylene diphosphonate (MDP) bone scan imaging following directed three-phase examinations.

Materials and Methods: Four-hundred consecutive patients aged 1-90 in whom combined directed three-phase and delayed whole body Tc-99m MDP bone scan imaging was obtained for a variety of indications between October, 2007 and July, 2008 were reviewed. Mean contribution of whole body imaging to study duration was extrapolated during the exams of 15 consecutive patients. Clinical indication, findings, and recommendations were recorded. Recommendations were characterized by strength. Clinical outcome was assessed by retrospective chart review.

Results: Tc-99m MDP three-phase bone scans were performed on 244 (61%) female patients, 52 (13%) pediatric patients, and 236 (59%) patients over 40 years of age. Mean increase in study duration due to whole-body imaging was 25 minutes (range: 21-31 minutes). Clinician-written requisitions were tabulated: 334 (84%) indicated focal symptoms in one or two areas, 15 (4%) indicated multiple foci, 29 (7%) indicated diffuse arthralgias or fibromyalgia, and 22 (6%) indicated a known marrow disorder or cancer. Excluding the three-phase region of interest, the whole body portion of the exam demonstrated a normal tracer distribution in 131 (33%) exams, solely degenerative changes in 103 (26%), and other finding(s) unrelated to the region of interest in 166 (41%). The findings outside the region of interest did not alter diagnosis or diagnostic certainty of the multiphase study in any case, but did generate 82 recommendations for further evaluation. Thirty-seven (9%) soft and 45 (11%) hard recommendations were made to obtain the following: 41 plain films, eight unspecified imaging studies, four CT exams, 11 MR exams, two nuclear medicine exams, two ultrasounds, one lab, and 34 clinical correlatives. As a direct result of these recommendations, clinicians obtained: 18 plain films, two CT exams, one MR, one ultrasound, and two referrals to a consultant. Recommendations based on findings outside the multiphase area of interest affected treatment in one case: temporomandibular joint uptake resulted in a referral to physical therapy.

Conclusion: For most indications, delayed whole body imaging following directed three-phase Tc-99m MDP bone scan imaging does not improve diagnostic yield, does not alter patient management, and is an unnecessary use of medical resources.

10:40 am

230. Extracardiac Findings in Low Dose Attenuation Correction CT Thoracic Images: A Rubidium-82 PET-CT Study

Demehri, S.; Rybicki, F.; Nallamshetty, .; Ersoy, H.; Di Carli, M.; Dorbala, S. Brigham and Women Hospital, Brookline, MA*

Address correspondence to S. Demehri (sdemehri@partners.org)

Objective: The objective was to evaluate prevalence and cost of downstream testing for extracardiac findings in thoracic CT attenuation correction (CTAC) images in myocardial perfusion Rubidium-82 (Rb-82) PET-CT

Materials and Methods: A total of 1,071 consecutive patients underwent rest-stress Rb-82 PET-CT with CTAC (16 row, 140 kV, 10 mA, 5 mm reconstruction, slow tidal breathing) for evaluation of known/suspected ischemic heart disease. All CTAC images were prospectively reviewed by radiology trainees; positive findings were confirmed by attending radiologists. Extracardiac findings were classified as "significant" (previously unknown, further evaluation recommended) and further as "critical" if potentially life threatening. All patients had greater than six months follow-up using the institutional electronic medical record that included smoking history (smoker vs. non/ex-smoker). Downstream imaging testing costs for significant extracardiac findings were estimated with standard Medicare charges.

Results: The mean age = 63.2 years (range =20-93 years); 17% smokers. Significant and critical extracardiac findings were noted in 98 (9.1%) and five (0.5%) patients, respectively. The prevalence was higher in smokers (13.7% vs. 8.1%, $p<0.005$). Among 98 significant extracardiac findings, the most common was pulmonary nodules (n=53, 54.1%), followed by a pulmonary opacity concerning for infection (n=12, 12.2%), a breast lesion (n=7, 7.1%), liver lesions (n=7, 7.1%), ascending aortic aneurysm >4.5 cm (n=4, 4.1%), renal abnormality (n=4, 4.1%), mediastinal lymph node enlargement (n=2, 2%), and pancreatic abnormality (n=2, 2%). The eight critical findings were ascending aortic aneurysm (n=4), histology-confirmed lung neoplasm (n=2), invasive ductal carcinoma of the breast (n=1), and severe hydronephrosis from ureteral stent occlusion (n=1). The total cost of downstream testing was $25,306, or $3,163 per patient with a critical finding.

Conclusion: Myocardial perfusion Rb-82 PET-CT patients have significant incidental findings detected on attenuation correction CT images, with a higher prevalence in smokers. Critical findings are uncommon and have a cost of downstream testing of roughly $3,000. Low dose and thus inherently noisy, CT attenuation correction images warrant evaluation by appropriately trained physicians.

10:50 am

231. Comparison of PET-CT and Enhanced Multislice CT for Detecting Small Hepatic Metastasis

Kim, I.; Park, J.; Kim, S.; Shin, H.; Park, S.; Kim, Y. Soonchunhyang University Hospital, Cheonan, Korea*

Address correspondence to I. Kim (ilykim@schch.co.kr)

Objective: The sensitivity difference between PET-CT and enhanced multislice CT in detection of the hepatic metastasis (HM) was evaluated according to the size, numbers and location of the liver.

Materials and Methods: Of 102 consecutive patients known to have or suspected of having HM referred to FDG PET-CT from November, 2005 for two years and enhanced CT at least two mo intervals, 69 patients with HM (22 colon, 14 stomach, nine lung, 24 others) finally were enrolled in this study. HM was confirmed by enhanced CT, follow up imaging study at least 6 mo, or histologic examination. Both examinations were evaluated by consensus of two radiologists or two PET experts without knowing the results of other studies. All images were divided into positive, equivocal, or negative. Data were analyzed according to the numbers, size and location.

Results: The PET-CT images were interpreted as one negative, three equivocal and 65 positive, and the enhanced CT images were classified as 3 negative, 11 equivocal and 55 positive. Specifically, PET-CT identified 19 more patients with HM of the discordant cases (n=23) for grading. For the number of lesions, PET-CT detected more than CT in seven of 14 patients. For subcentimeter sized HM located in 15 subcapsular portion of liver, PET-CT demonstrated higher sensitivity than enhanced CT (80.0% vs. 26.7%, p=0.01).

Conclusion: Combination of PET-CT and enhanced CT proves to be more sensitive than PET-CT or CT alone in depiction of HM. Furthermore PET-CT is superior to enhanced CT for detecting small HM located in the subcapsular portion of liver.

11:00 am

232. FDG Uptake in the Neck on PET-CT: The Value of Symmetry in Evaluating the Normal and Abnormal Neck

Ulaner, G.; Go, J. University of Southern California, Los Angeles, CA*
Address correspondence to G. Ulaner (ulaner@usc.edu)

Objective: The objective was to define parameters which help differentiate physiologic from pathologic FDG avidity in the neck.

Materials and Methods: A retrospective study of 200 patients who underwent FDG-PET-CT was performed, comparing 170 patients without neck disease to 30 patients with tumors of the lymphoid or salivary tissues of the neck. Maximum standardized uptake values (SUVmax) were determined for the lymphoid and salivary tissues of the neck. Statistical analysis was performed to evaluate the magnitude of FDG uptake and symmetry.

Results: In the 170 patients without known neck disease, the SUVmax of the lymphoid and salivary tissues of the neck ranged from 1.1 to 10.6. Out of 850 comparisons of left-right paired lymphoid and salivary tissues (five comparisons for each of 170 patients), 846 had <35% asymmetry in SUVmax. In contrast, in 27 of the 30 patients with tumors of the lymphoid or salivary tissues of the neck, the malignant tissue displayed >40% left-right asymmetry as compared to the contralateral side. In three instances, FDG asymmetry in lymphoid tissues of the neck lead to biopsies which diagnosed the site of primary malignancy.

Conclusion: 1) In patients without known neck disease, FDG asymmetry of up to 35% in the lymphoid and salivary structures of the neck can be regarded as physiologic, even when the SUVmax is >10.2) Greater FDG asymmetry often indicates pathology. 3) FDG PET-CT is useful in detecting the site of primary malignancy in patients with lymphadenopathy of the neck without known primary.

11:10 am

233. Somatostatin Analogs in a Colon Carcinoid Cancer Mouse Model: Comparison with FDG and 18F-DOPA

Baier, N.[1,2]; Böhm, B.[2]; Reske, S.[2]; Harisinghani, M.[1] 1. Massachusetts General Hospital, Boston, MA; 2. Universitätsklinikum Ulm, Ulm, Germany*
Address correspondence to N. Baier (baier.nina@mgh.harvard.edu)

Objective: The objective was to determine the diagnostic accuracy of FDG, 18F-DOPA, 68Ga and 111In labeled somatostatin analogs for detecting human colon carcinoid tumors in a mouse model, using microPET, and to define time points providing maximum information.

Materials and Methods: Cultured human colon carcinoid tumor cells (LCC) were implanted subcutaneously into severe combined immunodeficiency mice. Four weeks after tumor injection, FDG, 18F-DOPA, 68Ga-Dotatoc, 68Ga-Dotasomo and 111In-Dotasomo were injected intravenously. MicroPET images were acquired continuously for 120 minutes. Mice were sacrificed at 5, 15, 30, 45, 60 and 120 minutes postinjection for quantitative radiotracer biodistribution studies and tumor organ uptake ratios (t/o) were compared.

Results: At sacrifice, tumor organ uptake ratios (t/o) was significantly highest for FDG at time point 120 minutes (tumor uptake 7.10 ± 1.84%ID/g, t/o 4.77) as compared to DOPA (tumor uptake 4.60 ± 0.80%ID/g, t/o 1.96, p<0.001) and 68Ga-Dotatoc (tumor uptake 0.73%ID/g, t/o 0.67, p<0.001). For all time points t/o of FDG was higher than t/o of all other substances at corresponding time points, this difference was significant at 15 minutes compared to 68Ga-Dotasomo (p<0.001) and 68Ga-Dotatoc (p<0.001), at 60 minutes compared to 111In-Dotasomo (p=0.033) and at 120 minutes compared to DOPA (p<0.001) and 68Ga-Dotatoc (p<0.001). Comparing the time points 15, 60 and 120 minutes postinjection, t/o was highest at 120 minutes for FDG (tumor uptake 7.10 ± 1.84% ID/g, t/o 4.77, p<0.001) and at 60 minutes for DOPA (tumor uptake 6.20 ± 1.93%ID/g, t/o 2.35, p<0.001). Furthermore there was no significant difference between somatostatin analogs labeled with either 68Ga or 111In (p=0.51).

Conclusion: FDG is superior to 18F-DOPA and all somatostatin analogs included in this study. Delayed images at 60 or 120 minutes are likely to be most informative for detection of colon carcinoid tumors.

11:20 am

234. PET of Medullary Thyroid Cancer: Comparison of FDG, 18F-DOPA and 68Ga-DOTA-TOC in a Cancer Mouse Model

Baier, N.[1,2]; Reske, S.[2]; Böhm, B.[2]; Harisinghani, M.[1] 1. Massachusetts General Hospital, Boston, MA; 2. Universitätsklinikum Ulm, Ulm, Germany*
Address correspondence to N. Baier (baier.nina@mgh.harvard.edu)

Objective: The objective was to determine the value of FDG, 18F-DOPA and 68Ga-DOTA-Tyr3-octreotide (DOTA-TOC) in a mouse model for detection of medullary thyroid cancer (MTC), using microPET and to define time points providing maximum information.

Materials and Methods: Cultured human medullary thyroid cancer cells (TT) were implanted subcutaneously into severe combined immunodeficiency mice. Five weeks after tumor implantation, FDG, 18F-DOPA and 68Ga-DOTA-Tyr3-octreotide were injected intravenously and microPET images were acquired continuously for 120 minutes. Mice were sacrificed at 15, 60 and 120 minutes postinjection for quantitative (%ID/g) radiotracer biodistribution studies and tumor/organ uptake ratios (t/o) were calculated and compared.

Results: Tumor/organ uptake ratios were highest for DOTA-TOC at time points 60 and 120 minutes (tumor uptake 10.54%ID/g, 8.45%ID/g, t/o 3.15, 3.31) as compared to FDG (tumor uptake 2.76 ± 0.69%ID/g, 4.35 ± 0.65%ID/g, t/o 2.21, 2.74) and DOPA at equivalent time points (tumor uptake 3.68 ± 0.46%ID/g, 2.46 ± 0.50%ID/g, t/o 1.46, 1.51). However these differences were not statistically significant (p=0.15-0.65). Tumor/organ uptake ratios of FDG was higher than t/o of DOPA at 15, 60 and 120 minutes (FDG 1.76, 2.21, 2.51; DOPA 0.82, 1.45, 1.51) and this difference was statistically significant at 15 and 120 minutes ($p<0.001$, p=0.01). For DOPA at 15 minutes background uptake was higher than tumor uptake (t/o 0.82). Optimum time point for all tracers was 120 minutes; this was statistically significant for FDG and DOPA (FDG p=0.043, DOPA p=0.005).

Conclusion: 68Ga-DOTA-Tyr3-octreotide is superior to both FDG and 18F-DOPA, and FDG is superior to 18F-DOPA for evaluation of MTC. For all tracers delayed images at 120 minutes are likely to be most informative for detection of MTC.

GASTROINTESTINAL (LIVER) IMAGING PAPERS

Room: 310, Level 3
Thursday, April 30, 2009, 1:30 pm–3:30 pm
Abstracts 235-245

Moderators: *D. Nakamoto, B. Choi*
Keynote Address: Imaging of Hepatocellular Carcinoma with MR Contrast Agent—*B. Choi*

1:40 pm

235. Incidence of New Foci of Hepatocellular Carcinoma in Patients Who Underwent Radiofrequency Ablation of Hepatocellular Carcinoma: Role of MDCT

Bartolotta, T.; Taibbi, A.; Putignano, L.; Galia, M.; Lo Re, G.; Malizia, G.; Midiri, M.; Lagalla, R. University Hospital, Palermo, Italy*
Address correspondence to A. Taibbi (taibbiadele@hotmail.com)

Objective: The objective was to assess the incidence of new foci of hepatocellular carcinoma (HCC) by means of MDCT in patients who had undergone radiofrequency ablation (RFA) of HCC.

Materials and Methods: MDCT studies of 129 patients (92 men and 37 women; age: 48-89 years - mean: 72 years), with RFA-treated HCCs followed-up for one to 68 months (mean: 22 months), were retrospectively reviewed to detect the presence of new foci of HCC, defined as hypervascular focus in the arterial phase with wash-out in the portal-venous or equilibrium phases, arising at least at 2.1 cm from the treated nodule either in the same or in a different liver segment. All new nodules were definitively proven through biopsy and/or MR imaging and contrast-enhanced ultrasound findings.

Results: A total of 189 new HCCs (size:1-5 cm; mean: 1.7 cm) were detected in the same (n=38; 20%) or in a different (n=151;80%) liver segment ($p<0.001$) in 70/129 (54.3%) patients, followed-up for one to 59 months (mean: 26 months); 25/70 patients had a single new HCC, whereas 45/70 patients had two (17 patients), three (10 patients), four (six patients), five (four patients), six (three patients), seven (two patients) or eight (three patients) new HCCs. The remaining 59 patients without new HCCs were followed-up for 1-68 month (mean: 15 months) ($p<0.001$). Disease free interval-time was three to 54 months (mean: 14.5 months).

Conclusion: MDCT follow-up in patients with RFA-treated HCCs reveals, especially when follow-up is longer than one year, a high incidence of new HCCs mainly detected in a liver segment different from that of treated HCC.

1:50 pm

236. Correlation Between Fatty Liver Grading and Abdominal Fat, Using Hepatic Attenuation Value and Fat Volume

Jang, S.; Lee, C.; Kim, K.; Choi, J.; Lee, J.; Park, C. Korea University School of Medicine, Seoul, South Korea*
Address correspondence to S. Jang (tiancai0505@naver.com)

Objective: It has been generally recognized that fatty liver can often be seen among the obese population. This study was conducted to evaluate the association between fatty liver grading and abdominal fat volume by using the hepatic attenuation value.

Materials and Methods: A total of 310 patients underwent fat CT scans who visited our obesity clinic over the last six months. Liver and spleen attenuation measurements were taken with the region of interest (ROI) of the liver in three areas and two areas from the spleen. The hepatic attenuation index (HAI) is measured as follows: (1) hepatic parenchymal attenuation (CT_{LP}), (2) liver to spleen attenuation ratio (LS ratio), and (3) difference between hepatic and splenic attenuation (LS_{dif}). Abdominal fat volume was measured using a 10 mm slice CT scan at the aortic bifurcation level and was automatically calculated with a workstation (Philips Healthcare, Bothell, WA). Abdominal fat was classified into total fat (TF), visceral fat (VF) and subcutaneous fat (SF). We used the bivariate correlation method to assess the correlation between HAI and (1) total fat (TF), (2) visceral fat (VF), and (3) subcutaneous fat (SF), respectively.

Results: There was significant negative correlation between CT_{LP}, LS ratio and LS_{dif} with total abdominal fat, visceral fat, and subcutaneous fat. The CT_{LP} showed strong negative correlation with TF and VF ($r= -0.412$ and -0.414, respectively $p=0.000$). The correlation between CT_{LP} and SF was less significant than VF or TF ($r = -0.265$, $p=0.000$)

Conclusion: Fat infiltration of the liver is correlated with the amount of total abdominal fat and visceral fat was found to be more strongly associated with fatty liver than subcutaneous fat.

2:00 pm

237. Density Change in Colon Cancer Hepatic Metastasis Treated with Yttrium-90 on MDCT: Does it Predict PET Activity?

Tochetto, S.; Rezai, P.; Yaghmai, V. Northwestern University, Chicago, IL*
Address correspondence to V. Yaghmai (v-yaghmai@northwestern.edu)

Objective: The objective was to evaluate the correlation between PET activity and change in density of hepatic metastasis of colon cancer treated with Yttrium-90 radioembolization.

Materials and Methods: Fifty-eight colon cancer hepatic metastases in 22 patients were evaluated pre- and post-treatment with CT and PET scans. The average time interval between pre- and post-treatment scans was 44.6 ± 12.1 days (range 29 to 77 days). Pre- and post-treatment PET evaluations were compared and the results were qualitatively categorized in three groups: (A) No change; (B) Mild/moderate interval improvement; (C) Complete interval improvement. The mean density and volumetric measurements of the hepatic lesions were calculated. The percentage of change in density and volumetric measurements for the three groups was calculated comparing pre- and post-treatment measurements. $p<0.05$ was considered significant.

Results: The percentage of change in density correlated with PET evaluation of tumor response to Yttrium-90 radioembolization treatment (r=0.65). The percentage of change in density between pre- and post-treated lesions was 2.16% for Group A (SE ± 2.84%, n=13); -9.80% for Group B (standard error ± 2.56%, n=33) and -23.53% for Group C (SE ± 7.88, n=12). A significant difference was observed among the groups A, B and C (ANOVA, $p<0.001$). The percentage of change in volume and RECIST measurement did not correlate with PET and no significant difference was observed among the groups A, B and C ($p>0.05$).

Conclusion: The change in density of colon cancer hepatic metastasis treated with Yttrium-90 correlates with PET activity and may be a better predictor of monitoring therapeutic response than volumetric and RECIST measurements.

2:10 pm

238. Imaging Findings of Hepatic Focal Nodular Hyperplasia in Gadoxetic Acid vs. Gadobenate Dimeglumine–Enhanced MR: Preliminary Results

Taibbi, A.; Bartolotta, T.; Putignano, L.; Galia, M.; Lo Re, G.; Toro, A.; Midiri, M.; Lagalla, R. University Hospital, Palermo, Italy*
Address correspondence to A. Taibbi (taibbiadele@hotmail.com)

Objective: The objective was to evaluate imaging features of focal nodular hyperplasia (FNH) at MR performed with two different hepatocellular-specific gadolinium-based contrast agents.

Materials and Methods: Eleven patients (eight women, three men; mean age 37.8 years) with 14 confirmed FNHs (mean size 2.4 cm) underwent MR (1.5T) before (T2-weighted fast spin-echo sequences without and with fat-saturation and T1-weighted GRE in phase, out-of phase and fat-saturation sequences) and after (T1-weighted gradient echo volumetric fat-saturation sequences) intravenous bolus administration of both hepatospecific contrast agents: gadobenate dimeglumine (Gd-BOPTA): 0.1 mmol/kg and gadoxetic acid (Gd-EOB-DTPA): 0.025 mmol/kg. Arterial, portal-venous, equilibrium and hepatospecific phases - this latter at time interval of 1-2 hours (Gd-BOPTA) and 30-40 minutes (Gd-EOB-DTPA) were acquired. Contrast-enhancement patterns, central scar and, in the hepatospecific phase (HP), signal intensity (SI) of FNH compared with those of the surrounding liver parenchyma were evaluated by two blinded readers in consensus.

Results: All 14 FNHs (100%) showed strong arterial enhancement appearing hyperintense during portal-venous and equilibrium phases after Gd-BOPTA and Gd-EOB-DTPA injection without any statistically significant difference ($p>0.05$). In the HP all lesions retained both contrast-media but five out of 14 FNHs revealed inhomogeneous aspect with hypointense central oval area different from central scar. This latter was evident in 10/14 (71.4%) patients studied with either Gd-BOPTA or Gd-EOB-DTPA. In the HP, SI mean values were not statistically significant different (Gd-BOPTA: 1,301.9 and Gd-EOB-DTPA: 1,415.4) ($p>0.05$).

Conclusion: Imaging findings of FNHs evaluated with the two different hepatospecific MR contrast-agents are highly similar but Gd-EOB-DTPA allows for reduction in total time for the MR examination.

2:20 pm

239. Focal Liver Lesions in Patients with Cavernous Transformation of the Portal Vein: MR Imaging Features

Galluzzo, A.[1]; Brancatelli, G.[1]; Plessier, A.[2]; Midiri, M.[1]; Condat, B.[2]; Lagalla, R.[1]; Vilgrain, V.[3] 1. University of Palermo, Palermo, Italy; 2. Service d'hépatologie, Hopital Beaujon, AP-HP, Clichy, France; 3. Service de Radiologie, Hopital Beaujon, AP-HP, University of Paris, Clichy, France*
Address correspondence to A. Galluzzo (annagalluzzo@gmail.com)

Objective: The objective was to evaluate retrospectively MR imaging findings of focal liver lesions in patients with cavernous transformation of the portal vein.

Materials and Methods: Clinical, pathological and MR imaging findings were retrospectively reviewed in 58 patients with cavernous transformation of the portal vein. Two radiologists evaluated the presence of focal liver lesions. In patients with hepatic lesions, size, number and MR features (signal and enhancement of each lesion) were assessed. Diagnosis of the liver lesions was based on typical imaging or liver biopsy.

Results: Eighteen patients showed focal liver lesions and 12 had focal nodular hyperplasia (FNH) like lesions (20.6% of all patients). In ten patients was found a solitary lesion: five FNH-like lesions and five hemangiomas. Eight patients had multiple lesions: five with FNH-like lesions, one with hemangiomas and two with the association respectively of FNH-like lesions and liver adenoma and FNH-like lesions and hemangioma. The diagnosis of FNH-like lesion and liver adenoma were confirmed at pathology in three patients. The mean size of FNH-like lesions was 12.9 mm (range: 5-42 mm). The mean delay time between diagnosis of the portal vein thrombosis and the detection of FNH-like lesions was 4.3 years (range: 0-13 years).

Conclusion: Most lesions observed in patients with cavernous transformation of the portal vein are FNH-like lesions. These lesions probably arise as a consequence of portal inflow reduction.

2:30 pm

240. Comparison of Multislice CT and Gadolinium-Enhanced MRI for Detection of Small (<3 cm) Hepatic Lesions in Patients With Chronic Liver Disease

Wable, S.; Kaplan, M.; Wang, P.; Naqvi, S. Albert Einstein Medical Center, Philadelphia, PA*
Address correspondence to M. Kaplan (kaplanmc@einstein.edu)

Objective: The objective was to compare multislice CT and MRI for the detection of small hepatic lesions in patients with chronic liver disease.

Materials and Methods: Approximately 2,484 triple phase CT and MRI examinations were retrospectively reviewed from 2005. This yielded a study population of 30 patients with cirrhosis or chronic hepatitis who had lesions less than 3 cm and both MRI and multislice CT within a period of eight weeks. Eleven patients had CT with a 64-slice CT scanner and 19 with a 16-slice CT scanner. All but two patients had both MRI and CT within six weeks. All but six patients had no follow up or follow up for less than six months. The other patients had either follow up greater than six months to two years, had histological diagnosis or were

treated with radiofrequency ablation or chemoembolization for presumed hepatocellular carcinoma based on their characteristic imaging findings.

Results: A total of 32 lesions were seen on CT and 43 on MRI. Of the 11 additional lesions on MRI, two were additional foci of hepatocellular carcinoma (HCC), three were stable for two years, one was stable for eight months, three were subcentimeter lesions and thought to be foci of arterioportal shunting and two were characteristic of hemangiomas. Of the 32 lesions seen on both MRI and CT, three lesions were better characterized on MRI, one was characteristic for a hemangioma, one represented a portosystemic venous shunt, and one was thought to be a regenerative nodule stable for two years. The two lesions better characterized on CT demonstrated interval growth on three month followup. Of the six patients who had no follow up or follow up less than six months, two had imaging characteristics for benign lesions and one was atypical on both CT and MR and has remained stable for two months. In two, both CT and MRI showed lesions suspicious for HCC. In the sixth patient, both CT and MR detected the radiofrequency ablated nonviable lesions.

Conclusion: MRI appears to have only a slight advantage over multislice CT in lesion detection and characterization. Although more lesions were seen on MRI, only two of them represented additional foci of HCC. In patients unable to tolerate long imaging times and MRI, triple phase CT examination would be an adequate study. Based on the above data multislice CT will have a similar detection rate for small hepatic lesions as MRI. More pseudolesions are seen in MRI and familiarity with these varied patterns of enhancement is essential for interpretation.

2:40 pm

241. Differentiating a Benign From Malignant Liver Lesion in the Pretransplant Cirrhotic Liver on Triphasic MDCT: When to Worry, When to Relax

Liu, Y.; Shin, L.; Kamaya, A.; Jeffrey, R. Stanford University, Stanford, CA*
Address correspondence to Y. Liu (yliu@stanford.edu)

Objective: Hypervascular lesions are frequently seen in end-stage cirrhotic livers. Differentiating hepatocellular carcinoma (HCC) from benign entities such as regenerative nodules or arterial-portal shunts is often difficult yet of utmost importance. Candidacy for transplantation according to the Milan criteria and priority according to the United Network for Organ Sharing (UNOS) are determined based solely on hypervascularity for diagnosis of HCC without biopsy confirmation. This study aims to identify the sensitivity and positive predictive value of arterial phase imaging in detecting HCC and the added value of portal venous and delayed phase imaging. Other characteristics, including morphology and size, were also considered.

Materials and Methods: We reviewed all patients who underwent liver transplantation at our institution from 2003 to 2007 and identified 48 arterially enhancing lesions in 25 patients within six months of transplantation. Previously chemoembolized and lesions <1 cm were excluded. Enhancement profiles and other characteristics were recorded for each hypervascular lesion. All explanted livers were serially sectioned to 10 mm slices and examined for focal lesions.

Results: The mean lesion size was 1.8 cm. Based on pathologic correlation of the explanted liver, 18 active (i.e., not chemoembolized) HCCs were identified. 14 of the 18 lesions were hypervascular on arterial phase, resulting in a 77.8% sensitivity and 29.2% positive predictive value. Three of the four lesions that were not hypervascular were well differentiated HCCs. The presence of delayed wash-out provided a much higher sensitivity (93%) and specificity (97%) compared to hypervascularity alone. Two additional lesions showed partial wash-out on the delayed phase which proved to be a mixed HCC/cholangiocarcinoma and a focally-hemorrhagic HCC. There is also significant correlation between lesion size and HCC, as well as between lesion morphology and HCC.

Conclusion: Although UNOS uses hypervascularity as critieria for diagnosis of HCC without biopsy confirmation, the presence of wash-out on delayed images has a higher sensitivity and specificity in diagnosis of HCC and may be a better indicator of malignancy than arterial hypervascularity alone which only provided 78% sensitivity. Partial wash-out may be signs of mixed malignancies or HCC complicated by hemorrhage.

2:50 pm

242. Hepatic Lesions Imitating Neoplasms on Advanced Imaging (CT/MR/PET)—Experience in 74 Patients with Percutaneous Image-Guided Biopsy

Ma, X.; Sahani, D.; Gervais, D.; Hahn, P.; Mueller, P. Massachusetts General Hospital, Boston, MA*
Address correspondence to X. Ma (xma@partners.org)

Objective: The objective was to investigate hepatic lesions that mimic neoplasms on imaging from a cohort of 869 patients who underwent image-guided percutaneous biopsies.

Materials and Methods: From a cohort of 869 patients having had image-guided percutaneous focal liver lesion biopsy with both core biopsy and fine needle aspiration (FNA), (724 without liver cirrhosis and 145 with cirrhosis), 74 lesions were considered as pseudolesions based on the histopathology results, lesion stability/resolution on imaging follow-up more than six months or surgery diagnosis. Preprocedure image studies done within three months were reviewed for the reasons of biopsy. The prevalence of pseudolesions in cirrhotic and noncirrhotic liver and incidence of different lesion sizes (<=3cm vs. >3cm) was assessed for statistical significance using Chi-square test. Data was also reviewed to study lesion characteristics on imaging (CT/MRI/PET).

Results: Seventy-four (8.5%) of 968 lesions biopsied were considered pseudolesions. Lesion biopsy was undertaken due to suspicious imaging appearance/enhancing features on MRI (n=37), CT (n=32), or increased FDG uptake on PET (n=5). Histopathology revealed 23 (31%) inflammatory changes, 21 cirrhotic nodules, 20 focal steatosis, five regenerative changes and five perfusion abnormalities. On six months follow up imaging, 58 lesions were stable, whereas 15 disappeared and one patient underwent resection. 53/74 (71.6%) were in the 724 noncirrhotics, whereas 21/74 (28.4%) were found in the 145 cirrhotics ($p=0.0048$). Fifty-four (73%) pseudolesions measured <3cm and 20 (27%) in lesion size >3cm. ($p<0.001$) Small size (<3cm), poor conspicuity on delayed phase images, lack of T2 signal abnormalities, or mild FDG-uptake were features discovered in these lesions.

Conclusion: Pseudolesions are commonly encountered on liver imaging studies, more frequently in cirrhotics and they can present suspicious features. However, small lesion size and lack of visualization on delayed phase or T2-weighted images should raise the possibility of a benign diagnosis. A second imaging test or follow up can be a reasonable alternate as the majority disappears or remain stable.

3:00 pm

243. Acoustic Radiation Force Impulse Technology and Fibroscan in the Evaluation of Liver Diseases

Clevert, D.[1]; Zachoval, R.[2]; Reiser, M.[1] 1. Department of Clinical Radiology, University of Munich-Grosshadern Campus, Munich, Germany; 2. Internal Medicine II., Grosshadern Campus, Munich, Germany*
Address correspondence to D. Clevert (Dirk.Clevert@med.uni-muenchen.de)

Objective: Fibroscan is an accepted method in the detection of fibrotic and cirrhotic changes of the liver. The aim of our study was to compare this method with the new acoustic radiation force impulse (ARFI)-technology in patients with liver diseases.

Materials and Methods: Twenty-five healthy patients (group 1) age 25 to 37 years were examined with the fibroscan and with ARFI-technology. In addition, 28 patients age 48-77 years with histological proven liver cirrhosis by hepatitis C were examined (group 2). The examination time and the stiffness of the liver were measured. In addition, the healthy probands were examined through subcostal and intercostal windows with the ARFI technology.

Results: Fibroscan and ARFI showed a good correlation in the 25 healthy probands as well as in the 28 patients with histologically proven liver cirrhosis. The velocity of ARFI was between 0.7-4.89 m/s and the stiffness of Fibroscan was between 3.7-75 kPa. There were no significant differences in the velocity between the subcostal and intercostal measurement using the ARFI technology. The mean examination time for Fibroscan/ARFI was 5.2/1.7 minutes in group one and 6.8/3.1 minutes in group two. Due to ARFI one unknown hepatocellular carcinoma was found.

Conclusion: The measured data correlated well between the ARFI technology and Fibroscan in both groups. The examination time with ARFI can be reduced up to 67 % in comparison to Fibroscan. The subcostal ARFI examination has advantages for patients with considerable ascites. Due to the principle of ARFI, additional information is available with impact in the treatment of the patients.

3:10 pm

244. Characterization of Hypoechoic Focal Hepatic Lesions in Patients with Fatty Liver: Diagnostic Performance and Confidence of Contrast-Enhanced Ultrasound

Bartolotta, T.; Taibbi, A.; Galia, M.; La Grutta, L.; Malizia, G.; Midiri, M.; Lagalla, R. University Hospital, Palermo, Italy*
Address correspondence to A. Taibbi (taibbiadele@hotmail.com)

Objective: The objective was to assess the diagnostic performance of contrast-enhanced ultrasound (CEUS) in the characterization of hypoechoic focal hepatic lesions (HFHLs) in patients with fatty liver (FL) in comparison with baseline ultrasound (US).

Materials and Methods: A total of 105 consecutive patients with 105 HFHLs (52 malignant and 53 benign; mean size: 2.8 cm) in FL underwent CEUS after sulphur hexafluoride (Bracco, Milan, Italy) administration. Two blinded readers independently reviewed baseline US and CEUS scans classifying each lesion as malignant or benign on a five-point scale of confidence by means of definite diagnostic criteria. Moreover they recorded if further imaging was needed for lesion characterization. Sensitivity, specificity, areas under the receiver operating characteristic (ROC) curve (Az) and interobserver agreement were calculated.

Results: Diagnostic confidence improved after reviewing CEUS scans for both readers (A_z=0.706 and 0.999, 0.665 and 0.990 at baseline US and CEUS respectively: $p<0.0001$). Inter-reader agreement increased (weighted k=0.748 at baseline US vs 0.882 at CEUS). For both readers, after CEUS correctly characterized lesions increased (from 27/105 [27.5%] to 94/105 [89.5%] and from 19/105 [18.1%] to 93/105 [88.6%] respectively: $p<0.0001$) and the need for further imaging decreased (from 93/105 [88.6%] to 26/105 [24.8%] and from 96/105 [91.4%] to 40/105 [38.1%] respectively ($p<0.0001$).

Conclusion: CEUS improves the diagnostic performance of radiologists in the characterization of HFHLs arising in FL reducing the need for further radiological work-up.

3:20 pm

245. Role of Contrast-Enhanced Ultrasound in the Characterization of Incidentally Discovered Focal Liver Lesions

Bartolotta, T.; Taibbi, A.; Galia, M.; Lo Re, G.; La Grutta, L.; Midiri, M.; Lagalla, R. University Hospital, Palermo, Italy*
Address correspondence to A. Taibbi (taibbiadele@hotmail.com)

Objective: The objective was to assess the role of contrast-enhanced ultrasound (CEUS) to characterize incidentally discovered focal hepatic lesions (IDFHLs).

Materials and Methods: A total of 155 patients (112 women, 43 men; age range: 18-77 years, mean: 48.2 years) with 155 IDFHLs (size range: 0.5-13.1 cm; mean: 3.1 cm) at baseline ultrasound (US) underwent CEUS after sulphur hexafluoride (Bracco, Milan, Italy) administration. Standard of reference was histology (n=3: two focal nodular hyperplasia [FNH], one hepatocellular adenomas), core-biopsy (n=21: two hepatocellular adenomas, 16 FNHs, one intrahepatic extramedullary hematopoiesis nodule, one solitary necrotic nodule, one inflammatory pseudotumor) and typical CT and/or MRI findings (n=131: 86 hemangiomas, 28 FNHs, one echinococcus cyst, 16 hyper/hyposteatosis areas). Two blinded readers independently reviewed baseline US and CEUS scans and classified each lesion as malignant or benign on a five-point scale of confidence and recorded if further imaging work-up was needed. Sensitivity, specificity, areas under the receiver operating characteristic (ROC) curve (A_Z) and interobserver agreement were calculated.

Results: Diagnostic confidence improved after reviewing CEUS scans for both readers (A_Z= 0.606 and 0.899, 0.565 and 0.890 at baseline US and CEUS respectively: $p<0.0001$). Inter-reader agreement increased (weighted k=0.648 at baseline US vs. 0.782 at CEUS). For both readers, after CEUS correctly characterized lesions increased (from 44/155 [28.4%] to 138/155 [89%] and from 32/155 [20.6%] to 135/155 [87.1%] respectively ($p<0.0001$) and the need for further imaging decreased (from 132/155 [85.2%] to 48/155 [30.1%] and from 140/155 [90.3%] to 52/155 [33.5%] respectively ($p<0.0001$).

Conclusion: CEUS improves the diagnostic performance of radiologists in the characterization of IDFHLs and reduces the need for further imaging work-up.

GENERAL AND EMERGENCY RADIOLOGY PAPERS

Room: 309, Level 3
Thursday, April 30, 2009, 1:30 pm–3:00 pm
Abstracts 246-251

Moderators: *H. Abujudeh, M. Bruno*
Keynote Address: Organizing Patient Care and Enhancing Communication in Emergency Radiology with an Electronic Whiteboard System—*H. Abujudeh*

2:00 pm

246. Success of a Simple and Safe Algorithm to Reduce Utilization of CT Pulmonary Angiography in the Emergency Department

Stein, E.; Haramati, L.; Chamarthy, M.; Sprayregen, S.; Davitt, M.; Freeman, L. Albert Einstein College of Medicine, Montefiore Medical Center, Bronx, NY*
Address correspondence to L. Haramati (lharamati@aecom.yu.edu)

Objective: CT pulmonary angiography (CTPA) has supplanted ventilation-perfusion scanning (V/Q) as the primary imaging modality in patients with suspected pulmonary embolism (PE) despite its higher radiation exposure. We sought to determine if utilization of V/Q could be safely increased through an educational intervention with emergency department (ED) clinicians.

Materials and Methods: Collaborative educational seminars were held between radiology, nuclear medicine, and emergency medicine departments in December, 2006 regarding the radiation dose and comparable sensitivities of V/Q and CTPA for PE. A new imaging algorithm was introduced in which patients for whom there was a clinical suspicion of PE underwent chest radiography (CXR). If CXR was normal, V/Q was recommended, otherwise CTPA was recommended. To determine the intervention's safety and efficacy, we retrospectively tallied the number and results of CTPA and V/Q**s** before (2006) and after the intervention (2007). Medical records were reviewed for thromboembolism (false negative rate) and Social Security Death Index for mortality within 90 days after a negative study.

Results: The number of CTPAs performed for suspected PE decreased from 1,473 in 2006 to 920 in 2007 while the number of V/Qs increased from 745 in 2006 to 1216 in 2007, [CTPA: V/Q ratio 2006- 1.7:1, 2007- 0.8:1, $p<0.0001$]. The patients were similar in age for CTPA and V/Q in 2006 while the patients who underwent V/Q were significantly younger in 2007. The proportion of CTPA and V/Q interpreted as negative and positive, and indeterminate for V/Q, did not change between 2006 and 2007. V/Q was more often negative than CTPA in both 2006 (89.4% vs. 84.8%) and 2007 (89.4% vs. 81.8%), $p<0.0001$, each. There was no significant difference in false negative rate (range 0.8-1.2%) between CTPA and V/Q in 2006 and 2007. Among patients with negative imaging, 90 day mortality for CTPA (2006-10%, 2007-14%) was higher than for V/Q (2006-6%, 2007- 4%), $p<0.0001$, both years and decreased for V/Q in 2007 vs. 2006, ($p<0.0001$).

Conclusion: Practice patterns of ED physicians changed rapidly in response to an interdepartmental educational intervention promoting simple CXR triage for patients with suspected PE. Utilization of V/Q increased while CTA decreased, resulting in a reduction of patient radiation exposure without compromising safety and efficacy.

2:10 pm

247. Does Oral Contrast Increase Radiation Dose in mA Modulated MDCT Scanners? Estimated and Measured Dose Using a Body Phantom on 4-, 16- and 64-Detector Row Scanners

Beland, M.[1,2]; Kim, J.[2]; North, D.[2]; Collins, S.[2]; Mayo-Smith, W.[1,2]*
1. Brown University, Providence, RI; 2. Rhode Island Hospital, Providence, RI
Address correspondence to M. Beland (mbeland@lifespan.org)

Objective: Current MDCT scanners have a variable mA feature to reduce patient radiation dose. Use of oral contrast will increase the density of the patient on both scout and axial acquisitions and could lead to increased dose. The purpose of this project was to assess the effect of oral contrast on estimated and measured absorbed radiation dose utilizing a CT body phantom in 4-, 16- and 64-detector row scanners.

Materials and Methods: A CT body phantom containing gastric and colonic reservoirs was serially filled with air, sterile water, neutral oral contrast agent and barium sulfate. The phantom was scanned on six different variable mA CT scanners from different manufacturers on the same day utilizing routine abdomen/pelvis protocols for each contrast agent. A single detector row fixed mA scanner was used as a control. CT scanners included a 4-detector (one), 16-detector (four) and 64-detector (one) row. Cranial caudal coverage, field of view and kV were kept constant across all scanners. Slice thickness, collimation, pitch and rotation speed were kept constant for individual CT scanners. Internal radiation dosimeters were placed inside the phantom in the right upper quadrant and the left pelvis, to measure actual deep tissue absorbed dose. CT dose index (CTDI) and dose length product (DLP) were also recorded.

Results: The mean CTDI and DLP increased for water, a neutral oral contrast agent and barium sulfate when compared with air across all scanners except for one 16-detector row scanner. The mean CTDI was 9.23, 9.53, 9.60 and 9.48 mGy and the mean DLP was 505, 525, 526, 523 mGy-cm for air, water, volume and redi-cat respectively. As expected, the CTDI and DLP did not change for the single slice scanner with fixed mA protocol (300 mA). The measured deep tissue dose both in the abdomen and pelvis varied for each of the scanners without a trend toward increasing or decreasing dose. The mean measured dose in the abdomen was 1,577; 1,567; 1,561 and 1,696 mrad and in the pelvis was 1,159; 1,119; 1,211; 1,086 mrad for air, water, neutral oral contrast agent and barium sulfate respectively.

Conclusion: Oral contrast preparations denser than air generally lead to an increase in the average mA and therefore a higher DLP when all other parameters are held constant on variable mA MDCT scanners.

2:20 pm

248. Venous Thrombosis Head to Toe: Importance of Local Predisposing Factors

Kanekar, S.; Dykes, T.; Coquia, S. Penn State Milton S. Hershey Medical Center, Hershey, PA*
Address correspondence to S. Coquia (scoquia@hmc.psu.edu)

Objective: The purpose of this study was to identify the importance of local primary and secondary risk factors for venous thrombosis for various compartments of the body namely head, neck, chest, abdomen, pelvis and extremities.

Materials and Methods: We studied 121 patients with venous thrombosis from head to toe from our archive system from 2002 to date. Baseline clinical, blood work up and imaging data were analyzed. Imaging studies include CT, CT angiography, MR, MR angiography, DSA, USG and Doppler scans. These cases were further classified into six compartments from head to toe.

Results: Eighty-three men and 38 women were studied with venous thrombosis of various sites. Distribution of cases was as follows: intracranial sinus thrombosis=14 patients (11 cortical and three deep veins); neck vein= 8 patients, chest=29 patients, abdomen=18 patients; pelvis=seven patients, extremities= 45 patients, lower (36) and upper (nine). Local predisposing factor were found to be very different for different compartments. For intracranial, in pediatric patients dehydration and local infection (mastoiditis, sinusitis) while in adults it was trauma, extra-axial neoplasm and infection that were the major predisposing causes. Neck and upper extremities thrombosis was commonly seen following catheterization while tumor invasion was the primary risk factor in abdomen. All three cases of SVC thrombosis in the chest were due to neoplasm while pulmonary thrombosis/ embolism (venous blood) was following deep vein thrombosis. Classical Virchow triad was the major predisposing factors for the lower extremity (DVT) venous thrombosis, followed by local trauma.

Conclusion: Though the primary pathology in the blood or vessel could be the main cause for the venous thrombosis, local pathology and predisposing factors plays an important role in the development and extension of venous thrombosis. Identification and treatment of local predisposing factors should be the primary aim and is of vital importance for prevention and extension of venous thrombosis.

2:30 pm

249. CT Utilization and Effects on the Negative Appendectomy Rate at Harborview Medical Center from 1995-2007

Pugsley, J.; Raman, S.; Relyea-Chew, A.; Albrecht, E.; Richardson, M.; Bresnehan, B.; Maier, R.; Gunn, M.; Pugsley, J. University of Washington, Seattle, WA*
Address correspondence to S. Raman (sraman3@u.washington.edu)

Objective: The objective was to determine trends CT utilization prior to appendectomy over the last 13 years, and to determine the effect of CT utilization on the "negative appendectomy" rate.

Materials and Methods: The pathology reports for all patients undergoing appendectomy for any reason between 1995-2007 at Harborview Medical Center were reviewed, and classified as positive, negative or indeterminate for acute appendicitis. Patients were excluded if they underwent an incidental appendectomy (appendectomy in passing). The available accompanying preoperative CT reports were reviewed and classified as positive, negative or indeterminate for acute appendicitis.

Results: Over a 13-year period, 813 patients underwent nonincidental appendectomy. The patient population consisted of 69% men and 31% women, and the average age was 34 years. The percentage of patients undergoing preoperative CT imaging has steadily increased over time from 13% to 84%. The percentage of negative appendectomies has steadily declined over time from 25% to 4%. Previously, the rate of negative appendectomy in women was significantly higher than men, but has declined in recent years to a similar rate as men. Over the entire study period the negative appendectomy rate was 19.7% in those patients without a preoperative CT and 6.7% with CT. The cumulative negative appendectomy rate for patients with a positive CT was 4.1%. The length of stay in the hospital for patients with positive and negative appendectomies in recent years was approximately 2.5 days and 1.5 days, respectively.

Conclusion: Increased preoperative CT utilization was associated with a significant decrease in the negative appendectomy rate. Although both men and women have benefitted from increased CT utilization, women had a greater decrease in the negative appendectomy rate and have received the greatest benefit from increased utilization of CT. Although the negative appendectomy rate has declined over time and patients with a negative appendectomy average shorter hospital stays, this still represents a large healthcare cost and further efforts at reduction in the negative appendectomy rate are warranted.

2:40 pm

250. Disc and Ligamentous Injuries: Something New to Consider on MDCT?

Ramos, J.; Crawford, H.; Kumaravel, M.; Jarolimek, A.; Kim, J.; Sitton, C.; West, O. University of Texas Medical School at Houston, Houston, TX*
Address correspondence to J. Ramos (juan.m.ramos.gonzalez@uth.tmc.edu)

Objective: Advanced technology in newer generation CT scanners allow for better evaluation of cervical soft tissues. The purpose of this study is to compare the performance of CT to MRI for identification of cervical spine soft tissue injuries (STI), independent of state of consciousness. Also, this study will determine how often CT of the cervical spine correctly depicts STI in trauma patients.

Materials and Methods: This retrospective study evaluated 576 consecutive blunt trauma patients who had both cervical spine CT and MRI during September, 2006 to August, 2008 at a single large Level I trauma center. All CT and MRI reports were reviewed. Comparison and subgroup analysis of CT and MR findings was accomplished using pivot tables. Cases with cervical STI reported on either modality, CT and MRI were reviewed by three radiologists blinded to original diagnosis.

Results: MRI identified 85.5% (212/248) of traumatic findings noted by CT; 90.2% (212/235) of CT findings were present on MRI; 8.9% (21/235) had traumatic findings on MRI not detected on CT. Two more had equivocal findings on CT. Of 23 discordant cases, eight consisted of bone contusions with or without underlying cord edema. 15 had ligamentous injury with or without traumatic disc injury. A total of 8.5% (21/248) had traumatic findings on CT not present on MRI. Seven more had equivocal findings on MRI. All discordant cases were fractures and/or dislocations. Seventy-one patients had traumatic disc rupture on MRI. Nine were diagnosed on CT and 12 were equivocal for disc injury for a total of 21 (30%). Ninety-nine patients had ligamentous injury on MRI. Nine were diagnosed on CT and 15 equivocal for ligamentous injury for a total of 24 (24%). During the review of images, we identified two CT findings that indicated underlying STI: avulsion fracture adjacent to the disc space correlated with discoligamentous injury on MRI; midline soft tissue mass between the semispinalis cervicis muscles represented interspinous ligament injury on MRI.

Conclusion: Neither CT nor MRI detected all cervical spine injuries. CT detected a greater number of injuries, while MRI performed better for STI. In a small number of cases, CT depicted STI, indicating that STI should be sought when reading CT. Further, our review of cases identified two novel CT findings that may improve the sensitivity of CT for detection of STI.

2:50 pm

251. Imaging Women with Acute Abdominal Pain: Diagnostic Performance of Pelvic Ultrasonography and CT

Levsky, J.; Stein, M.; Khalef, V.; Zaidi, F.; Rozenblit, A. Montefiore Medical Center, New Rochelle, NY*
Address correspondence to M. Stein (mstein17@aol.com)

Objective: The objective was to evaluate and compare the diagnostic performance of abdominal/pelvic CT and pelvic ultrasonography (US) in women presenting with nontraumatic abdominal or pelvic pain.

Materials and Methods: We retrospectively studied the medical records of 490 consecutive patients (mean age 35 years) who underwent both CT and US within 48 hours of each other during the emergency work-up of abdominal pain. CT and US reports were reviewed at separate times by the consensus of two readers blinded to the clinical details. The performance of each exam in diagnosing a cause of pain was scored as (1) definite, (2) possible, or (3) none identified. Classifications were compared on a patient-by-patient basis across modalities for concordance.

Results: Definite, possible and no cause of pain were identified in 233 (48%), 53 (11%) and 204 (42%) USs, respectively, and in 236 (48%), 76 (16%) and 178 (36%) CTs, respectively. Pain etiologies identified by imaging (n=280) were: ovarian cysts (51%), pelvic inflammatory disease (PID) (15%), ovarian masses (10%), gastrointestinal (GI) diseases (9%) urological diseases (5%) and others (10%). Concordance for a definite cause of pain was found in 145/490 (29%) cases while concordance for no definite cause of pain was found in 137/490 (28%). In 56/490 (11%) cases one test gave a possible diagnosis while the other test was definitive and in 79/490 (16%) cases one test demonstrated no cause of pain while the other was definitive. The diagnoses provided by US and not identified by CT (n=65/490, 13%) included ovarian cysts (69%), PID (20%) and ovarian masses (5%). The diagnoses provided by CT and not identified by US (n=68/490, 14%) included GI diseases (41%), urological diseases (19%), ovarian cysts (17%) and degenerating uterine myomas (12%). In 22/490 (4%) cases US and CT gave different diagnoses.

Conclusion: US and CT performed similarly in this group of patients with a predominance of gynecologic abnormalities. Each modality provided a definite cause of abdominal pain in about half of patients. In about one quarter of patients only one modality provided a definite diagnosis. US was superior in identifying ovarian and tubal pathology and CT was superior in identifying GI and urological etiologies of pain. This data suggests the feasibility of an US first diagnostic algorithm for imaging women with abdominal pain to lower the radiation burden inherent to CT with the understanding that there will be cases that require CT for diagnosis.

MUSCULOSKELETAL (SYSTEMIC DISEASE/SPINE) IMAGING PAPERS

Room: 310, Level 3

Friday, May 1, 2009, 10:00 am–12:00 noon

Abstracts 252-263

Moderators: M. Robbin, B. Sabb

10:00 am

252. Association of Vertebral Wedging Patterns with Acute Fractures at the Thoracolumbar Junction

Cabay, M.[1]; Rosas, H.[2]; De Smet, A.[2] 1. University of Wisconsin, Madison, WI; 2. University of Wisconsin, Madison, WI*
Address correspondence to M. Cabay (mcabay1@yahoo.com)

Objective: Symmetric anterior wedging of T12 and L1 on radiographs has been attributed to normal variation or projection related to x-ray beam centering. Thus symmetric wedging at T12 or L1 on radiographs is considered unlikely to represent a fracture unless other fracture findings are present. The objective of this study was to compare the frequency of fractures at T12 and L1 detected on CT with symmetric and asymmetric vertebral wedging on lumbar spine radiographs in the trauma setting.

Materials and Methods: A total of 154 consecutive patients (mean age 38 years; 107 males/47 females) had radiographs and CT of the lumbar spine for acute trauma. The vertebral level of the central x-ray beam on the lateral lumbar radiograph was determined. Two observers without knowledge of the CT findings retrospectively evaluated the lumbar spine radiographs classifying T12 and L1 vertebral body shape as normal, symmetrically wedged, or wedged superiorly or inferiorly, and assessed for signs of fracture other than wedging. CT was used as the gold standard for the presence of acute fracture.

Results: The location of the central x-ray beam had a similar distribution in vertebrae with and without symmetric wedging. Eight patients had acute body fractures of T12 and L1, 11 had fractures of T12 and not L1 and 26 had fractures of L1 and not T12. Seventeen of the 45 patients with T12 or L1 fractures had vertebral fractures at other levels. Of the 19 T12 vertebral body fractures, 13 had superior wedging, three had symmetric wedging and three had no endplate depression. Of the 34 L1 vertebrae with body fractures, 28 had superior wedging, one inferior wedging, four symmetric wedging and one had no endplate depression. For T12 and L1 combined, CT demonstrated acute vertebral body fractures in 33% of the vertebrae with inferior wedging, 77% with superior wedging, 12% with symmetrical wedging and 2% without wedging. Of the 53 T12 and L1 vertebrae with body fractures on CT, 85% of those with superior wedging but only 29% of those with symmetrical wedging had definitive radiographic signs of a fracture such as cortical disruption or lucent fracture line.

Conclusion: Although acute vertebral body fractures at the thoracolumbar junction most commonly have superior wedging, 12% of symmetrically wedged vertebrae had acute fractures with only 29% showing other radiographic signs of a fracture. In acute trauma, any pattern of vertebral wedging at the thoracolumbar junction should suggest an underlying fracture.

10:10 am

253. Stress Fractures of the Anterior Arch of the Atlas

Hughes, T.; Hiller, L. University of California-San Diego, San Diego, CA*
Address correspondence to T. Hughes (thughes@ucsd.edu)

Objective: We had noted several patients that have an open anterior arch of C1 with associated hypertrophic margins. They all had associated congenital nonunion of the posterior arch. The literature suggests that such anterior findings are due to nonfusion of secondary ossification centers. We considered that they were stress fractures from loss of hoop strength due to the open posterior arch.

Materials and Methods: We retrospectively reviewed 840 CT scans of the cervical spine requested by the trauma team taken from a one-year period, to assess for the presence of nonfusion of the posterior arch and also an open anterior arch with accompanying hypertrophic margins. Those with open posterior arches and age/sex matched normal studies were measured in the midline anteriorly for the areal density in Houndsfield units of a 1mm sagittal slice to assess for hypertrophy.

Results: Twenty-six of the 840 patients had a congenitally open posterior arch. Five of these 26 had a degree of congenital fusion of the occiput to the atlas. One of the 26 had an open hypertrophic anterior arch. No patient had an open anterior arch without an open posterior arch.

Conclusion: Congenital nonunion of the posterior arch of C1 is relatively common and usually causes no symptoms. It does however weaken the ring of C1 with loss of hoop strength. Due to the alignment of the lateral masses of C1, there are increased forces on the anterior arch causing hypertrophy and stress fracture. The synchondrosis between the anterior arch (hypochondral bow) and the two lateral masses are not in the midline and not the cause of the open anterior arch.

10:20 am

254. The Importance of Sagittal 2D Reconstruction in Pelvic and Sacral Trauma: Avoiding Oversights of U-Shaped Transverse Fractures of the Sacrum

Porrino, J.; Holden, D.; Taljanovic, M.; Rogers, L. University of Arizona Health Science Center, Tucson, AZ*
Address correspondence to L. Rogers (lfrogers@comcast.net)

Objective: We describe an uncommon form of sacral fracture, a U-shaped transverse sacral fracture, which can be easily overlooked in the absence of clinical suspicion and if appropriate images are not obtained. If unrecognized and untreated, such fractures can result in sacral plexus compression with subsequent serious neurologic deficits of bowel, bladder, and sexual dysfunction. We have found that the only consistent means of disclosing the transverse component of sacral fractures is by CT with 2D reconstructed images in the sagittal plane.

Materials and Methods: We encountered seven patients with U-shaped sacral fractures spanning a six year period from 2003 thru 2009. There were three males and four females ranging in age from 19 to 83 years. The mechanism of injury included fall from heights, bicycle vs. motor vehicle and motor vehicle

accident. Anteroposterior (AP) radiographs, as well as axial, sagittal, and coronal CT imaging of the pelvis were obtained. All images were reviewed by three of the authors to determine the best means of identifying these unusual fractures.

Results: U-shaped sacral fractures generally occur in association with a variety of pelvic fractures. However, in one of the seven cases, the anterior arch of the pelvis was spared, making the presence of a sacral fracture seem much less likely. We found that transversely oriented sacral fractures are nearly nondiscernable, even in retrospect, on standard AP radiographs of the pelvis, as well as axial and coronal 2D and 3D CT images of the pelvis. However, we note that such fractures are readily apparent and easily identified on reformatted 2D CT images in the sagittal plane.

Conclusion: Initial evaluation of the multisystem trauma patient routinely involves MDCT. This provides images that are of superb quality with image reconstruction in multiple planes relatively easily obtained. In most trauma centers it is standard procedure to reconstruct pelvic CT 2D images in the coronal plane and 3D images of the entire pelvis. Reconstruction of images in the sagittal plane as a matter of routine is less common. We advocate the routine reconstruction of CT images of the pelvis in the sagittal plane in multisystem trauma patients in order to assure identification of transverse fractures of the sacrum, and in an attempt to avoid the potential unfortunate consequence of sacral neurologic injury and subsequent bowel, bladder, and sexual dysfunction associated with U-shaped transverse fractures of the sacrum.

10:30 am

255. Imaging of Intracortical Chondroma

Ruble, C.[1]; Murphey, M.[1]; Tyszko, S.[2]; Fanburg-Smith, J.[1]; Franklin, J.[1]; Zbojniewicz, A.[3] 1. Armed Forces Institute of Pathology, Bethesda, MD; 2. National Naval Medical Center, Bethesda, MD; 3. No Institutional Affiliation*
Address correspondence to C. Ruble (chadruble@mac.com)

Objective: The objective was to describe the imaging characteristics of intracortical chondroma with pathologic correlation.

Materials and Methods: We retrospectively reviewed 21 cases of intracortical chondromas, pathologically proven in 19 cases. Radiologic studies including: radiographs (n=21), bone scintigraphy (n=2), CT (n=6), MR (n=8), were reviewed by three radiologists with agreement by consensus. Evaluation included patient demographics, clinical presentation, lesion location/shape/size/margin, bone expansion, mineralization, radionuclide uptake pattern and intrinsic characteristics on CT and MR. Histologically, the presence of cellular atypia was also evaluated.

Results: Patients included ten males and 11 females with an age range of two to 58 years (average 19 years). Clinical presentation included asymptomatic (39%), pain (15%), painful mass (15%) and painless mass (31%). Lesion shape was oval in 52% and elongated in 48% of cases. Cortical expansion was graded as mild (29%), moderate (42%), or marked (29%). Lesions were located in the tibia (29%), humerus (24%), femur (14%), radius (9%) or hand (24%) and were centered in the diaphysis (76%), metaphysis (19%) or epiphysis (5%). Physeal involvement was seen in 33% of cases. Lesion size averaged 4.2 X 1.2 cm with a range from 0.8 X 0.4 cm to 13.3 X 2.0 cm. At radiography, all lesions showed geographic lysis with a narrow (43%) or focal wide zone of transition (57%). Radiographs revealed mineralization in 43% of cases compared to 67% on CT. Bone scintigraphy showed mild uptake in all cases. CT revealed intact cortical/periosteal margins in all cases. The attenuation of the nonmineralized areas was similar to muscle in 50% and lower than muscle in 50% of cases. On MR, all lesions demonstrated lobular margins, signal intensity similar to muscle on T1-weighting and high intensity on T2-weighting. Postcontrast MR showed peripheral and septal (50%), peripheral (33%) or diffuse (17%) enhancement patterns of mild degree. Cellular atypia was seen histologically in 76% of cases.

Conclusion: Intracortical chondroma is a rare benign osseous neoplasm. Imaging features that strongly suggest the diagnosis include an intracortical location, elongated shape, physeal involvement, lobular margins and intrinsic features suggesting chondroid matrix. Radiographs and histology may suggest a more aggressive lesion because of apparent cortical destruction and cellular atypia, respectively. However, CT and MR show an intact cortical margin reflecting the lesion's benign etiology.

10:40 am

256. Granulocytic Sarcoma of the Spine: MR Imaging and Clinical Review

Seok, J.[1]; Park, J.[2]; Kim, s.[1]; Choi, J.[3] 1. The Catholic University of Korea, Seoul, South Korea; 2. St. Mary's Hospital, Seoul, South Korea; 3. St. Paul's Hospital, Seoul, South Korea*
Address correspondence to J. Park (jmpark@catholic.ac.kr)

Objective: Granulocytic sarcoma (chloroma) is a tumor formed by myeloid precursors in an extramedullary site and is associated with myeloid leukemias and other myeloproliferative disorders. We present the MR imaging findings and clinical manifestations of 33 cases of spinal chloroma.

Materials and Methods: The average age of the patients (22 males and 11 females) was 32 years. There were 24 acute myelogenous leukemias, four acute lymphocytic leukemias and five chronic myelogenous leukemias. Nine patients manifested with granulocytic sarcoma as a presenting sign and the remaining 24 were diagnosed during remission phase or relapse period. All patients received radiotherapy with combined chemotherapy and three patients underwent surgical decompression. MR imaging of spine was performed in all patients with follow up MR imaging in 24 patients

Results: All patients complained of lower back pain, with other complaints including radioculathies, numbness and pain in the extremities, and paraplegia. The lumbosacral (15 cases) and thoracic (13 cases) spines were commonly involved, and three of the 33 patients exhibited multiple noncontiguous areas of involvement. MR imaging demonstrated multiple epidural masses and obliteration of the spinal canal with parameningeal extension mainly through the neural foramina, resulting in thickening of multiple nerve roots. Lesions were isointense to bone marrow on both T1- and T2-weighted MR images with homogeneous enhancement after injection of contrast medium.

Conclusion: Increased awareness of imaging findings of granulocytic sarcoma will facilitate early diagnosis and minimize potentially preventable neurological morbidity.

10:50 am

257. Diabetic Myopathy: Imaging Diagnosis and Prevalence in a Hospital Population

Huang, B.; Sarang, T.; Tamrazi, B.; Dieudonne, G.; Seo, G.; Monu, J. University of Rochester, Rochester, NY*
Address correspondence to J. Monu (johnny_monu@urmc.rochester.edu)

Objective: This study evaluates and correlates clinical parameters with the occurrence and the distribution of diabetic muscle infarction in the lower extremities within a large hospital population.

Materials and Methods: MRI reports from July, 1999 through January, 2006 were retrospectively evaluated and correlated with clinical parameters for patients diagnosed with diabetic muscle infarctions. Fifteen patients met the study criteria and parameters including the type of diabetes, hemoglobin A1C (HbA1C), creatine kinase (CK), erythrocyte sedimentation rate (ESR) and presence of complications were recorded. The distribution of involvement by individual muscles and by muscle groups was reviewed.

Results: Over the study period, 15 patients were identified, and 18 extremities were imaged (nine thighs and nine calves). Two patients had bilateral involvement of the thighs and one patient had involvement of the thigh and calf. 13 (87%) of the study patients had Type 2 diabetes, while the remaining two (13%) had Type 1 diabetes. Approximately half of the patients with Type 2 diabetes were on an insulin regimen at presentation. The anterior compartment was most commonly affected muscle group in eight (89%) of the nine thighs. In the thigh, the vastus lateralis and medialis were the most commonly affected muscles overall, each accounting for eight (89%) muscles. The posterior compartment was the most commonly muscle group affected in eight (89%) of the nine calves. The medial head of the gastrocnemius was most commonly affected individual muscle in eight (89%) calves. Rim enhancement with a low signal intensity centrally was indicative of muscle infarct and necrosis and was seen in five (28%) of 18 extremities imaged. Five (28%) extremities exhibited hyperintensity within the affected muscles on unenhanced T1-weighted images, likely representing hemorrhagic necrosis. CK, ESR, and HbA1C were elevated in the majority of cases. Coexisting nephropathy, neuropathy, and retinopathy was present in eight (53%), seven (47%), and four (27%) cases respectively.

Conclusion: Diabetic muscle infarction affects patients with Type 2 diabetes more frequently than previously reported. Because it has a self-limiting course, the diagnosis should be made confidently potentially harmful biopsies avoided.

11:00 am

258. New Mechanisms and Imaging Findings of Tumor Induced Osteomalacia

Feldman, F., Columbia Presbyterian Medical Center, New York, NY*
Address correspondence to F. Feldman (friedafeldman@hotmail.com)

Objective: The objective was to demonstrate and discuss imaging and biochemical and genetic characteristics of oncogenic osteomalacia involving the musculoskeletal system.

Materials and Methods: Forty-five patients with malignant, benign or developmental lesions which induced oncogenic osteomalacia were studied with radiographs, CT, PET-CT and/or 1.5 or 3T MR magnets (GE Healthcare, Milwaukee, WI). Dedicated pelvic and extremity coils were used with multiple T1and fluid sensitive sequences in multiple planes.

Results: Correlation of results of above noted imaging modalities with specific biochemical and genetic markers increased the accuracy and specific identification of the often elusive lesions responsible for imaging findings and clinical symptoms.

Conclusion: Numerous bone and soft tissue lesions, not all of mesenchymal origin, are well defined on advanced imaging modalities but are usually nonspecific. Despite recognition of some of these entities, i.e. benign or malignant lesions per se, they should not be taken at "face value" in view of their overlapping features one of which is osteomalacia. These lesions play an otherwise unexplainable role in concomitant but deemed to be "idiopathic osteomalacia". Their full clinical significance may be more readily appreciated if imaging findings are correlated with specific biochemical and genetic markers which will be discussed.

11:10 am

259. Comparative Evaluation of Diffusion Characteristics and ADC Values in Patients With Intra- and Extramedullary Myelomatous Lesions

Kaushik, C.; Yousaf, A.; Pandey, T.; Viswamitra, S.; Jambhekar, K. University of Arkansas for Medical Sciences, Little Rock, AR*
Address correspondence to T. Pandey (drtarunpandey@hotmail.com)

Objective: Patients with extramedullary myeloma have different management and prognosis compared to patients with intramedullary disease. We tested the hypothesis that there may be a difference in ADC values in intra- vs. extramedullary myeloma lesions.

Materials and Methods: Twenty-four patients with multiple myeloma were the subjects of our study. These included 11 patients with extramedullary involvement, ten patients with only intramedullary lesions and three patients with both intra- and extramedullary involvement. There were 15 male and nine female patients, with age range of 49-73 years. All imaging was performed using 1.5T MRI scanner (Siemens Medical Solutions, Erlangen, Germany). Diffusion-weighted images (DWI) were obtained using single-shot echo planar sequence (repetition time [TR]/echo time [TE] 4200/ 82 milliseconds, matrix 124x192, b-values 0/ 50/ 400/ 800 mm^2 /second). Direct measurements of ADC values of these lesions were obtained on a workstation (Siemens Medical Solutions, Erlangen, Germany). The mean and standard deviation of the ADC values was calculated. Statistical analysis was performed using Student's t-test.

Results: Extramedullary locations were: 12 liver, two skeletal muscle, two ischiorectal fossa, one breast, one pancreas, one adrenal, one renal and one pararenal lesions. The ten patients with intramedullary involvement showed diffuse pattern of marrow involvement in seven and focal involvement in three. The bone lesions had a mean ADC of 1.4×10^{-3} mm^2/second, SD ± 0.5 compared to extramedullary lesions which had a mean ADC

1.1 x 10^{-3} mm^2/second, SD ± 0.5 which was not statistically significant (p=0.15). However there was a trend toward bone lesions having higher ADC values.

Conclusion: Extramedullary and intramedullary myelomatous lesions tend to have similar ADC values. A higher trend of ADC values in bone lesions was noted which needs studies in larger patient population to evaluate true statistical significance.

11:20 am

260. Prospective Study of High Resolution Ultrasound Evaluation of Rib Metastases from Renal Cell and Prostate Carcinoma

Lee, K.; De Smet, A.; Liu, G. University of Wisconsin-Madison, Middleton, WI*
Address correspondence to K. Lee (kenlee8799@yahoo.com)

Objective: In a prior study, high resolution ultrasound (US) was shown to be accurate for evaluating possible rib metastases detected on a bone scan. However, that study did not address if the US appearance was different for osteoblastic and osteolytic metastases. Our objective was to determine the US appearance of known rib metastases from osteolytic renal cell carcinoma and osteoblastic prostate carcinoma.

Materials and Methods: Institutional review board approval and informed consent were obtained for this prospective study. We obtained high resolution US of eight rib metastases in three male patients with renal cell carcinoma and 16 rib metastases in four patients with prostate carcinoma metastases. All patients had rib metastases proven by radiographs, CT and/or bone scan. High resolution US scanning was performed by an experienced musculoskeletal radiologist using a 12-5 MHz linear array transducer. Transverse and longitudinal scans were obtained of each rib metastasis and of a normal rib in each patient as a baseline.

Results: All seven normal ribs had a smooth continuous appearance of the superficial surface of the rib. All 16 prostate carcinoma metastases demonstrated mild cortical irregularity of the superficial surface of the rib without associated soft tissue mass, cortical disruption, or bone destruction. Seven of eight (88%) renal cell carcinoma rib metastases demonstrated cortical disruption or extensive bone destruction without soft tissue mass. One of eight (12%) renal cell carcinoma rib metastases demonstrated only minimal superficial cortical irregularity at the site of a healed metastasis.

Conclusion: Osteolytic renal cell and osteoblastic prostate carcinoma rib metastases have a distinctive appearance on US. Our success in visualizing these lesions suggests that US may be useful to assess if a bone scan abnormality in a rib represents either an osteolytic or osteoblastic metastasis.

11:30 am

261. Radiographic Screening for Facial Fractures: A Sensitive and Accurate Alternative to Facial CT

Daffner, R. Allegheny General Hospital, Pittsburgh, PA*
Address correspondence to R. Daffner (rhdaffner@netscape.net)

Objective: The objective was to demonstrate that routine screening for facial injuries using Waters and lateral radiographs is a sensitive and accurate procedure. Furthermore, radiography provides a lower radiation dose when compared with CT.

Materials and Methods: One hundred patients with known facial fractures selected from a teaching file and data base who underwent both radiographic and CT examinations of the face prior to 2000 were studied. Forty-two patients had zygomatic arch/zygomaticomaxillary complex fractures; 29 had orbital injuries; 17 had maxillary/LeFort injuries; and 12 had mandible fractures. Radiographs consisted of Waters and lateral views. Patients with mandible fractures also had panoramic and Towne views. All studies were examined for direct (fracture lines seen) and indirect (asymmetry, malocclusion, sinus opacification, displacement/duplication) signs of injury.

Results: Waters and lateral radiographs correctly identified all the zygomaticomaxillary complex, orbital, and maxillary/LeFort injuries. Two nondisplaced zybomatic arch, four mandible condylar, and three mandible parasymphyseal fractures were not demonstrated on the radiographs. All injuries were shown on CT. Supplementary panoramic and Towne views showed all the mandible fractures; submentovertex views showed the zygomatic arch fractures.

Conclusion: Screening with Waters and lateral radiographs is a sensitive method for identifying facial fractures. The radiation dose is less than for CT. If clinical examination findings are added, appropriate supplemental views (panoramic, Towne, and submentovertex) can be obtained to increase the accuracy of radiography.

11:40 am

262. Radiographic Finding of Lumbar Epidural Gas with CT and MR Correlation

Liu, W.[1]; Choi, G.[1]; Choi, J.[2]; Lee, S.[1]; Park, H.[1]; Paeng, S.[1] 1. Wooridul Spine Hospital, Seoul, South Korea; 2. Samsung Medical Center, Seoul, Korea*
Address correspondence to W. Liu (weichiang@mac.com)

Objective: The main purpose of this study was to evaluate CT imaging finding of lumbar epidural gas in correlation with MR imaging and radiculopathy.

Materials and Methods: From March, 2004 to August, 2008, 41 consecutive patients with 47 lumbar epidural gases proven by CT were retrospectively reviewed in our institution. These were composed of eight men and 33 women. The average age of the patients at the time of admission was 66 years, ranging from 43 to 84 years. We categorized lumbar epidural gas as four groups i.e. epidural gas with disc material (honeycomb appearance, air contained herniated disc) and without disc material (air cyst and air pseudocyst), to evaluate CT imaging finding is correlated with MR finding and radiculopathy.

Results: CT finding of lumbar epidural gas showed in six of 47 (12.8%) as honeycomb appearance, 17 of 47 (36.2%) as air contained herniated disc, seven of 47 (14.9%) as air cyst, and 17 of 47 (36.2%) as air pseudocyst. On MR image, lumbar epidural cyst showed in 17 of 47 (36.2%) on T1-weighted image and 17 of 47 (12.8%) on T2-weighted image. Honeycomb appearance and air contained disc were associated with radiculopathy more than air cyst and air pseudocyst (p=0.0018).
Conclusion: Lumbar epidural gas with disc material (honeycomb appearance, air contained herniated disc) on CT image is associated with radiculopathy.

11:50 am

263. Imaging Raises the Bar for Remission in Rheumatoid Arthritis

Monu, J.; Anandarajah, A.; Dhillon, G.; Mooney, S. University of Rochester, Rochester, NY*
Address correspondence to J. Monu (johnny_monu@urmc.rochester.edu)

Objective: Current methods used in evaluating disease remission in rheumatoid arthritis (RA) rely on composite scores base entirely on clinical and laboratory assessments. The purpose of this presentation is to show that it is inadequate to rely on clinical and laboratory data alone in monitoring disease progress in RA.

Materials and Methods: Clinical and laboratory data of two patients with RA who have been monitored over a period of 3-8 years are presented. Serial imaging studies including plain radiographs, MRI and ultrasound studies were used at various times to monitor disease progress. Surgical biopsy specimens were reviewed for disease activity and correlated with the clinical, laboratory and radiographic results.

Results: Over the period the patients' disease were apparently controlled and in remission using clinical and laboratory parameters. Pathologic material from biopsy showed continued disease activity and correlated positively with imaging findings.

Conclusion: Clinical and laboratory parameters used in assessing disease activity do not directly measure inflammation at primary site of disease and may be subject to confounding factors whereas imaging does not suffer from this disadvantage. Imaging therefore should be used continuously and in conjunction with clinical and laboratory parameters to evaluate disease activity.

The Roentgen Fund® gratefully acknowledges its top 2008 contributors.

Radiology has been an inseparable part of my life for 50 years. As I have grown and raised an ever-expanding family, so has the field of radiology grown and expanded. Radiology has been good to me, and has given me much, personally, professionally and intellectually. I am also fortunate in having prospered materially as a result of my involvement in radiology. But nothing in life is a one-way street; I have taken much from radiology, and in return I am morally committed to giving something of value back to it. My wife's and my contribution to the ARRS Roentgen Fund, to be used to educate and support young men and women so that they, too, can enjoy the fruits of and benefit from radiology, is but one small way by which I can attempt to repay the enormous debt that I owe to my profession; it is but one small way of saying, 'thank you'.

Dr. Leonard Berlin

2008 Top Individual Contributors

Philip O. Alderson
Norman J. Beauchamp
Leonard Berlin and Phyllis Berlin
Stephen Bravo
Stephen M. Brown, Intl. Med. Imaging Cons. Inc.
M. Paul Capp
Barbara L. Carter and Jeffery Moore
William J. Casarella and Kay Vydareny
Mauricio Castillo
John K. Crowe
Sandeep Deshmukh
N. Reed Dunnick
Anton N. Hasso and Peggy Fritzsche
Marcia Javitt
Chuck Kahn
Joseph K.T. Lee
Jonathan Lewin
Brian Meagher
Neil Messinger
Lee F. Rogers
Melissa Rosado de Christenson
William P. Shuman
Robert J. Stanley
Richard G. Stiles
James H. Thrall
Paula Yehiayan
David Yeh

The Roentgen Fund® also gratefully acknowledges support by Bracco Diagnostics Inc. and Philips Healthcare.

Donations to The Roentgen Fund® are deductible as a charitable gift contribution. Please call Keri Sperry at 703-858-4306 if you have any questions about contributing to the fund. Contributions can be mailed to The Roentgen Fund®, c/o ARRS, 44211 Slatestone Court, Leesburg, VA 20176. Log onto www.arrs.org to contribute online.